DOE/FE/60181-26
(DE84002700)

LOW-RANK COAL RESEARCH UNDER THE UND/DOE COOPERATIVE AGREEMENT

Quarterly Technical Progress Report for the Period July–September 1983

By
George A. Wiltsee, Jr.

Work Performed Under Contract No. FC21-83FE60181

Energy Research Center
University of North Dakota
Grand Forks, North Dakota

Technical Information Center
Office of Scientific and Technical Information
United States Department of Energy

DISCLAIMER

DISCLAIMER

This report has been reproduced directly from the best available copy.

Available from the National Technical Information Service, U. S. Department of Commerce, Springfield, Virginia 22161.

Price: Printed Copy A11
Microfiche A01

Codes are used for pricing all publications. The code is determined by the number of pages in the publication. Information pertaining to the pricing codes can be found in the current issues of the following publications, which are generally available in most libraries: *Energy Research Abstracts (ERA); Government Reports Announcements* and Index (*GRA* and I); *Scientific and Technical Abstract Reports (STAR);* and publication NTIS-PR-360 available from NTIS at the above address.

DOE/FE/60181-26
(DE84002700)
Distribution Category UC-90

LOW-RANK COAL RESEARCH UNDER THE UND/DOE COOPERATIVE AGREEMENT

QUARTERLY TECHNICAL PROGRESS REPORT FOR THE PERIOD JULY 1983-SEPTEMBER 1983

George A. Wiltsee, Jr.

University of North Dakota
Energy Research Center
Grand Forks, North Dakota 58202

Prepared for the
U.S. Department of Energy
Office of Fossil Energy
Under Cooperative Agreement DE-FC01-83FE60181

TABLE OF CONTENTS

TABLE OF CONTENTS--Continued

TABLE OF CONTENTS--Continued

TABLE OF CONTENTS--Continued

TABLE OF CONTENTS--Continued

TABLE OF CONTENTS--Continued

HIGHLIGHTS

COAL CONVERSION RESEARCH

Gasification Wastewater Treatment and Reuse

- Two long gasification tests were accomplished (66 and 72 hours of slagging operation) this quarter, and the balance of the wastewater needed for the second cooling tower (CT) test (~11,000 gallons) was generated.

- Eleven thousand gallons of slagging fixed-bed gasifier (SFBG) wastewater were solvent extracted and ammonia stripped (AS) to nominal levels of 160 mg/l phenol and 600 mg/l NH_3. This wastewater is being further treated by activated sludge (AS) and granular activated carbon (GAC) processing to prepare a high quality makeup for the second CT test.

- Component material balances have been completed for some key species from the first UNDERC CT test based on rates and composition of makeup, blowdown, drift, and evaporate. Phenol mass balances indicated that >90 pct of the phenol was stripped from the tower, indicating that previous assumptions of high levels of biodegradation were erroneous. Over 80 pct of the ammonia and about 25 pct of the methanol were also stripped.

- Data collected during steady state operation of the bench-scale rotating biological contactor indicate complete removal of phenolics and alcohols, and 94 pct removal of BOD. Nitrification also occurred in this unit, with over 30 pct removal of ammonia. Operating conditions for the unit included a hydraulic detention time (HDT) of 0.48 days and a hydraulic loading of 0.1 gal/ft^2/day. Operation of this unit on SGL was exceptionally good. Considering the low initial investment, low operating costs, and the stability of this type of biological treatment process, its use should be evaluated at a larger scale.

- Some problems have been encountered in operation of the pilot-scale AS system, including foaming and variable levels of COD in the influent. Nevertheless, operation has been good and steady state samples with an HDT of 3 days and a sludge age of 20 days have shown complete removal of phenolics and alcohols and over 94 pct reduction in BOD. With the relatively short sludge age, little nitrification was expected and none was seen.

- Problems due to individual bacteria, present in the biotreated wastewater, passing through the multi-media filter and thus decreasing the carbon adsorption efficiency of the GAC system, have resulted in lower treatment rates than originally anticipated. Since chemical addition may present problems when reusing wastewater at high cycles of concentration in a cooling tower and could affect UNDERC's analytical techniques, only a physical filtration step (multi-media filtration) is used when preparing water for the carbon columns. As a result, to achieve the desired treatment, the contact time of the wastewater with the carbon in the

granular activated carbon system has been increased. Since this has decreased the treatment rate, a larger carbon adsorption system has been designed and is presently being constructed.

Hydrogen Production from Low-Rank Coals (LRCs)

- It is planned to utilize a relatively large-scale TGA apparatus for the major portion of the test work in H_2 production from LRCs. The design has been completed, and construction has begun of a unit in which samples of up to 1 pound can be tested. While the main operating areas of interest for H_2 production are temperatures of ~650°C at atmospheric pressure, the TGA apparatus was designed for use in Coal Science projects to approach reaction temperatures of 1000°C and pressures up to 1000 psig.

Fine Coal Cleaning

- The "forms of sulfur" analytical procedures at UNDERC have been completed and will be used on a variety of projects. The sulfate ion will be measured directly using an ion chromatograph. A modified ASTM method D2492, using AA rather than ICAP analysis for iron, was selected as a more rapid method to determine pyritic sulfur content in the coal samples.

Coal-Water Slurry Preparation

- Contract construction of the hot-water/coal drying process development building was completed the last week in September, nearly two months later than scheduled. The general contractor completed the painting requirements, while the electrical and plumbing subcontractors finished installation of the lighting and heating systems. The building is now ready for occupation and erection of work structures, and the placement of process equipment has started.

- Pilot plant construction during the quarter included fabrication of the main work platform, the coal feeder stand, the coal storage hoppers, the overhead crane support structure, and the vacuum pump stand. In addition, several small pump bases and pedestal stands were also completed.

- Fabrication of a bench-scale hot-water/steam drying apparatus designed to operate in a cold-charge batch mode, drying up to a maximum of one gallon of coal in slurry per cycle, was completed. The apparatus has the versatility to operate with either liquid or vapor phase water for coal drying purposes. The test fixture consists of two high-temperature/high-pressure autoclaves, one acting as the coal dryer while the second accumulates evolved gases and water condensate. Thus, material balances can be closed and the product gases analyzed.

Low-Rank Coal Liquefaction

- Hexane-soluble portions of chloroform Soxhlet extracts of seven liquefaction coal samples have been partially characterized. These fractions contain alkanes such as terpane, triterpanes, and pristane, which are considered biological markers. While there were some correlations as a function of coal rank, such as an increasing pct of pristane and a decreasing average chain length with rank, others, such as weight pct

n-alkanes, showed no apparent rank effect. Nonetheless, each coal extract gave a unique capillary GC profile, which may serve as an identifier.

- At "normal" liquefaction temperatures (420°C in the presence of H_2S to 460°C without H_2S) increasing the fraction of hydrogen in the feed gas generally results in increased liquid yield (i.e., distillate plus soluble residuum) and increased hydrocarbon gas yield. These same trends were noted for the staged runs where the second-stage temperature was 440°C. However, at low liquefaction temperatures typically used in the first-stage reactions (i.e., 380°C), the total liquid yield declined with increasing hydrogen concentration in the feed gas. Thus, it is seen that roles of the CO and H_2 feed gas constituents vary depending on the reaction temperature.

- Time sampled batch autoclave data at low temperatures simulating proposed first-stage operation (320° to 400°C) with CO reductant suggest either different mechanisms or competing reactions begin influencing conversion at ~375°C. Below 375°C a conversion maximum is reached in less than five minutes, whereas above 375°C, conversion initially appears lower than obtained at lower temperature and continually increases through the entire 60-minute test.

COAL UTILIZATION RESEARCH

SO_x/NO_x Control

- Bench scale testing of potential catalysts for NO_x reduction has shown synthetic mordenite to be the most reactive. Synthetic mordenite is a hydrated aluminum silicate whose open structure may indicate that surface area is the critical catalyst property.

Particulate Characterization

- Examination of coal ash characteristics and fabric filter performance indicates a strong correlation between Na_2O level and collection efficiency. Increased sodium levels appear to result in increased collection efficiency.

Waste Characterization

- Leaching tests on ashes generated by combustion of pulverized low-rank coals from the Gulf Coast and Fort Union Regions indicate significant levels of Cr, Se, and Mo in leachates from selected coal ashes.

Combustion Research and Ash Fouling

- Combustion of micronized (<15 μm) high-sodium lignite indicates a slight decrease in deposition rate and bonding strength for deposits formed during pilot scale testing when compared to conventional (80 pct <74 μm) grind coal.

- Operation of the bench-scale combustion device at UNDERC indicates coal particles are exposed to heating rates of approximately 5 x 10^4°K/ sec. This is based on a gas temperature of about 1200°C at the exit to the high temperature furnace.

Fluidized-Bed Combustion of Low-Rank Coals

- Operation of the 2.25 sq ft AFBC on a high sodium lignite with about 0 pct excess air and a silica sand bed did not result in bed agglomeration in 100 hours of operation. A rapid rise in bed Na_2O content and an increase in bed particle size were observed, which may indicate a potential problem if the run duration had been increased.

COAL SCIENCE

Ash and Slag Characterization

- An in-house sample bank has been established which so far contains 16 low-rank coal samples from five states. The purpose of this activity was the collection of samples for laboratory ashing studies; however, the samples will actually be of use in all Coal Science projects.

- Preliminary data on ashing of five coals at 150°, 750°, and 1000°C has shown a number of interesting mineral transformations as a function of ashing temperature. Of particular interest are the oxidation of pyrite to hematite and magnetite, the fixation of sulfur by calcium as anhydrite, and the formation of the melilite aluminosilicate solution series.

- Viscosity vs temperature tests on low-rank coal ash slags confirmed earlier observations that the viscosity at a given temperature is significantly higher in air than in neutral or reducing atmospheres.

- Analysis of slag phases found in the hearth section of the UNDERC slagging gasifier, after runs which had aborted early, suggests that the failure mechanism is a reaction of alkalies or alkaline earths with the refractory to produce phases which would be fluid at the high temperatures of the tuyere blast but would solidify in the relatively cooler taphole region.

Organic Structure

- Development of a method for determination of cellulose in lignite has proven to be difficult. The methods utilized do not appear to go to completion. Nevertheless, the amounts of cellulose found so far are quite small, ranging from .003 to .015 pct in as-received coal.

- Lignin is determined by measuring the methoxy ether content by oxidizing the coal sample with pertrifluoroacetic acid followed by hydrolysis of the product esters and gas chromatographic determination of the resulting methanol. The yield of methanol from Indian Head lignite by this procedure is comparable to that obtained by supercritical water extraction

and by hot water slurry drying, suggesting that one effect of these two processes is to degrade the lignin residues in the coal structure.

- Oxidation of lignite with sodium periodate is a specific measure of o-methoxyphenol structures. Preliminary results suggest that at least one-third of the methoxy groups in lignite are located ortho- to free hydroxy groups.

- Studies of model compounds and polymers by pressure differential scanning calorimetry confirmed the previous assignment of the low-temperature peak in the thermogram to the aliphatic portion of the structure and the high temperature peak to the aromatic portion. An interesting model polymer found to have lignite-like combustion characteristics is polyvinyl toluene.

Distribution of Inorganics

- The technique for chemical fractionation was extended to incorporate an additional ammonium acetate extraction, to insure full removal of the ion-exchangeable cations.

- A method for determination of carboxylic acid groups was modified for use on lignites. The principal features of the method are the reaction of demineralized coal with barium acetate under an inert atmosphere. The acetic acid formed in the reaction is a measure of the carboxylic group content of the coal.

- Electron microscopy techniques were used to distinquish between syngenetic pyrite, formed in the early stages of coalification, and epigenetic pyrite resulting from postdepositional processes. These techniques have been applied to a detailed study of minerals and inorganic element associations in a vertical section of coal in the Beulah (North Dakota) lignite seam.

- The separation of lignite and subbituminous lithotypes into durain, fusain, and vitrain has been accomplished successfully. The application of traditional petrographic techniques to low-rank coals has required solving problems associated with high-moisture contents of the coals, and mainly has required always keeping the exposed part of the polished specimen covered with the oil used for the oil-immersion microscope lenses.

Physical Properties and Moisture

- A battery of simple tests has been developed to predict and compare the shift in particle size for different coals subjected to comparable degrees of thermal and mechanical treatment. The shape of the resulting size distribution curves indicates which coals are most subject to thermal or mechanical comminution and whether the mechanical degradation arises from fracture by impact and compression or by abrasion. The mechanical friability of low-rank coal increase sharply with the amount

of drying prior to tumbling. The shrinkage of lignite particles on drying also has an effect on size distribution in addition to that caused by fracturing.

- The distribution of pore diameters was determined for Beulah lignite by small angle x-ray scattering. The distributions are unusual in that they have neither an upper nor lower bound for pore size and have no extremum. The effect of heating to 550°C is the creation of very small pores, probably by the escape of volatile matter, but leaving the coal matrix largely intact.

Supercritical Solvent Extraction

- Twenty-three tests were made using supercritical water to extract Indian Head (North Dakota) lignite. The maximum conversion noted was 54.4 pct. Most of the conversion occurs in about the first 15 minutes of operation, with further conversion occurring slowly thereafter. A slight increase in percentage conversion with increase in operating temperatures was noted, but the percentage conversion increased significantly with operating pressure up to 4000 psia. The aqueous phase was found to contain methanol, acetone, phenol, and cresols. The tarry extract is difficult to analyze. The residual solid had a surface area of 13 to 17 m^2/g.

Pyrolysis and Devolatilization

- The principal focus of work was small-scale pyrolysis using an externally heated tubular reactor and using the thermogravimetric analysis apparatus. The data being obtained will be a guide to further design and development of a large sample thermogravimetric unit now under construction. Tests using the residual char from the supercritical solvent extraction work showed it to have a high reactivity, similar to a highly reactive coal-based activated carbon.

2. - GASIFICATION WASTEWATER TREATMENT AND REUSE

Project No.: 7102, 7103 B&R No.: AA8540000
AA8545050

Submitted by: W.G. Willson, Manager, Coal Conversion Division

Prepared by: J.G. Hendrikson and G.G. Mayer, Research Supervisors, Gasification Wastewater Treatment and Reuse

Assigned UNDERC Personnel:
W.G. Willson
G.G. Mayer
J.G. Hendrikson
C. Turner
B.W. Farnum
M.D. Mann
R.E. Shockey
J.R. Gallagher
M.M. Fegley

Assigned AWU Personnel:
J. Worman
Chia-Yuan Chao
S. Galegher
J. Meyer
K. Kempf
S. Karner

2.1 GOALS AND OBJECTIVES

The principal goal of the University of North Dakota Energy Research Center (UNDERC) Wastewater Treatment program is to develop public data on environmentally acceptable means of treatment, either for reuse or disposal, of wastewater derived from slagging fixed-bed gasification (SFBG) of lignite. All wastewater treatment and reuse unit operations at UNDERC are designed to yield scalable data and are operated on a real gasification effluent. To the degree that SFBG wastewater is representative of commercial fixed-bed gasification, an immediate goal is to assess the consequences, both process and environmental, for the use of solvent-extracted and ammonia stripped wastewater (stripped gas liquor--SGL) as makeup to a cooling tower. To the extent that problems are expected with the use of SGL as cooling tower makeup, another objective is to test alternative treatments that may be necessary if disposal is used rather than zero discharge. The long-range goal is to develop and validate a working model for wastewater treatment design ultimately capable of using as input basic coal characterization data.

To accomplish these objectives, the four major activities in the gasification wastewater treatment and reuse program during the first year of the cooperative agreement are:

1. Phase I cooling tower assessment using SGL as makeup, to determine environmental parameters and process fouling rates in cooling tower circuit. Wastewater will be prepared by tar/oil/water separation, filtration, solvent extraction, and ammonia stripping.

2. Phase II cooling tower assessment using SGL treated by single-stage activated sludge processing followed by carbon adsorption as makeup.

3. Characterization of the organic contaminants in lignite-derived wastewater, before and after each stage of treatment. Emphasis will be placed on the mechanism and kinetics for hydantoin formation and on methods development as needs arise in characterizing the different process streams.

4. Development of models for solvent extraction, inorganic fouling of the cooling tower, and (for the first time) the effects of key organics in the cooling tower.

2.2 ACCOMPLISHMENTS

2.2.1 Summary of Operations

Water for use in the Phase II cooling tower tests was produced in the UNDERC slagging fixed-bed gasifier, then processed in a solvent extraction-ammonia stripping train. This was followed by processing in an activated sludge reactor to reduce organic loading and remove the BOD content. The final step was passage through a granular activated carbon adsorption train. A summary of these operations follows.

2.2.1.1 Gasification

Three gasifier tests were made during the quarter, two of which provided a total of approximately 11,000 gallons of wastewater for future use. Tables 2-1 and 2-2 present data from the tests.

Run UND-6 was terminated because of the inability to initate any slag flow even though a concerted effort was made to open the taphole through use of the taphole burners.

Slagging operation for UND-7 totalled 66.4 hours before a leaking hearth plate caused stoppage of slag flow which resulted in termination of the run. Slag flow was erratic during the latter portions of the test due, in part, to the hearth plate problems.

UND-8 was operated to a scheduled shutdown when the lignite supply was exhausted. A total of 72.2 hours of slagging on the new hearth plate produced approximately 6,000 gallons of wastewater.

In an effort to verify or disprove a theory that the hydantoin formation during gasification was the result of the low offtake temperature (≅325°F), the product gas sidestream sampler was fitted with a preheater. This preheater was operated at temperatures of 530°F (the anticipated offtake temperature of the GPGA Lurgi gasifiers) and at 800°F (the offtake temperature of the Sasol gasifiers). Hydantoins form when ketones react with ammonia, ganide, and CO_2 in the course of tar/oil/water separation; therefore, if the acetone (or higher ketones) were removed from the heated exit gas stream, hydantoin formation should be eliminated. Acetone will thermally decompose in the 600° to 1200°F range and at 800°F the decomposition is rapid (1). The reaction involved in the decomposition is shown in equation 1.

TABLE 2-1

SUMMARY OF PROCESS VARIABLES

Run Number	UND-6	UND-7	UND-8
Date: Start:	07-11-83	08-08-83	08-22-83
End:	07-11-83	08-11-83	08-25-83
Feedstock, Hours of Slagging:			
Indian Head lignite	0	66.40	72.18
Controlled Variables:			
Pressure, psig	300	300	300
O_2 feed rate, scf/hr	6500	6500	6500
O_2/steam molar ratio	0.9	0.9	0.9
Design Conditions:			
Hearth plate number	24	24	25
Vertical distance, tuyeres to taphole, inches	3 5/8	3 5/8	3 5/8
Integral ring taphole burner	Yes	Yes	Yes
Slagging section relined	Yes	No	No
Response Variables:			
Coal feed, lb/hr		2043.5	1946.0
Coal feed, maf, lb/hr		1329.5	1255.0
Product gas, IGF, scf/lb coal		17.27	16.74
O_2 use, scf/lb coal		3.18	3.30
Steam use, lb/lb coal		.17	.17
Heating value of gas, Btu/scf		319.8	319.9
Average offtake gas temp., °F		342.0	342.7
Reasons for Shutdown:			
Voluntary (test completed)	--	--	Yes
Hearth plate leak	--	Yes	--
Loss of slag flow	Yes	Yes	--

TABLE 2-2

SUMMARY SHEET

Run number:	UND-7	UND-8
Total slagging hours	66.40	72.18
Data period, hours	65.02	57.52
Oxygen/steam molar ratio	.90	.89
Operating pressure, psig	300	300
Oxygen rate, scf/hr	6497.0	6420.5
Steam rate, lb/hr	342.5	337.6
Fuel rate, lb/hr	2043.5	1946.0
Fuel rate, lb maf/hr	1329.5	1255.0
Fixed carbon rate, lb/hr	669.9	640.4
Flux rate, lb/hr	0	0
Flux ratio, lb flux/lb fuel ash	0	0
Total gas, inert gas free, scf/hr	35288	32568
Slag recovered, lb/hr	106.8	101.9
Oxygen consumption, inert gas free:		
Per 1000 scf product gas, scf	184.12	197.14
Per 1000 scf $CO + H_2$, scf	216.97	231.07
Per lb fuel, scf	3.18	3.30
Per lb maf fuel, scf	4.89	5.12
Steam consumption, inert gas free:		
Per 1000 scf product gas, lb	9.71	10.37
Per 1000 scf $CO + H_2$, lb	11.44	12.15
Per lb fuel, lb	0.17	0.17
Per lb maf fuel, lb	0.26	0.27
Gas production, inert gas free:		
Per lb fuel, scf	17.27	16.74
Per lb maf fuel, scf	26.54	25.95
Cold gas efficiency, pct	79.0	76.5
Operational efficiency, pct	83.9	82.2
$CO + H_2$ production, scf/lb maf fuel	22.52	22.14
Average offtake temperature, °F	342.0	342.7
Gas liquor production, lb/hr	591.0	648.4

$$\begin{matrix} CH_3 \\ CH_3 \end{matrix}\!\!>\!C = O + \text{heat} \rightarrow \underset{\text{Ketene}}{CH_2 = C = O} + CH_4 \qquad [1]$$

The ketene formed by the decomposition will react with water to yield a fatty acid (in this case acetic acid) as shown in equation 2.

$$\underset{\text{Ketene}}{CH_2 = C = O} + H_2O \rightarrow \underset{\text{acetic acid}}{CH_3 - \overset{\overset{O}{\|}}{C} - OH} \qquad [2]$$

Table 2-3 gives the analysis from the condensate collected in the side-stream sampler with no preheat and with the two preheat conditions. While the results are somewhat inconclusive, there does appear to be a reduction in the acetone concentration under conditions of preheat to some "equilibrium" value of about half the initial concentration and, with one exception, a subsequent reduction in the dimethylhydantoin formation.

A column which will give us the capability to analyze for organic acids on the ion chromatograph is currently on order. These samples have been preserved and will be analyzed for acetic acid in the near future. If the acetone reductions are accompanied by an increase in acetic acid, then the reactions shown in equations 1 and 2 are probably operative.

TABLE 2-3

EFFECT OF OFFTAKE TEMPERATURE ON GASIFIER CONDENSATE COMPOSITION

Date	8/23	8/23	8/25	8/23	8/25
Preheat Temp., °F	None	530	530	800	800
Sampler gas flow, scfm	3.2	3.8	1.0	2.7	1.0
Preheater residence time, sec	--	1.53	5.88	1.82	4.96
Total phenols, mg/ℓ	6770	7270	7020	7080	6230
5-5-dimethyl hydantoin, mg/ℓ	120	20	30	130	20
5-methyl-5-ethyl hydantoin, mg/ℓ	60	60	50	60	40
Acetone, mg/ℓ	830	400	420	390	550
Acetonitrile, mg/ℓ	310	200	180	180	200
Propionitrile, mg/ℓ	30	20	20	10	20
Methanol, mg/ℓ	1700	1200	1100	1200	1020
Ethanol, mg/ℓ	10	10	10	10	10
1-propanol, mg/ℓ	120	80	50	50	50

2.2.1.2 Solvent Extraction-NH_3 Stripping Train

Five solvent extraction-ammonia stripping train tests, each of 4 to 5 days duration, were made during this quarter. The objective was again to produce wastewater with phenol and ammonia concentrations similar to Great Plains Gasification Associates (GPGA) expected concentrations of 150 mg/ℓ and 600 mg/ℓ, respectively. Table 2-4 gives results for the five tests. Wastewater feed for the five tests came from gasifier runs UND-4, UND-7, and UND-8.

TABLE 2-4

RESULTS OF SOLVENT EXTRACTION AND STEAM STRIPPING

Run No.	Water Processed, Gallons	Total Phenol Exit Treatment Train Average, mg/ℓ	Total NH_3 Exit Treatment Train Average, mg/ℓ
15	4250	160	593
16	4300	179	530
17	5100	122	597
18	4000	137	570
19	4000	146	649

Averages of the daily analyses available from Runs 15 through 17 are given in Table 2-5. Sample S-2 is the raw wastewater produced in the UNDERC slagging gasifier. Oils and tars were gravity separated, and the water was rough filtered prior to charging to the extraction column. Sample S-7 is the wastewater after solvent extraction with diisopropyl ether, and S-10 is the processed wastewater after both solvent extraction and ammonia stripping. All of this water will be processed in the activated sludge biological treatment unit in preparation for the Phase II cooling tower studies.

2.2.2 Cooling Tower--Phase I Test

The Phase I cooling tower test was completed May 26, 1983, and preliminary results have been reported (2, 3, 4). Data reduction and reporting have continued in an effort to issue a final report (draft) on the Phase I testing by October 31. Analytical results received this quarter verify speculations concerning biological fouling. Results from drift and evaporate sampling have also been received and reported (5, 6, 7).

2.2.2.1 Atmospheric Emissions

During Phase I testing, sampling was performed to determine the atmospheric emissions from the cooling tower. Several types of equipment were used in the Phase I cooling tower test for the collection and retention of components in the tower evaporate and to quantify the total drift. Methods and results are presented here, with more detailed information reported elsewhere (5, 6, 7).

TABLE 2-5

WASTEWATER ANALYSES FOR SOLVENT EXTRACTION-AMMONIA STRIPPING RUNS

Run Number	15			16			17		
Sample Location	S-2	S-7	S-10	S-2	S-7	S-10	S-2	S-7	S-10
Methanol	ND	ND	ND	1250	1210	110	1280	ND	90
Ethanol	ND	ND	ND	0	0	0	0	ND	0
Acetone	ND	ND	ND	150	130	0	303	ND	0
2-Propanol	ND	ND	ND	0	20	0	0	ND	0
Acetonitrile	ND	ND	ND	300	280	0	293	ND	0
DIPE	ND	ND	ND	40	420	0	30	ND	0
1-Propanol	ND	ND	ND	30	0	0	33	ND	0
Propionitrile	ND	ND	ND	30	30	0	40	ND	0
Phenol	3760	167	167	4470	175	140	3800	157	107
o-Cresol	533	0	0	585	5	0	577	0	0
p-Cresol	677	3	3	1620	10	10	990	0	0
m-Cresol	907	3	3				877	3	3
Dimethyl Hydantoin	1193	1153	1100	ND	ND	ND	753	ND	933
Ethyl-methyl Hydantoin	347	290	287	ND	ND	ND	290	ND	300
pH	8.4	8.7	8.8	8.6	8.8	8.6	8.4	8.6	8.2
Alkalinity	16800	16750	1140	15800	16500	800	17130	16430	1020
NH_3	5778	5942	480	5485	6125	460	6277	6060	637
Sulfide	233	158	0	200	105	10	300	183	10
Cyanide	51	42	44	28	39	34	37	42	28
Thiocyanate	393	308	153	300	205	185	210	220	223
COD	29050	11475	7135	29800	10710	6270	37230	15570	8130

ND = Not Determined

2.2.2.2 Air Stream Sampling Equipment

The sampling train used for collecting components of the overhead tower exhaust was comprised of a five-stage multicyclone, an XAD-2 resin trap, a set of four cooled impingers, and a vacuum pump equipped with a calibrated orifice meter. An illustration of this equipment as it was assembled for air stream sampling is presented in Figure 2-1.

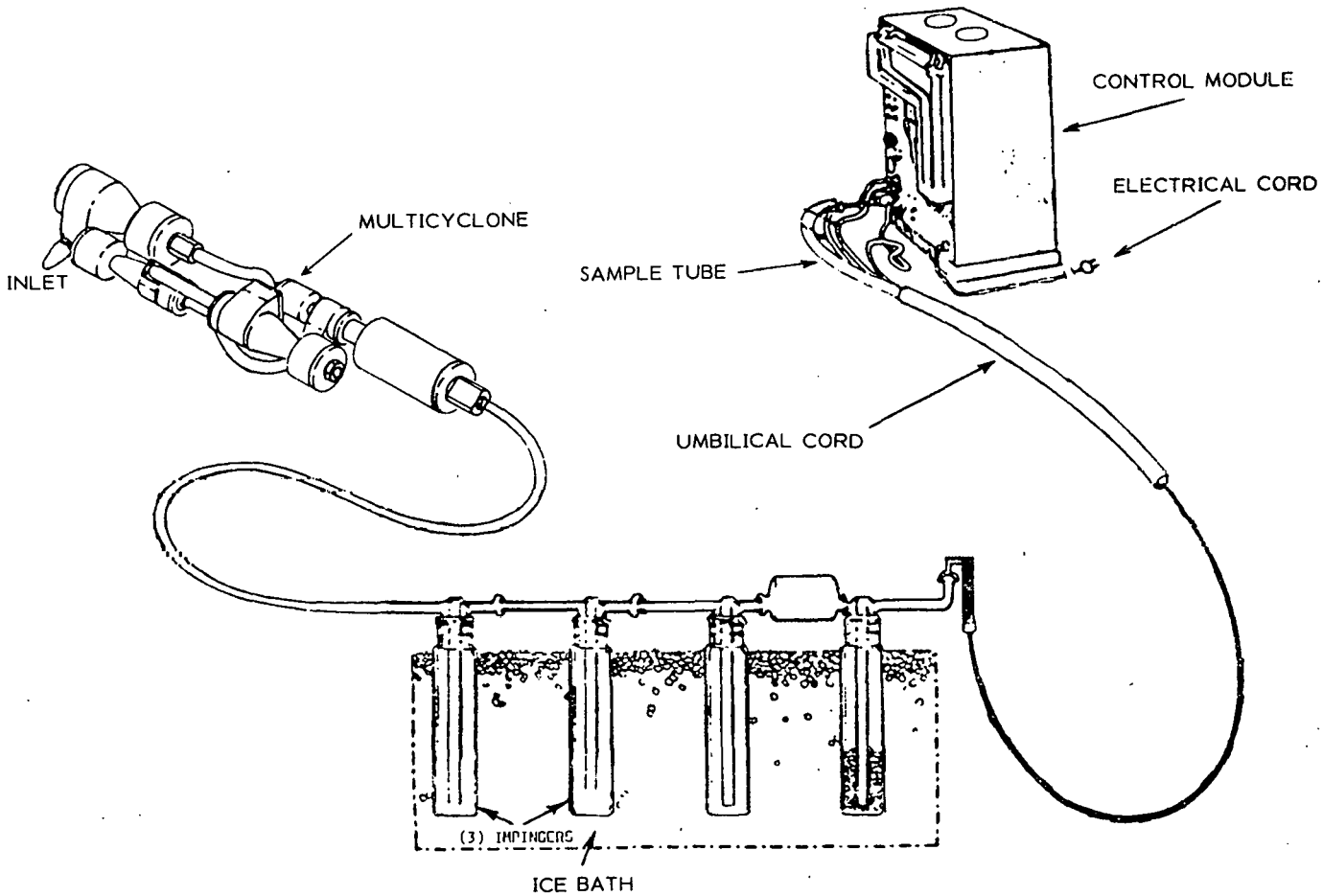

FIGURE 2-1: Assembled exhaust sampling train used at UNDERC.

During sampling runs, the entire multicyclone unit was located in a horizontal position within the cooling tower exhaust duct. In an attempt to prevent condensation from occurring within the cyclones, a thermister probe was inserted into the unit and sampling was begun only afer the recorded temperature reached that of the exhaust gas. Following the multicyclone the gas sample was drawn through a series of three dry impingers, through the XAD-2-filled resin trap, and finally through a silica-filled impinger prior to reaching the vacuum pump. The four impingers were partially submerged in an ice bath to promote condensation of the evaporate. The impinger and resin trap portion of the sampling train was mounted just outside the exhaust duct sampling port so as to minimize the amount of interconnecting tubing needed.

A five-stage stainless steel multicyclone, the Gram Slam Sampler, manufactured by Flow Sensor Corporation (FSC), was used for this aerosol sampling work. The largest available straight nozzle, ½ inch in diameter, was used to carry out isokinetic sampling of the UNDERC test cooling tower exhaust. The operating principle of a multicyclone sampler is to size fractionate particles in an air stream by drawing the sample through a series of consecutively smaller diameter cyclones. The basis for its use in this work was to try to separate and size fractionate cooling tower drift emissions. The droplet size

fraction collected in each cyclone is dependent on the viscosity of the gas stream and the sample flow rate. This flow rate and the appropriate nozzle size were determined from the results of stack velocity and temperature traverses. Manufacturer specifications for this sampler state that it may be operated in any orientation without affecting its particle collection characteristics.

Empirical equations have been derived for predicting the mean cut diameter, referred to as the D_{50}, of each cyclone from known flow rates and gas viscosity (8). The gas viscosity, in turn, can be calculated from polynomial fits to published data using the gas temperature and approximate composition (9). A computer program has been developed which uses these polynomial curve fits and empirical equations to obtain mean cyclone cut diameters and also the mass loading characteristics of each droplet size range. The latter is done by assuming the droplets collected in each cyclone to have diameters between the D_{50} of that cyclone and the D_{50} of the preceding cyclone.

The impingers used in this sampling train were designed to minimize the number of turns the gas stream would be pulled through. As such, the outlets and inlets of consecutive impingers were located on the same horizontal plane, and the resin trap was inserted such that its connections were also directly in line. In order to prevent contamination of the samples by joint sealing lubricants, only non-grease glass-to-glass connections were used in this sampling train.

A 4-inch diameter pyrex cylinder with internal porous pyrex membranes served as the sampling train resin trap. The trap was filled with XAD-2 synthetic resin. This particular resin was chosen because of its effectiveness in retaining a wide variety of organic vapors, and because the retained organics are easily extracted with a number of different solvents.

A Misco Model 7200 source sampler was used to draw samples isokinetically from the tower exhaust stream. This control module is an enclosed vacuum pump equipped with manometers, a calibrated orifice, wet and dry test meters, and an umbilical cord which connects it to the final silica-filled impinger.

Sampling of the drift was performed using a Heated Glass Bead Isokinetic (IK) Sampling System developed by Environmental Systems Corporation (ESC) (10). The IK system employs Pyrex sampling tubes filled with Pyrex beads and wrapped with heating tape. One end of the tube is attached to a vacuum source and the tube is placed at the measurement point such that the air flow is directed into the tube opening. The mean flow velocity through the tube is then adjusted so that it is equal to that of the air surrounding the tube to achieve isokinetic sampling. Current is applied to the heating tape surrounding the tube, elevating the temperature of the glass surface inside. Drift droplets are transported through the tube opening and evaporate after impinging on the hot internal surfaces of the Pyrex tubing, leaving a residue of the minerals contained in the droplets. After the exposure period, the mineral residue is washed from the tube and analyzed for selected components.

The Sensitive Paper Method (SP), developed by ESC, was also used to measure drift. This method utilizes a water-sensitive paper that has been chemically treated such that a drop of water striking the surface of the paper

will produce a stain whose size is related to that of the original droplet. The sensitive paper is exposed to the exhaust stream for a preset time period to produce a paper stained by the drift droplets. The droplet stains are measured and counted and used along with corresponding data on duct dimensions, impingement velocity, and sampling time and location. With these data, a determination is made of the drift particle size distribution and mass flux distribution, which can then be used to compute the total drift mass emission rate.

Other methods of drift determination were done using process and concentration data recorded during the test period.

2.2.2.3 Atmospheric Emission Sampling Results

The cooling tower operating parameters are presented in Table 2-6. The makeup and blowdown rates were determined from flow totalizer data, while the exhaust and evaporation rates were calculated from linear velocities and collected psychrometer data. All conditions remained unchanged with the exception of evaporation rate, which varied from day to day due to differences in inlet air humidity.

TABLE 2-6

COOLING TOWER WATER STREAM AND EXHAUST PARAMETERS

Tower recirculation rate (gpm)	8.2
Net makeup rate (gpm)	0.3129
Blowdown rate (gpm)	0.0317
Drift rate (gpm)	0.0044
Cycles of concentration[a]	9.0
Air Circulation Rates:	
Spray chamber (m^3/min)	21
Non-spray chamber (m^3/min)	38
Total (m^3/min)	59
Evaporation Rates:	
Spray chamber (gpm)	0.1031-0.1322
Non-spray chamber (gpm)	0.0291-0.0846
Total (gpm)	0.1322-0.2168

[a]Cycles based on Cl^- concentration

Four independent sampling runs were made. The results from the droplet size distribution collected in the five-stage multicyclone are presented in Tables 2-7 and 2-8. Table 2-7 presents the moisture collection rates from the sampling. Collection rates in the cyclones average 0.035 g/min with good

reproducibility between runs. The drift rate measured for the UNDERC cooling tower was less than 0.046 pct, depending upon measurement techniques, which corresponds to a rate of 0.002 g/min through the 1/2-inch sample nozzle (5, 7). This drift rate is up to 20 times lower than the total collection rate in the cyclones, indicating that over 95 pct of the moisture collected in the cyclones was due to condensation of the evaporate in the multicyclones. Also, no hydantoins were detected in the samples collected in cyclones. At the level of hydantoin present in the basin water, hydantoins would be detected in the cyclones if the drift rate was over 0.15 pct of the total catch. These data indicate that the five-stage multicyclone used for this test was not adequate for separating the drift from the evaporate. Rather, it collected a significant amount of evaporate in the cyclones along with the drift.

TABLE 2-7

MOISTURE COLLECTION RATES FROM SAMPLING OF COOLING TOWER (SPRAY CHAMBER) EXHAUST

Sampling Run Number	Multicyclone Collection Rate g/min	Total Impinger Collection Rate g/min	Total Moisture Collection Rate g/min
CES-1	0.03	0.23	0.26
CES-2	0.04	0.20	0.24
CES-3	0.03	0.20	0.23
CES-4	0.04	0.25	0.29
Averages	0.035	0.22	0.26

TABLE 2-8

DROPLET SIZE DISTRIBUTION RESULTS FOR FIVE-STAGE MULTICYCLONE COLLECTION

Distribution Parameters	Cyclone I	Cyclone II	Cyclone III	Cyclone IV	Cyclone V
D_{50} = Mean cut diameter, μm	11.9	6.6	4.0	2.7	2.0
Pct of total mass collected	24.3	37.5	10.8	18.3	9.1
Cumulative pct of mass with $d<D_{50}$	75.7	38.2	27.4	9.1	0.0

The droplet size distribution for the fractions collected in the five-stage multicyclone is given in Table 2-8. The individual and cumulative mass fractions for each of the staged cyclones is shown in addition to the mean cut from each stage. This analysis indicates that 75 pct of the particles collected have a mean diameter less than 12 microns. Fog, or evaporate condensate, generally has a mean diameter of approximately 10 microns (11), which was the size range predominantly measured and collected in the multicyclones. The cyclone cuts from the two sample runs show good reproducibility.

The fractions collected from each cyclone, the impingers, and the XAD-2 resin were weighed and analyzed. These data were used to compute mass flow rates and total exhaust concentrations. Exhaust concentrations for the major species are presented in Table 2-9. Component material balances on the UNDERC cooling tower were then derived using the measured exhaust rates and the makeup, blowdown, and drift rates already known. The phenol balance on the system indicated that an average of 91 pct of the phenol in the makeup to the cooling tower was stripped during the cooling cycle. Eighty-one pct of the ammonia and 25 pct of the methanol were also stripped. This is summarized in Table 2-10. Material balances also indicate that approximately 75 pct of the methanol was available for biodegradation, while only a small portion of the phenol was available for consumption by the microorganisms.

TABLE 2-9

UNDERC COOLING TOWER EXHAUST CONCENTRATIONS

Component	Concentration	
	$\mu g/m^3$	ppm
Ammonia	26900	39
Phenol	8000	2.0
Methanol	2500	2.0
Cresol	1300	0.3
5-Ethyl-5-methyl hydantoin	ND	ND
5,5-Dimethyl hydantoin	ND	ND

ND = Not Detectable

TABLE 2-10

PERCENT OF INFLUENT EMITTED IN UNDERC COOLING TOWER EXHAUST FOR MAJOR SGL MAKEUP CONSTITUENTS

Component	Percent of Influent Stripped
Phenol	91
Ammonia	81
Methanol	25

Two independent direct measurements were taken to determine the drift rate from the UNDERC cooling tower: The Sensitive Paper Method (SP) and the Heated Glass Bead Isokinetic Sampling Method (IK). Results from the SP indicate a drift rate of 0.0025 pct of circulation. This drift rate was calculated from point measurements assuming a uniform drift over the entire exit plane. The drift rate determined from IK sampling was 0.031 pct based on the sodium ion.

The IK indicated higher drift rates than that indicated by the SPs. This is typical and associated with at least two phenomena. The first is that as the droplets evaporate, the droplet mineral-to-liquid concentration increases. Since the IK measures mineral deposition, the implied liquid flux, if appreciable while evaporation is occurring, will be greater than actual. The second phenomenon is that the surrounding air deposits additional quantities of various minerals, again making the implied liquid flux greater than actual (10, 12). The fact that no hydantoins were detected in the multicyclone collections also supports the lower drift rate determined by the SP.

Two indirect methods were also used to approximate the drift rate. A material balance over the system indicated a drift rate of 0.059 pct. The "concentration equation," which determines specific ion concentrations as a function of time and drift rate, approximated the drift at 0.048 pct. These indirect determinations of the drift rate are extremely sensitive to small errors in the measured makeup rate and ion concentrations. Therefore, variations of an order of magnitude are not uncommon. These methods are discussed by Mann (4).

Based on the various measurements and the sensitivity of each, the drift from the UNDERC cooling tower is estimated at 0.0025 pct. This drift rate is relative to the drift elimination system of the UNDERC tower during Phase I testing and will therefore vary from other commercial towers. The emission rates measured, however, are independent of the drift elimination system, and packed towers with similar L/G ratios can expect similar emission rates of phenol, ammonia, and methanol.

2.2.2.4 Biological Evaluation

Identification of the microorganisms in the cooling tower recirculation water was continued. Pseudomonas aeruginosa is the predominant microbe isolated and identified. Other microbes identified thus far include pseudomonas stutzeri and CPC Group V E-1. Yeast, filamentous fungi, as well as some Gram positive bacilli, have been isolated. Sulfur oxidizers, iron oxidizers, and nitrifiers were not found in either the suspended or attached growth from the cooling tower.

Solids were scraped from the cooling tower at various locations and extracted with CH_2Cl_2; 15 to 30 pct of the solids were soluble in the CH_2Cl_2. The CH_2Cl_2 was evaporated to give mainly dimethylhydantoin. The CH_2Cl_2 insoluble portion was subjected to C, H, N, and ash analysis. The analysis indicated the residue was highly organic: average carbon was approximately 35 pct; hydrogen approximately 5 pct; nitrogen approximately 11 pct; and ash was approximately 20 pct. Sodium, silica, sulfur, iron, and aluminum were the major species in the ash, while phosphorus, potassium, calcium, and magnesium were found as minor components. The infrared spectra of typical samples were

remarkably similar to amino acids (see Aldrich Catalogue of Infrared Spectroscopy Non-Aromatic Amino Acids). The compounds, which were highly insoluble in most solvents, contained -OH, amide, and acid-type carbonyl stretching. They dissolved in DMSO and DMF, and appeared to react in trifluoroacetic acid.

It is suspected that the insoluble portion of these sludge deposits is primarily biological fouling material. A significant amount of hydantoins was found in these deposits as well. The mechanism of formation of these deposits is not known. Biological fouling may have occurred first, followed by precipitation of hydantoins into the biological matrix; or hydantoins may have fouled the surfaces and the biological growth attached to these surfaces; or both may have occurred simultaneously.

2.2.2.5 Blowdown Trace Metal Analysis

An analysis of the blowdown water for the EPA priority pollutants and RCRA trace element levels has been performed, with the results listed in Table 2-11. This determination is important as the metals present in the blowdown will ultimately end up in a disposal stream. In the GPGA proposed treatment scheme, these metals will be present in the ash from the incineration of the residue from the multi-effect evaporators (cooling tower blowdown will be used as feed to the evaporators).

TABLE 2-11

EPA PRIORITY POLLUTANTS AND RCRA TRACE ELEMENT LEVELS IN COOLING TOWER BLOWDOWN

Element	Blowdown Concentration, ppm
Ag*	A
As*	0.3
Ba*	0.13
Cd*	A
Cr*	<0.1
Cu	<0.1
Ni	0.028
Pb*	<0.1
Se*	A
Zn	0.3
Be	B
Hg*	B
Sb	B
Ti	B

* = RCRA elements
A = Not detected
B = Not determined

2.2.3 Activated Sludge - Granular Activated Carbon Adsorption

The Phase II cooling tower assessment will involve the operation of a cooling tower utilizing wastewater treated to a greater degree than in Phase I. Treatment steps will include solvent extraction, ammonia stripping, activated sludge processing, multimedia filtration, and granular activated carbon adsorption.

The objective of this portion of the Phase II study is to use activated sludge treatment and granular carbon adsorption on pretreated (extracted and stripped) wastewater to prepare a satisfactory feed to the cooling tower. The major goals of this work will be to:

1. Optimize the operation of the activated sludge process in combination with granular activated carbon adsorption.

2. Develop scalable biokinetics.

3. Demonstrate hydantoin (COD) removal with granular activated carbon adsorption.

4. Determine the lowest "reasonable" hydraulic detention time for operation of the activated sludge process using SGL.

A flow diagram showing the test equipment is presented in Figure 2-2.

2.2.3.1 Biological Treatment

The pilot-scale activated sludge unit is being operated in a manner that will produce the greatest amount of kinetic and operational data possible while ensuring the production of 20,000 gallons of biologically-treated SGL for use in the pilot cooling tower. The pilot-scale treatment unit is an aerobic, completely mixed activated sludge system with a separate solids separation tank and activated sludge recycle. Two 1500-gallon tanks provide feed for the activated sludge (AS) reactor. The tanks are nitrogen purged to minimize biological activity and are continuously mixed and "topped off" daily to reduce the variability of feed to the AS unit.

Operating conditions for the activated sludge process are shown in Table 2-12. The feed rate to the reactor is 180 gallons per day. This corresponds to a hydraulic residence time (HRT) of three days (the tank volume is 540 gallons). The unit will be operated at this HRT for the majority of the test. Near the end of the test period, the HRT will be reduced (feed rate increased) until sludge bulking or other operational problems are encountered.

Air to the reactor is controlled in order to maintain a dissolved oxygen (DO) level between 2 and 3 milligrams per liter. Complete mixing of the liquor in the reactor is accomplished using hydraulically driven stirrers. Wastewater to the reactor is maintained at 80°F. These operational parameters should allow the development of scalable biokinetics.

Operation of the unit is aimed at producing steady state conditions at various food-to-microorganism (F/M) ratios, so that kinetic coefficients can be determined. However, development of these data may be limited by the

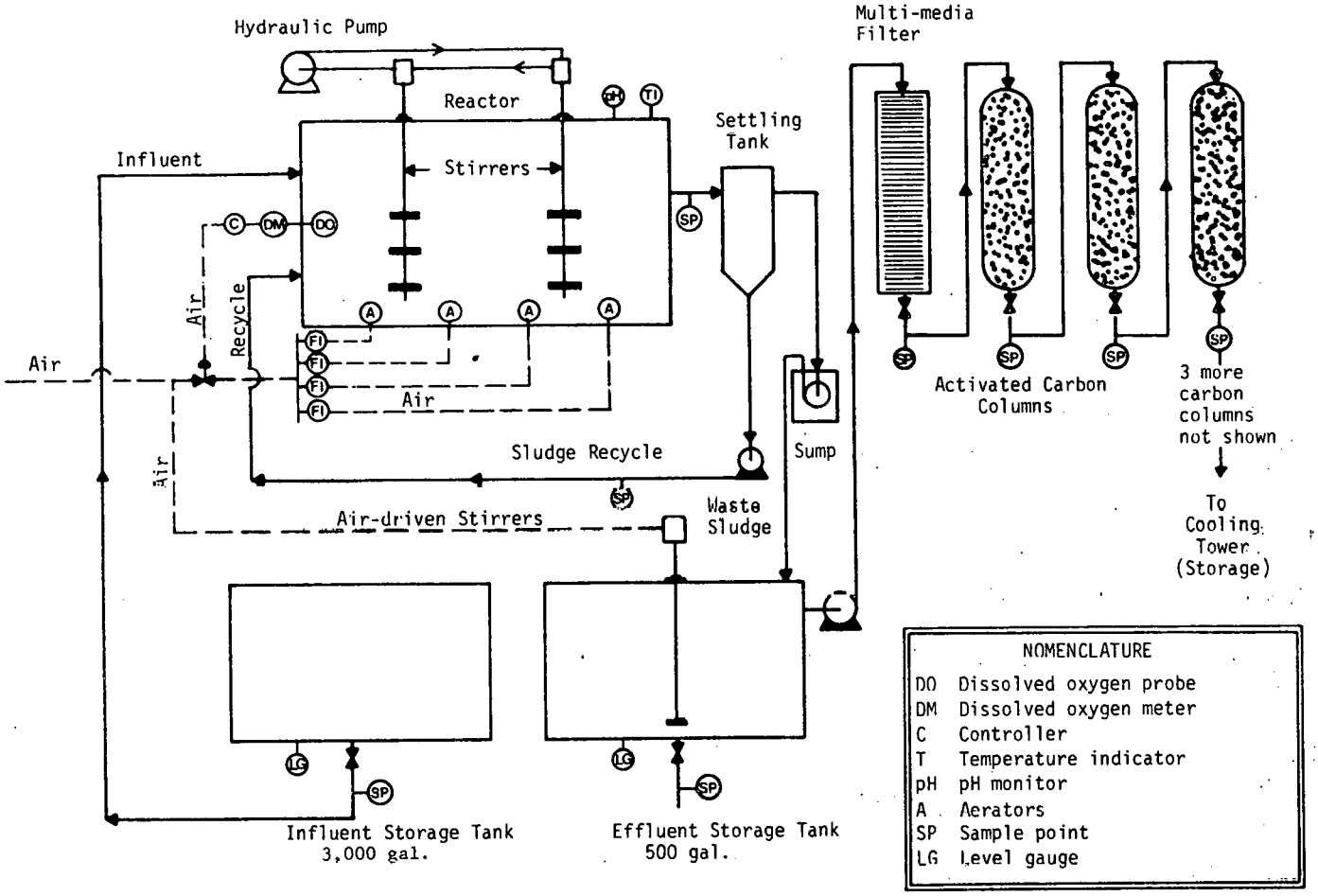

FIGURE 2-2. Flow schematic of activated sludge carbon adsorption process.

TABLE 2-12

ACTIVATED SLUDGE PILOT PLANT OPERATING CONDITIONS

Activated Sludge Treatment:	
Influent flow rate	0.125 gpm
Inlet H_2O temperature	80°F
Mixed liquor O_2 concentration	2 - 3 mg/ℓ
Stirrer speed	27 rpm
Hydraulic detention time	72 hours
Sludge age	15 - 25 days

quantity of SGL available. Long periods of operation at each condition are necessary to collect data for determination of kinetic parameters.

2.2.3.2 Activated Carbon Adsorption

The activated sludge process is highly efficient in removing phenolic compounds, yet it has little effect on the two major organic compounds, 5,5-dimethylhydantoin and 5-methyl-5-ethylhydantoin, found in the SGL. Granular activated carbon adsorption is used in conjunction with biological treatment for the removal of the organic compounds which are resistant to biological treatment, such as the hydantoins.

A multi-media filter is used to prefilter the incoming wastewater stream before it enters the activated carbon bed. This process decreases the suspended solids content of the wastewater and eliminates deposition of these materials in the carbon beds. The filter has backflush capability to remove solids when flow through the filter becomes restricted.

Carbon adsorption consists of six equi-sized columns filled with granular carbon. As the biotreated and filtered wastewater passes through and adsorption proceeds, the saturated zone moves forward until the breakthrough point is reached. As each set of three columns becomes contaminant saturated, it is taken out of service for reloading. Table 2-13 shows the design operating conditions for the pilot plant carbon adsorption unit.

TABLE 2-13

ACTIVATED SLUDGE-CARBON ADSORPTION DESIGN OPERATING CONDITIONS

Granular Activated Carbon Adsorption:

Carbon	Filtrasorb 400
Contact time	120 minutes
Carbon bed depth/column	5 feet
Optimum mass transfer zone	15 feet
Hydraulic loading	0.65 gpm/ft^2

2.2.3.3 Status of Activated Sludge - Carbon Adsorption Activities

Fabrication and installation of all equipment needed for continuous activated sludge and carbon adsorption processing of wastewater was completed this quarter. Activated sludge processing of SGL began July 25, with wastewater collection for the Phase II cooling tower assessment beginning August 15, 1983. Activated carbon adsorption of the biotreated wastewater was initiated August 29, 1983.

Table 2-14 presents data collected from the steady state operation of the pilot plant activated sludge unit. Samples were taken daily and analyzed. Results were averaged, with the average analysis being presented. Test re-

sults indicate complete removal of phenolics and alcohols, 94 to 98 pct removal of BOD, and approximately 45 pct removal of the COD. The low rate of removal of the COD is due primarily to the non-biodegradable hydantoins present in the wastewater.

TABLE 2-14

PILOT PLANT ACTIVATED SLUDGE UNIT

	Influent, (mg/ℓ)	Effluent, (mg/ℓ)
BOD_5	2410	55
COD	7620	3290
Alcohols	80	0
Phenols	150	0
SCN^-	225	20
CN^-	15	10
NH_3	660	660
Hydantoins	1175	1185

Problems encountered in the operation of the continuous activated sludge unit include the variability of the COD in the feed and the foaming tendencies of the mixed liquor in the reactor. Conversion from a 500-gallon feed tank to a 3000-gallon capacity system with mixing has minimized feed variability problems. Although feed variability has not had a pronounced effect on constituent removal efficiencies within the activated sludge system, steady state operation for development of biokinetics necessitated the change. A silicon-based antifoaming agent from Calgon (CL-37), which does not interfere with UNDERC's analytical techniques for wastewater analysis, is used to control the foaming in the activated sludge reactor. This is the same antifoaming agent used to control the foaming within the cooling tower.

Problems associated with the operation of the granular activated carbon system have resulted in lower treatment rates than originally anticipated. Since chemical addition may present problems when reusing wastewater at high cycles of concentration in a cooling tower and could affect UNDERC's analytical techniques, a physical filtration step (multi-media filtration) is used only when preparing water for the carbon columns. Individual bacteria, present in the biotreated wastewater, pass through the multi-media filter, decreasing the carbon adsorption efficiency. As a result, to achieve the desired treatment, the contact time of the wastewater with the carbon in the granular activated carbon system has been increased. Since this has decreased the treatment rate, a larger carbon adsorption system has been designed and is presently being constructed. Completion of this unit and installation are planned for the month of October. Even though treatment rates in the carbon adsorption system at the present time are low, the rate of contaminant removal from the biotreated wastewater is quite good. Data indicate over 96 pct removal of hydantoins present in the wastewater and 88 pct removal of the COD. Much of the COD remaining in granular activated carbon treated water is due to the bacteria passing through this system.

2.2.4 University of North Dakota Bench-Scale Studies

The University of North Dakota Civil Engineering Department is performing bench-scale studies in support of wastewater treatment activities at UNDERC. The major goals involved in this effort are to:

1. Obtain design data for pilot plant operations through bench-scale modeling;

2. Assess problems associated with pilot plant operations; and

3. Assess alternative treatment methods.

A series of batch and continuous bench-scale activated sludge acclimation tests were performed to obtain data for the design of the pilot plant activated sludge system. This work has been completed, with results being presented in a previous quarterly report (4).

Studies currently in progress utilize a variety of treatment techniques, with each being evaluated as to its effectiveness in the treatment of fixed-bed gasification wastewaters. Emphasis is presently on bench-scale work to support PDU activity at UNDERC; however, this will change, with future work focusing on multistage biodegradation nitrification/denitrification studies to remove organics and ammonia from wastewater if the final goal is discharge. Status of the work follows.

2.2.4.1 Powdered Activated Carbon - Activated Sludge Treatment

The objective of this project is to determine the effectiveness of adding powdered activated carbon to a bench-scale model of an activated sludge system, in order to improve mixed liquor characteristics and to remove hydantoins and other nonbiodegradable organics.

In the activated sludge process using powdered activated carbon (PAC), PAC is added directly to the aeration tanks of a conventional activated sludge system. This combination permits more complete treatment of the wastewater. Some of the advantages of adding powdered activated carbon to a biological process that have been cited in literature include:

1. Added system stability against shock loading and temperature changes.

2. Improved nonbiodegradable organics removal.

3. Color removal.

4. Improved removal of compounds on EPA's priority pollutant list.

5. Resistance to biologically toxic substances in the wastewater.

6. Improved hydraulic capacity of existing plants.

7. Improved nitrification of ammonia.

8. Suppressed foaming in aerators.

9. Improved sludge settling/thickening/dewatering.

10. Reduced sludge bulking.

The unit to be used in this study has been operating as a standard activated sludge process to establish baseline operating conditions. Steady state operation of this unit was achieved during the first week of August. Table 2-15 presents data collected from the steady state operation of the bench-scale activated sludge unit. Results indicate complete removal of phenolics and alcohols, 96 pct removal of BOD, and approximately 50 pct removal of COD. Operating conditions for the unit include a hydraulic detention time of 1.8 days and a sludge age of 26 days with a biomass concentration (MLVSS) of 3600 mg/ℓ. PAC addition to the unit is scheduled to begin the second week of October 1983. The powdered activated carbon used in this research will be Nuchar Type S-A. An initial concentration of 2000 mg/ℓ of PAC will be used in the study with higher concentrations being tested as time permits.

TABLE 2-15

BENCH-SCALE ACTIVATED SLUDGE UNIT

	Influent (mg/ℓ)	Effluent (mg/ℓ)
BOD_5	1380	48
COD	5870	2910
Alcohols	230	0
Phenols	160	0
SCN	220	<10
CN	32	9
NH_3	570	460

2.2.4.2 Effects of Nutrient Addition on Cooling Tower Operation

One of the most critical and often neglected areas of a cooling water treatment program is microbiological control. Inadequate biological control can lead to fouling of surfaces, thus reducing heat transfer. Even if that by itself doesn't reduce heat transfer rates, the gelatinous nature of the colonies tends to trap particulate matter from the fluid, resulting in a dense mass which can seriously interfere with water distribution and can restrict air flow in a cooling tower. Biomass on metal surfaces can also lead to under deposit corrosion. The combination of these problems tends to degrade the efficiency of the cooling tower system.

In general, the differences in appearance, quantity, or consistency of slime are not inherent in the organisms generating it, but rather are connected with the availability of nutrients (13). During respiration, under

conditions of limited nutrients, one-fourth to one-third of the carbon removed from organic substrates is transformed into extracellular polysaccharides in the form of slime, instead of new protoplasm. This can, under adverse conditions, serve as a source of food for the organisms; however, it also translates into severe fouling problems in a cooling tower system.

The primary objective of this investigation is to conduct a preliminary study on the effects of using SGL as makeup water to cooling towers. Independent bench-scale cooling towers are being operated to determine the difference in biological and chemical fouling, and contaminant removal efficiences of nutrient-enriched and nutrient-deficient wastewater recirculated through the towers. It is anticipated that this study will show whether nutrient addition is required for optimum cooling tower operation.

The pilot-scale cooling tower in operation at UNDERC, upon which the bench-scale units at UND are based, is a packaged Baltimore Air Coil Company model VXT-20WC with a forced-draft fan which operates in a counterflow mode. The air and water are contacted on a corrugated packing constructed of molded PVC sheets.

At UND the bench-scale cooling towers are similar to trickling filters, and the BOD loading is the main criterion used to establish steady state operation. The BOD loading at UNDERC, based on a makeup water BOD concentration of 1200 mg/ℓ, was determined to be approximately 550 lb BOD/1000 ft^3/day. This value was used to calculate flow rates for the bench-scale units. Based on the BOD loading at UNDERC, which most closely resembles loadings for two-stage trickling filters (14), a flow rate of 83.7 ml/min is used. The depth of the cooling tower basin was determined to be 1.4 inches based on a detention time of 20 minutes and reactor dimensions of 6 inches by 12 inches.

Operation of these units and collection of the resulting data is scheduled for completion the middle of October 1983. Preliminary results indicate a significant difference in the biological communities present in each of the cooling towers. The cooling tower with phosphorous addition appears to have a more diverse growth of organisms compared to the unit without phosphorous addition. More rapid build-up of both attached and suspended growth was also noted in the unit with phosphorous addition. Table 2-16 presents data from the first month of operation of the two cooling towers. Table 2-17 presents data from the final month of operation of the units. The towers were operated at three cycles of concentration based on chloride content in the makeup and recycle. BOD removal was 81 pct and 96 pct, respectively, for the unit without and with phosphorous addition. Analysis for polysaccharides present in the deposits on cooling tower surfaces and the quantity of deposits present in each of the towers has not been completed and will be reported later.

2.2.4.3 Multistage Activated Sludge Nitrification

The purpose of this research is to determine the feasibility of a two-stage activated sludge process for removal of ammonia from coal gasification wastewater (SGL). Kinetic parameters, optimum sludge age, and minimum hydraulic detention times are to be evaluated through use of a bench-scale: 1) continuous flow stirred tank, activated sludge reactor (CFSTR); and 2) multiple batch reactors with various mixed liquor concentrations obtained from the activated sludge CFSTR.

TABLE 2-16

COOLING TOWER ANALYSIS
JULY 1983

Parameter	Makeup Water	Basin Water Without Addition of Phosphorus	Basin Water With Phosphorus Addition
BOD (mg/ℓ)	1368	1554	1520
COD (mg/ℓ)	6091	14545	16248
Phenol (mg/ℓ)	160	76	18
NH_3 (mg/ℓ)	535	465	344
Plate count (microbs/mℓ)	--	1.1×10^8	4.1×10^8
V SS (mg/ℓ)	--	54	79

TABLE 2-17

COOLING TOWER ANALYSIS
SEPTEMBER 1983

Parameter	Makeup Water	Basin Water Without Addition of Phosphorus	Basin Water With Phosphorus Addition
BOD (mg/ℓ)	1584	869	165
COD (mg/ℓ)	5840	6433	5680
Phenol (mg/ℓ)	125	29	5
NH_3 (mg/ℓ)	460	350	375
Plate Count (microbs/mℓ)	--	1.5×10^8	9.5×10^7
V SS (mg/ℓ)	--	61	52

Nitrification, by definition, is the biological oxidation of ammonium, first to the nitrite, then to the nitrate form. This oxidation is accomplished in a two-step process by two specialized aerobic, autotrophic bacteria, Nitrosomonas and Nitrobacter. Equations three and four define the stoichiometric relationship of nitrification.

$$2NH_4^+ + 3O_2 \xrightarrow{\text{Nitrosomonas}} 2NO_2^- + 4H^+ + 2H_2O \quad [3]$$

$$2NO_2^- + O_2 \xrightarrow{\text{Nitrobacter}} 2NO_3^- \quad [4]$$

In comparison with carbonaceous removal, nitrification is a slower process, and is more sensitive to environmental conditions such as pH, temperature, dissolved oxygen, nutrient concentrations, heavy metals, and toxins. Each of these conditions must be maintained at levels that are non-limiting to the nitrification process to ensure that accurate kinetic rate coefficients may be determined.

As shown in Figure 2-3, an 8-liter, plexiglass tank serves as the basic CFSTR unit. Feed (activated sludge effluent) is continuously pumped into the reactor at an initial rate of 1.5 liter/day, allowing for a hydraulic detention time of 5.33 days. The hydraulic detention time will be varied until a stable, steady state condition occurs in CFSTR. Continuous waste procedures are provided by a hydraulic head differential between the reactor and the clarifier. Intermittent sludge return from the clarifier to the CFSTR is pumped at hourly intervals with a pump duration time of one minute. A mechanical stirrer and a submerged air diffuser are used to ensure a homogeneous mixed liquor and a sufficient oxygen supply.

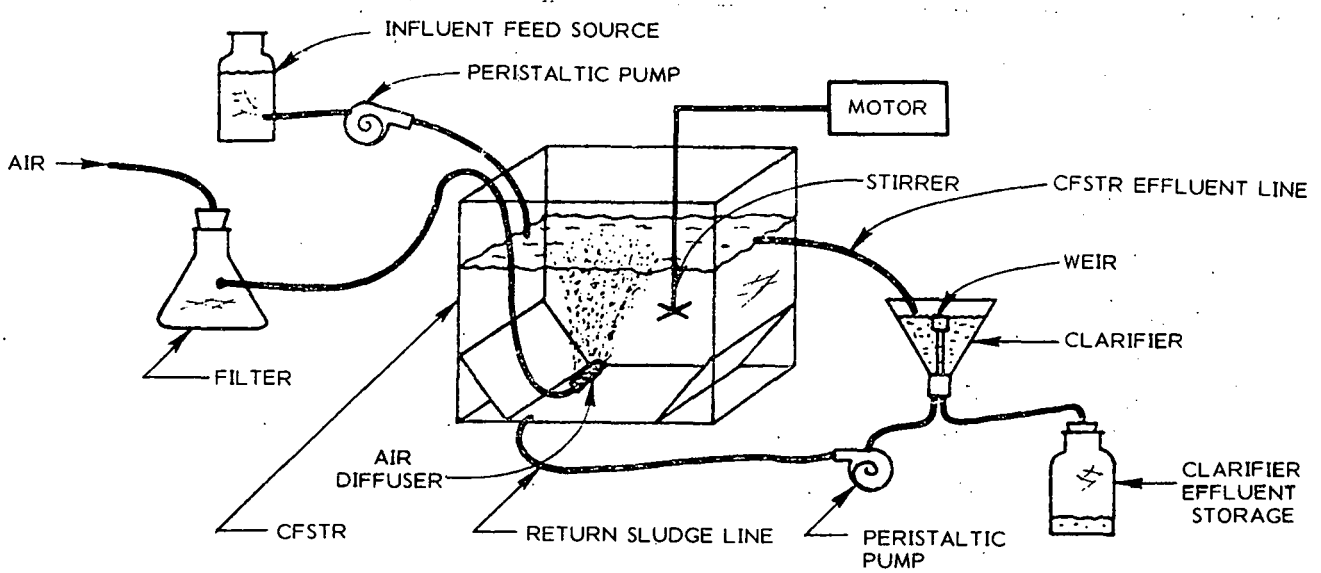

FIGURE 2-3. Bench-scale activated sludge CFSTR.

The clarifier consists of an inverted 1000-ml Erlenmeyer flask with its base removed. An internal weir allows the effluent to flow from the clarifier to a storage container. An opening located at the bottom of the clarifier provides for return and waste of the settled sludge. The clarifier volume is varied by adjusting the weir height in the clarifier unit. A hydraulic detention time in the clarifier of less than 4 hours is desirable; this is varied until adequate settling in the clarifier occurs and a steady state condition exists in the entire CFSTR system.

Up to this point, operation of this unit for removal of ammonia has not been successful. The activiated sludge nitrification process is very susceptible to upsets caused by influxes of cyanide and thiocyanate. Direct PAC addition to the nitrification unit is being considered in order to remove

toxic substances that are inhibiting the growth of the nitrosomonas and nitrobacter bacteria. This should also aid in system stability against shock loading.

2.2.4.4 Attached Growth Treatment - Rotating Biological Contactors

The purpose of this study is to determine the feasibility of rotating biological contactors (RBC) for the carbonaceous substrate removal of wastewater generated by coal gasification using bench-scale reactors.

After completion of the solvent extraction and ammonia stripping the wastewater (SGL) is used for biological treatment. The RBC consists of parallel circular discs attached perpendicularly to a horizontal shaft. The discs are slowly rotated with 40 pct of their surface area submerged in the tank. As the SGL flows past these discs, a film of biomass develops on the discs. Rotation of the discs aids in the transfer of oxygen and nutrients to the biomass. When the biomass, which uses certain organic components of the SGL for growth and energy requirements, becomes too thick, the shearing forces overcome the adhesion forces of the biomass, and it is sloughed into the effluent. The discharged biomass has good settling characteristics and is removed in a settling tank.

The RBC consists of 21, 6-inch discs connected on a 3/8-inch nickel-plated shaft. The area of the discs was determined by the flow. The ratio used in this study for determination of disc surface area is 0.625 gal/ft^2/day. The total area of disc is 8.24 ft^2. The volume of the tank was determined using an industry standard of 0.12 gal/ft^2(15). The total volume of the RBC tank used in this study is 0.128 ft^2. The discs are mounted so that the flow will be pumped perpendicular to the disc. The discs will be rotated by a variable motor and the influent will be delivered by a master flux pump.

Table 2-18 presents data collected during steady state operation of the bench-scale rotating biological contactor. Results indicate complete removal of phenolics and alcohols, and 94 pct removal of BOD. Nitrification also occurred in this unit, with over 30 pct removal of ammonia. Operating conditions for the unit included a hydraulic detention time of 0.48 days and a hydraulic loading of 0.1 gal/ft^2/day. Operation of this unit on coal gasification wastewater was exceptionally good. Considering the low initial investment, low operating costs, and the stability of this type of biological treatment process, its use in industrial coal gasification facilities should be evaluated.

TABLE 2-18

ROTATING BIOLOGICAL CONTACTOR

	Influent (mg/ℓ)	Effluent (mg/ℓ)
BOD_5	1380	74
COD	5870	4884
Alcohols	230	0
Phenols	160	0
SCN	220	92
CN	32	15
NH_3	570	395

2.3 REFERENCES

1. Brinton, R.K. "The High Temperature Photolysis of Acetone," J. Amer. Chem. Soc. 83, 1541-1546 (1961).

2. Willson, W.G., J.G. Hendrikson, M.D. Mann, G.G.Mayer, and E.S. Olson. "Pilot Plant Wastewater Treatment Project Status at UNDERC," Proceedings, 12th Biennial Lignite Symposium, May 1983, Grand Forks, North Dakota.

3. Willson, W.G., G.G. Mayer, M.D. Mann, and J.G. Hendrikson. "Addendum to Pilot Plant Wastewater Treatment Project Status at UNDERC," Internal Report. June 14, 1983.

4. Wiltsee, G.A. "Low-Rank Coal Research Under the UND/DOE Cooperative Agreement; Quarterly Technical Progress Report for the Period April-June 1983" (DOE/FE/60181-17).

5. Mann, M.D. "Drift Determination of the UNDERC Cooling Tower," September 1983. Internal Report.

6. Mann, M.D., and S.J. Galegher. "Determination of Emission Levels from the UNDERC Cooling Tower," Internal Report, September 1983.

7. Galegher, S.J. "Atmospheric Emissions From a Gasifier Wastewater-Fed Cooling Tower." Master's Thesis, University of North Dakota, Draft.

8. Parons, C.T., and L.G. Felix. "Operators Manual for the Five-Stage Multicyclone," p. 12, Southern Research Institute, Birmingham, Alabama, 1980.

9. Reid, R.C., J.M. Prausnitz, and T.K. Sherwood. "The Properties of Gases and Liquids," 3rd Edition, pg. 457-463, McGraw-Hill, New York, 1977.

10. Shofner, F.M., G.O. Schrecker, T.B. Carlson, and R.O. Webs. "Measurement and Interpretation of Drift-Particle Characteristics," Proceedings, 1974 Symposium on Cooling Tower Environment, March 4-6, 1974, University of Maryland.

11. Hanna, S.R. "Fog and Drift Deposition from Evaporating Cooling Towers," Nuclear Safety, Col. 15, No. 2, March-April, 1974, pg. 190-195.

12. Missimer, J.R. "Results of Isokinetic and Sensitive Paper Analysis," TIN 83-1077, prepared for M.D. Mann, Grand Forks Energy Technology Center, June 23, 1983.

13. McCoy, J.W. "Microbiology of Cooling Water," Chemical Publishing Company, New York, NY, 1980.

14. Clark, J.W., W. Viessman, and M.J. Hammer. "Water Supply and Pollution Control," A Dun-Donnelley, New York, NY, 1977.

15. Grady, C.P., and Henery C. Lim. "Biological Wastewater Treatment-Theory and Applications," Marcel Dekker, Inc., New York, NY, 1980.

3. - HYDROGEN PRODUCTION FROM LOW-RANK COALS

Project No.: 7108 B&R No.: AA8545050

Submitted by: W.G. Willson, Manager, Coal Conversion Research Division

Prepared by: R.C. Ellman, Senior Research Associate

Assigned UNDERC Personnel: R.C. Ellman
M.M. Fegley
P.A. Kongshaug

3.1 GOALS AND OBJECTIVES

The goal of this project is to enhance the production of hydrogen in gasification of low-rank coals by increasing the already high reactivity of these coals through the use of catalysts. The approach will be to increase the gasification rate and the water-gas shift reaction by use of catalysts at temperatures and pressure conditions which are unfavorable to methane production. An additional goal of the project is to expand the data base on the contributions of catalysts to gasification of low-rank coals, both as inherent minerals which catalyze the reactions and as additives; and to establish those conditions of temperature, pressure, catalyst application techniques, and coal source which optimize or influence the production of hydrogen.

3.2 ACCOMPLISHMENTS

3.2.1 Literature Survey

Catalytic coal gasification has been the subject of extensive research. The goal of the major portion of this research has been to increase production of methane. The inherent high reactivity of low-rank coals is recognized in the literature, but contributing differences in ash compositions and physical structural properties have not been defined to any satisfactory extent. The literature review is a continuing effort in progress by which the project work plan and candidate catalysts for initial testing will be selected.

3.2.2 Test Apparatus

It is planned to utilize a relatively large-scale TGA apparatus for the major portion of the test work. The design has been completed and construction has begun of a unit in which samples of up to 1 pound can be tested. While the main operating areas of interest for H_2 production are temperatures of ~650°C at atmospheric pressure, the TGA apparatus was designed for use in Coal Science projects to approach reaction temperatures up to 1000°C and pressures up to 1000 psig. The external water-cooled pressure vessel has been completed and installed in a test bay for high-pressure operations.

Fabrication of a thin-walled, stainless steel sample chamber, surrounded by heating elements and suspended from a load cell, is in progress. Preheated reactants (steam) will be passed into the sample chamber and sampled and analyzed after reaction. Calibration and shakedown operation of the apparatus will be performed in the next quarter, initially for devolatilization studies. Subsequent modification for catalytic gasification tests will be made after apparatus capabilities are established.

In addition, smaller-scale reaction units are being considered. These have advantages for screening functions, so that the number of tests performed in the larger-scale unit can be reduced.

Selection of instrumentation for temperature recording and control and gas analyzing has not been finalized, but no particular problems are anticipated.

4. - FINE COAL CLEANING

Project No.: 7104 B&R No.: AA052000

Submitted by: W. G. Willson, Div. Mgr., Coal Conversion Research

Prepared by: M. J. Mitchell, Div. Mgr., Analytical Research

Assigned AWU Personnel: D. Brown
A. Marg
T. Sawatzke

4.1 GOALS AND OBJECTIVES

The goals for the Fine Coal Cleaning project are two-fold. The first concern is to support PETC in building a uniform data base on fine coal cleaning of western coals by float-sink methods. The second goal is to investigate advanced coal cleaning methods for selected low-rank coals, with emphasis on upgrading the quality of low-rank coal/water slurries.

4.1.1 Uniform Data Base on Fine Coal Cleaning of Western Coals

The Pittsburgh Energy Technology Center (PETC) is providing 156 samples for centrifugal float-sink analysis. The testing plan is given in Figure 3-1 Fine Size Centrifugal Float-Sink Procedure, Quarterly Progress Report, April-June 1983, this project. Splits of coal, prepared to 65, 200, and 325 mesh top size will be separated at specific gravities of 1.3, 1.4, and 1.6. Washability studies on these same coal samples in the conventional size range is being performed in other PETC-funded projects.

The specific objectives of the float-sink studies scheduled to continue through 1985 are as follows:

1. Establish consistent comminution methods to provide usable size fractions for the float-sink studies.

2. Establish limits of applicability for float-sink methods used in this study with regard to fine coal particle sizes, while performing the float-sink cleaning studies. Specifically, identify the smallest coal particle size that is amenable to wet gravity separation in float-sink tests performed at specific gravities of 1.30, 1.40, and 1.60.

3. Evaluate the impact of surface and bound moisture on the fine coal cleaning procedure used in this study.

4. Determine the degree of segregation of inorganic constituents of selected low-rank coals as a function of coal source, coal moisture (after conventional or steam drying), and size fraction. In addition, identify the separation of coal components as a function of size fraction of the comminuted samples.

5. Compile and reduce data leading to evaluation of the levels of physical removal of inorganics from the fine coals investigated (in conjunction with PETC).

Objectives for this reporting period included:

1. Determine the size distribution of tested samples by wet screening. Analyze each fraction to establish base data.

2. Select and standardize a method for pyritic sulfur determination; and

3. Initiate the heavy media separation studies.

4.2 ACCOMPLISHMENTS

1. Size analysis by wet screening was completed on the first 24 samples prepared for the float-sink tests. Differences between wet and dry screening methods were noted for some western coals. It appears that particles swell when wetted for some coals. Dry particles pass screen sizes in the large size range (65 mesh as an example) but will not when wet. When redried, the material again passes the screen.

2. Analytical determinations on the size fractions of samples obtained by wet screening is near completion. For some of the finer size fractions of some coals, insufficient material was obtained with which to perform all of the analytical tests. The selection of which determinations to make will depend on the availability of data on the rest of the coal as established with PETC. The analytical data on the finer sizes of the float-sink portion of the study may also be required to select the most needed analysis.

3. The "forms of sulfur" analytical procedures at UNDERC are completed and will be used on a variety of projects. The sulfate ion will be measured directly using an ion chromatograph. The $SO_4^=$ appears as a clean peak of sufficient intensity for quantitative use on the instrument and is reproducible. The instrument has been calibrated for this procedure, but blanks have not been run due to high utilization of the ion chromatograph by other projects.

   ASTM method D2492 using AA rather than ICAP analysis for iron in a modified method was selected to determine pyritic sulfur content. The AA method is faster and more available at this time.

4. Float-sink analysis at 1.30 specific gravity on 65-mesh top size samples is complete. Results for the last four samples have not been reported. The range for float values at 1.3 specific gravity ranges from ~0 on W-2 (Upper Hartshorne Bed, Lamar Co., Arizona) and 0.22 pct on W-11 (Bull Creek Bed, Coleman Co., Texas) to 37 pct on W-10 (San Pedro Bed, Webb Co., Texas) and 59 pct on W-9 (Secor Bed, Wagner Co., Oklahoma). Float-sink separations at 1.4 specific gravity have started. No problems have been encountered with the separations.

Work planned for third quarter 1983 includes:

1. Proximate analysis determinations will be resumed in late October. The proximate analysis unit is down; parts delivery is now expected in late October.

2. The sulfate analysis procedure will be completed and samples will be analyzed for pyritic sulfur.

3. Float-sink testing and analyses of the finely-ground coal samples will continue.

5. - COAL-WATER SLURRY PREPARATION

Project No.: 7105

B&R Nos.: AA0520000
AA2530100
AA3515050

Submitted by: W.G. Willson, Manager, Coal Conversion Research Division

Prepared by: G.G. Baker, Research Supervisor, Coal-Water Slurry Preparation

Assigned UNDERC Personnel:
D.J. Maas
M.J. Mitchell
J.E. Tibbetts
L.H. McEwen
R.A. Sweeney

UND Faculty Participants:
D.N. Baria
A.R. Hasan

AWU Student Participants:
J. Brungardt
B. Olson
G. Huber
S. Seaborn
R. Sears

5.1 GOALS AND OBJECTIVES

The overall project objective is to develop methodology to prepare stable low-rank coal-water slurries with high enough solids and Btu contents to be economically utilized as replacement fuel for oil-fired combustors, feed to high-pressure gasifiers, and/or to be transported by pipeline. The key to accomplishing this goal is the development of an economical coal drying procedure that gives a product which is resistant to moisture reabsorption. One of the most promising processes is hot-water drying of finely ground coal in slurry.

Hot-water drying is a process for removal of liquid water from high-moisture coal by heating the coal-water slurry under pressure. The drying temperature may be sufficiently high so that some carboxylic groups in the coal decompose to form carbon dioxide. Dewatering is enhanced when the carbon dioxide formed in the pores of the coal forces the liquid out of the pores and into the carrier medium. Drying also occurs because of surface modification which reduces the ability of the coal to bind water. This is due to the replacement of the hydrophilic carboxyl groups on the surface of the coal by hydrocarbon groups which are hydrophobic. Energy requirements for drying can be minimized because vaporization of the water is not required, and feed/effluent heat exchange can be employed. Hot-water drying of low-rank coals produces a product that will reabsorb a minimum amount of water. Further, evidence exists that this process will reduce sodium resulting in a higher quality fuel. Some of the more attractive features of this process include: high coal throughput; good heat recovery; and the potential to incorporate

fine coal cleaning and coal beneficiation via ion removal. An additional benefit may be that the water removed in drying may be used for slurrying the solids, resulting in reduced surface or groundwater usage, which may be an important consideration in the western United States, where most of the low-rank coals occur, and where water is relatively scarce.

Specific objectives for the current budgetary year are: (a) perform autoclave tests on North Dakota lignite to produce data necessary for the successful design of a hot-water/coal drying process development unit (PDU) and perform autoclave tests on other coals to develop a low-rank coal hot-water drying data base, and (b) design and construct a hot-water/coal drying process development unit to prepare high solids-content low-rank coal-water slurries. The initial design will include steps for coal-water mixing, heating, drying, and concentration by flash evaporation.

Near-term objectives of the project for the period of July through September 1983, were:

1. Continue construction of the hot-water coal drying process development unit.

2. Continue procurement of major equipment items needed for the fabrication of the process development unit for the analysis of hot-water-dried coal-water slurries.

3. Design and construct a bench-scale hot-water/steam drying apparatus to provide comparative data on hot-water and steam-dried coals.

4. Design and build an extrusion viscometer for testing hot-water-dried coal-water slurries under conditions similar to pipeline flow and atomization.

5. Continue studies relevant to the analysis of hot-water-dried coal and to the design of the coal-water slurry pilot plant.

5.2 ACCOMPLISHMENTS

5.2.1 Hot-Water/Coal Drying Process Development Unit

The Hot-Water/Coal Drying Process Development Unit (HWCD-PDU) is designed to dry 100 pounds per hour of lignite continuously under pressure, and at elevated temperature in a water slurry. The main product from the plant consists of a low-rank coal-water slurry that has been concentrated to 60 or 70 wt pct "bone dry" solids. The design of the PDU used existing pumps, vessels, instrumentation, and other equipment to minimize costs. A majority of this process equipment was salvaged from the decommissioned Project Lignite coal liquefaction process development unit.

Construction of the HWCD PDU was initiated in April 1983. The salvage of structural steel, floor plate, and stairways from the Project Lignite Coal Preparation building was completed. Approximately 620 square feet of floor plate, 340 linear feet of "H" and "I" beam, 240 linear feet of stairway stringer, and 65 pieces of stair tread were recovered. Almost all of this

will be reused in building the work platforms and vessel support structures for the hot-water/coal drying preparation facility. Savings for the project because of structural steel salvage was estimated at between $5,000 and $10,000 based on current-day replacement costs less labor costs for recovery. In addition to the structural steel, a 5-ton electric hoist was also removed from the Project Lignite facility and transported to the Energy Research Center. The hoist was rewired for monorail use and tested. The hoist will be installed in the new coal preparation facility and will be used to load coal into the coal feeder by hoisting 2-ton feed hoppers into position. Estimated cost savings by reuse of the 1945 model hoist range from $20,000 to $25,000 depending on options.

Outside contract construction of the hot-water/coal drying process development building was completed the last week in September, nearly two months later than scheduled. The general contractor completed the painting requirements, while the electrical and plumbing subcontractors finished installation of the lighting and heating systems. The building is now ready for occupation and erection of work structures, and the placement of process equipment has started.

Pilot plant construction during the quarter included fabrication of the main work platform, the coal feeder stand, the coal storage hoppers, the overhead crane support structure, and the vacuum pump stand. In addition, several smaller pump bases and pedestal stands were also completed.

The main work platform is a three-level structure measuring approximately 4½ feet wide by 22 feet long by 28 feet high. Each level is 7 feet above the one below it, with the first level 7 feet off the concrete floor. On both sides of the structure and at the 28-foot level are mounted ½-ton air hoists to facilitate vessel mounting and removal. The east side of the platform will support the slurry recovery and concentrating equipment (Figure 5-1), while the west side supports the slurry heaters and the coal drying reactors (Figure 5-2). This structure has been completely framed and erection of the uprights has begun. It is anticipated that final erection and assembly will be complete by the second week of October.

The coal feeder stand was completed and moved into the coal drying preparation facility. The structure measures approximately 5 feet by 7 feet by 9 feet tall. At the top are mounted four load cell capsules designed to mate with and weigh the coal supply hoppers (Figure 5-3). Below these is mounted the volumetric coal feeder, which also rests on load cells. Beneath that and off to the side is the multistage, horizontal slurry mix tank, which again rests on load cells for weight measurement. The coal feeder stand also houses the low-pressure slurry circulation pump and the precision metering water feed pump. Both pumps are mounted to permit easy access and to facilitate floor maintenance and clean-up.

Three coal storage/supply hoppers were fabricated by a local weld shop. The hoppers are cylindrical in design with right angle cones terminated by knife gate valves to facilitate unloading. Each hopper is 4 feet in diameter by 9 feet high with sufficient volume to hold roughly 3,000 pounds of pulverized coal. They were constructed of ¼-inch mild steel plate rolled and coned to meet design dimensions. When the pilot plant is operating, these hoppers will be used to transport coal from the coal grinding facility to the hot-water coal drying building--a distance of approximately 500 feet.

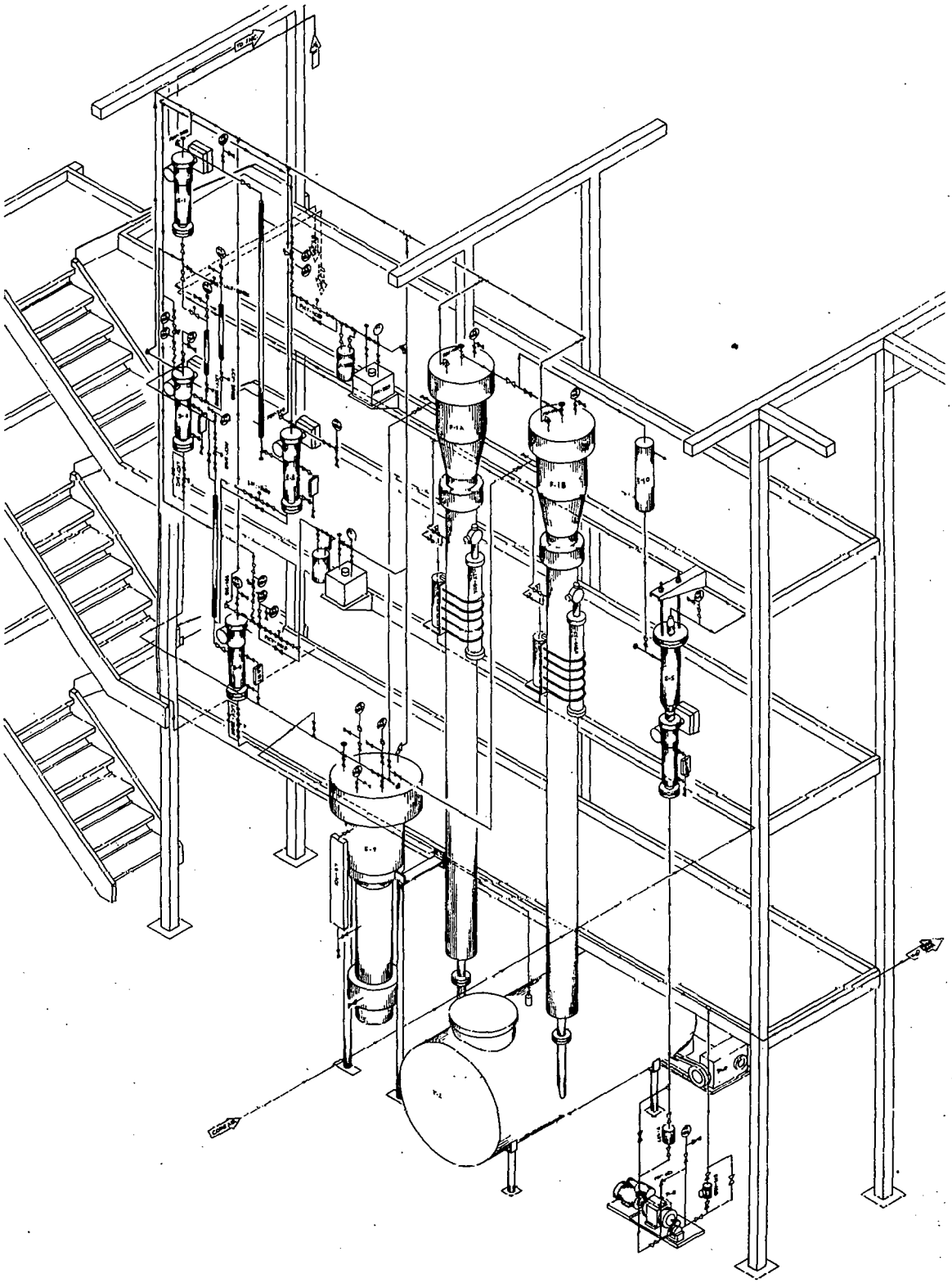

FIGURE 5-1. Isometric drawing of the center work platform with the slurry recovery and concentrating equipment mounted on the east side.

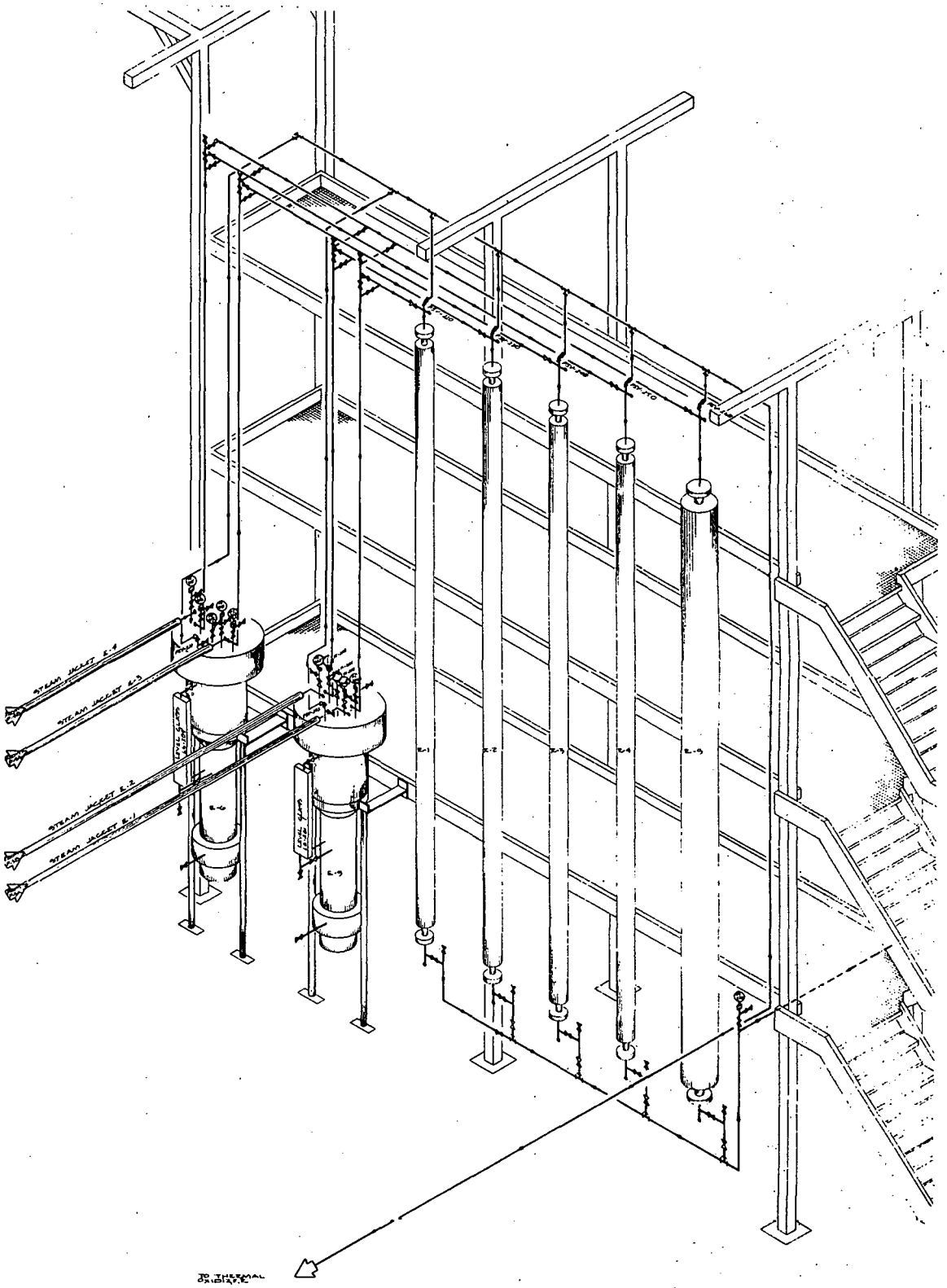

FIGURE 5-2. Isometric drawing of the center work platform with the slurry heaters and the coal drying reactors mounted on the west side.

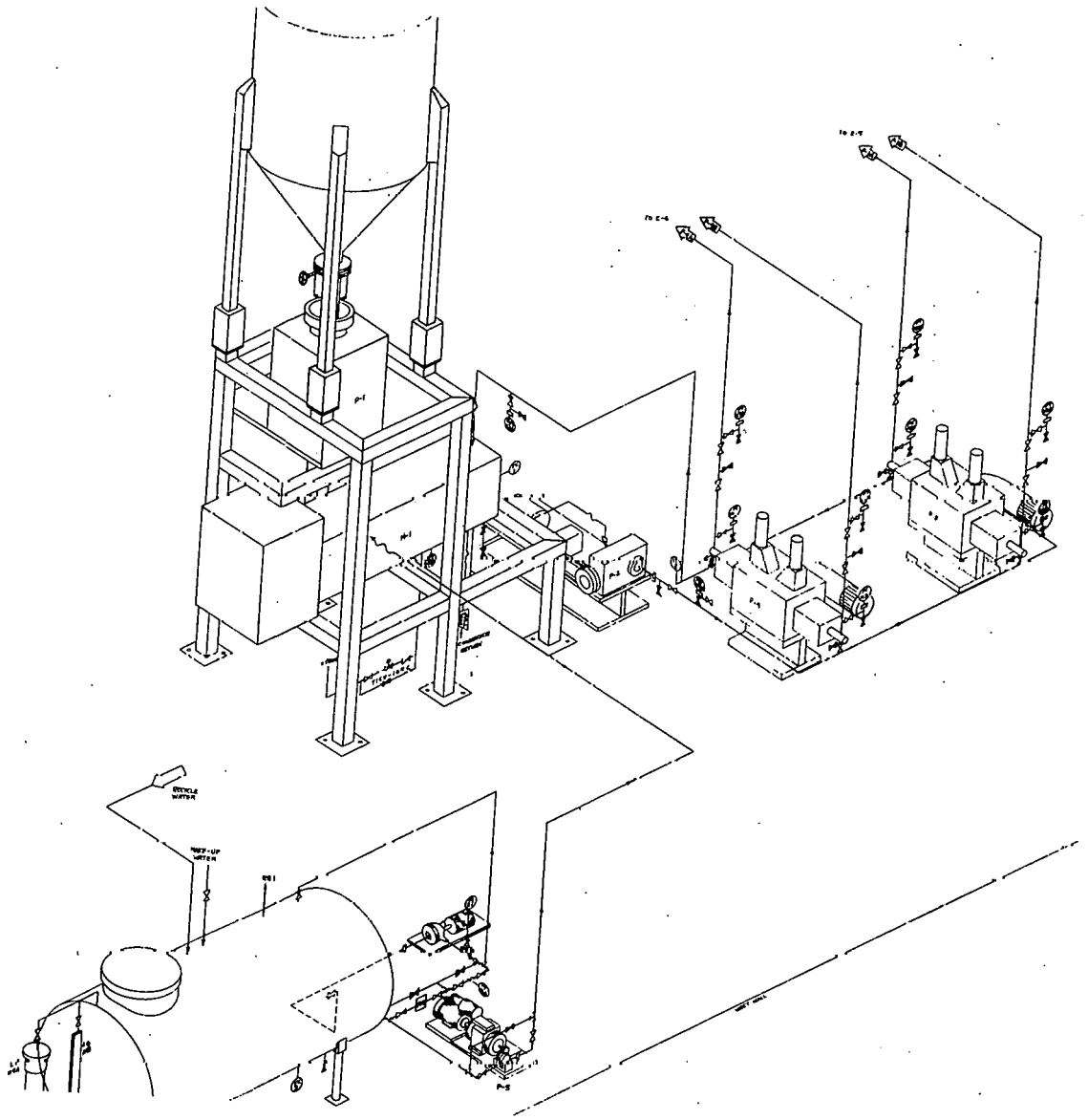

FIGURE 5-3. Isometric drawing of the coal feeder support stand and ancillary equipment.

Also completed this quarter were the overhead crane support structure and the vacuum pump stand. The overhead crane support structure consists of two 27-foot stanchions and a 27-foot horizontal monorail. The stanchions were built in the shape of a capped "H" using salvaged 6"-25 lb/ft wide flange beams with reinforcement and stabilization accomplished by cross bracing with 2-inch angle iron. The monorail is a single length of 18"-55 lb/ft I-beam. This structure was framed on the ground and then erected in the building. The 5-ton electric hoist was installed shortly thereafter.

The vacuum pump stand was the final item completed this reporting period. It consists of a metal table approximately 3 feet by 8 feet with vertical racking along one of the longer edges. Mounted on this were three vacuum pumps with motors, two knockout pots, two cold traps, a pressure transmitter, a control valve, and a positive displacement gas meter. The unit was completely piped and is ready for relocation to the hot-water coal drying facility.

In addition to PDU construction, other activities included procurement of structural steel tubing to build the stairways and landings for the main work platform; design of the slurry heater coils; and making a preliminary outlay of the process instrument panel.

5.2.2 Procurements

Several major items were procured or ordered as needed for constructing the HWCD-PDU or for analyzing hot-water-dried products. These included: 1) a laboratory-scale pulverizer with an a.c. frequency speed controller to vary hammer speed up to 14,000 rpm. This pulverizer will be used to extend the grinding studies on lignite and to prepare coal samples of a variety of particle size distributions for hot-water-water drying in the autoclaves and for slurry rheology studies; 2) a multi-point data acquisition system complete with a 16-bit personal computer and dual 320 K 5-inch floppy disc drives. The data logger features 100 separate input and 40 individual output channels along with an RS 232 interface for communications by hardwire to the personal computer and by telephone modem to the IBM 370 main frame computer on the UND campus. As an end use, the system will become part of the control and monitoring instrumentation for the continuous hot-water/coal drying unit; 3) a low-temperature incubator featuring 19.9 cubic feet of storage capacity and temperature adjustability from -10° to 50°C. The incubator is used in conjunction with performing equilibrium moisture tests on dried lignite samples as per ASTM procedures; and 4) three custom-built coal storage hoppers each capable of holding approximately 3,000 pounds of pulverized coal, enough coal to provide 30 hours of operation on the hot-water coal drying PDU. The bins complete the equipment requirements for the coal-water slurry mixing section of the pilot plant.

In addition to the previously cited procurements, the UNDERC coal-water slurry project also acquired the use of a Haake Rotovisco viscometer which was purchased by the Grand Forks Federal Project Office through actions initiated before the defederalization of the DOE's Grand Forks Energy Technology Center. The viscometer, a Rotovisco RV 100, features a shear rate programmer, an xy-t-recorder and co-axial rotational cylinders of the Searle type. All functions of the instrument and calibration of the recorder are pushbutton controlled. The speed controller is programmable and can be started with a hold time at zero speed to allow the sample to reach a predetermined temperature or structure recovery. It is followed by a time linear speed increase up to the chosen maximum rotor speed which can be any value between 0.5 and 500 rpm. The maximum speed can be maintained for a selected hold time and then the speed program reversed. Following this routine, the thixotropy of a sample can be measured and recorded. The instrument is also suitable for measuring the samples' yield stress at zero shear and for determining the rheological properties of fluids as a function of time at a constant shear

rate. The viscometer is used to characterize dried lignite-water slurries and to a limited extent quantify their storage stability by measuring yield stress at zero shear.

5.2.3 Coal Hot-Water/Steam Drying Apparatus

The hot-water/steam drying apparatus is a bench-scale unit designed to operate in a cold-charge batch mode, drying up to a maximum of one gallon of coal per cycle. The apparatus has the versatility to operate with either liquid or vapor phase water for coal drying purposes. The test fixture consists of two high-temperature/high-pressure autoclaves, one acting as the coal dryer while the second accumulates evolved gases and water condensate. Thus, material balances can be closed and the product gases analyzed. Figure 5-4 is a photograph of the coal hot-water/steam drying apparatus.

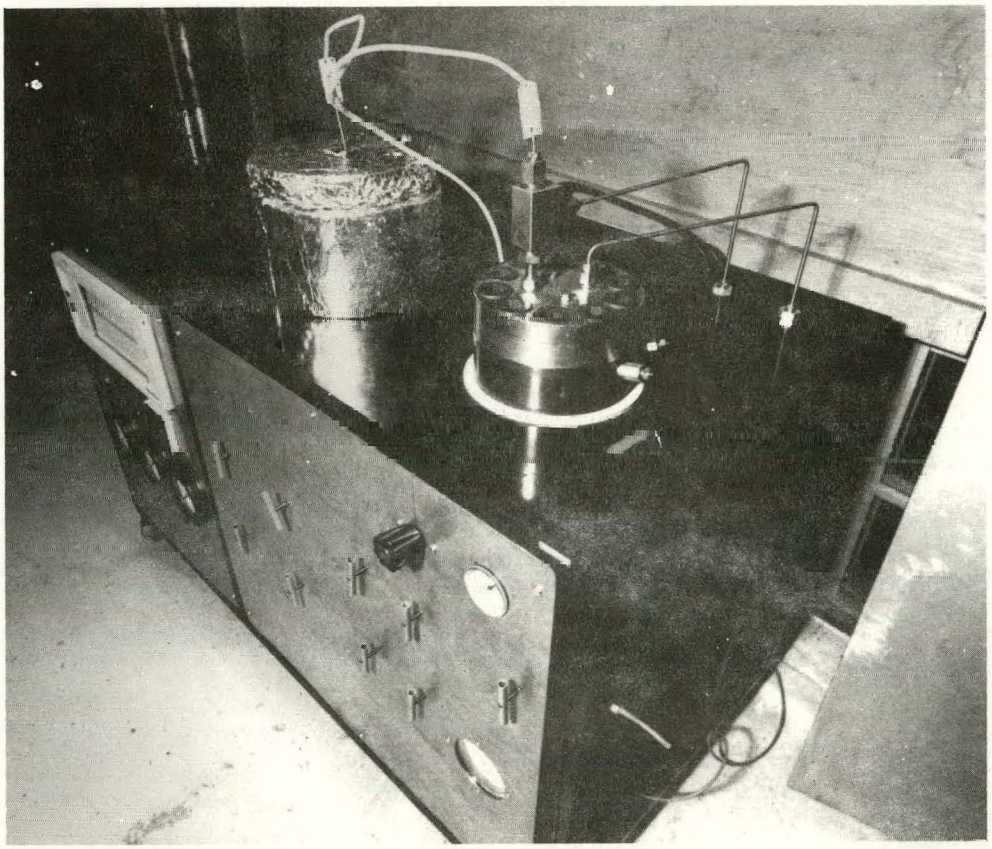

FIGURE 5-4. Steam drying apparatus.

A 2-gallon autoclave with a removable stainless steel insert is utilized as the coal dryer. A preweighed charge of coal is placed into a basket and is either submerged in a known amount of water for hot-water drying or placed above the liquid level in the vapor space for steam drying inside the removable insert. The insert is placed in the 2-gallon autoclave, the autoclave closure is bolted down, and the autoclave is heated to the desired drying temperature with external temperature-controlled electrical heaters. The temperature of the coal bed is monitored by a thermocouple protruding from the

bottom or the top of the autoclave depending upon the drying medium used. The autoclave closure has a centrally located dip tube which is connected to a condenser and a 1-gallon autoclave. The pressures of the autoclaves are monitored using pressure gauges.

In steam drying, after the prescribed drying time, live steam and evolved gases are passed through the condenser and into the cold 1-gallon autoclave. Also, any remaining water is vaporized and the 2-gallon autoclave is cooled. In hot-water drying, the 2-gallon autoclave is cooled prior to venting the evolved gases, after the prescribed drying time. The products of drying are then recovered, measured, and analyzed.

Hot-water and steam drying runs are planned using North Dakota lignite in the apparatus. The results of the testing will be used to compare the two drying methods, and the coal slurry products from the hot-water drying testing will be used for rheological studies. Experiments will also be conducted with the apparatus to aid in designing the slurry separation and slurry flash concentration sections of the HWCD-PDU.

5.2.4 Slurry Rheology

The Haake Rotovisco RV 100 viscometer, with an assortment of spindles, was received and set up. Testing was started using coal-water slurries to define and develop a standard procedure for slurry preparation, handling, and viscosity measurement; and to become familiar with operation of the instrument in general.

Besides the preliminary work with the rotational viscometer, an extrusion rheometer was fabricated in-house. This instrument will be used for measuring rheological properties of coal-water slurries by using tube flow data. These data will be used to supplement the measurements obtained by other viscometry methods and to give a more accurate simulation of slurry rheological properties in pipeline flow and in atomization nozzles.

The extrusion rheometer consists of a cylindrical, water-jacketed, reservoir with interchangeable tubes of different inner diameters (see Figure 5-5). A selectable timing device is used for controlling the electrically-actuated tube flow valve mounted at the bottom of the unit. The temperature of the sample is measured by a thermocouple in the reservoir. A digital readout scale, accurate to the nearest gram, is used in conjunction with the timing device for measuring flow rates. A variable speed cylindrical stirrer is mounted within the reservoir and is used for maintaining slurry suspension. Also included are controls for pressuring the unit to 200 psig.

The apparatus was tested using a Newtonian viscosity standard. Several runs were made with the unit pressured from 5 to 30 psig at 23.7°C and from 35 to 65 psig at 24.7°C. The data and results are shown in Table 5-1. A significant rise in sample temperature was detected as the shear rate increased. This may account for the lower experimental viscosities compared to the reported viscosities for the standard. The extrusion rheometer is fitted with a water jacket, and a constant temperature water circulation system will be added to attempt to improve the correlation between the measured and reported viscosities.

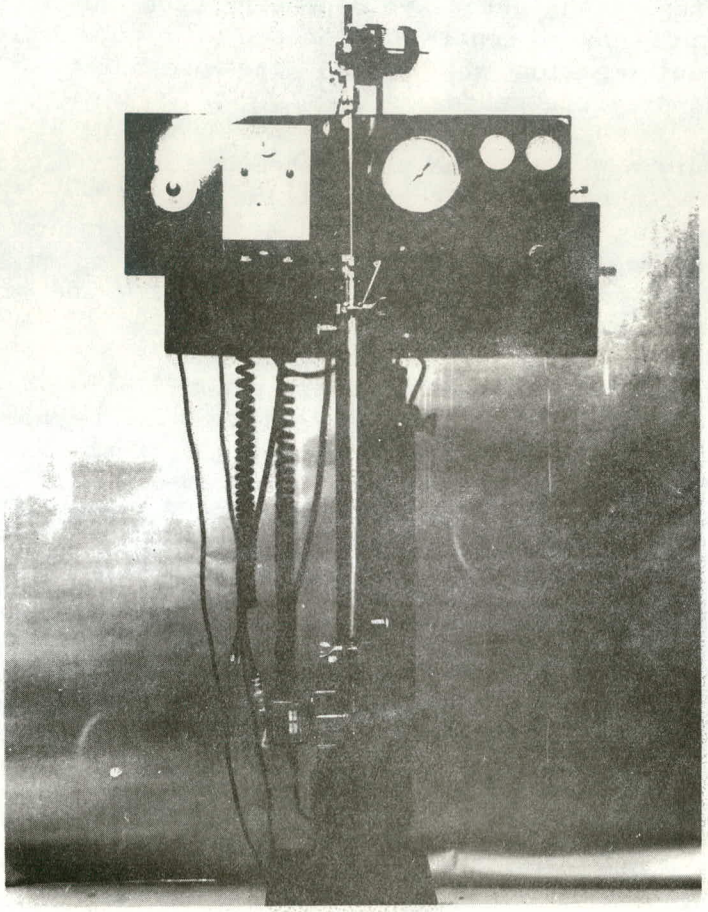

FIGURE 5-5. Extrusion rheometer.

TABLE 5-1

CALIBRATION TESTS ON EXTRUSION RHEOMETER

Sample temp., °C	23.7	24.7
Shear stress range, $g/cm \cdot sec^2$	554-3079	3519-6154
Shear rate range, sec^{-1}	748-3135	3666-6467
Actual viscosity, poise	1.180	1.109
Experimental viscosity, poise	1.044	0.954
Percent error	11.5	14.0
Correction factor	1.13	1.16

Viscosity standard: S60 Lot No. 75106
Extrusion tube length: 49.15 cm
Extrusion tube I.D.: 0.318 cm

5.2.5 Special Studies and Methods Development

5.2.5.1 Coal Grinding Studies

Particle size distribution is an important factor in stable coal-water slurry prepration and, therefore, will be one of the parameters investigated in hot-water drying tests and during operation of the process development unit.

In order to determine which particle size distributions can be obtained with existing equipment, tests were conducted on the Mikro-pul Model 2DH pulverizer. The pulverizer can be operated with hammer speeds of 3300, 4000, or 6800 rpm by changing the sheave on the hammer shaft. The selection of removable screens include: 1/2-inch, 3/8-inch, 1/8-inch, and 1/32-inch round perforated, 1/4-inch jump-gap, 0.027 and 0.010 wedge bar, and a 1/32-inch herring bone.

Initially, pulverizing tests were run using an eastern coal. From these tests, it was found that at the same hammer speed there is little difference between the particle size distributions for coal ground with 1/2-inch and 3/8-inch round perforated screens or between 0.027 and 0.10 wedge bar screens. It was also found that particle size distributions obtained at 4000 rpm could also be obtained with the 3300 and 6800 rpm hammer speeds.

Indian Head lignite from west-central North Dakota was used in the second series of pulverizing tests. The high and low hammer speeds were used to give the total range of particle size distributions obtainable with the existing equipment.

Figures 5-6 and 5-7 show particle size distributions for Indian Head lignite pulverized at 3300 rpm and 6800 rpm, respectively. The sieve analysis to determine these distributions was run according to the ASTM D410-38 procedure. In Figure 5-6, it is apparent that there is little difference among particle distributions for coal pulverized at the same hammer speed using the 1/16-inch and 1/32-inch round perforated screens or the 1/32-inch herring bone screen.

In general, the results of the grinding work showed considerable differences between the grinding characteristics of different coals, with the differences not solely attributable to the differences in coal rank. For instance, in grinding the Indian Head lignite to match the particle size distribution obtained with a Texas lignite ground at 6800 rpm hammer speed using the 1/8-inch round perforated screen, it was necessary to first grind the Indian Head coal at 6800 rpm using the 1/8-inch round perforated screen and then to regrind it using the same hammer speed but with the much finer 0.027 wedge bar screen.

Grinding work thus far has shown that the most significant variable in grinding coal with this pulverizer was hammer speed and that the effects of screen size are much smaller.

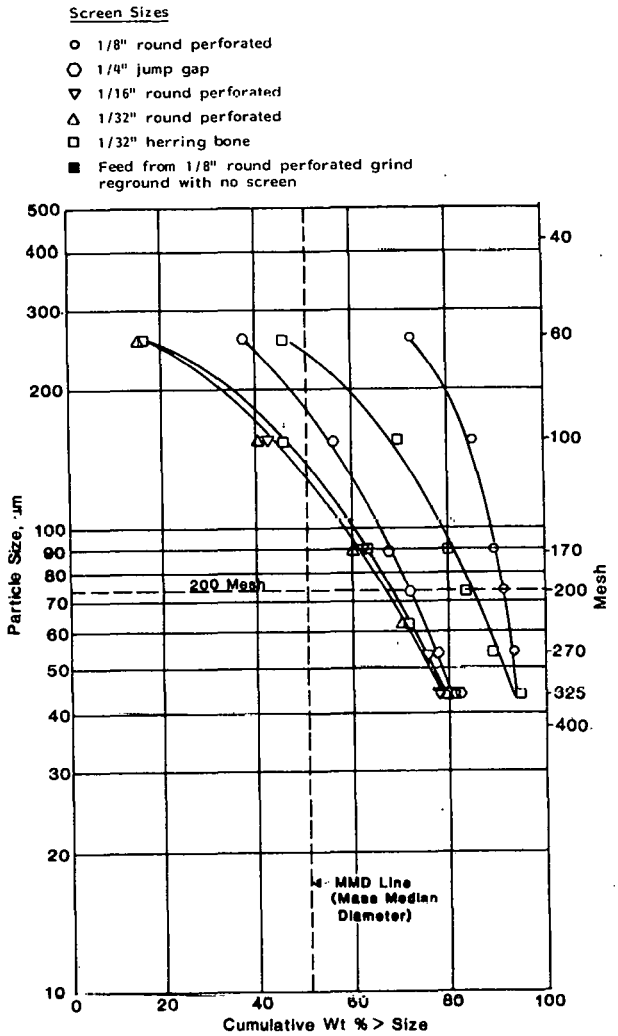

FIGURE 5-6. Particle size distributions for Indian Head lignite pulverized in a Model 2DH Mikro-pulv pulverizer at a hammer speed of 3300 rpm.

5.2.5.2 Methods Development for Determination of Equilibrium Moisture Content of Coal

The procedure for determining equilibrium moisture in coal was further developed and refined. Equilibrium moisture is used as an indicator of how much moisture can be reabsorbed by dried coal and can also be used to compare drying effectiveness for different drying processes. Comparing the equilibrium moisture of "as received" coal to the equilibrium moisture for hot-water-dried coal is especially useful because of the difficulty in determining the inherent moisture of coal in a slurry.

The current method of determining equilibrium moisture is similar to that outlined in the ASTM D1412 procedure. The procedure is as follows: From 10 to 15 g of pulverized coal are placed into a 250-mℓ Erlenmeyer flask with 50 mℓ of freshly distilled water. The slurry is stirred magnetically for 30

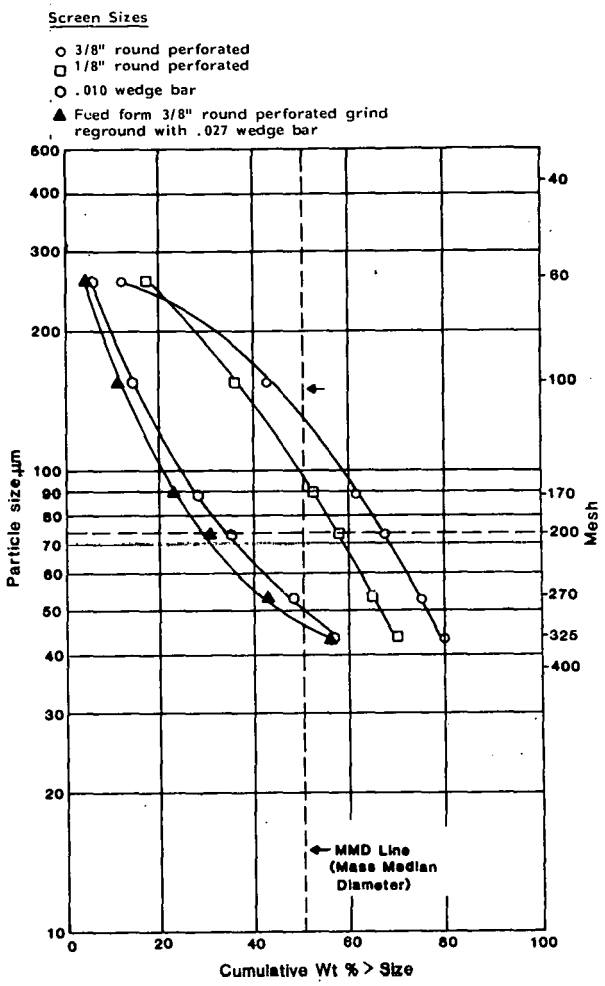

FIGURE 5-7. Particle size distributions for Indian Head lignite for Indian Head lignite pulverized in a Model 2DH Mikro-pulv pulverizer at a hammer speed of 6800 rpm.

minutes and then placed in an incubator at 30°C for 3 hours. At the end of the wetting period, the excess water is removed from the coal on an 11.0-cm Büchner funnel with a water aspirator supplying suction. The coal is transferred to the filter with a minimum of distilled water.

During filtration, air saturated with water vapor is passed through the filter cake in a closed system to prevent drying of the coal. After filtration, about 5.0 g of the wet coal is placed uniformly in a preweighed 7.0 cm diameter low-form, flat-bottom weighing bottle.

The weighing bottle is placed in a 160-mm diameter vacuum-type desiccator containing a saturated solution of K_2SO_4. Excess crystalline K_2SO_4 extends above the solution level at the bottom of the desiccator. The desiccator is evacuated to 30 mm mercury absolute pressure and placed in an incubator at 30°C for 72 hours.

After 72 hours, the pressure in the desiccator is restored to atmospheric in no less than 15 minutes by bubbling air through H_2SO_4. The rate of air flow is controlled with a needle valve.

The weighing bottle is removed from the desiccator and weighed to the nearest 0.1 mg. After weighing, the weighing bottle is placed in a moisture oven for 1½ hours at 105°C and then cooled in a desiccator for 30 minutes. The weighing bottle is then reweighed to the nearest 0.1 mg to determine the dry weight of coal.

5.2.5.3 Development of Procedure for Filtering Coal-Water Slurries

A procedure for filtering coal-water slurries was developed as an additional aid in analyzing hot-water-dried coal-water slurries and for concentrating these slurries for additional rheology and stability study. As-received coal was slurried with distilled water and this was used to develop the proper techniques.

The procedure for filtering the as-received coal-water slurry is as follows: 150 to 250 g of as-received pulverized coal is placed in a preweighed 50 mℓ Erlenmeyer flask containing a magnetic stir bar. Water is added to the flask so that the concentration is at least 50 wt pct water.

The coal and water are well mixed and stirred for 10 minutes using a magnetic stirrer before filtering. After mixing, the slurry is transferred to a 24-cm Büchner funnel and filtered for one hour. The slurry is transferred to the funnel with a minimum of water from a preweighed wash bottle. During filtration, a cold trap cooled with isopropyl alcohol and dry ice collects evaporated water between the filter and vacuum pump.

After filtering is complete, the filtrate is collected in a preweighed bottle. The filter cake is scraped from the filter paper and the loose coal is then transferred to a second preweighed bottle.

When filtering hot-water-dried slurry, 300 to 500 g of slurry is used. Water is not used to transfer the slurry to the Büchner funnel. After transfer of the hot-water-dried slurry to the funnel, the procedure is the same as for the as-received slurry.

Filtering tests were conducted on a variety of test coals to check the procedure. Material balance closures ranged from 94 to 96 pct without the cold trap and from 96 to 100 pct after the cold trap was added.

5.3 TRAINING

A seminar and workshop on measurement of absolute viscosity was attended on July 19, 1983, in Minneapolis, Minnesota. The seminar was sponsored by Haake Buchler Instruments, Incorporated, and brought out the importance of uniformity in sample preparation and shear history prior to making the viscosity measurements, mainly because of the thixotropic nature of some materials.

A conference and workshop on particle characterization was attended on September 20-22 in Rosemont, Illinois. The workshop was sponsored by Micrometrics. Topics covered at the workshop included: surface area, pore structure, density, zeta potential, particle size analysis, and chemisorption. Background information was given in each area, developments in the state-of-the-art instrumentation capabilities, applications and limitations were presented.

6. - LOW-RANK COAL LIQUEFACTION

Project No.: 7106

B&R No.: AA1515100
AA2515050
AA2530100

Submitted by: W.G. Willson, Manager, Coal Conversion Research Division

Prepared by: J.R. Rindt, Research Engineer

Assigned UNDERC Personnel:

R. Brown
S. J. Cisney
D. Como
R.A. DeWall
B. W. Farnum
S. A. Farnum
H. J. Foster
L. Haug
B. Hewitt
F. Jones
R. Kulas
D.R. Moe
S.S. Moore
D. Miller
T. Ogawa
A. Ruud
R. Timpe

UND Faculty:
T. Owens
L. Radonovich
V. Stenberg

Visiting Faculty:
H. Hattori-Hokkaido University

AWU Participants:
A. Wolfson

UND Students:
J. Albrecht
P. Weideroder

6.1 GOALS AND OBJECTIVES

The overall goal of the Low-Rank Coal Liquefaction project is to continue developing the technical data base necessary to adapt direct liquefaction expressly for low-rank coals (LRC), including both lignites and subbituminous coals. The data base includes correlations of process yields with operating parameters and with process modifications, such as use of synthesis gas and catalysts, that effectively capitalize on unique properties of LRC. These properties include high moisture, high reactivity associated with oxygen functionality, and alkaline mineral matter.

During the term of the Cooperative Agreement, four major research areas are to be pursued. They are: a) catalytic liquefaction, with increased attention on understanding the effects of adding H_2S, particularly in the presence of iron-containing materials; b) staged liquefaction, with emphasis on low-temperature first stage reactions using CO as the reductant where differences in coal rank will be most evident; c) mechanism/kinetic studies using labeled reactants and reductants, to determine the effects of CO reactions with coal and to elucidate the role of H_2 in LRC liquefaction; and d) determining the effects of solvent on LRC liquefaction (specifically, to evaluate how start-up solvent composition influences lined-out product) and continued characterization of liquefaction products.

6.2 ACCOMPLISHMENTS

6.2.1 Catalyst Preparation and Testing

6.2.1.1 Background

Various catalysts have been used in coal liquefaction with molybdenum (Mo) and iron (Fe) catalysts being the most frequently used. In most cases, the Mo and Fe are combined with other metal oxides to form the catalysts. A catalyst formed using oxides of molybdenum and cobalt (Co) supported on alumina is used in the H-coal process. In other processes iron in the form of "red mud" is used, sometimes after mixing with elemental sulfur.

It is our objective in this study to design a highly active catalyst for LRC liquefaction. A series of supported iron catalysts was prepared with the guidance of Professor Hideshi Hattori, a catalyst expert from Hokkaido University who spent two months at Grand Forks this summer, and tested with model compounds (diphenylmethane (DPM) and diphenylether (DPE)) and coal/anthracene oil solvent with hydrogen gas (H_2) and hydrogen sulfide (H_2S). Selection of the specific iron catalysts to be prepared was based on the following experimental observations:

1. Adding H_2S when an iron catalyst was present promoted hydrocracking of DPM.

2. The effect of adding H_2S depended on the nature of the support for the iron catalyst. Comparing iron catalysts supported on SiO_2, ZrO_2, and TiO_2, the Fe_2O_3/SiO_2 catalyst had the greatest activity for hydrocracking DPM when H_2S was added.

3. The activities of Fe_2O_3/SiO_2 catalysts depended on the method of support preparation. Iron (III) oxide supported on high surface area silica exhibited higher activity than did Fe_2O_3 on low surface area SiO_2. An Fe_2O_3-SiO_2 catalyst prepared by coprecipitation did not have high activity.

4. Adding a small amount of molybdenum to an Fe_2O_3/SiO_2 catalyst caused an increase in activity.

5. An Fe_2O_3/TiO_2 catalyst was active not only for hydrocracking DPM but also for hydrocracking diphenylether DPE.

The catalysts that were prepared are listed in Table 6-1. The reasons for preparing the particular catalysts follow.

1. To determine the effect of SiO_2 (support) surface area, catalysts 1, 2, and 3 were prepared at different pH values from a Na-free Si source.

2. To examine the effect of different sources of the SiO_2 support, catalysts 4, 5, and 6 were prepared at the same pH values but using sodium metasilicate as the source.

TABLE 6-1

LIST OF CATALYSTS PREPARED

No.	Catalyst Composition (wt. ratio)	Source of Fe_2O_3	Support: Starting Material	Support: Precipitation Reagent	Support: pH
1.	Fe_2O_3/SiO_2 (1/9)	$Fe(NO_3)_3$	$Si(OC_2H_5)_4$	HNO_3	1
2.	Fe_2O_3/SiO_2 (1/9)	$Fe(NO_3)_3$	$Si(OC_2H_5)_4$	HNO_3	5
3.	Fe_2O_3/SiO_2 (1/9)	$Fe(NO_3)_3$	$Si(OC_2H_5)_4$	NH_4OH	11
4.	Fe_2O_3/SiO_2 (1/9)	$Fe(NO_3)_3$	Na_2SiO_3	H_2SO_4	1
5.	Fe_2O_3/SiO_2 (1/9)	$Fe(NO_3)_3$	Na_2SiO_3	H_2SO_4	5
6.	Fe_2O_3/SiO_2 (1/9)	$Fe(NO_3)_3$	Na_2SiO_3	H_2SO_4	11
7.	Fe_2O_3/SiO_2 (1/9)	$Fe(NO_3)_3$	$Si(OC_2H_5)_4$	H_2SO_4	1
8.	Fe_2O_3/SiO_2 (1/9)	$Fe(NO_3)_3$	$Si(OC_2H_5)_4$	NaOH	11
9.	Fe_2O_3/CaO (1/9)	$Fe(NO_3)_3$	$Ca(OH)_2$	-(calcined at 600°C)-	
10.	Fe_2O_3/La_2O_3 (1/9)	$Fe(NO_3)_3$	$La(NO_3)_3$	NH_4OH	9
11.	Fe_2O_3/ZrO_2 (1/9)	$Fe(NO_3)_3$	$ZrOCl_2$	NH_4OH	9
12.	Fe_2O_3/ZnO (1/9)	$Fe(NO_3)_3$	$Zn(NO_3)_2$	NH_4OH	9
13.	Fe_2O_3/SnO_2 (1/9)	$Fe(NO_3)_3$	$SnCl_2$	NH_4OH	9
14.	Fe_2O_3/TiO_2 (1/9)	$Fe(NO_3)_3$	$TiCl_4$	NH_4OH	9
15.	Fe_2O_3/TiO_2 (1/9)	$Fe(NO_3)_3$	$TiCl_4$ + $(NH_4)_2SO_4$	NH_4OH	9
16.	$MoO_3 \cdot Fe_2O_3/SiO_2$ (1/9/90)	$Fe(NO_3)_3$ + $(NH_4)_6MO_4O_{24}$	Commercial silica gel		
17.	$WO_3 \cdot Fe_2O_3/SiO_2$ (1/9/90)	$Fe(NO_3)_3$ + $(NO_4)_{12}W_{12}O_{41}$	Fisher Sci. Co.		
18.	$Co_3O_3 \cdot Fe_2O_3/SiO_2$ (1/9/90)	$Fe(NO_3)_3$ + $Co(NO_3)_3$	Catalog No. S-156, 14-20 mesh		
19.	$NiO \cdot Fe_3O_3/SiO_2$ (1/9/90)	$Fe(NO_3)_3$ + $Ni(NO_3)_2$	Lot No. 744571		
20.	Fe_2O_3/SiO_2 (1/9)	$Fe(NO_3)_3$			
21.	Fe_2O_3/SiO_2 (1/9)	$Fe_2(SO_4)_3$			
22.	$Na/Fe_2O_3/SiO_2$ (2/9/89)	$Fe(NO_3)$			
23.	$K/Fe_2O_3/SiO_2$ (2/9/89)	$Fe(NO_3)$			
24.	Fe_2O_3/TiO_2 (1/9)	$Fe(NO_3)$	Commercial, MCB, TX0685-1, Anatase		
25.	Fe_2O_3/TiO_2 (1/9)	$Fe(NO_3)$	Not prepared, rutile form of TiO_2		
26.	Fe_2O_3/Active C (1/9)	$Fe(NO_3)$	Commercial, Union Carbide, LCK, Columbia®		
27.	Fe_2O_3	$FeCl_3$	Vapor phase oxidation of $FeCl_3$		
28.	Fe_2O_3 + SiO_2	$FeCl_3$	Commercial JMC, Puratronic + Fisher SiO_2		
29.	$Co \cdot Mo/Al_2O_3$	$FeCl_3$	Harshaw Co-Mo-0401		

3. To examine the effect of precipitating agent, SiO_2 supports for catalysts 7 and 8 were prepared using a Na-free source of Si, but precipitating with H_2SO_4.

4. Catalysts of varying basicity were prepared to observe the effect of support basicity on activity (catalysts 9 through 15).

5. Sodium (Na)- and potassium (K)-poisoned catalysts were prepared to determine the effect of acidic sites on catalysis (catalysts 22 and 23). Poisoning acidic sites may avoid coke formation. At the same time, the interaction of Fe and K in a catalyst, which is present in Fischer-Tropsch and ammonia syntheses, will be examined.

6. Evaluation of additives to Fe_2O_3/SiO_2 resulted in catalysts 16 through 19. The additives were Mo, W (tungsten) , Co, and Ni (nickel).

7. A relatively high surface area TiO_2-supported catalyst (catalyst 15) was prepared in the presence of sulfate ions.

8. Because active carbon has very high surface area, an Fe_2O_3/Active C catalyst was prepared (catalyst 26). Highly dispersed Fe_2O_3 is expected, while resistance to coke formation may also result.

The catalysts were subjected to three types of reaction, and the reaction products were characterized. The three reactions were:

1. Hydrocracking of DPM to benzene and toluene; this is a model reaction for C-C bond cleavage.

2. Hydrocracking of DPE to phenol and benzene; this is a model reaction for C-O bond cleavage.

3. Liquefaction of Zap (North Dakota) lignite.

Reaction conditions are summarized in Table 6-2. The reactions were carried out using the tubing bomb apparatus. The surface areas of the catalysts were measured, and selected catalysts were to be subjected to detailed analyses using scanning electron microscopy (SEM) and electron probe micro analysis (EPMA).

6.2.1.2 Results

Table 6-3 summarizes the results obtained from testing the catalysts using the two model compounds and the surface areas of the support alone and of the prepared catalyst. Tables 6-4 and 6-5 show more detailed results obtained in the reactions of the model compounds, DPM, and DPE, respectively. Several observations have been made. For the hydrocracking of DPM:

1. Catalyst activity varies depending on the character of the support. This indicates interaction of the Fe_2O_3 with the support, and that the "state" of the Fe_2O_3 depends on the catalyst support.

TABLE 6-2

REACTION CONDITIONS

Reaction	Reaction Temperature, °C	Ratio of Reactant/ Catalyst by wt.	Pressure, psig (Cold Charge) H_2S	H_2	Reaction time, min.
Hydrocracking of diphenylmethane	425	10/1	100	700	20
Hydrocracking of diphenyl ether	425	10/1	100	1400	60
Liquefaction of coal	360	10/1	100	1400	20

2. Catalyst activity increased with increasing surface area of the support. Additional characterization of the catalyst and of Fe_2O_3/support interactions are required before definitive reasons can be established.

3. Adding oxides of Mo, W, Co, and Ni to the Fe_2O_3/SiO_2 catalyst enhanced catalytic activity. This may be caused either by multifunctional behavior of the additives and Fe_2O_3 or by altering the "state" of Fe_2O_3.

4. Adding Na and K reduced catalyst activity. This indicates the importance of acidic sites for the hydrocracking of DPM.

For the hydrocracking of DPE:

1. Catalysts containing Mo were more active than Fe-containing catalysts. Large quantities of hydrogenated products such as methylcyclopentane and cyclohexane were produced in the presence of the Mo-containing catalyst.

2. For Fe_2O_3 catalysts, activity increased with increased surface area of the support.

3. Adding Mo and W oxides to Fe_2O_3/SiO_2 catalysts enhanced activity.

4. Poisoning effects of adding Na and K were not as noticeable as compared with the hydrocracking of DPM.

It should be noted that the first tests with lignite were made at 425°C, and conversions were high for all catalysts, thus making differentiation virtually impossible. Therefore, reaction conditions for screening the catalysts with coal were modified so that the "base case" conversion and

TABLE 6-3

SUMMARY OF RESULTS FROM CATALYST TESTING

No.	Catalyst*	Wt. Ratio	Support: Start. Reagent	Support: pH	Support: Precip. Reagent	Surface Area, m^2/g: Support	Surface Area, m^2/g: Fe_2O_3/Support	Conversion, %: DPM	Conversion, %: DPE
1.	Fe_2O_3/SiO_2	1/9	$Si(OC_2H_5)_4$	1	HNO_3	704	579	74.1	35.1
2.	Fe_2O_3/SiO_2	1/9	$Si(OC_2H_5)_4$	5	HNO_3	459	382	25.0	19.0
3.	Fe_2O_3/SiO_2	1/9	$Si(OC_2H_5)_4$	11	NH_4OH	27.3	28.1	2.3	6.6
4.	Fe_2O_3/SiO_2	1/9	Na_2SiO_3	1	H_2SO_4	686	578		<14.5
5.	Fe_2O_3/SiO_2	1/9	Na_2SiO_3	5	H_2SO_4	404	349	5.6	<12.0
6.	Fe_2O_3/SiO_2	1/9	Na_2SiO_3	11	H_2SO_4		318	<1.0	< 6.3
7.	Fe_2O_3/SiO_2	1/9	$Si(OC_2H_5)_4$	1	H_2SO_4	633	568	14.0	<11.7
8.	Fe_2O_3/SiO_2	1/9	$Si(OC_2H_5)_4$	11	NaOH	41.2	38.8	<1.0	<15.5
9.	Fe_2O_3/CaO	1/9	$Ca(OH)_2$			12.7	0.89	<1.0	3.9
10.	Fe_2O_3/La_2O_3	1/9	$La(NO_3)_3$	9	NH_4OH	59.3	11.2	<1.0	7.2
11.	Fe_2O_3/ZrO_2	1/9	$ZrOCl_2$	9	NH_4OH	94	74.3	2.7	4.6
12.	Fe_2O_3/ZnO	1/9	$Zn(NO_3)_2$	9	NH_4OH	4.7	4.6	1.8	<11.5
13.	Fe_2O_3/SnO_2	1/9	$SnCl_2$	9	NH_4OH	29.2	28.4	5.7	<5.1
14.	Fe_2O_3/TiO_2	1/9	$TiCl_4$	9	NH_4OH	43.3	41.2	4.3	19.2
15.	Fe_2O_3/TiO_2	1/9	$TiCl_4+(NH_4)_3SO_4$	9	NH_4OH	61.1	56.3	12.5	10.2
16.	$MoO_3 \cdot Fe_2O_3/SiO_2$		Commercial silica gel			707	477	80.2	58.2
17.	$WO_3 \cdot Fe_2O_3/SiO_2$		Commercial silica gel			707	496	89.0	36.5
18.	$Co_3O_4 \cdot Fe_2O_3/SiO_2$		14-20 mesh			707	550	80.3	12.1
19.	$NiO \cdot Fe_2O_3/SiO_2$		Lot 71			707	502	81.2	24.1
20.	Fe_2O_3/SiO_2		Lot 71			707	521	71.2	33.3
21.	Fe_2O_3/SiO_2		Lot 71			707	344	36.7	<20.7
22.	$Na_2O/Fe_2O_3/SiO_2$		Lot 71			707	200	<1.0	5.6
23.	$K_2/Fe_2O_3/SiO_2$		Lot 71			707	205	<0.1	2.9
24.	Fe_2O_3/TiO_2	1/9	Commercial, MCB Anatase, TX0685-1			7.6	11.1	2.3	6.0
25.	Not Prepared					--	--	--	--
26.	Fe_2O_3/Active C		Comm. Union Carbide, LCK, Columbia^R			1006	946	3.6	9.7
27.	Fe_2O_3		$FeCl_3$ vapor phase oxidation			--	--	--	--
28.	α-Fe_2O_3 + SiO_2		Comm. JMC Puratronic + Fisher Sci.				(Fe_2O_3)12.0	<1.0	4.7
29.	$Co \cdot Mo \cdot/Al_2O_3$		Harshaw Co-Mo-0401				195	48.3	98.8

*For more detail regarding catalysts, see Table 6-1.

TABLE 6-4

HYDROCRACKING OF DIPHENYLMETHANE

No.	Catalyst* Composition	Conversion, %	Product Yield/mol/100 mol Reactant Charged					
			Cyclohexane	Benzene	Toluene	Ethylbenzene	Benzylcyclohexane	Unknown (Wt %)
1.	Fe_2O_3/SiO_2	74.1	0	75.3	68.3	1.0	1.0	1.4
2.	Fe_2O_3/SiO_2	25.0	0	24.1	23.4	0	0.8	0.2
3.	Fe_2O_3/SiO_2	2.3	0	1.9	2.0	0	0.3	0
4.								
5.	Fe_2O_3/SiO_2	5.6	0	4.4	4.7	0	0.4	0.6
6.	Fe_2O_3/SiO_2	<1.0	0	tr**	tr	0	0	0.5
7.	Fe_2O_3/SiO_2	14.0	0	14.6	13.4	0	0.1	1.4
8.	Fe_2O_3/SiO_2	<1.0	0	0	0	0	0	tr
9.	Fe_2O_3/CaO	<1.0	0	tr	tr	0	0	0.5
10.	Fe_2O_3/La_2O_3	<1.0	0	tr	tr	0	tr	0.7
11.	Fe_2O_3/ZrO_2	2.7						
12.	Fe_2O_3/ZnO	1.8	0	0.4	0.5	0	0.5	0.8
13.	Fe_2O_3/SnO_2	5.7	0	3.3	1.5	0	0	3.4
14.	Fe_2O_3/TiO_2	4.3	0	3.1	3.2	0	0.4	0.8
15.	Fe_2O_3/TiO_2	12.5	0	11.0	11.4	0	0.6	0.6
16.	$MoO_3 \cdot Fe_2O_3/SiO_2$	80.2	0	77.0	70.6	1.0	0.4	0.5
17.	$WO_3 \cdot Fe_2O_3/SiO_2$	89.0	0	91.3	82.4	2.0	0.2	0.2
18.	$Co_3O_4 \cdot Fe_2O_3/SiO_2$	80.3	0	79.9	73.9	1.4	0.2	1.4
19.	$NaO \cdot Fe_2O_3/SiO_2$	81.2	0	83.1	74.5	1.6	0.2	0.5
20.	Fe_2O_3/SiO_2	71.2	0	63.5	60.0	1.0	0.2	0.9
21.	Fe_2O_3/SiO_2	36.7	0	37.6	35.2	tr	0.1	0.7
22.	$Na/Fe_2O_3/SiO_2$	<1.0	0	tr	tr	0	0	0.8
23.	$K/Fe_2O_3/SiO_2$	<1.0	0	tr	tr	0	0	0.9
24.	Fe_2O_3/TiO_2	2.3	0	1.1	1.2	0	0.3	0.8
25.								
26.	Fe_2O_3/Active	3.6	0	2.2	2.4	0	0.4	0.3
27.								
28.	α-Fe_2O_3+SiO_2	<1.0	0	tr	tr	0	0	0.7
29.	$Co \cdot Mo/Al_2O_3$	49.6	0.4	46.4	42.4	0	6.9	1.4

* For more detail on catalysts, see Table 6-1.
** trace

TABLE 6-5

HYDROCRACKING OF DIPHENYL ETHER

No.	Catalyst Composition	Conversion, %	Product Yield/mol/100 mol Reactant Charged: Methyl cyclopentane	Cyclohexane	Benzene	Phenol	Unknown (Wt %)
1.	Fe_2O_3/SiO_2	35.1	8.0	4.7	25.3	20.4	0.4
2.	Fe_2O_3/SiO_2	19.0	4.0	5.5	14.8	14.1	0
3.	Fe_2O_3/SiO_2	6.6	0	3.0	3.5	6.3	0
4.	Fe_2O_3/SiO_2	<14.5	tr	tr	4.2	3.7	0
5.	Fe_2O_3/SiO_2	<12.0	0	2.1	3.4	3.6	0
6.	Fe_2O_3/SiO_2	< 6.3	0	0	0	0	0
7.	Fe_2O_3/SiO_2	<11.7	0	1.8	2.8	2.4	0
8.	Fe_2O_3/SiO_2	<15.5	0	0.9	2.4	2.5	0
9.	Fe_2O_3/CaO	3.9	0	1.4	3.2	3.0	0
10.	Fe_2O_3/La_2O_3	7.2	0	3.4	5.0	5.7	0
11.	Fe_2O_3/ZrO_2	4.6	0	2.6	4.7	2.0	0
12.	Fe_2O_3/ZnO	<11.5	0	1.0	2.2	1.8	0
13.	Fe_2O_3/SuO_2	< 5.1	0	tr	2.8	2.4	0
14.	Fe_2O_3/TiO_2	19.2	0	6.5	20.3	1.6	0.2
15.	Fe_2O_3/TiO_2	10.2	0	1.9	10.4	0.1	0
16.	$MoO_3 \cdot Fe_2O_3/SiO_2$	58.2	19.8	8.5	45.6	26.2	0.3
17.	$WO_3 \cdot Fe_2O_3/SiO_2$	36.5	9.1	5.1	30.3	25.9	0.2
18.	$Co_3O_4 \cdot Fe_2O_3/SiO_2$	12.1	2.4	3.2	12.3	9.5	0
19.	$NiO \cdot Fe_2O_3/SiO_2$	24.1	2.9	2.9	13.4	13.5	0
20.	Fe_2O_3/SiO_2	33.3	8.4	4.2	31.7	24.7	0.3
21.	Fe_2O_3/SiO_2	<20.7	1.2	2.4	9.6	10.5	0
22.	$Na/Fe_2O_3/SiO_2$	5.6	0	1.2	4.7	5.0	0
23.	$K/Fe_2O_3/SiO_2$	2.9	0	0.2	1.8	0.6	0
24.	Fe_2O_3/TiO_2	6.0	0	2.7	3.5	5.3	0
25							
26.	Fe_2O_3/Active C	9.7	0	2.8	6.5	9.8	0
27.							
28.	α-$Fe_2O_3+SiO_2$	4.7	0	2.2	3.2	3.7	0
29.	$Co \cdot Mo/Al_2O_3$	99.5	15.6	86.8	72.8	0	1.7

yields were reduced and so that differences between catalysts became more apparent. Figure 6-1 summarizes the runs performed to obtain the catalyst screening conditions. All runs were for 20 minutes using Zap lignite and A04 solvent with H_2 feed gas, while the temperature was varied from 350° to 400°C. At a temperature of ~360°C overall conversion of 65 pct (wt) allows for significant improvement because of increased catalytic activity. Also, at that temperature the yield of distillate is quite low (14 wt pct) and that of the soluble residum quite high (48 wt pct), again allowing room for improvement when a good liquefaction catalyst is present.

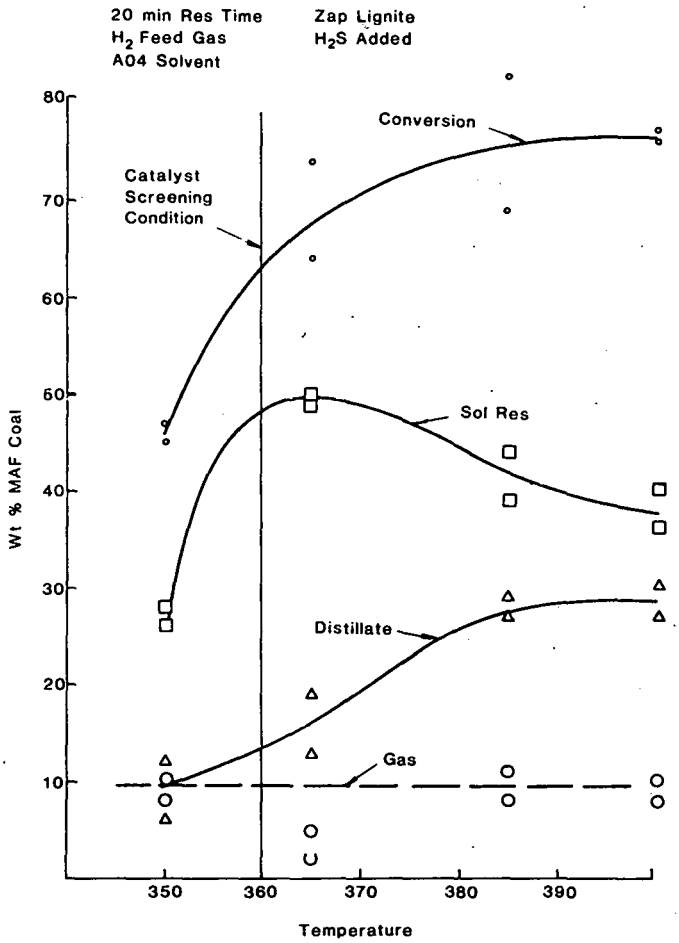

FIGURE 6-1. Conversion and yields of distillate, solid residuum, and gas as a function of temperature.

6.2.2 Low-Temperature Liquefaction

Hot-charge autoclave experiments were continued in the program to study low-temperature liquefaction of low-rank coal. Specific reaction conditions included using anthracene oil (A04) solvent, Zap lignite (from the Indian Head Mine) as the feed coal, and pure CO as the reductant at low temperature (typically 365° to 375°C). The reaction time was 60 minutes unless there was a subsequent, higher-temperature stage, in which case the low-temperature reaction time was 20 minutes.

Results presented last quarter indicated that low-temperature liquefaction (i.e., 365° to 380°C) was attractive because of relatively high overall conversion and high liquid yield as compared with results obtained at more commonly used reaction temperatures (420° to 460°C) using either syngas or pure hydrogen as the feed gases. Figure 6-2 shows time-sampled data obtained for low-temperature liquefaction using A04 solvent and pure CO as the feed gas. These data form the basis for the time-at-low temperature in staged liquefaction experiments. Although we hesitate to draw firm conclusions from time-sample results, the data do suggest that, up to a reaction temperature of 365°C, the conversion reaches its maximum value in less than 10 minutes. At temperatures of 375°C and higher, the conversion was initially lower than at lower temperatures, but the conversion increased with time over the 60-minute reaction time. The data may indicate a change in reaction mechanism in the 363°-375°C range of temperature, and the time-at-temperature is relatively unimportant at times greater than 10-15 minutes. Thus in staged operation, the time at the lower temperature in the presence of A04 solvent and CO was maintained at 20 minutes. These results led to a series of experiments to evaluate using low-temperature pretreatment in the presence of CO in the liquefaction scheme.

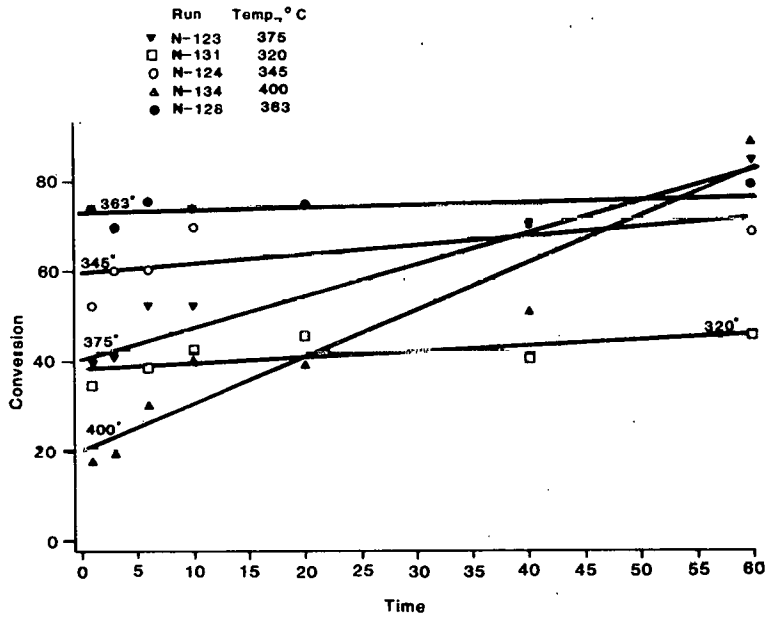

FIGURE 6-2. Conversion of Zap, North Dakota lignite as a function of time for a variety of temperatures (non-catalyzed).

6.2.2.1 Staged Liquefaction

In the staged reaction runs using the hot-charge autoclave equipment, the coal/solvent slurry is first hot-charged to an autoclave containing the reaction gas. The reaction mixture is held in the first-stage autoclave for the desired time; then it is discharged into the second reactor that contains solvent and gas. Thus, the solvent can be modified (i.e., a more hydrogenated solvent added) and the gas composition changed, although the first-stage solvent and a portion of the first-stage gas enter the second stage.

Figure 6-3 shows the results obtained when Zap lignite was subjected to low-temperature (365°-370°C) reduction in the presence of pure CO prior to being fed to a higher-temperature reactor (440°C). The higher-temperature reactor contained pure CO in one case (Run N175) and pure hydrogen in the other (Run N174). The high temperature second stage, with added hydrogen, converts the heavy fraction to lighter components--both distillate and hydrocarbon gases. This results in a lower yield of total liquid and higher gas yield, and the overall conversion was reduced somewhat, presumably because reactive species formed during hydrocracking recombine to form THF-insoluble organic matter (IOM).

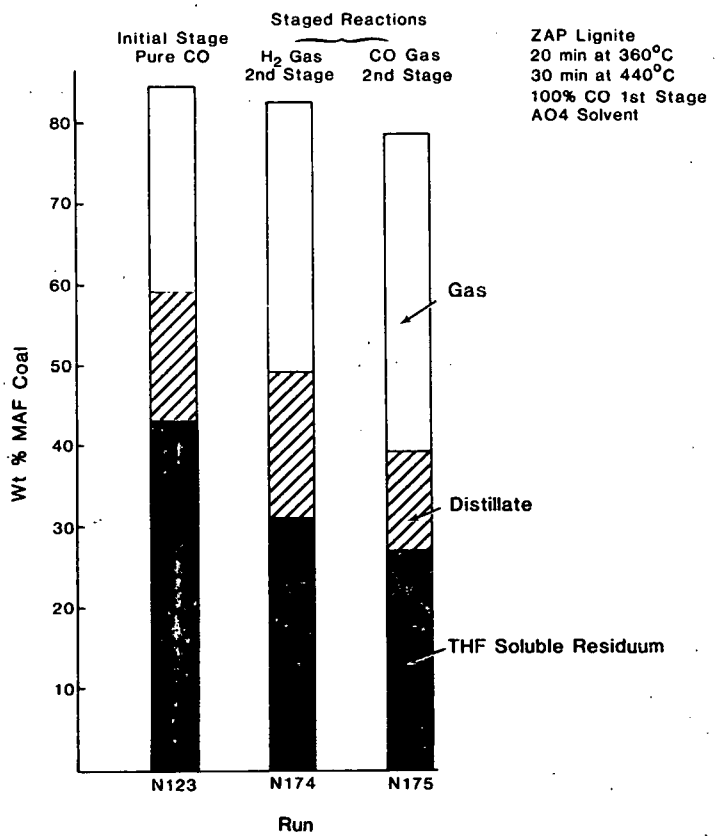

FIGURE 6-3. Comparison of varied reaction gas in staged reactions (non-catalyzed).

Using pure CO in the higher-temperature stage results in even higher yields of distillate and hydrocarbon gases at the expense of the heavier distillate and soluble residuum. The overall conversion dropped from 85.3 pct of the maf coal to 78.9 pct, indicating increased coking/repolymerization at the higher reaction temperature when hydrogen is not present. Also the total liquid yield is significantly reduced from 58.6 pct of the maf coal fed (at the low-temperature condition) to 38.0 pct after the high-temperature stage.

Figure 6-4 shows the effect of increasing temperature in the second stage in the staged liquefaction scheme. In each of the three runs, the first stage

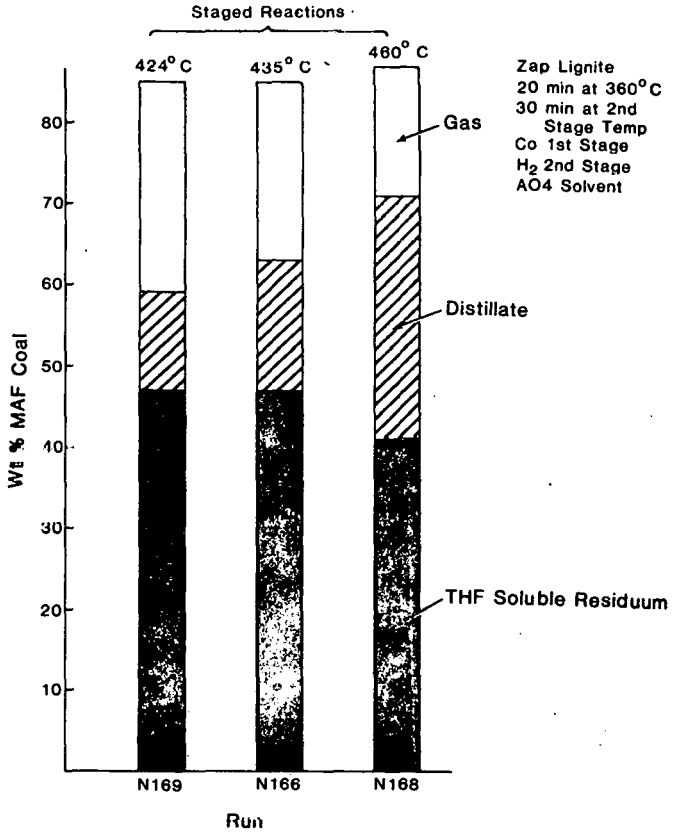

FIGURE 6-4. Effect of varied second stage temperature during staged operation (non-catalyzed).

temperature was about 350°C, the solvent was non-hydrogenated anthrancene oil (AO4), and the feed gas was pure CO. After 20 minutes, the reactor contents were forced into the second-stage reactor containing pure hydrogen and hydrogenated solvent (HA061) at higher temperature. The reaction mixture was held at the higher temperature for 30 minutes. The hydrogenated solvent presumably made hydrogen available to products resulting from thermal cracking at "normal" liquefaction temperatures (i.e., 420° to 460°C). The results show the overall conversion increasing slightly (from 85 to 87 pct) when the second-stage temperature increased from 424° to 460°C. In addition, the distillate yield increased from 12.1 pct of the maf coal fed at the lowest temperature to 29.3 pct at 460°C. The distillate material also became lighter with increasing temperature with a concurrent increase in hydrocarbon gases, and the yield of soluble residuum decreased.

Figure 6-5 summarizes the results obtained using the staged liquefaction scheme and compares those results with single-stage results at a variety of conditions. Some of the results have been reported previously and are shown here for completeness. Run N123 is a single-stage, low-temperature run using AO4 solvent and pure CO gas, while Run N174 is a two-stage experiment using

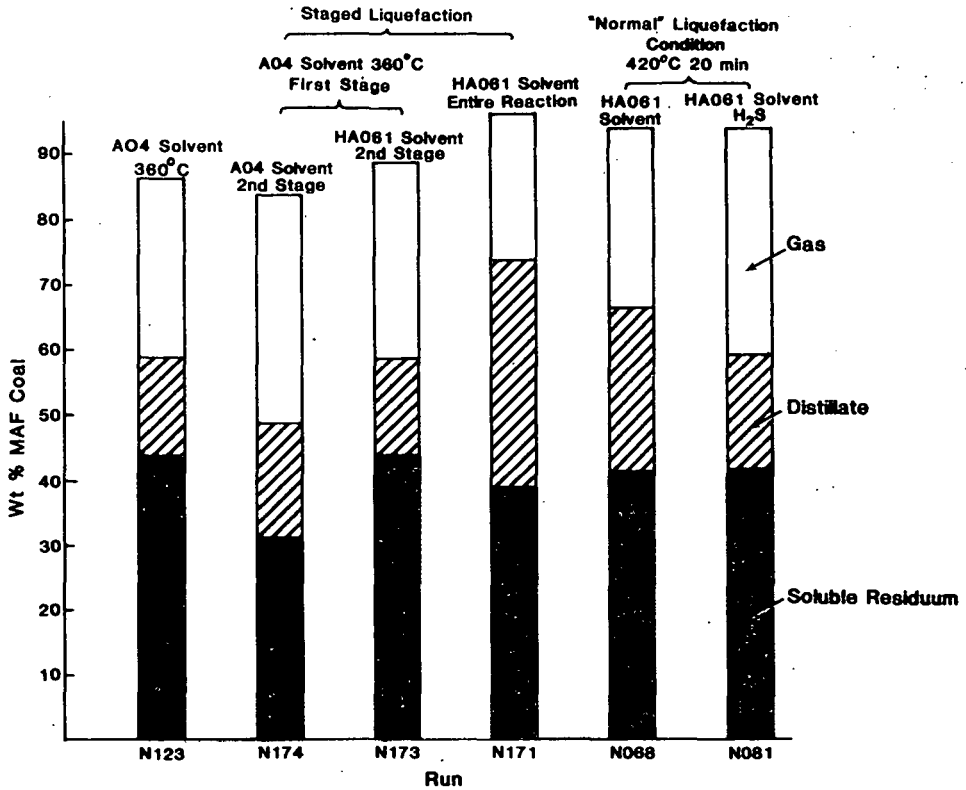

FIGURE 6-5. Effect of added hydrogen-donor solvent (HA061) in staged liquefaction.

A04 solvent in both stages; the second-stage temperature was 440°C. Carbon monoxide gas was used in the first-stage reactor, while pure hydrogen was charged to the second stage. In Run N173 a hydrogenated solvent was added in the high-temperature stage. Adding the second, high-temperature stage with hydrogen gas caused increased hydrocarbon gas production and increased yields of lighter distillate materials, while the yields of soluble residuum and heavy distillate decreased. Also, the overall conversion of maf coal declined slightly. This is consistent with earlier observations that heavy constituents are thermally cracked to light products at the higher liquefaction temperatures, but that some of the reaction products "repolymerize" to form THF-insoluble material. Making hydrogen available in the form of a hydrogenated solvent in the high-temperature stage causes conversion of heavy distillate to a lighter distillate product with a slight decrease in the yield of distillate. The yield of soluble residuum is unchanged when compared with the low-temperature run (Run N123), but higher than in Run N174 when non-hydrogenated solvent was used at high temperature.

In Run N171, the hydrogenated solvent was present in both the high- and low-temperature stages. All other conditions were nominally the same. It is clear from the results that distillate yield, at 34.2 pct of the maf coal fed, was the highest of any of the runs, and the overall conversion was high, 94 pct of the maf coal fed. The hydrocarbon gas yield does not indicate extensive cracking of the solvent as had been seen previously at high temperatures.

The data from staged liquefaction runs, when compared with single-stage "higher" temperature, indicate that the low-temperature stage contributes to higher distillate yields at the expense of soluble residuum. Also the fraction of light distillate is greater in staged operation. Total liquid yield (distillate plus soluble residuum) is 72 pct of the maf coal for the staged run, 65 pct for the single-stage operation at 420°C, and 58 pct when H_2S was added for single-stage liquefaction.

There are a number of additional sets of conditions, including adding H_2S, that will be run in an effort to further improve low-temperature operations. However, at this point, it appears that low-temperature liquefaction with nearly pure CO present offers promising possibilities in staged low-rank coal liquefaction.

6.2.2.2 Gas Composition

Table 6-6 summarizes data that have been collected over a relatively long period of time. The data show the effects of changing feed gas composition at different temperatures, for two different low-rank coals, in the presence/absence of H_2S, and for two different solvents (i.e., AO4--an unhydrogenated anthracene oil; and HAO61--hydrogenated AO4). There are four pairs of runs from which comparisons can be drawn. The following observations can be made:

1. At "normal" liquefaction temperatures (420°C in the presence of H_2S and 460°C) increasing the fraction of hydrogen in the feed gas generally results in increased liquid yield (i.e., distillate plus soluble residuum) and increased hydrocarbon gas yield. These same trends were noted for the staged runs where the second-stage temperature was 440°C.

2. At low liquefaction temperature (i.e., 380°C), the total liquid yield declined with increasing hydrogen concentration in the feed gas, and hydrocarbon gas yield was relatively low in all instances.

Thus, it is seen that the roles of the CO and H_2 feed gas constituents vary depending on the reaction temperature.

6.2.3 Solvent Effects

A significant effort is underway to determine the effect of various parameters, including coal, start-up solvent, and catalysts (i.e., H_2S), on low-rank coal liquefaction recycle solvent. Work has included several CPU recycle runs followed by extensive product analysis. Recycle solvent can be separated into two general physical classes, distillate and non-distillate. The light distillate has been analyzed in great detail by methods developed at UNDERC under previous DOE sponsorship, while characterization of the non-distillable or heavy ends have been limited in detail. Increased emphasis has been directed at more detailed analysis of the non-distillable recycle solvent.

6.2.3.1 Comparison of Aromaticity in the Distillate

Silica gel column fractionation of CPU recycle slurry ASTM D-1160 distillates is commonly used at UNDERC to prepare fractions for capillary GC and

TABLE 6-6

EFFECTS OF GAS COMPOSITION ON LOW-RANK COAL LIQUEFACTION

Run Number	NO93	NO94	NO29	NO30	NO36	NO35
Coal	Big Brown	Big Brown	Big Brown	Big Brown	Zap	Zap
Solvent	HA061	HA061	A04	A04	A04	A04
Additive	H_2S	H_2S	None	None	None	None
Run Time, min.	20	20	20	20	20	20
Avg. Temperature	418	419	457	455	457	456
Max. Press., psig	3800	3940	3695	3790	3805	3820
Pct H_2 Feed Gas	.0	44.2	52.3	100.0	51.5	100.0
Moisture, gms	99.6	99.6	95.8	94.9	96.4	96.5
Net Yields, wt % maf coal charged):						
C_1-C_3	2.2	2.4	5.9	8.2	6.8	5.3
Gas + H_2O	26.2	19.8	37.8	27.9	34.2	17.6
Lt. and Mid. Oil	10.0	17.1	15.4	30.2	28.0	33.1
Hvy. Oil	12.1	6.6	-11.3	-7.9	-6.6	-6.6
Total Liquid	69.7	74.1	31.7	45.2	41.8	46.7
Solvent Rec.	109.1	109.8	88.0	88.3	90.3	92.3
Conversion	95.9	94.0	69.5	73.2	76.0	64.3
Mat. Bal. Closure	93.3	98.8	95.9	95.1	94.1	91.6

TABLE 6-6 (Continued)

EFFECTS OF GAS COMPOSITION ON LOW-RANK COAL LIQUEFACTION

Run Number	N175	N174	N160	N159	N157	N158
Coal	Zap	Zap	Zap	Zap	Zap	Zap
Solvent	A04-A04	A04-A04	A04	A04	A04	A04
Additive	None	None	None	None	None	None
Run Time, min	20-60	20-60	60	60	60	60
Avg. Temperature	365-440	370-439	380	383	380	383
Max. Press., psig	4000-2385	4000-2275	3490	3550	3500	3580
Pct H_2 Feed Gas	.0	78.6	.0	24.9	50.2	75.1
Moisture, gms	72.9	69.1	99.3	100.1	97.6	105.2
Net Yields (Wt % maf coal charged):						
C_1-C_3	4.6	6.8	.6	.7	.7	.7
Gas + H_2O	40.9	34.6	5.2	13.0	27.7	26.0
Lt. and Mid. Oil	26.8	16.3	26.4	9.0	23.4	22.5
Hvy. Oil	-15.2	2.3	1.4	9.9	-15.2	-15.6
Total Liquid	38.0	49.1	82.4	61.5	54.4	49.4
Solvent Rec.	101.5	102.2	108.8	103.1	99.8	98.4
Conversion	78.9	83.7	87.5	79.5	82.1	75.3
Mat. Bal. Closure	93.7	103.7	95.3	93.9	97.4	95.8

GC/MS. In a recent GC/MS study, the heavy aromatic fractions from CPU runs with four coals (Beulah, North Dakota, lignite; Big Brown, Texas, lignite; Wyodak, Wyoming, subbituminous coal; and Powhatan, Ohio, bituminous coal) processed at 460°C with H_2 at 2600 psig total pressure, showed a correlation between the sum (wt pct of oil) of these fractions and coal rank. With the exception of the Beulah lignite, an increase in aromaticity of the solvent is shown with increasing rank (Figure 6-6). The sum of silica gel column fractions 5 through 10 was used as it has been suggested that it is a better measure of solvent aromaticity than f_a values from ^{13}C or ^{1}H NMR spectra of unseparated samples. This is due to the presence of phenols and alkanes in the unseparated samples making these NMR measurements very inaccurate. GC/MS work during this study resulted in identification of five previously unreported compounds. These include 1-phenylnaphthalene, 2-phenylnaphthalene, 1-phenyltetralin, 2-phenyltetratin, and 2,2^{1}-binaphthyl.

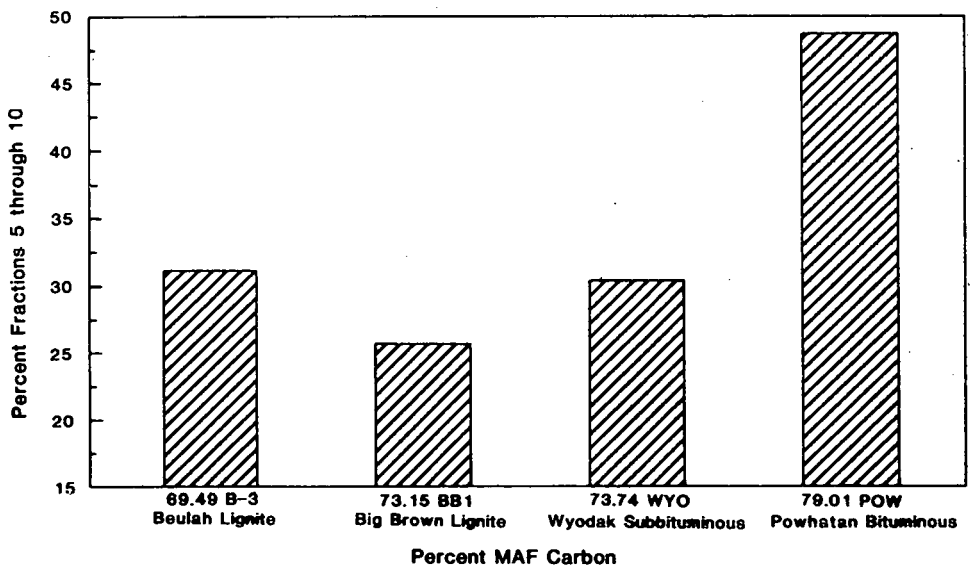

FIGURE 6-6. Percent fractions 5 through 10 versus coal rank.

These results were presented at the American Chemical Society 186th National meeting in Washington, D.C., August 28 to September 3, in a paper entitled "Characterization of Liquefaction Recycle Slurry by Capillary GC/MS" by David J. Miller and Sylvia A. Farnum (Analytical Division Abstract No. 64).

6.2.3.2 Comparison of Distillate/Non-distillate Separations

An ASTM D1160 distillation subjects the non-distillate portion of the recycle solvent to rather severe conditions, including temperature up to its smoke point. As a result, analysis of the non-distillate portion of the recycle solvent after being subjected to an ASTM D1160 distillation was questionable. A comparison of the non-distillate before and after an ASTM D1160 distillation was recently initiated.

The non-distillable portion from ASTM D-1160 distillation of the CPU recycle product contains the minerals from the lignite as well as non-volatile heavy organic materials. To separate the minerals and intractable organics, a Soxhlet extraction (20 hours) with chloroform was carried out. Further extraction with tetrahydrofuran gave only a 5- to 9-pct additional yield. The chloroform soluble extract was freed of solvent using a rotary evaporator and chromatographed on an open silica gel column using a modified Mobil SESC separation (1). The results are shown in Table 6-7. The scheme was successful in separating the extract into compound classes as shown by the ^1H NMR spectra. Assignment of compound class in Table 6-7 was based in part on these NMR spectra and in part on infrared analyses of the fractions. The ^1H NMR spectra were also different for comparable fractions of CPU runs with different coals. Those for Run 53 which processed POW1, a bituminous coal, showed the most marked differences from the rest.

TABLE 6-7

ANALYSIS OF FRACTIONS, $CHCl_3$ SOLUBLE VACUUM BOTTOMS, CPU BOTTOMS RECYCLE RUNS, 450°C, 2600 PSIG

CPU Run Parameters:				
Run No.	45	53	64	66
Coal[a]	B3	POW1	BB1	BB1
Startup Solvent	HAB1[b]	SSOL[c]	SSOL	SSOL
Recycle Pass No.	12	19	13	13
Processing Gas	H_2	H_2	H_2	H_2/CO
Wt % of Bottoms Extracted by $CHCl_3$	28.7	44.5	50.9	39.5
Modified SESC Separation:		Wt % of $CHCl_3$ Soluble Extract		
Fraction No.--(Compound Class)				
1 & 2 (alkanes)	0.23	0.14	0.60	0.29
3 (aromatics)	34.0	2.61	32.2	31.7
4 (heavier aromatics)	11.6	6.25	8.55	18.9
5 (heavy aromatics)	7.26	6.69	6.52	4.48
6 (phenols)	13.1	5.79	14.7	13.3
7-10 (undefined polars)	25.8	25.4	23.9	28.4
Recovery	92.0	46.9	86.5	97.1

[a] B3, North Dakota Beulah lignite
POW1, Ohio bituminous coal, Powhatan
BB1, Texas Big Brown lignite

[b] HAB1, hydrogenated anthracene oil bottoms

[c] SSOL-surrogate solvent, 60% anthracene oil, A04, 40% SRC II middle distillate Ft. Lewis, WA.

[d] In our modification Fraction 3 is eluted with benzene.

When the NMR spectrum for each coal pot residue fraction was compared with the spectrum of a corresponding distillable oil fraction, there was a very close correspondence. Recognizable features of the well-characterized distillable fraction were repeated in the nondistillable fraction. This very notable similarity confirms that the structure of the heavy pot residue resembles that of the distillate. Differences lie in the size of molecules and in polarity.

Having determined that the pot residue resembles the distillate, it was possible to address two other related areas: 1) Since the pot residue is likely to begin to undergo decomposition when heated to the smoke point in the D-1160 distillation, it is desirable to separate the heavy ends in some other way. If such a separation were used, the overlap between distillable oil from the ASTM distillation and the lighter fraction from the second separation would have to be investigated; and 2) It is desirable to design a simpler separation for the heavy ends that would yield larger fractions and have less chance of chromatography solvent adulteration. The solvents used in the SESC separation, especially tetrahydrofuran and pyridine, are difficult to maintain in a pure condition and often add a considerable amount of non-coal-derived material to column fractions.

6.2.3.3 Separation of Heavy Ends by Solubility and Comparison of Method With Distillation

Product slurry (5g-20g) was separated into methylene chloride solubles and insolubles using a 40:1 volume-to-weight ratio of solvent-to-slurry at room temperature with stirring under N_2 gas for 4 hours. Methylene chloride insoluble material (including mineral matter, insoluble organic materials, and unreacted coal) was removed with a fritted glass funnel (40-60 micron) and was set aside for later consideration. The methylene chloride soluble extract was stripped of solvent using a rotary evaporator at room temperature and was further separated with the same amount of pentane as methylene chloride originally used. The pentane soluble fraction (PSHE) and the pentane insoluble fraction (PIHE) were analyzed separately. An NMR comparison of the polar fractions is shown in Figure 6-7.

To compare the two methods of separation, the distillate from the ASTM distillation and the pshe fraction from the solubility separation were both fractionated and analyzed by UNDERC standard methods (silica gel column separation followed by fraction analysis by capillary GC). It appears that, except for small differences, the PSHE fraction closely resembles the ASTM distillate.

When the PIHE fraction derived from the solubility separation method is compared with the ASTM-D1160 pot residue from ASTM distillation of the same slurry, short silica column separations (pentane, issoctane, methylene chloride, methanol) gave different fraction distributions, with the aromatic fraction larger in the distillation pot residue. This shows differences in composition, probably due to heat-induced reactions (such as aromatization) when the pot residue is heated to its smoke point. The PIHE extract also differed considerably in volatility from the ASTM D-1160 pot residue.

For these reasons our further efforts in characterization will center on the slurry separated heavy fraction, not the pot residue from ASTM D-1160 distillation.

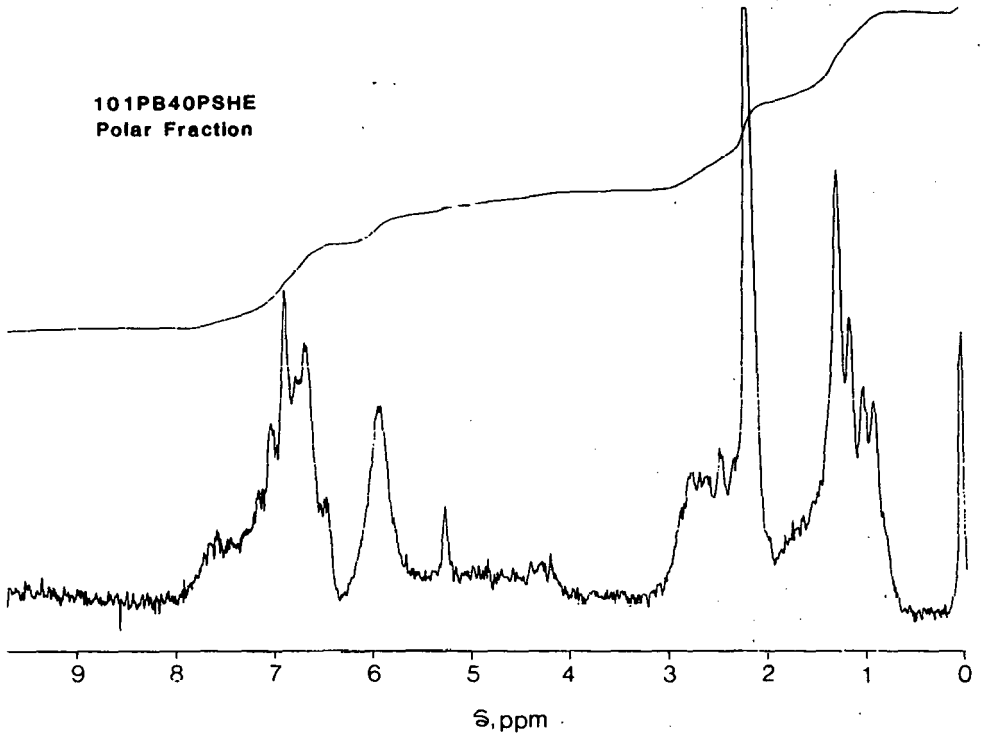

a.)

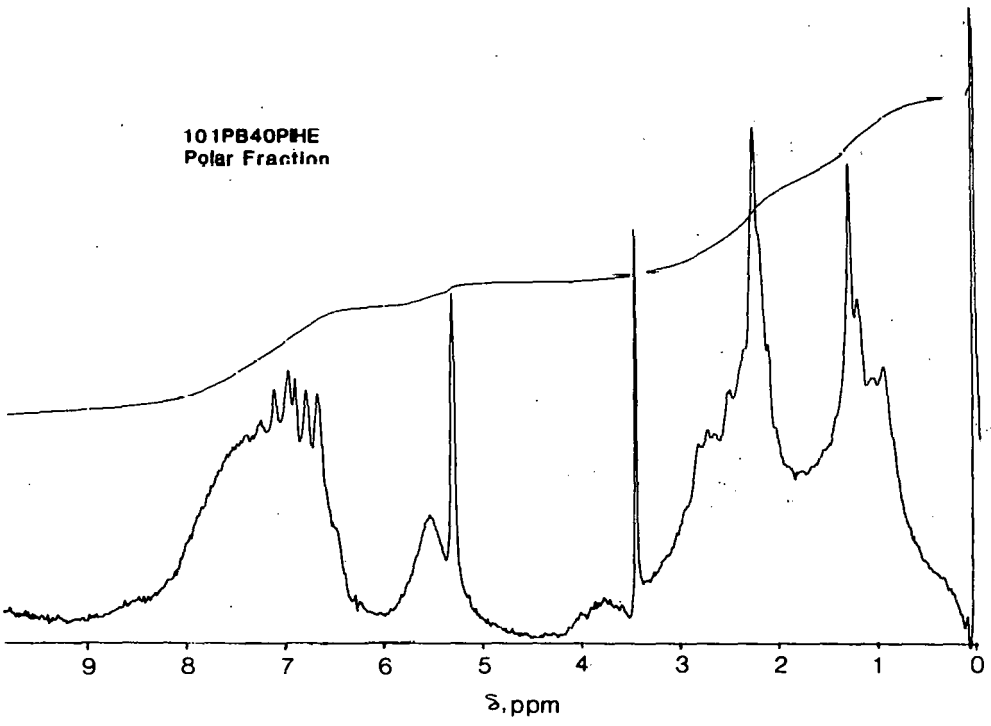

b.)

FIGURE 6-7. NMR comparison of liquefaction product polar compound fractions separated by methylene chloride extraction.
a) pentane soluble fraction
b) pentane insoluble fraction

6.2.4 Extraction of Hydrocarbons From Liquefaction Coals

6.2.4.1 Purpose Of Study

Extractions of seven coal samples used in CPU liquefaction studies were carried out to: 1) Compare n-alkanes produced in bottoms recycle coal liquefaction with n-alkanes extracted from coal under mild conditions; 2) Provide baseline extraction data for supercritical extraction; 3) Compare extract profiles from the coal tested by capillary GC; and 4) Carry out preliminary screening for the presence of biological markers and waxes.

6.2.4.2 Experimental Procedure and Results

The seven coal samples extracted are listed in Table 6-8 with their elemental and ash analyses.

TABLE 6-8

ANALYSIS OF COALS EXTRACTED

	% maf Coal					% mf Coal
	C	H	N	S	O	Ash
Beulah 3 (ND)	69.49	4.43	0.99	2.81	22.28	16.44
Morwell (Aust.)	70.64	5.01	0.46	0.33	23.56	3.55
Big Brown 1 (TX)	73.15	5.22	1.40	1.30	18.93	13.29
Big Brown 2 (TX)	74.00	6.09	1.22	1.21	17.48	18.74
Wyodak (WY)	73.74	5.38	1.22	0.53	19.13	8.15
Highvale (AL)	74.41	4.92	0.95	0.20	19.52	12.61
Powhatan (OH)	79.01	5.43	1.29	3.92	10.35	10.22

The extraction procedure is shown in Figure 6-8. Extractions were carried out in a Soxhlet apparatus with the solvents indicated on the figure. Each extracted fraction was divided into a hexane soluble and a hexane insoluble fraction. The results are shown in Table 6-9. Each of these fractions contained some long chain waxes, tentatively identified as long chain alcohol esters of long chain fatty acids. The only fraction that contained the hydrocarbons of interest was the chloroform soluble-hexane soluble fraction (CHX). The CHX fraction was chromatographed to yield the characteristic profile for the coal. The best results were obtained using a J&W DB5 60M fused silica capillary column with H_2 carrier gas and a flame ionization detector. Temperature programming from 50° to 125°C at 0.5°C/min, from 125°C to 250°C at 1.0°C/min, and from 250° to 350°C at 1.5°C/min, followed by an isothermal plateau at 350°C was used. Thermogravimetric analyses showed that >90 pct of the extracts were volatile.

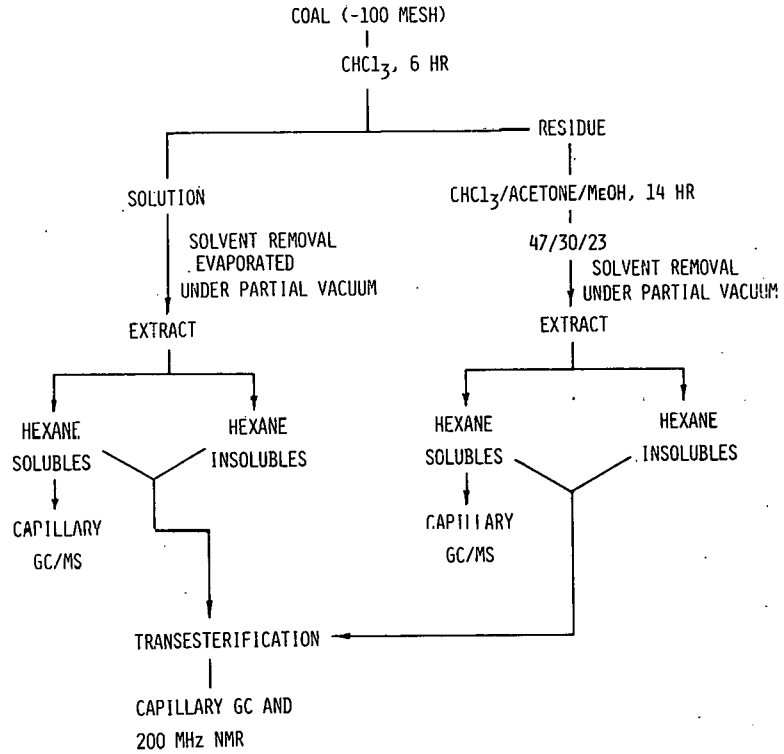

FIGURE 6-8. Sequential soxhlet extraction of coal.

TABLE 6-9

SEQUENTIAL EXTRACTION OF COALS WITH $CHCl_3$ (SOXHLET), $CHCl_3$: ACETONE: METHANOL, 47:30:23, AZEOTROPE (SOXHLET) AND SEPARATION OF HEXANE SOLUBLES (WT % MAF COAL, DUPLICATES WERE AVERAGED)

	Total $CHCl_3$ Soluble (Soxhlet)	Hexane Soluble Portion of $CHCl_3$ Extract	Total Azeotrope Soluble (Soxhlet)	Hexane Soluble Portion of Azeotrope Extract
B3	2.8	1.0	1.6	0.13
MOC[a]	0.82	0.58	1.7	0.59
BB1[a]	4.2	1.7	2.2	0.16
BB2	3.7	1.7	2.4	0.19
WY01	3.2	2.9	5.0	0.21
ALB1	0.58	0.35	1.8	0.28
POW1	0.70	0.51	5.8	1.1

[a]Values given from single extraction only.

There were some striking similarities and differences between profiles for the coal CHX extracts. The profiles for CHX extracts of MOC, BB1, and BB2 were very similar. They show no detectable alkanes and very few peaks until 230 min when the maximum temperature was reached. Between 230 and 320 minutes a large group of peaks form a dense envelope.

The capillary GC profiles for B3 and WY01 extracts are also strikingly similar, with nearly every major GC peak having a counterpart in each chromatogram. The ALB1 extract chromatogram shows some similarity to the WY01 trace, while the POW1 extract profile is different. All of the GC profiles for B3, WY01, ALB1, and POW1 CHX extracts have continuous baseline resolved peak distributions from about 50 to 350 minutes with various recognizable patterns. From duplicate extractions of the same coal and by comparing BB1 and BB2 extracts, it was seen that the profiling of the hydrocarbon extracts was reproducible and thus may be used to identify and group coals.

Each CHX fraction was also subjected to analysis by GC/MS. A total ion current (TIC) chromatogram was obtained which matched the FID profile. From the TIC chromatogram, selected ion chromatograms were obtained using the HP-5985B software. Some of the ions selected were M/Z 141 for alkanes, methyl- and dimethylnaphthalenes, M/Z 91 for alkyl benzenes, M/Z 105 for disubstituted benzenes, M/Z 198,183 for cadalene, M/Z 206,191 for sesquiterpenes, M/Z 208, 193 for sesquiterpanes, M/Z 191 for nearly all terpanes, and M/Z 217 for steranes. The compounds identified using these methods are given in Tables 6-10 and 6-11.

The sesquiterpenes (M/Z 206) found in the B3, WY01, and ALB1 extracts were tentatively assigned bicyclic C_{10} structures with 5 substituent carbon atoms. Baset, Pancirov, and Ashe (2) reported at least 9 M/Z 206 compounds in extracts of Wyodak coal which probably correspond to those we found. Pyrolyates of Wyodak did not contain the M/Z 206 compounds (2). No mass spectra were included in the Baset reference so no direct comparisons were made. Gallegos (3) also reported M/Z 206 sesquiterpenes. Interestingly, these compounds were found in pyrolysates of Wyodak as well as five other coals. No attempt was made to assign structures.

Figure 6-9 shows the M/Z 206 and TIC chromatograms for the WY01 extract. The individual mass spectra of the M/Z 206 sesquiterpenes found in our study lead us to propose structures similar to those shown in Figure 6-10 reported by Philip et al. (4) and Richardson and Miller (5). The M/Z 206 compounds would, however, have a double bond in one of the two rings.

The individual mass spectrum (M/Z 276) of another hydrocarbon identified in WY01, B3, and ALB1 (Highvale, Alberta subbituminous coal) (Figure 6-11) is identical with that reported by Philip and was assigned the structure I shown in Figure 6-11.

A number of pentacyclic triterpenes with M/Z 398, 412, 426, 440, and 454 were detected. Only one was positively identified. The compound having Mass 412 was assigned the structure II, Figure 6-12, oleanane (6).

The pristane percentages were low or not-detected in lignites, but were appreciable in the POW1 bituminous coal extract.

TABLE 6-10

ACYCLIC HYDROCARBONS FOUND IN EXTRACTS OF COALS AND THEIR DISTILLABLE LIQUEFACTION PRODUCTS
(Capillary GC, Area Percent, FID)

	Retention Time, min.	B3 Coal Extract	WY01 Coal Extract	ALB1 Coal Extract	POW1 Coal Extract
Isoprenoids:					
pristane (2,6,10,14,tetramethyl-pentadecane)	168.9	0.15			1.35
n-alkanes:					
C-14					
C-15	125.8	0.82			
C-16					
C-17					
C-18					
C-19	194.1	0.74			0.49
C-20	205.0	0.99			0.41
C-21	215.6	1.38			0.26
C-22	223.9	1.22	1.04		0.46
C-23	232.7	0.69	0.73	1.38	0.31
C-24	241.2	0.67	0.33	0.43	0.46
C-25	249.2	1.89	0.82	1.85	0.34
C-26	256.9	1.55	0.57	0.37	0.29
C-27	264.5	2.92	0.99	0.92	0.33
C-28	271.6	0.42	0.31	0.31	0.25
C-29	278.5	0.76	0.98	0.77	0.25
C-30	285.1	0.57	0.52	0.2	0.25
C-31	290.2	0.29	0.56	0.59	0.10
C-32	296.1				0.02
C-33	300.1				0.03
C-34	304.3				0.001
C-35	308.7			0.19	0.03
C-36	312.0			0.09	0.004
C-37	316.6				0.01
C-38	320.4				0.006
C-39	324.0				0.008

TABLE 6-11

OTHER HYDROCARBONS FOUND IN EXTRACTS OF COAL CAPILLARY
GC AND GC/MS, AREA %, FID

		Retention Time, Min.	m/e, Parent Ion	Capillary GC, Area %						
				B3	MOC	BB1	BB2	WY01	ALB1	POW1
Miscellaneous:										
naphthalene		47.9			0.32			0.18	0.12	1.2
2-methylnaphthalene		72.0			0.29			0.19	0.38	2.7
1-methylnaphthalene		75.6			0.04			0.09	0.13	2.0
C_2-naphthalene		95.3								0.68
cadalene		160.4	198	0.31					1.3	1.3
Alicyclic terpenoids:										
$C_{15}H_{26}$ sesquiterpene	a	100.7	206					2.8		
"	b	104.8	206					1.0		
"	c	106.8	206	1.9				13.2	0.70	
"	d	108.9	206	1.12				3.3		
"	e	111.2	206	0.24				8.3	0.17	
"	f	113.0	206					4.6	0.27	
"	g	114.9	206	2.3				1.5	1.9	
"	h	116.2	206	0.10				0.96	0.17	
$C_{20}H_{36}$ tricyclic alkane		230.3	276	1.7				0.96	0.46	
?		233.4	252						0.50	
$C_{17}H_{30}$ tricyclic alkene		236.4	234	1.2				1.0	0.10	0.10
?		272.5	Not Shown				0.66			
$C_{29}H_{50}$		284.6	298						0.27	0.13
$C_{30}H_{52}$		285.2	412							0.13
$C_{31}H_{54}$		287.0	426				3.3			
$C_{31}H_{54}$		295.8	426							0.03
$C_{32}H_{56}$		312.0	440		0.29	3.0	1.1			
$C_{33}H_{58}$		321.7	454	0.07	0.10	1.7	3.5			

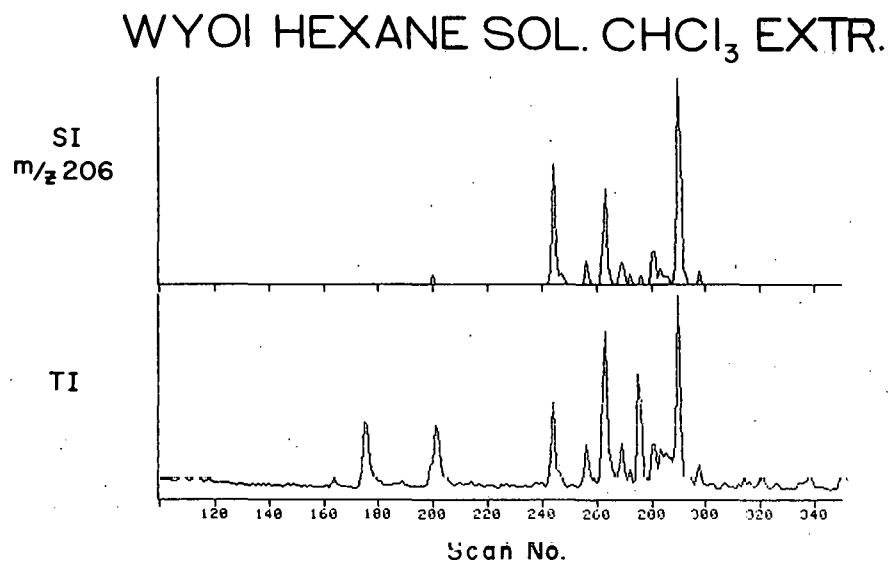

FIGURE 6-9. a) M/Z 206 and b) TIC chromatograms of Wyodak subbituminous coal HCL_3.

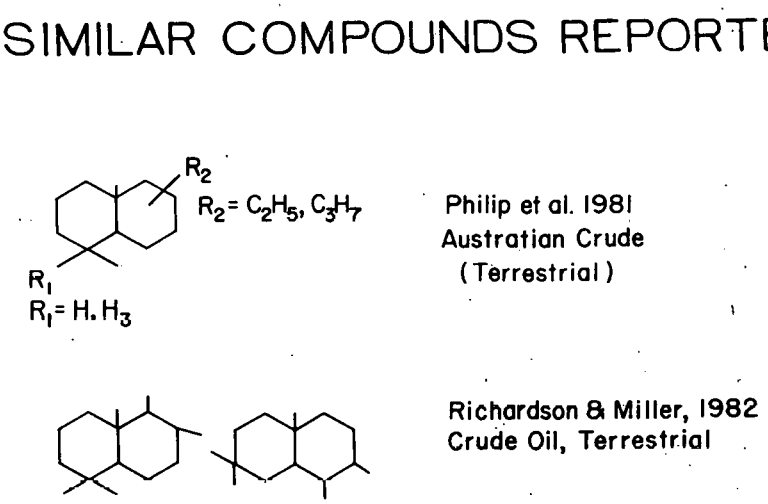

FIGURE 6-10. Proposed structures for M/Z 206 sesquiterpenes.

The n-alkane extract distributions for B3, WYO1, and POW1 were compared with the distribution of n-alkanes in CPU bottoms recycle liquefaction runs after 13-19 recycle passes (Figures 6-13, 6-14, and 6-15). Odd/even carbon number preference indices (CPI) are shown in the figures. If the percentages

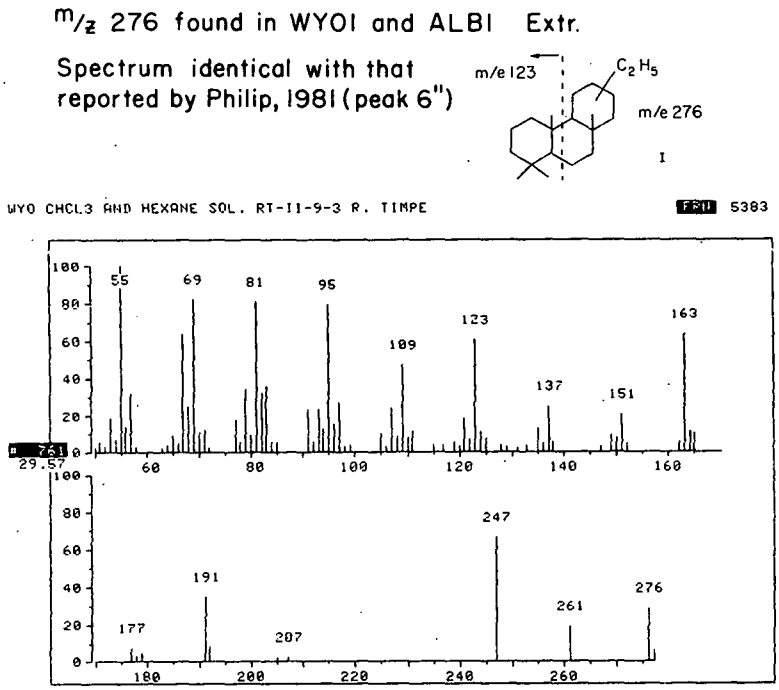

FIGURE 6-11. Individual mass spectrum of Wyodak and Highvale subbituminous coal extracts.

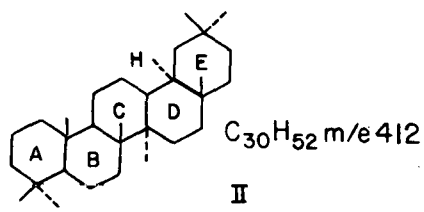

Oleanane

Ekweozor et al., 1979

FIGURE 6-12. Compound structure for oleanans identified and assigned M/Z 412.

of n-alkanes are calculated as wt pct maf coal, the results show (Table 6-12) that there are approximately 5 to 10 times larger quantities of n-alkanes formed during liquefaction than can be extracted. The distribution and CPI are very different for the coal liquefaction products. The same trend was seen by Baset (2). He reported 0.4 wt pct maf alkanes extracted from Wyodak coal and 2.4 wt pct maf alkanes obtained by pyrolysis of the coal.

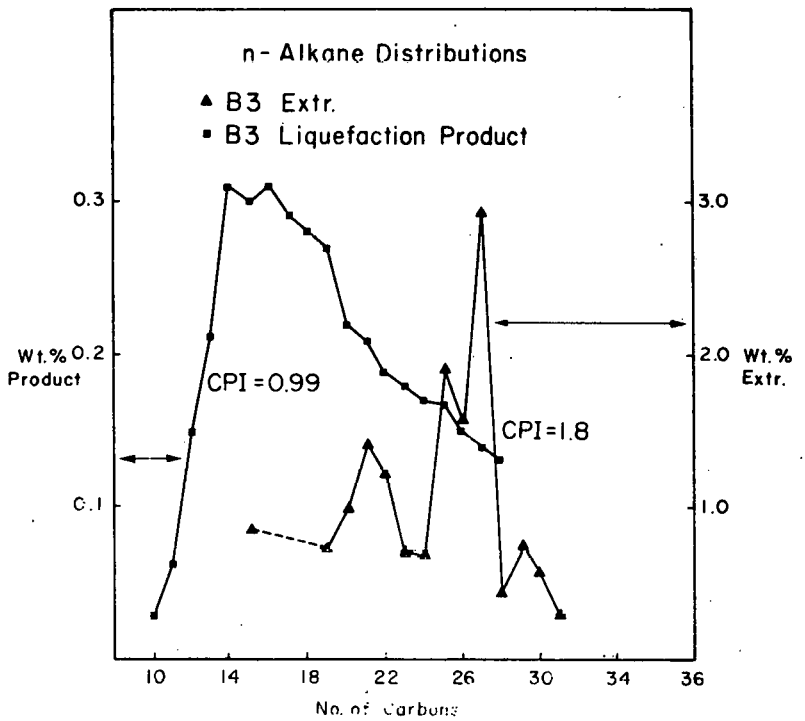

FIGURE 6-13. Comparison of n-alkane extract distribution from Beulah lignite, n-alkane distribution from CPU bottoms recycle product (Beulah lignite feed coal).

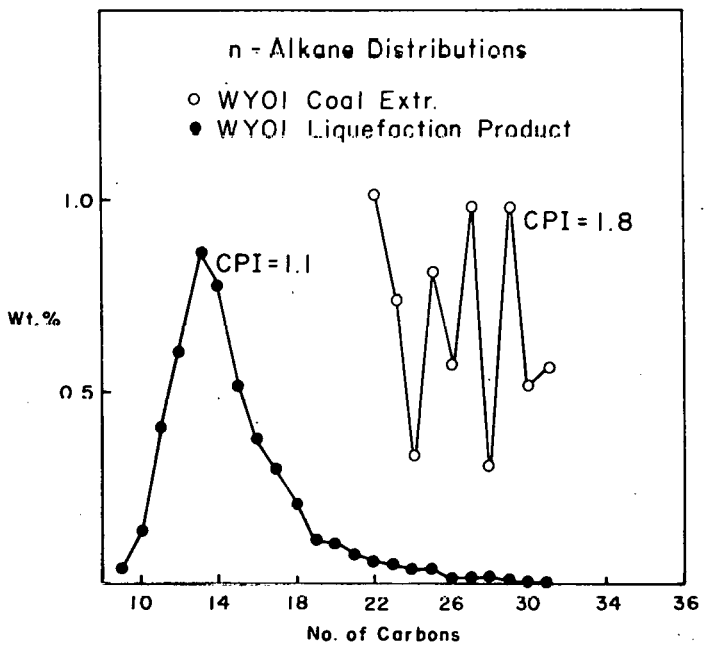

FIGURE 6-14. Comparison of n-alkane extract distribution for Wyodak subbituminous coal and n-alkane distribution from CPU bottoms recycle product (Wyodak subbituminous feed coal).

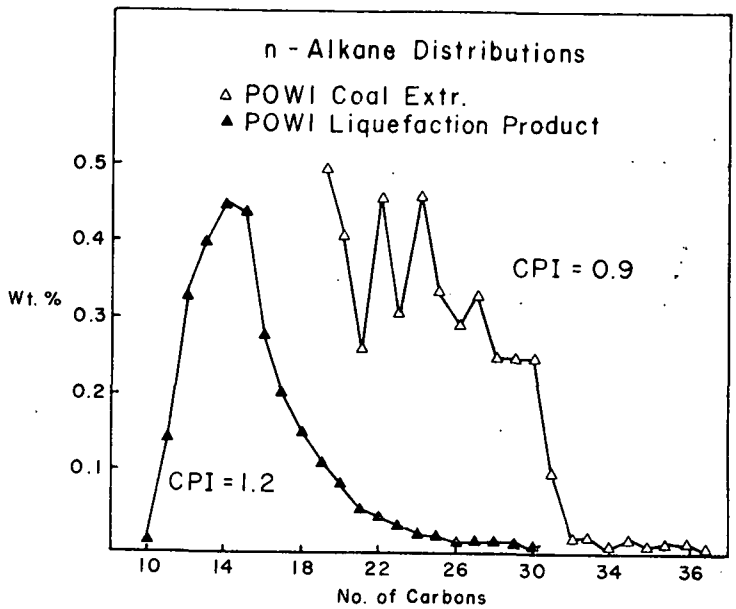

FIGURE 6-15. Comparison of n-alkane extract distribution for Powhatan bituminous coal and n-alkane distribution from CPU bottoms recycle product (Powhatan bituminous feed coal).

TABLE 6-12

EXTRACTED/SEPARATED n-ALKANES
(WT % MAF COAL)

Coal	HX Soluble $CHCl_3$ Extract	CPU Liquefaction Product After 13 Recycle Passes
B3	0.15	1.7
MOC	ND	NA
BB1	ND	3.8
BB2	ND	NA
WY01	0.20	1.7
ALB1	0.025	NA
POW1	0.022	0.96

ND = Not Detected
NA = Comparable values not available

Chaffee and coworkers (7) also reported that solvent extractable alkanes made up less than 70 pct of the alkanes formed from pyrolysis. Since considerable additional amounts of alkanes are produced by pyrolysis and liquefaction, these additional amounts of alkanes must arise through bond-breaking reactions.

6.2.4.3 Summary

The hexane soluble portions of chloroform Soxhlet extracts of seven liquefaction coal samples have been partially characterized. These fractions contain alkanes, including those alkanes considered biological markers. Among the components found were a number of bicyclic sequiterpenes, at least one tricyclic terpane, several pentacyclic triterpanes, pristane and n-alkanes. Steranes were not detected in any of these extracts.

Each coal extracted gave a characteristic capillary GC profile. The profiles for B3 and WYO1 extracts were very similar. The Morwell Australian coal, MOC, gave an extract that in general contour resembled those of BB1 and BB2.

Pristane percentages increase with rank; lignite contained small or non-detectable amounts. There was no apparent correlation between wt pct n-alkanes extracted and rank. The distribution maximum chain length decreases slightly with rank and CPI values decreased with rank. Over 90 pct of n-alkanes produced during liquefaction or pyrolysis are non-extractable, leading to the supposition that bond-breaking reactions during liquefaction lead to the formation of alkanes.

Portions of this work were reported at the American Chemical Society National Meeting in Washingotn, D.C., August 28 through September 2, 1983 (7) and will become a chapter in "Chemistry of Low-Rank Coals", an ACS Symposium Series volume edited by Harold H. Schobert, UNDERC.

6.3 REFERENCES

1. Whitehurst, D.D., T.O. Mitchell, and M. Farcasiu. Coal Liquefaction. 1980 Academic Press, New York, NY, Chapter 3.

2. Baset, Z.H., R.J. Pancirov, and T.R. Ashe. Advances in Organic Geochemistry, 1979, Editors A.G. Douglas and J.R. Maxwell, publ. 1980, Pergamon Press, NY, p. 619-630.

3. Gallegos, E.J. J. Chromatog. Science, 1981, 19, 156-160.

4. Philip, R.P., T.D. Gilbert, and J. Friedrick. Geochemistry Cosmachim. Acta, 1981, 45, 1173-1180.

5. Richardson, J.S. and D.E. Miller. Anal. Chem., 1982, 54, 765-768

6. Ekweozor, C.M., J.I. Okogun, D.E.U. Ekong, and J.R. Maxwell. Chem. Geol, 1979, 27, 11-28.

7. Chaffee, A.L., G.J. Perry, and R.B. John. Fuel, 1983, 62, 311-316.

8. Farnum, S.A., R.A. Timpe, D.J. Miller, and B.W. Farnum. American Chem. Soc. Fuel Div. Prepr. 1983, 28 (4), 93-101

7. - SO_x/NO_x CONTROL

Project No: 7202 B&R No.: AA0505000

Submitted by: M.L. Jones, Manager, Coal Utilization Research Division

Prepared by: G.F. Weber, Research Supervisor, SO_x/NO_x Control

Assigned UNDERC Personnel:
K.L. Grohs
G.L. Schelkoph
B.M. Gumeringer
D.K. Rindt
D.L. Toman

Assigned AWU Personnel:
M. Bobman
J. Eisenhuth

7.1 GOALS AND OBJECTIVES

The overall project objective is to develop an economical process for simultaneous control of SO_x/NO_x emissions derived from combustion of low-rank coals. The key to accomplishing this goal is the development of a dry process readily adaptable to retrofit situations and useful in areas of the West where water supplies are scarce. A promising process involves the direct injection of a calcium based sorbent material with subsequent collection of flue gas particulate (including the calcium based sorbent material) in a high temperature baghouse (1000°F). Use of a catalytic or noncatalytic NO_x reduction step in conjunction with the high temperature baghouse provides for simultaneous control of SO_x/NO_x emissions.

The specific goals of the project during the first year of the Cooperative Agreement are:

1. Identify and evaluate materials which have the potential for use as throwaway NO_x reduction agents.

2. Identify and evaluate additives or dopants for calcium-based compounds to enhance SO_x capture and sorbent utilization.

3. Investigate the use of a pressure hydrator as a means of combining additives and dopants with calcium-based compounds and increasing sorbent utilization.

4. Evaluate NO_x emissions control using an ammonia injection catalytic system incorporated into the 130-scfm propane-fired combustor/high temperature baghouse system.

5. Investigate simultaneous SO_x/NO_x emissions control by direct calcium injection for SO_2 control, and ammonia SCR and/or ammonia throwaway reagents for NO_x control, using the 130-scfm propane-fired combustor/high temperature baghouse system.

6. Investigate simultaneous particulate/SO_x/NO_x control using a high temperature baghouse and ammonia-SCR or ammonia throwaway system coupled with the pulverized coal-fired particulate test combustor.

7. Conduct an engineering/economic evaluation and begin work in preparation for a field test of simultaneous particulate/SO_x/NO_x control, to be cost-shared with a utility company in 1985.

The planned activities in the second quarter of the Cooperative Agreement included the following:

1. Complete evaluation of identified throwaway NO_x reduction agents using a bench-scale packed-bed reactor system.

2. Complete preliminary evaluation of NO_x reduction capabilities of promising throwaway materials (as identified from bench-scale packed-bed testing) on the 130-scfm propane-fired combustor/high temperature baghouse PDU.

3. Complete preliminary evaluation of the Selective Catalytic Reduction (SCR) NO_x control system installed in the 130-scfm propane-fired combustor/high temperature baghouse PDU.

4. Complete preliminary testing of a pressure hydrator in conjunction with additives identified in the literature survey as having the potential to enhance utilization of calcium-based sorbent materials for SO_2 control.

5. Complete preliminary testing of additive enhanced calcium-based sorbents produced in the pressure hydrator in the 130-scfm propane-fired combustor/high temperature baghouse PDU.

7.2 ACCOMPLISHMENTS

7.2.1 Packed Bed Reactor Evaluation of Throwaway NO_x Reduction Agents

Screening tests on identified throwaway NO_x control agents using the bench-scale packed-bed reactor system were completed during the quarter. The bench-scale packed-bed reactor was constructed to evaluate the effect of various throwaway materials on the ammonia injection catalytic reduction of NO_x in a simulated flue gas stream. Table 7-1 provides data on inlet gas composition.

Figure 7-1 illustrates the reactor configuration. The component gases are introduced at the top of the preheater, traversing downward through a 2-inch I.D. tube, heated by a Sybron/Thermolyne Model F21125 Tube Furnace. Hot gases then pass through the reactor, which consists of a 2-inch I.D. stainless steel tube externally heated by heat tape, a removable holder to contain bed material, and two type-K thermocouples. The holder is fitted with a wire mesh screen and porous Kaowool pads to prevent entrainment of bed material. Static pressure drop across the bed is measured by a manometer.

TABLE 7-1

PACKED-BED REACTOR INLET GAS COMPOSITION

Constituent	Concentration (Vol. %)
Nitrogen	78.3
Carbon Dioxide	16.0
Oxygen	5.7
Oxides of Nitrogen	1000 ppm
Anhydrous Ammonia	1500 ppm

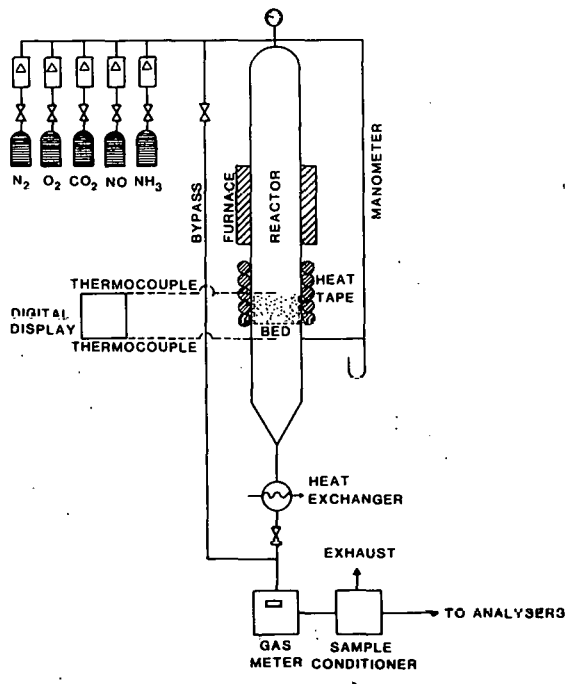

FIGURE 7-1. Bench-scale packed-bed reactor.

After passing through the reactor, the gas stream is cooled to 25°C and then flows through a gas metering device. Subsequently, the gas stream enters a sample conditioner, from which slip streams are removed for analysis. NO_x concentrations are recorded by a Thermo Electron Model 10 Chemiluminescent Analyzer, O_2 concentrations by a Beckman Model 755 Analyzer, and CO_2 concentrations by Beckman Model 865 Infrared Analyzer.

To conduct a test, about 50 g of minus 40 mesh material are placed in the bed; the weight of reducing agent used varies with its bulk density, since a fixed bed volume is desired. During heat-up, N_2 is purged through the system, and when the selected temperature is achieved, the sample gases are introduced into the preheater. The gas flow rate is kept at about 30 scfh, with the bed temperature operated from 400° to 850°F. Experimental conditions monitored throughout a run include bed and reactor wall temperatures, inlet and outlet gas flow rate and composition, and pressure drop across the bed. Space velocities are about 15,000 hr^{-1}.

Packed-bed reactor evaluation of the throwaway NO_x reduction agents identified in the literature survey has been completed. A list of the materials tested in order of decreasing reactivity with respect to NO_x reduction, is as follows: Zeolon 900H (synthetic mordenite), Fisher Iron, Coal Creek fly ash (lignite), Center fly ash (lignite), Magnetite, Cohassett fly ash (subbituminous), Flue Dust, and Nahcolite. Tabulated results of the packed-bed reactor testing are presented in Table 7-2. One aspect of the data in Table 7-2 should be noted. When preheater wall temperatures exceeded 1800°F noncatalytic NO_x reduction occurred which, in the case of some of the materials tested (fly ash, magnetite, flue dust, and nahcolite), produced unexpectedly high NO_x reduction values. Test results which were affected by noncatalytic NO_x reduction have been identified in Table 7-2. Figures 7-2 and 7-3 illustrate the noncatalytic reduction which occurred at specific conditions during tests conducted on magnetite and flue dust, respectively.

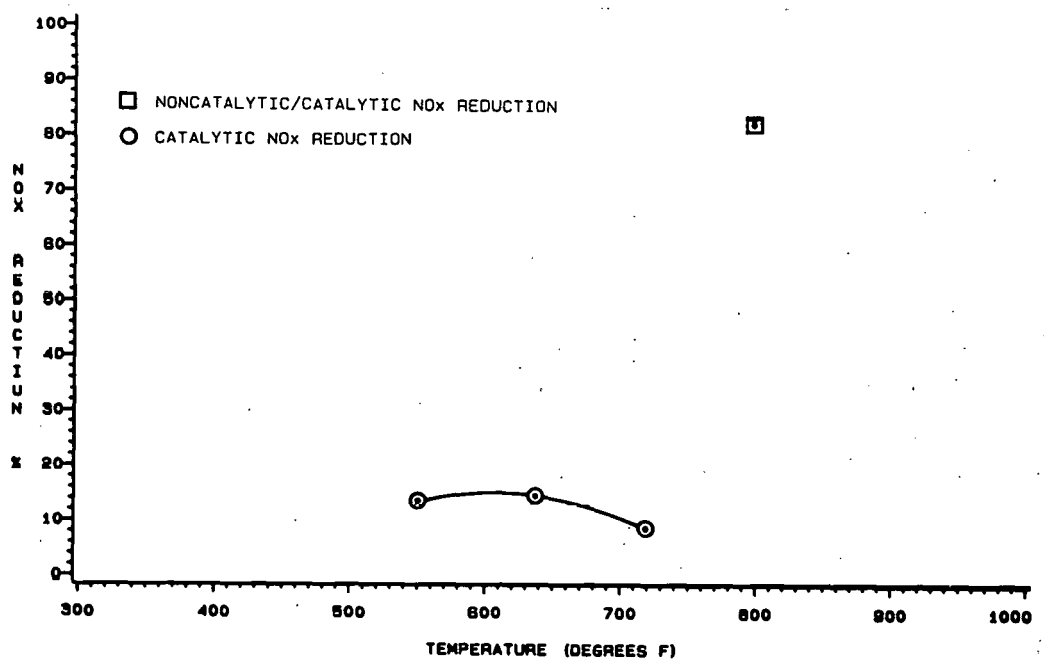

FIGURE 7-2. NO_x reduction versus reactor bed temperature for magnetite.

TABLE 7-2

RESULTS FROM PACKED BED REACTOR EVALUATION
OF POTENTIAL THROWAWAY NO_x REDUCTION CATALYSTS

Test No.	Catalyst Material[a]	Preheater Wall Temp., °F	Average Exit Bed Temp., °F	Space Velocity hrs^{-1}	Inlet NO_x Concentration (ppm)	Exit NO_x Concentration (ppm)	% Reduction of NO_x[b]
1-1	Fisher Iron	935	380	14000	980	718	27.7
1-2	Fisher Iron	1290	500	14000	970	453	52.3
1-3	Fisher Iron	1290	608	14000	980	438	55.0
1-4	Fisher Iron	1920	805	14000	1060	169	84.0*
1-5	Fisher Iron	2010	856	14000	1120	136	88.0*
1-1	Zeolon 900H	930	424	13000	880	616	30.0
1-2	Zeolon 900H	1200	540	13000	890	463	48.0
1-3	Zeolon 900H	1380	651	13000	1050	294	72.0
1-4	Zeolon 900H	1560	731	13000	995	276	72.2
2-1	Zeolon 900H	1500	690	15000	1250	300	76.0
2-2	Zeolon 900H	1940	700	15000	1250	230	81.6*
1-1	Coal Creek Fly Ash	1380	590	13000	990	921	7.0
1-2	Coal Creek Fly Ash	1450	660	13000	1000	896	10.4
1-3	Coal Creek Fly Ash	1510	723	13000	910	742	18.5
1-4	Coal Creek Fly Ash	1830	800	13000	1110	162	54.5*
1-1	Center Fly Ash	1150	401	13000	1150	1150	0.0
1-2	Center Fly Ash	1400	481	13000	950	893	6.0
1-3	Center Fly Ash	1470	565	13000	980	839	14.4
1-4	Center Fly Ash	1830	694	13000	980	113	88.5*
1-1	Magnetite	1380	550	14000	915	790	13.6
1-2	Magnetite	1380	637	14000	980	838	14.5
1-3	Magnetite	1470	719	14000	900	822	8.7
1-4	Magnetite	1830	797	14000	1000	181	81.9*
1-1	Cohassett Fly Ash	932	412	14000	850	814	4.2
1-2	Cohassett Fly Ash	1360	530	14000	930	865	7.0
1-3	Cohassett Fly Ash	1430	590	14000	780	717	7.8
1-4	Cohassett Fly Ash	1830	735	14000	860	183	78.7*
1-5	Cohassett Fly Ash	1650	780	14000	840	512	39.0
2-1	Flue Dust	1360	727	15000	1070	1070	0.0
2-2	Flue Dust	1830	736	15000	1100	1100	0.0
2-3	Flue Dust	1990	743	15000	1130	380	66.4*
1-1	Nahcolite	878	353	13000	1000	1000	0.0
1-2	Nahcolite	986	464	13000	900	900	0.0
1-3	Nahcolite	1290	570	13000	980	980	0.0
1-4	Nahcolite	1830	716	13000	850	213	75.0*
1-	Silica Sand	1830	716	13000	940	202	78.5*
2-1	Silica Sand	1300	644	16000	1200	1200	0.0

[a] Average particle size for the catalyst materials was 40 mesh or less except for the silica sand which had an average particle size of 20 mesh.

[b] "*" Indicates possible combined non-catalytic/catalytic reduction of NO_x.

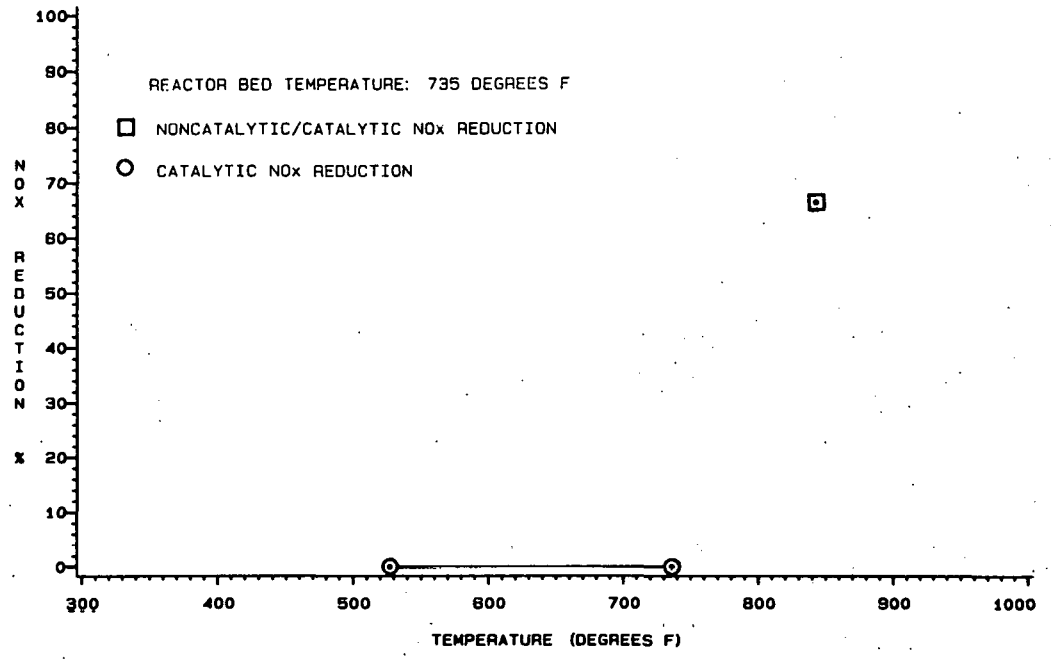

FIGURE 7-3. NO_x reduction versus preheater wall temperature for flue dust.

The Zeolon 900H, a synthetic mordenite, was found to be the most reactive of the materials tested for reducing NO_x emissions. Mordenite is a hydrated aluminum silicate. Results from packed bed reactor tests show NO_x reduction increasing with increased reactor bed temperature. For reactor bed temperatures ranging from 400° to 750°F NO_x reduction ranged from 30 to 80 pct, respectively, as shown in Figure 7-4. Space velocity for the mordenite tests ranged from 13,000 to 15,000 hrs^{-1}.

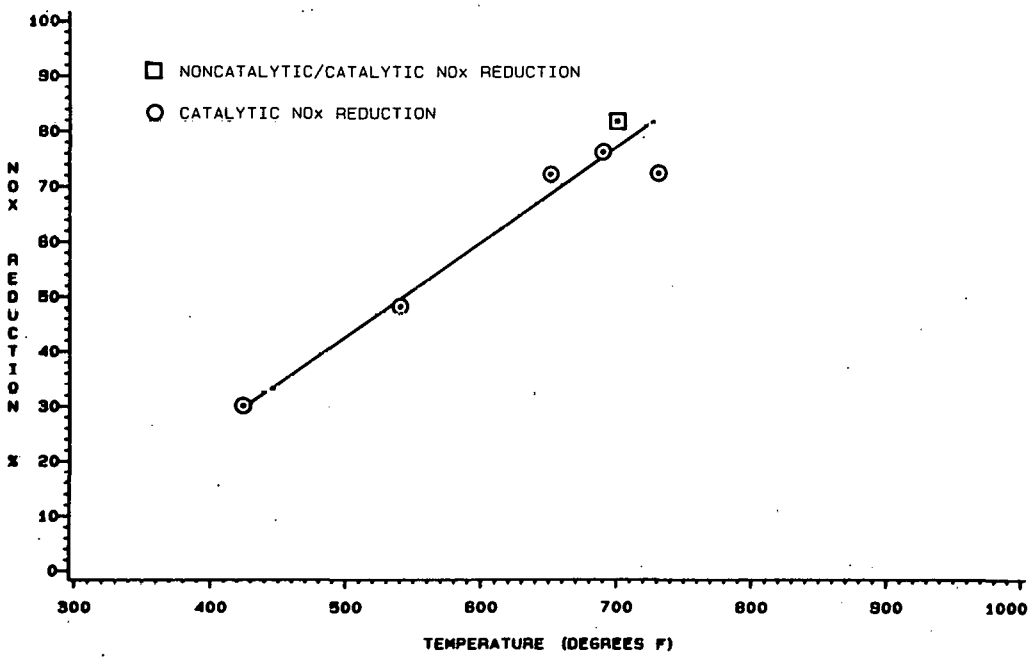

FIGURE 7-4. NO_x reduction versus reactor bed temperature for Zeolon 900H (synthetic mordenite).

Fisher Iron (40 mesh Fe) also exhibited good NO_x reduction capabilities during packed bed reactor testing. Reduction of NO_x was found to increase with increasing reactor temperature for reactor temperatures ranging from 380° to 850°F. Values for NO_x reduction ranged from 28 to 88 pct, respectively, as shown in Figure 7-5. Space velocity for the iron (Fe) tests was approximately 14,000 hrs^{-1}.

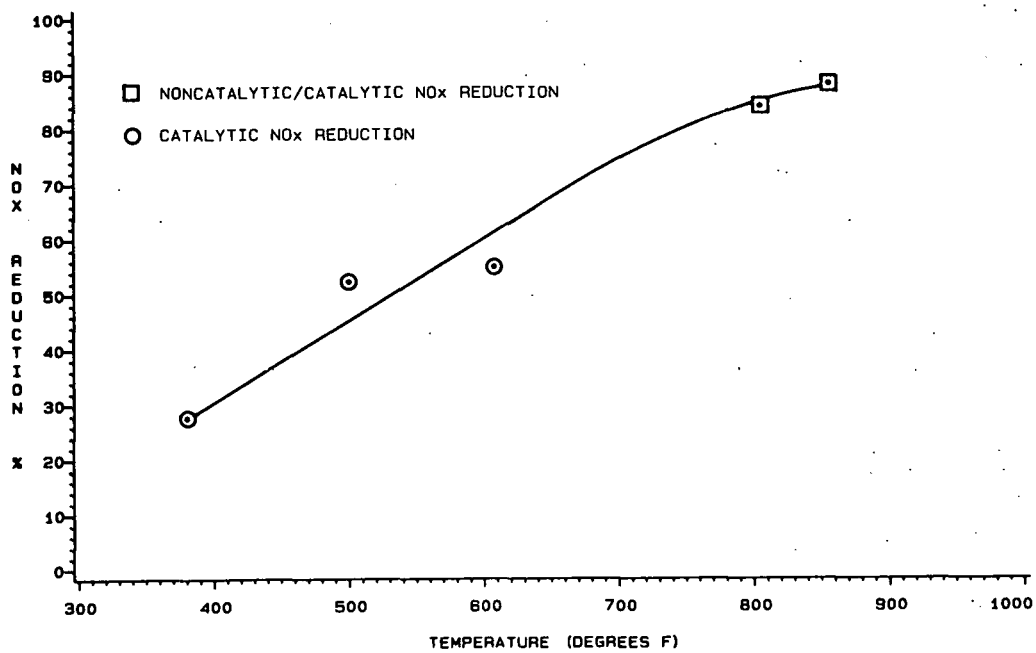

FIGURE 7-5. NO_x reduction versus reactor bed temperature for Fisher Iron (40 mesh).

Two lignite fly ashes were tested as possible throwaway NO_x reduction catalysts. Both fly ashes showed some NO_x reduction capabilities, but neither lignite fly ash exhibited NO_x reduction capabilities comparable to mordenite or Fisher Iron. The high NO_x reduction values seen in Figures 7-6 and 7-7 are a direct result of noncatalytic NO_x reduction. Space velocity for the lignite fly ash tests was approximately 13,000 hrs^{-1}.

Additional testing with the bench-scale packed-bed reactor is not planned at this time, but would be considered if other potential NO_x control agents are identified.

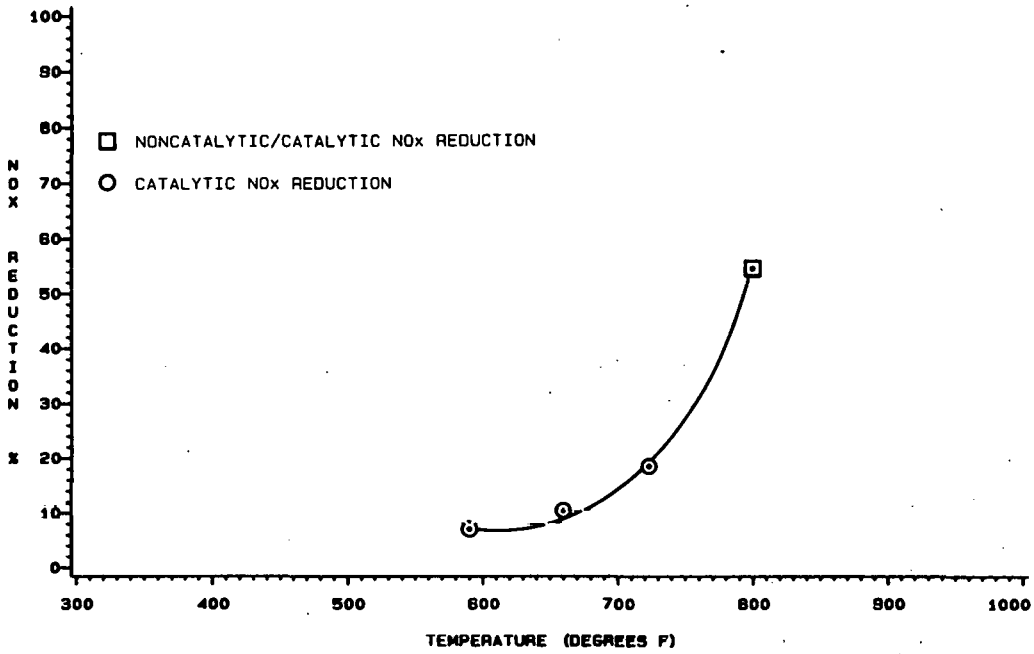

FIGURE 7-6. NO_x reduction versus reactor bed temperature for a lignite fly ash (Coal Creek).

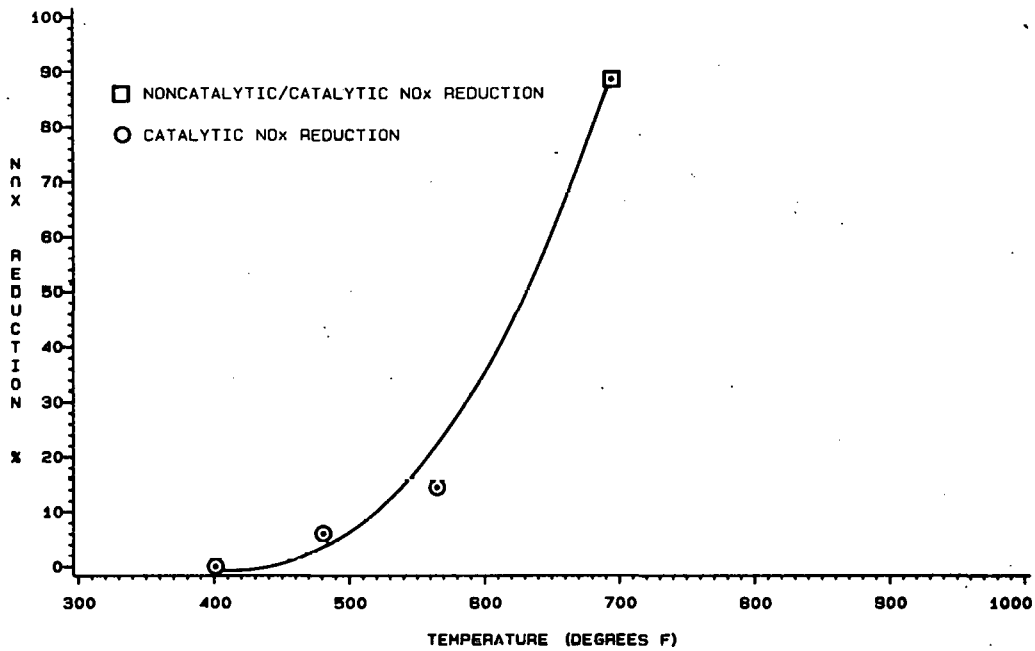

FIGURE 7-7. NO_x reduction versus reactor bed temperature for a lignite fly ash (Center).

7.2.2 Evaluation of Throwaway NO_x Reduction Reagents in the 130-scfm PDU

Six runs (83 tests) were performed on the 130-scfm propane-fired combustor/high temperature baghouse PDU during the quarter indicating fifty-seven tests to evaluate throwaway NO_x reduction compounds. The materials evaluated were two lignite fly ashes, iron filings (two particle sizes), flue dust, a synthetic mordenite (Zeolon 900H), and a natural mordenite. Injection was accomplished prior to the baghouse at temperatures ranging from 1000° to 1750°F. Baghouse temperatures ranged from 500° to 950°F.

A schematic of the 130-scfm combustor-baghouse is presented in Figure 7-8. The combustor burns propane gas to generate a flue gas containing approximately 11 pct moisture. Anhydrous ammonia (to produce NO) and SO_2 can be added to the flame at any desired rate. Sorbent or NO_x reduction materials may be injected through any sample injection port. The baghouse can be operated over a temperature range extending from the flue gas dewpoint up to about 1000°F. Ceramic filters are used at flue gas temperatures ranging from 500°-1000°F.

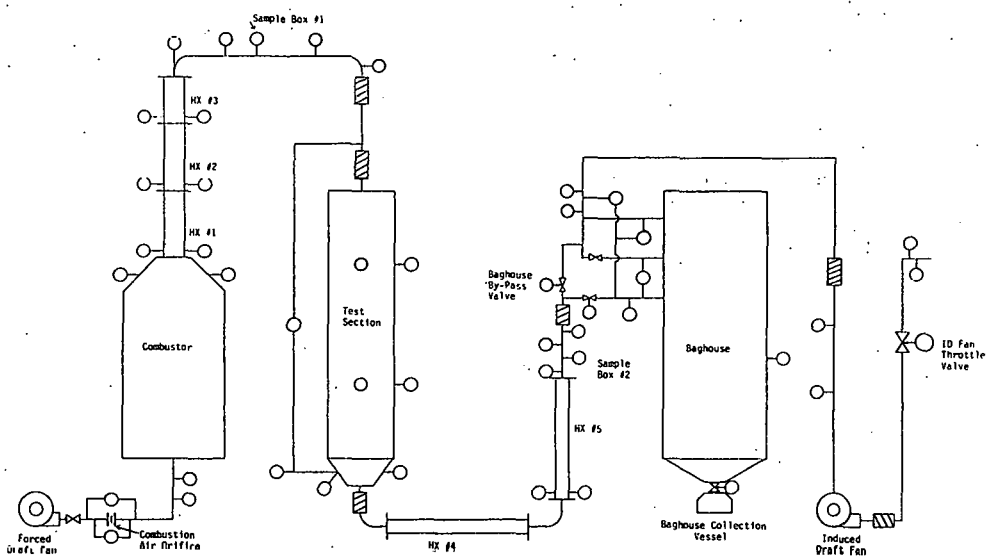

FIGURE 7-8. Dry sorbent unit, facility configuration.

A review of the literature indicated that iron compounds are effective catalysts for reducing NO_x emissions when combined with ammonia injection. The effective temperature range is reported to be 550° to 900°F, with maximum NO_x reduction occurring at 750° to 800°F.

The iron oxide content of lignite and subbituminous fly ash can vary from 2 pct up to 35 pct, with typical values for most ashes around 10 pct. Therefore, NO_x reduction may be possible by collecting the low-rank coal derived fly ash on ceramic filters in a flue gas temperature range of 550° to 900°F.

Experiments were conducted on the 130-scfm high temperature baghouse PDU to characterize NO_x reduction by iron oxide and other compounds collected on ceramic filters in the high-temperature baghouse. The results of the NO_x reduction experiments, with ammonia injection, are presented in Table 7-3.

Two lignite fly ashes have been tested as potential throwaway NO_x reduction catalysts. Data for the first lignite fly ash (Center) is presented in Figure 7-9 as NO_x reduction versus temperature for both packed-bed reactor and 130-scfm PDU data. Maximum NO_x reduction was approximately 28 pct at a baghouse temperature of 850°F. Space velocity for tests conducted with the first lignite fly ash (Center) ranged from 16,700 to 23,000 hrs^{-1}.

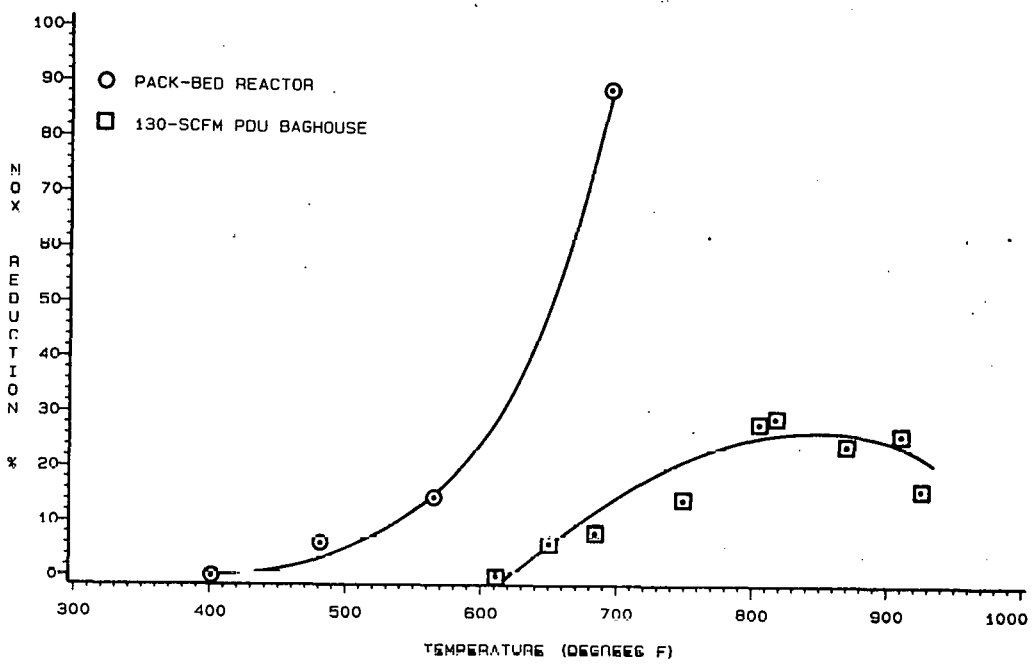

FIGURE 7-9. NO_x reduction versus temperature for a lignite fly ash (Center).

Data reduction has not been completed for the second lignite fly ash (Coal Creek), but preliminary observations indicate that overall results will be similar to those reported for the first lignite fly ash (Center).

A series of tests was conducted on the 130-scfm PDU evaluating the NO_x reduction capabilities of iron filings (40 mesh Fe). Packed-bed reactor data indicated the iron filings should significantly reduce NO_x emissions. Values for NO_x reduction tests on the 130-scfm PDU were less than 20 pct for baghouse temperatures ranging from 650° to 950°F. Space velocity for this test series ranged from 16,000 to 26,000 hrs^{-1}. The poor results seen with the iron filings may have been caused by fallout of the 40 mesh iron filings (Fe) in the baghouse resulting in limited contact between the flue gas and iron filing particles. Figure 7-10 illustrates results for both packed-bed reactor and 130-scfm PDU testing.

TABLE 7-3

NO_x REDUCTION BY POTENTIAL THROWAWAY COMPOUNDS IN A HIGH-TEMPERATURE BAGHOUSE

Test No.	Additive[a,b,c]	Injection Temp., °F	Baghouse Temp., °F	Anhydrous Ammonia, scfh[d]	Total NO_x Reduction, %[e]	A/C ft^3/ft^2	Baghouse ΔP inch-W.C.
0883.7	Iron filings	1535	640	6.3	18	5.7	4.6-4.9
0883.8	Iron filings	1470	727	6.3	12	6.1	5.0-5.3
0883.9	Iron filings	1560	790	6.8	8	7.0	6.0
0883.10	Iron filings	1560	870	6.7	4	7.3	2.9-5.2
0883.11	Iron filings	1750	951	7.5	1	8.7	6.1-6.5
0883.12	Iron filings	1750	950	3.7	0	8.7	6.6
0883.13	Iron filings	1190	955	7.1	2	9.0	5.5-6.4
0983.7	Lignite fly ash	1560	650	6.6	6	6.1	3.0-5.4
0983.8	Flue dust	1560	675	6.8	6	6.4	5.4-8.0
0983.9	Flue dust	1590	720	6.8	8	6.6	8.4
0983.10	Flue dust	1535	800	6.8	7	7.0	8.9
0983.11	Flue dust	1525	865	6.7	5	7.3	3.5-9.8
0983.12	Flue dust	1640	940	7.1	7	8.2	7.4
0983.13	Flue dust	1640	940	7.2	8	8.2	7.7
0983.14	Flue dust	1140	935	7.0	4	8.0	5.3-7.6
1083.1a	Zeolon 900H	980	500	5.6	--	4.4	3.6
1083.1b	Zeolon 900H	980	510	5.3	3	4.2	3.5-4.0
1083.2	Zeolon 900H	1090	585	6.7	20	5.8	5.5-6.2
1083.3	Zeolon 900H	1115	660	6.5	30	6.0	6.4-6.5
1083.4	Zeolon 900H	1350	655	6.5	32	5.9	4.0-6.0
1083.5	Zeolon 900H	1225	720	6.7	50	6.5	4.4-6.2
1083.6	Zeolon 900H	1160	805	6.6	64	6.9	4.0-5.7
1083.7	Zeolon 900H	1215	875	6.6	65	7.2	4.3-7.2
1083.8	Zeolon 900H	1260	935	6.8	55	7.8	4.4-6.8
1083.10	Lignite fly ash	1225	870	6.7	24	7.3	4.0-6.1
1083.11	Lignite fly ash	1255	910	5.4	26	7.6	4.0-6.0
1183.8	Lignite fly ash	1525	805	6.6	28	6.8	6.2-6.8
1183.13	Lignite fly ash	1725	925	7.0	16	8.0	6.5

[a] Particulate concentration from additive injection was about 3.0 gr/scf.

[b] Fe_2O_3 in lignite ash, 9.6 pct.

[c] Particle sizes for the additives were 40 mesh for the iron filings and <325 mesh for the fly ash, flue dust, and Zeolon 900H.

[d] All anhydrous ammonia was injected immediately upstream of the baghouse.

[e] Flue gas inlet NO concentrations were maintained at about 700 ppm.

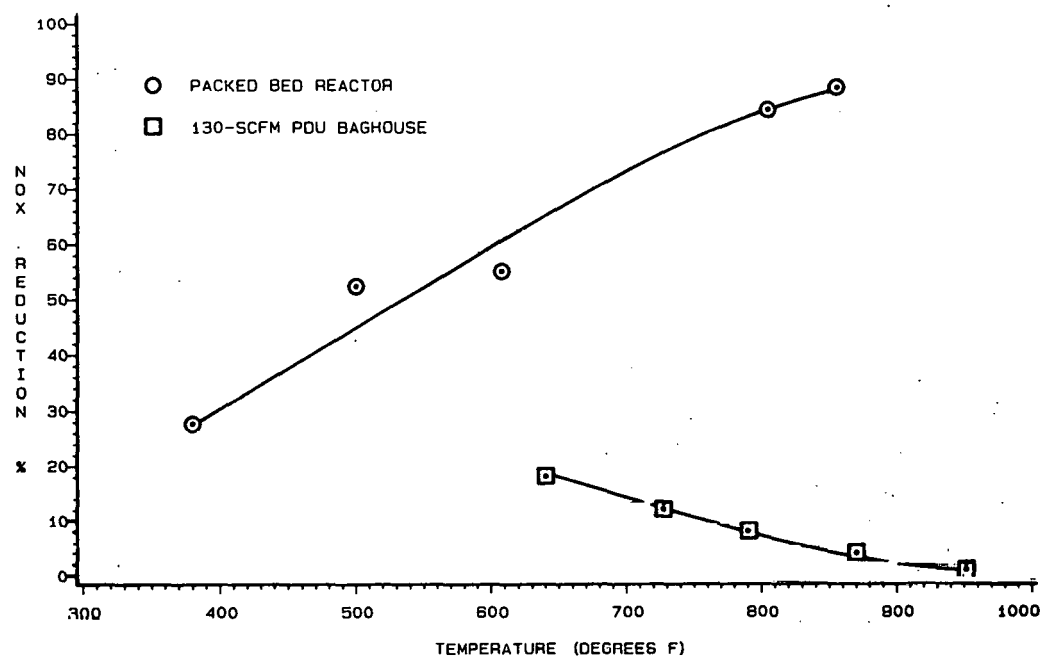

FIGURE 7-10. NO_x reduction versus temperature for 40 mesh iron filings.

A second series of tests was performed using -325 mesh iron filings (Fe). The small particle size was used in an effort to prevent particle fallout in the baghouse. Data reduction has not yet been completed for this test series but preliminary observations indicate that NO_x reduction was generally less than 30 pct.

Flue dust (FeO) was also evaluated on the 130-scfm PDU for NO_x reduction capabilities this past quarter. Overall results were poor. Reduction of NO_x emissions was less than 10 pct for all tests performed.

Zeolon 900H, the synthetic mordenite found to be the most effective NO_x reduction compound during packed bed reactor testing, was evaluated on the 130-scfm PDU this past quarter. Maximum NO_x reduction was 65 pct at a baghouse temperature of approximately 850°F. Space velocity for this test series ranged from about 10,000 to 22,000 hrs^{-1}. Figure 7-11 illustrates NO_x reduction as a function of temperature for both packed-bed reactor and 130-scfm PDU data.

The synthetic mordenite (Zeolon 900H) is an expensive material even for use as an experimental NO_x reduction agent. Therefore, a source of natural mordenite was located and tested on the 130-scfm PDU. Data reduction has not yet been completed for the natural mordenite test series but preliminary observations indicate maximum NO_x reduction was less than 30 pct. An attempt will be made to explain the poor results experienced with the natural mordenite when analysis of both mordenite samples has been completed.

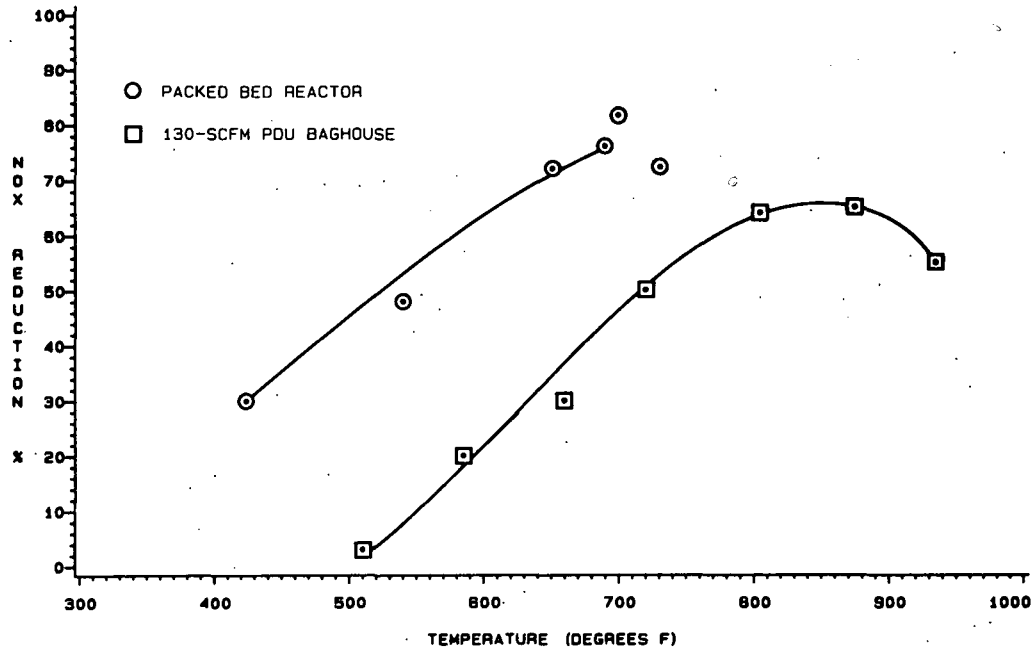

FIGURE 7-11. NO_x reduction versus temperature for a synthetic mordenite (Zeolon 900H).

Preliminary testing of potential throwaway NO_x reduction agents on the 130-scfm PDU has been completed. Additional testing would be considered if other potential NO_x control agents are identified or if data currently being correlated generates questions or exhibits unexplained inconsistencies.

7.2.3 Preliminary Evaluation of Selective Catalytic Reduction (SCR) System

Preliminary testing of the Selective Catalytic Reduction (SCR) reactor has been completed. All data support the findings reported for the first quarter of the Cooperative Agreement. Reactor temperatures below 700°F will not produce 80 pct NO_x reduction.

The supplier of the SCR reactor, Engelhard Industries, was contacted after the completion of all data reduction in an effort to establish an explanation for the poor results. Engelhard Industries agreed to review the test procedures and resulting data.

After reviewing the test procedures and resulting data Engelhard Industries recommendations were as follows:

- All ammonia (NH_3) injection for catalytic reduction of NO_x with the SCR reactor should be downstream of the baghouse where flue gas temperatures are less than 900°F. This step would reduce the chance of NH_3 reacting prior to entering the SCR reactor.

- Ammonia injection should be accomplished with multiple point injection rather than single point. In addition, static mixing devices should be used to assure homogeneous mixing of the NH_3 with the flue gas upstream of the SCR reactor.

- Measurement of flue gas NO_x concentration upstream of the SCR reactor should be performed upstream of the NH_3 injection point to eliminate possible NH_3 interference in the NO_x analyzer.

- Ammonia injection rates should be controlled to provide the desired degrees of NO_x reduction. Calculated NH_3/NO_x ratios should not be used as test control parameters but should be determined and reported as test results.

- Flue gas NH_3 concentration downstream of the SCR reactor is an important data point when evaluating performance of the SCR system. A simple colorimetric method makes use of a device called a Draeger tube.

During the test program conducted to evaluate the SCR reactor, NH_3 injection was performed in temperature regimes ranging from 775° to 2000°F. Results from the test program showed that for temperature regimes ranging from 775° to 1700°F, the location or temperature regime at which the NH_3 is injected is not critical as long as the NH_3 is thoroughly mixed with the flue gas prior to entering the SCR reactor. Injection of NH_3 into temperature regimes in excess of 1700°F is not recommended because of the probable oxidation of NH_3 to NO. During any future testing of the SCR reactor NH_3 injection will be performed downstream of the baghouse at flue gas temperatures below 900°F.

Ammonia injection during the test program was performed at several locations. Minimum distance upstream of the SCR reactor at which NH_3 injection was performed was approximately 19 pipe diameters. Ammonia injection was from a single point source directed into the flue gas stream. During any future testing of the SCR reactor NH_3 will be injected through a tube spanning the flue pipe with multiple injection points directed into the flue gas stream. In addition a static mixer will be installed immediately downstream of the NH_3 injection location to assure homogenous mixing of the NH_3 and flue gas.

Flue gas NO_x concentration upstream of the SCR reactor is measured upstream of the NH_3 injection point, therefore NH_3 interference in the NO_x analyzer is not possible. The Thermo Electron Model 10 NO_x analyzer uses a catalytic converter rather than a thermal converter therefore minimizing any possible NH_3 interference with NO_x determinations.

The NH_3 injection rate (scfh), as measured with a flow meter during the test program, was calculated based on the measured flue gas flow rate (scfm), NO_x concentration (ppm), and a desired 1:1 mole ratio of NH_3 to NO_x. The possibility does exist that the potential compounding of errors could result in an undesirable NH_3 injection rate. Data generated during the test program do not support the compounding error theory. A 50 pct increase or decrease in the NH_3 injection rate caused NO_x reduction values to range from 84 to 60 pct, respectively. These data would indicate that any error in the NH_3 injection rate was not significant enough to cause the SCR reactor's poor performance at reactor temperatures below 700°F.

Wet chemistry techniques were used to determine NH_3 concentration in the flue gas stream downstream of the SCR reactor. Although results are not conclusive, the limited testing performed indicated NH_3 concentrations of less

than 50 ppm. During any future testing of the SCR reactor, the colorimetric method using Draeger tubes will be tested which should give accurate NH_3 concentrations down to 5 ppm.

Future testing of the SCR system will be minimal until simultaneous SO_x/NO_x work begins in October 1983.

7.2.4 Operation of Bench-Scale Pressure Hydrator

During the second quarter of the Cooperative Agreement SO_2 control work has centered around the development and operation of a bench-scale pressure hydrator. The apparent advantages of an SO_2 control scheme using a pressure hydrator for direct injection of calcium-based compounds include the following:

1. Very small particles (average particle size ~0.4-micron) are generated in the pressure hydrator, which are further reduced in size by dehydration reactions after injection into a flue gas stream. Small particle size provides large surface area for reaction.

2. Additives can be readily incorporated in the hydration process to increase overall sorbent utilization to meet changing coal sulfur levels.

From previous results calcium hydroxide has proved to be the most reactive calcium-based material for direct injection into high temperature flue gas. If the reactivity of the hydrated product can be increased by addition of other compounds during the hydration process overall sorbent utilization may be significantly increased from the 40 pct value previously observed. Sodium is one of the additives proposed for testing, and will be added by hydrating quicklime with a solution of sodium hydroxide. Other additives being considered include iron oxide, sodium carbonate, sodium bicarbonate, copper oxide, and manganese oxide.

As a result of quicklime and water feed problems encountered when attempting to operate the pressure hydrator in a continuous mode, a decision was made to operate the pressure hydrator in a batch mode assuming the dry product was 100 pct hydrated with an average particle size of less than 1.0 μm. Work on the continuous pressure hydration system is continuing but is not a priority since industrial scale pressure hydration systems are available commercially.

Batch operation of the pressure hydrator involves charging the preheated reactor with a specific quantity of quicklime (~3 lbs), then injecting the desired amount of water from a pressurized container. The hydration reaction proceeds quickly, causing reactor temperature and pressure to increase. The continuously stirred reaction proceeds for approximately 20 minutes with reactor temperature and pressure reaching maximum values of 300°F and 150 psig, respectively. Once the hydration reaction is complete reactor temperature begins to decrease slowly. The hydration products are slowly expelled from the reactor for a period of about 40 minutes. A cyclone is used to collect the hydrated product or it can be directly injected from the reactor into a flue gas stream. The pressure hydration system has been successfully operated in this manner several times in the past two months.

Hydrated lime produced in the first couple of tests was collected with the cyclone. The hydrated product was found to be dry and analytical results, X-Ray Diffraction (XRD) and Scanning Electron Microscope (SEM), showed the product to be 100 pct hydrated with an average particle size of less than 1.0 μm. Figures 7-12 and 7-13 illustrate the conversion of calcium oxide to calcium hydroxide in the pressure hydrator. When coulter counter results are available a specific average particle size will be reported.

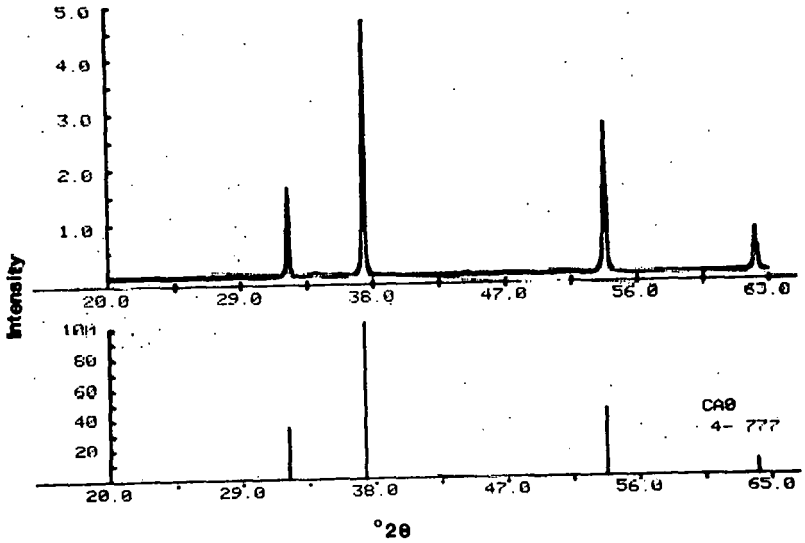

FIGURE 7-12. X-ray diffraction scan of quicklime feed to pressure hydrator.

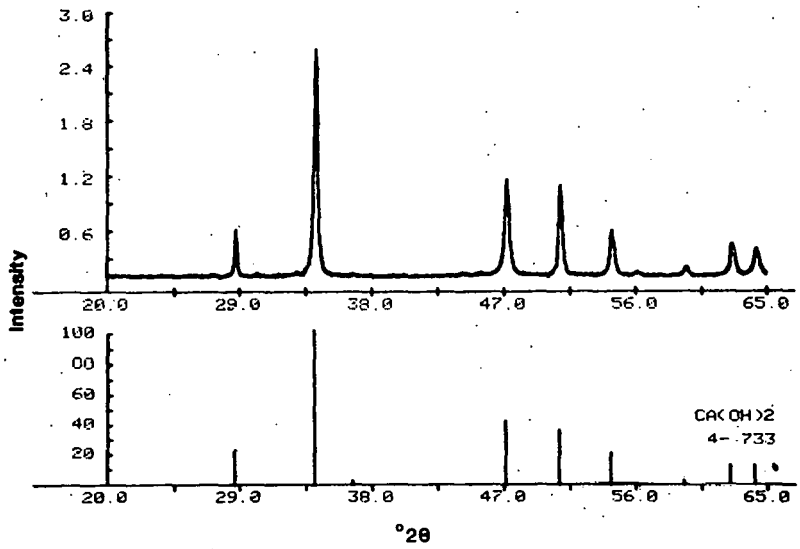

FIGURE 7-13. X-ray diffraction scan of hydrated product collected in cyclone.

Direct injection from the pressure hydrator into the flue gas stream of the 130-scfm propane-fired combustor/high temperature baghouse PDU was performed on three occasions with no significant operability problems. Data reduction and sample analysis have not yet been completed; therefore SO_2 removal and sorbent utilization data are not available at this time.

Preliminary testing of the pressure hydrator in conjunction with additives identified in the literature survey was not completed as scheduled due to problems encountered in the early development of the pressure hydration system. Completion of preliminary additive testing has been rescheduled for the third quarter of the Cooperative Agreement. Testing of additives in conjunction with the pressure hydrator was initiated this past quarter but analytical results are not yet available.

Preliminary testing of additive enhanced calcium based sorbents in the 130-scfm propane-fired combustor/high temperature baghouse PDU was not completed as scheduled due to the delay stated above. Completion of additive/sorbent testing in the 130-scfm PDU has been rescheduled for the third quarter of the Cooperative Agreement.

The two scheduling delays reported here should not significantly affect the completion of other intermediate milestones scheduled for the third quarter of the Cooperative Agreement.

8. - PARTICULATE CHARACTERIZATION

Project No.: 7203 B&R No.: AA0505000

Submitted by: M.L. Jones, Manager, Coal Utilization Research Division

Prepared by: S.J. Miller, Research Engineer

Assigned UNDERC Personnel: J.F. Grohs
S.J. Miller
D.R. Sears, Project Manager
A.L. Severson
L.A. Weckerly

Assigned AWU Personnel: R.C. Gehringer

8.1 GOALS AND OBJECTIVES

The purpose of the Particulate Characterization project is to measure and characterize particulate and trace element emissions to the atmosphere and relate these emissions to the fuel, ash, and particulate collector parameters, and to operation of upstream FGD, or simultaneous SO_x/NO_x reduction devices. The long range goal of this work is to develop a detailed understanding of coal- and collector-specific emissions, in order to reduce these emissions by improved collector and station design, coal preparation, or other strategies, based upon reliable predictive models. Another goal is to provide data to support development of new or revised emissions standards, which may relate to respirability, ultrafine particle emissions, or metal content.

8.2 ACCOMPLISHMENTS

8.2.1 Coal Specific Fabric Filtration Tests

Fly ash is generated at UNDERC in the nominal 75 lb coal/hr pc-fired particulate test combustor (PTC). The unit is equipped with a versatile 3-mode baghouse which can operate in shaker, pulse, or low-pressure expansion cleaning modes. Since July 1981 when the baghouse was first operational, 88 runs have been completed with the PTC and baghouse with 19 different coals. The runs have ranged in burn time from 8 hours to 100 hours. A wealth of data has been accumulated which includes runs with all three cleaning modes and with different fabric and cleaning cycle combinations. The body of our accumulated quantitative performance data is being applied to our efforts to develop a predictive model of fabric performance. The focus has been on efficiency, rather than pressure drop because project emphasis has shifted towards particulate emission characterization.

There are many parameters which are likely to have major effects on fabric filter performance. These can be divided into two categories--baghouse related and ash related. The most extensively published research in fabric filtration has concentrated on the baghouse related parameters such as fabric

type, cleaning mode, cleaning cycle, and air-to-cloth ratio. To a lesser extent studies have considered ash characteristics such as particle size distribution and specific filter resistance coefficient, K_2. Little research has been done relating coal or ash properties to fabric filter performance, even though in many cases fabric filtration is considered to be the economic choice for high efficiency particulate control for eastern and especially western coals. The particulate characterization research at UNDERC has focused on the coal-specific nature of fabric filtration. Objectives have been to 1) identify to what extent fabric filtration is coal specific, and 2) determine what specific ash characteristics have major effects on fabric filter performance.

For some coals, tests have been done with all three cleaning modes and several fabrics. However, in order to isolate ash effects from different coals, a number of tests have been done with the same fabric and cleaning combination. The most extensive tests that have been completed at UNDERC are with the shaker mode of cleaning and a woven glass fabric with 10 pct Teflon B coating. Seventeen coals have been tested with this configuration. For some coals, only brief data exists with only a single outlet dust loading, while for other coals, multiple testing has been completed.

Besides ultimate, proximate, and ash analyses of the coal, several fly ash characteristics have been considered. Particle size distribution (PSD) has been recognized by others (1) as affecting fabric filter performance. Because of this we have employed several methods to document PSD. These include aerodynamic methods (impactors and multicyclones) and non-aerodynamic methods (Coulter Counter and Scanning Electron Microscopy (SEM)).

We have also used SEM to determine particle morphology and SEM microprobe analysis to determine particle elemental composition as a function of particle size. Elemental composition of bulk fly ash is measured with x-ray fluorescence analysis (XRFA).

8.2.2 Baghouse Efficiency

Efficiency data for each of the 17 coals are included in Table 8-1. For clarity the data are plotted as pct penetration in Figures 8-1 through 8-3. The data reveal a wide variation in baghouse removal efficiency from an extremely low 76 pct for one Wilcox group Texas lignite (Big Brown) to 99.8 pct for two North Dakota lignites and a western subbituminous coal. One usually hears of high efficiencies for fabric filtration on the order of 99.9 pct; however, efficiency has been reported to be highly sensitive to air-to-cloth ratio (2). The air-to-cloth ratio for these tests is in the 3 to 3.5 range which will tend to cause lower efficiencies. Also it is not unusual for full scale utility baghouses to operate at efficiencies of 99.8 pct. For 23 utility baghouses the range of efficiencies reported was 98.4 to 99.97 pct with a median value of 99.8 pct (3). The efficiency for a full scale utility baghouse using a shake deflate cleaning mode and an air-to-cloth ratio of 3+ was reported to be 99.3 pct (4). This shows that it is not unreasonable to expect efficiencies of 99 to 99.9 pct with a shaker baghouse operating at an air-to-cloth ratio of 3:1. It is unusual, however, to see efficiencies in the range of 76 to 95 pct as in the first six values in Table 8-1. More will be said about this later.

TABLE 8-1

EFFICIENCY AND FLY ASH ANALYSIS

Name	Source	Rank	Inlet Dust Loading grains/scf	Baghouse Removal Efficiency, %	Baghouse Penetration, %	Fly Ash Analysis Pct Concentration as Oxides									
						SiO_2	Al_2O_3	Fe_2O_3	TiO_2	P_2O_5	CaO	MgO	Na_2O	K_2O	SO_3
Big Brown	Freestone Co., TX	Lignite	5.0	76.0	24.0	53.6	17.7	7.35	1.62	0	14.7	3.0	0.44	0.9	1.2
Choctaw (washed)	Choctaw Co., AL	Lignite	2.7	89.6	10.4	25.2	12.6	19.1	1.0	0.2	26.7	2.4	0.70	0.7	11.7
Pike Co.	Pike Co., Al	Lignite	3.6	90.0	10.0	34.4	18.8	6.9	1.6	0.1	27.5	1.9	0.71	0.3	8.5
Choctaw (unwashed)	Choctaw Co., Al	Lignite	4.6	92.2	7.8	32.2	13.2	26.8	0.9	0.1	13.8	2.5	0.54	1.1	9.4
Naughton	Lincoln Co., Wy	Subbit.	1.6	93.6	6.7	56.4	15.9	8.3	0.85	0.1	7.7	3.2	0.20	1.7	0.8
Arapahoe	Routt Co., Co	Subbit.	2.8	95.5	4.5	58.4	24.8	3.9	1.2	0.7	6.4	2.1	0.60	1.6	0.9
San Miguel	Atascosa Co., Tx	Lignite	12.0	99.1	0.9	60.2	20.1	3.7	1.1	0.04	5.4	1.1	3.6	2.6	1.2
Antelope High Na	Wyoming	Subbit.	1.5	99.1	0.9	35.9	10.4	7.1	1.2	0.5	28.6	6.1	2.4	0.6	7.3
Beulah Low Na	Mercer Co., ND	Lignite	3.2	99.3	0.7	38.2	7.4	12.1	1.7	0.2	19.3	5.2	5.8	0.2	9.7
Antelope Low Na	Wyoming	Subbit.	2.8	99.4	0.4	47.7	19.7	4.1	2.0	1.3	17.6	4.2	1.1	0.6	1.8
Caballo/ Spring Creek	Cambell Co., Wy	Subbit.	1.9	99.5	0.5	37.6	15.1	6.6	2.0	0.6	26.2	4.3	2.4	0.4	4.7
Velva V3	McLean Co., ND	Lignite	1.9	99.5	0.5	18.4	10.7	6.4	0.7	0.4	42.2	9.9	3.2	0.1	8.2
Antelope Medium Na	Wyoming	Subbit.	1.7	99.5	0.5	29.7	14.0	8.8	1.4	0.7	30.9	6.3	1.3	0.4	6.5
Indian Head I3	Mercer Co., ND	Lignite	2.5	99.7	0.3	29.2	12.4	11.5	1.0	0.4	20.6	5.3	10.2	1.1	8.3
Antelope/ Spring Creek	Wyoming	Subbit.	1.6	99.8	0.2	36.9	13.1	7.5	1.3	0.6	25.5	5.2	3.1	0.5	6.5
Velva V4	McLean Co., ND	Lignite	2.0	99.8	0.2	14.8	9.5	7.6	0.8	0.5	41.4	9.4	4.3	0.1	11.7
Beulah High Na	Mercer Co., ND	Lignite	2.1	99.8	0.2	25.5	12.3	11.2	1.1	0.5	18.1	4.3	13.7	0.6	12.9

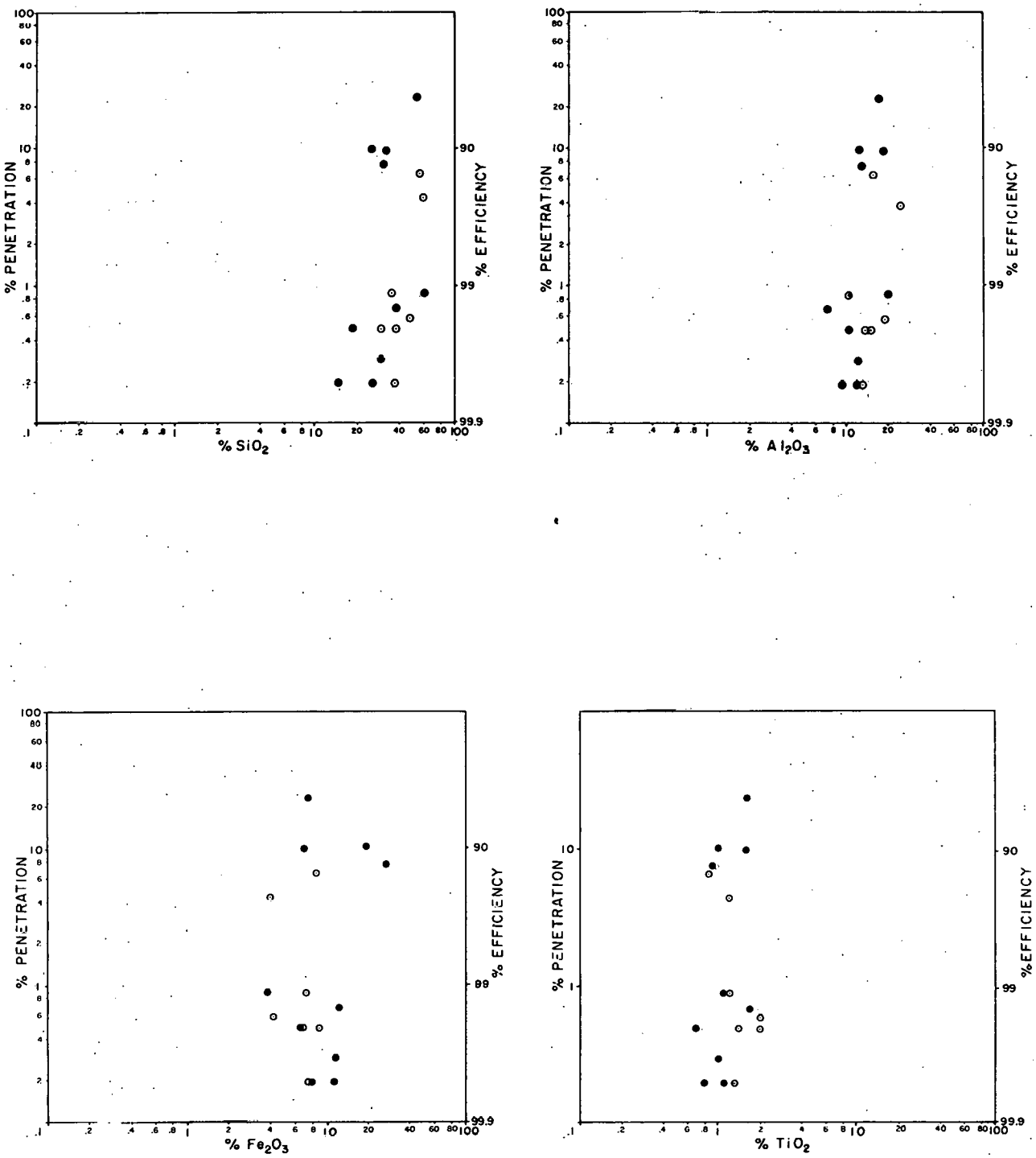

FIGURE 8-1. Penetration as a function of SiO_2, Al_2O_3, Fe_2O_3, and TiO_2 concentration in the fly ash for 17 coals.

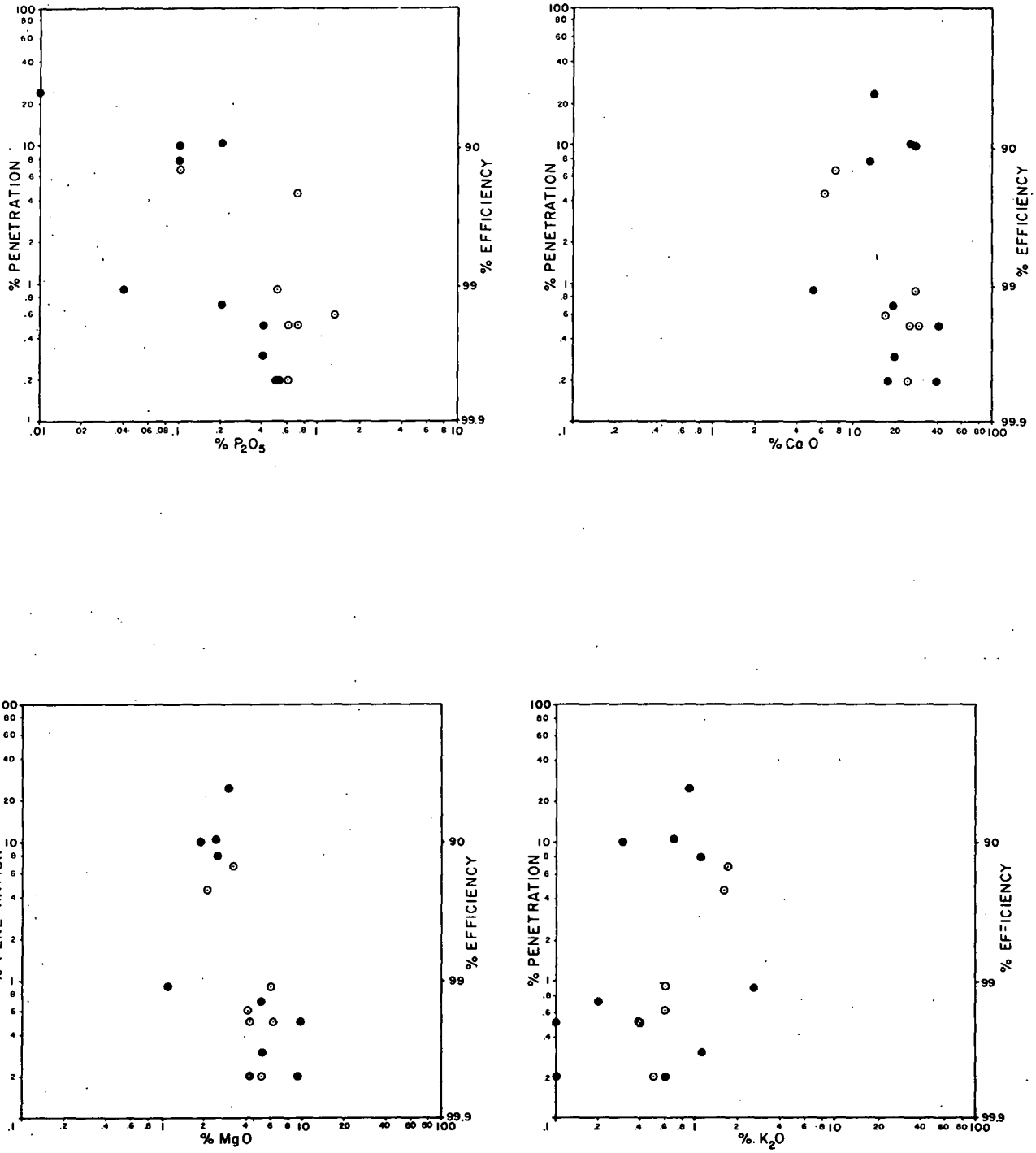

FIGURE 8-2. Penetration as a function of P_2O_5, CaO, MgO, and K_2O concentration in the fly ash for 17 coals.

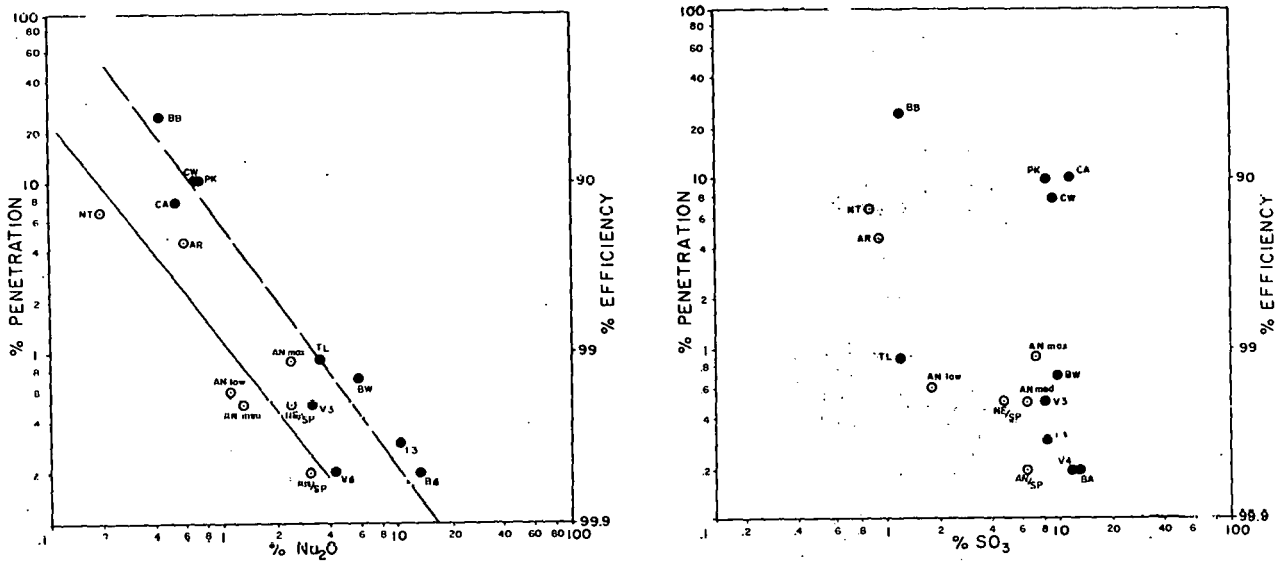

FIGURE 8-3. Penetration as a function of Na_2O and SO_3 in the fly ash for 17 coals.

All of the tests listed in Table 8-1 were with similar operating conditions and with the same fabric; therefore, any differences in reported fabric filter performance should be due to differences in the coals and their respective fly ashes. No attempt was made to optimize fabric filter performance for each coal. For example, coal A may have a better removal efficiency with a two-hour bag cleaning interval while coal B may have the best efficiency with a one-hour cleaning interval. A complete description of the bag material used for these tests and the baghouse operating parameters are given in Tables 8-2 and 8-3, respectively.

TABLE 8-2

FABRIC SPECIFICATIONS

Mfgr.[a] designation	601E
Fiber	Glass
Construction	Woven, 3x1 twill
Count, in^{-1}	54x30
Weight, oz/yd^2	10.3
Finish	10% Teflon B
Permeability, ft^3/ft^2..... (ASTM D737 @ 1/2" W.C.)	30-50

[a]Filter Media Products, Kennecott Corporation, Winchester, Va.

TABLE 8-3

BAGHOUSE OPERATING CONDITIONS

Mode	Shaker Chamber
Temperature	300°F
Fabric	10 oz woven glass (KFM 601E)
Air-to-Cloth Ratio	3-3.5
Cleaning Interval	1 hour
Shaker Frequency	8 Hz
Shaker Stroke Length	1.5 inches
Shake Time	15 seconds

The lowest efficiency by far was with the Big Brown Texas lignite. To date ten runs have been completed with this coal using several fabrics and all three cleaning modes. By changing fabrics the efficiency can be improved but, in all cases, this coal has shown the lowest efficiency when compared with other coals with the same fabric and cleaning configuration. This implies that the very poor efficiency with this coal must be related to the nature of the coal fly ash. More will be said about this in the discussion of possible reasons for differences in efficiency. The next lowest efficiencies in this group are with the three Alabama lignites which are Gulf Province lignites from the Wilcox and Midway groups. For these coals, only one run, each with two outlet dust loadings, was completed because of a limited amount of coal.

Most of the runs are "one day" runs with 8 to 16 hours of steady-state baghouse operation. With some coals, however, 100-hour runs have been completed in order to assess subtle longer term changes in performance. In these cases, pressure drop has remained quite steady and efficiency has had only minor fluctuations. One example of this is with the Naughton subbituminous coal where the average efficiency was only 93.6 pct. This was a 5-day run with dust loadings each day. Measured efficiency for the first day was low and it did not improve by the end of the week. Another example of this is with Velva North Dakota lignite where measured first-day efficiency was 99.8 pct and it remained there for the duration of the 98-hour run. This shows that differences among coals can be detected with one day tests. It does not imply that all long term effects (as in large scale reverse air baghouses where high residual dust cakes take months to stabilize) can be studied in one day tests. It is important to recognize however, that with the shaker chamber tests, the cleaning action is vigorous, leaving a light residual dust cake. Because of this, the time required for stable operation is much less for shaker cleaning than for conventional reverse air.

The next coal listed in Table 8-1, the Arapohoe subbituminous coal, gave a low efficiency of 95.5 pct. Later entries in the table show that a large number of coals fit into the efficiency range of 99.1 to 99.8 pct. Coals in this group include a Jackson group Texas lignite (San Miguel), several subbituminous coals and five North Dakota lignites. In all tests, the North Dakota lignites have consistently shown high removal efficiencies.

8.2.3 Reasons For Efficiency Differences

As previously mentioned, the particle size distribution (PSD) of the fly ash is likely to have a major effect on collection efficiency in a fabric filter. Tests have shown (1) that finer fly ash gives lower baghouse efficiency than coarse ash. Detailed information on PSD of the 17 coal fly ashes will not be presented here but briefly our data do not show higher levels of fines to be present in the fly ashes with poor removal efficiency. It would appear that there are other effects which override the PSD effects in causing differences in removal efficiency.

Particle morphology will likely have an effect on the caking characteristics of the ash as it collects on the bags. This in turn will affect the filtering of the fly ash and may cause poor efficiency if the ash does not form a good dust cake. In general any ash characteristic that affects the way the ash layer builds up on the bags will have an effect on fabric filtration of that ash. This could include PSD, particle morphology, ash "stickiness" or adhesive/cohesive properties, electrical properties, and chemical composition. Detailed investigation of particle morphology of fly ash has been initiated. Preliminary data do not reveal gross differences in particle morphology with differences in removal efficiency.

Among other ash characteristics that could have an effect on removal efficiency is the elemental composition of the fly ash. Table 8-1 includes average elemental oxide concentrations of the fly ash for each of the 17 coals. All data are from x-ray fluorescence analysis of the bulk fly ash except for the sodium values that are less than 1 pct which were obtained from atomic absorption analysis of digested fly ash. Baghouse pct penetration is presented as a function of oxide concentration in Figures 8-1 through 8-3. The data for the lignites are the solid points while the data for the sub bituminous coals are the open circles.

The graphs for SiO_2, Al_2O_3, Fe_2O_3, and TiO_2, shown in Figure 8-1, do not suggest any correlation between concentration and penetration. Figure 8-2 presents similar graphs for P_2O_5, CaO, MgO, and K_2O. It appears that there may be slight correlations especially if the lignites and subbituminous coals were considered separately. For phosphorous it appears that penetration increases with decreasing concentration but there is large data scatter. For calcium there is not much of a trend except that the two subbituminous coals with poor efficiency had a substantially lower calcium content than the other subbituminous coals. The magnesium graph indicates a slight inverse relationship between concentration and penetration. The graph for potassium shows too much data scatter to suggest any clear trend.

Figure 8-3 presents baghouse penetration as a function of sodium and SO_3 concentration. The graph for sodium indicates a definite inverse trend between concentration and penetration. The relationship appears for both the lignites and the subbituminous coals. If one applies a straight line fit on the log-log plots for the lignite and the subbituminous coals the two lines appear parallel with the subbituminous line shifted somewhat to the left. It appears that sodium concentration has a significant effect on baghouse efficiency for these tests. All of the coals which exhibited poor collection efficiency of 95 pct or less (penetrations of 5 pct or greater) had fly ash sodium concentrations of less than 1 pct. Conversely all of the high sodium

coals had good baghouse removal efficiencies. The graph for SO_3 also shows an inverse relationship between penetration and concentration; however, the three Alabama lignites do not appear to fit in with the other data.

Of all of the plots the element that shows the most consistent clear relationship between penetration and oxide concentration is sodium. Sodium is known to have major effects on ash fouling, precipitator performance, and bed agglomeration in AFBC. It is not surprising then to find that sodium also affects fabric filter performance. The mechanism by which sodium affects efficiency at this point is not clear. Sodium is one of the more volatile elements and is often found to be present in higher concentrations in the fine particles and may be enriched on the surface of larger particles (5). This may affect the caking characteristics of the ash on the fabric, which will affect the efficiency. We have observed that the low sodium Big Brown ash falls off the dust loading filter quite easily and we have not observed this with any of the other ashes. This indicates that the Big Brown ash has different adhesive properties which will affect its caking properties and retention on a fabric filter.

8.2.4 Significance of Results

These results should be considered highly significant. First, they show that fabric filter performance is indeed coal specific with large differences in removal efficiency with different coals. Second, the results reveal a definite inverse correlation between penetration and sodium concentration in the fly ash for the fabric and cleaning configuration considered. The tests do not rule out applying fabric filtration to the ashes which showed poor efficiency, but they do suggest that one would use a different approach in fabric filter design for the low efficiency ashes than for the high efficiency ashes. For the ashes that demonstrate poor performance in tests such as these, careful selection of the correct fabric along with a conservative air-to-cloth ratio and the optimum cleaning cycle may all be necessary in order to maintain an adequate residual dust cake and bring up the efficiency to an acceptable level. In other words, heavy dust cake formation may be necessary to achieve high efficiencies with these "problem" coals. On the other hand, residual dust cake for the coals that showed high efficiencies in these tests may not be important. These coals may then be candidates for high ratio filtration with conventional woven fabric. For example, the tests with the North Dakota lignites give excellent efficiencies even immediately after starting with new bags. This means that a heavy residual dust cake for these ashes is not necessary to achieve high removal efficiency. Apparently the ash builds up on the woven fabric layer in such a way that openings in the weave and pinholes are immediately bridged over resulting in high efficiency.

8.2.5 Future Tests

Most likely several ash characteristis like PSD, particle morphology, and elemental composition all contribute to differences in fabric filter performance with different coals. Future work will involve more detailed analysis of PSD and particle morphology in an attempt to evaluate their effects on fabric filter performance.

For the ashes with poor efficiencies it would be desirable to do additional testing with other fabrics and changes in cleaning configuration to

obtain better efficiencies. For these coals testing should also be done to determine if sodium additives such as soda ash will improve efficiency. Also the problem coals could be blended with high sodium coals to determine beneficial effects.

The sodium levels for the lignites tested to date jumped from 0.7 to 3.5 pct with no data points in the 1 to 3 pct range. It would be desirable to test both Fort Union region and Gulf Coast lignites in this sodium range to further assess the effect of sodium in fabric filtration performance.

8.3 REFERENCES

1. W. F. Frazier and W. T. Davis, University of Tennessee, "Effects of Fly Ash Size Distribution on the Performance of a Fiberglass Filter", presented at the Third Symposium on the Transfer and Utilization of Particulate Control Technology, March 1981.

2. K. E. Noll, W. J. Franck, and M. N. Patel, "Bench and Pilot Scale Fabric Filter Cleaning Studies for Fiberglass/Fly Ash Systems", presented at the 74th Annual Meeting of the Air Pollution Control Association, Philadelphia, Pennsylvania, June 21-26, 1981.

3. Walter Piulle and Robert Carr, Electric Power Research Institute, and Peter Goldbrunner, Burns and Roe, Inc, "1983 Update Operating History and Current Status of Fabric Filters in the Utility Industry", presented at EPRI Conference on Fabric Filter Technology for Coal-Fired Power Plants, Denver, Colorado, March 1983.

4. K. L. Ladd, R. L. Chambers, O. C. Plunk, and S. L. Kunka, Fabric Filter System Study: Second Annual Report, Southwestern Public Service Company, March 1981, EPA 600/7-81-037

5. S. A. Benson, D. K. Rindt, G. G. Montgomery, and D. R. Sears, "Microanalytical Characterization of North Dakota Fly Ash," presented at the 185th ACS National Meeting, Fuel Chemistry Division, Seattle, Washington, March 20-25, 1983.

9. - WASTE CHARACTERIZATION

Project No.: 7204 B&R No.: AA0515000

Submitted by: M.L. Jones, Manager, Coal Utilization Research Division

Prepared by: K.R. Henke, Chemist
D.R. Sears, Research Supervisor, Particulates and Waste Characterization

Assigned UNDERC Personnel: J.F. Grohs
K.R. Henke
D.R. Sears

9.1 GOALS AND OBJECTIVES

The goals of the Waste Characterization project are to 1) characterize the solid wastes derived from the direct utilization and conversion of low-rank western coals; 2) assess the environmental consequences associated with the disposal of coal-derived wastes, with emphasis on identification of deleterious major and trace elements which may be mobilized into groundwater; and 3) evaluate and develop measures to mitigate undesirable environmental impacts. These measures may include coal preparation, immobilization by fireside additives, ash treatment, direct utilization, resource extraction, or improved disposal methods and siting.

9.2 BACKGROUND

Long-range projection of the future utilization of western coals indicate significant increases in the quantities of coal-derived wastes which will require disposal using environmentally acceptable methods. Current federal regulations do not allow unrestricted disposal of coal wastes and in the future may require predisposal treatment to render them innocuous, or specially constructed disposal sites to prevent leachate from contacting surface or groundwater. Current practice usually employs landfill or pond disposal techniques. Many western utilities and proposed conversion plants are located adjacent to coal mines, and disposal in mined-out areas of neighboring strip mines is becoming an attractive alternative. Improper disposal of coal-derived wastes may permit dissolution of deleterious elements by meteoric water and groundwater. Once incorporated into the groundwater, these elements will migrate unless attenuated or isolated.

Attenuation of deleterious elements has been investigated under conditions typical of municipal landfills. Data on major and trace element soil attenuation based on the unique properties of low-rank coal alkaline fly ashes is very limited, and is expected to be very site- and coal (ash)- specific. Proper design of coal-derived disposal sites requires detailed knowledge of attenuation effects, with proper attention paid to site-specific effects.

The chemical and physical characteristics of coal-derived waste are partially defined with respect to major elements (calcium, magnesium, sodium), chemical leaching, and physical properties. Many low-rank fly ashes also contain significant quantities of toxic trace elements such as arsenic, selenium, and molybdenum. When these alkaline fly ashes are exposed to water, the resulting high-pH leachate enhances the mobility of some trace elements. The distribution of major and trace elements among the crystalline and amorphous phases of low-rank coal ash particles is not well defined. Detailed characterization of the major and trace element distribution in quartz, mullite, magnetite, and other ash mineral phases may help to suggest methods of immobilization of deleterious elements. For example, such information coupled with a knowledge of the high temperature phase behavior of the coal and ash minerals might lead to development of appropriate precombustion dopants or fireside additives. Ash treatment strategies also can employ such information.

9.3 ACCOMPLISHMENTS

9.3.1 Ash Leaching Investigations

Leaching tests have been performed on several fly ash and bottom ash samples obtained in the Particulate Test Combustor (PTC) pc-fired pilot plant, from a field test at a utility station, from the UNDERC Atmospheric Fluidized-Bed Combustor (AFBC) pilot plant, and from the U.S. Bureau of Mines Wellman-Galusha gasifier in Minneapolis.

We have chosen the ASTM "Method A" batch leaching protocol (1) because it is more applicable to alkaline western ashes than is the published alternative, the U.S. EPA "EP Method" (2). The ASTM method is designed for rapid evaluation of the extractability of inorganic species from finely divided wastes such as fly ash. Although it is intended to model leaching by groundwater, the ASTM "Method A" is not suitable for engineering design of disposal sites. For instance, it does not provide information about waste permeability and groundwater hydrology. Its value lies in the focus it places on leachability, which may be used to assess relative potential for groundwater contamination among various wastes, if other site-specific factors are equal.

9.3.2 The ASTM Method A Batch leaching Test

The following is an abbreviated summary of the published procedure (1):

> Using teflon or teflon-coated glassware, a 700 g solid waste sample is mixed with 2800 ml of water and agitated for 48 hours using an oscillating platform shaker operated at 60-70 strokes/min. The pH of the solution is recorded. The water is distilled or deionized to ASTM reagent Type IV (Specification D1193). Following settling of solids, the supernatant fluid is filtered through P040 Nucleopore or AP15 Millipore prefilter followed by a 0.45 μm membrane filter under 50 psi pressure of argon or other rare gas. Filtrate pH is recorded and then adjusted to 1.2 to 2.0 with nitric acid. The acidified fluid is stored in airtight plastic containers for subsequent chemical analysis. Calibration of the pH meters is done with commercially available certified buffer solution.

Because of sample size limitations, the quantities above were proportionately reduced to 200 g solid: 800 ml water.

Nitric acid acidification and refrigeration preserves samples for as much as 2 weeks prior to analysis; routinely, however, samples are analyzed within a few days of preparation. Major and trace elements are analyzed both by atomic absorption (AA) and inductively coupled argon plasma spectrometry (ICAP).

Table 9-1 describes several coal-derived wastes and the corresponding leachate analyses. Additional investigations performed under non-DOE funding are reported elsewhere.

Several samples are noted to display apparent pozzolanic behavior during the batch leaching test. An inherent limitation of this method is that this behavior, while observed, cannot be related quantitatively to what would actually occur in field conditions. Qualitatively, we expect that both laboratory and field leaching rates would be reduced by formation of dense masses of altered consolidated ash.

The samples in Table 9-1 were analyzed for selected trace elements including the RCRA trace elements, and molybdenum. The latter is included because of reports that it has appeared in unexpectedly high concentrations in groundwater affected by lignite ash disposal in North Dakota (3), and its reported presence in uraniferous North Dakota lignite deposits southwest of the Missouri River (4). Although there is no current U.S. water quality standard for molybdenum, the Soviet Union, for example, has published a quality criterion of 0.5 ppm (5).

9.3.3 Relation of Leaching Results to EPA Water Quality Criteria

In Table 9-2 we compare the observed leachate concentrations with the U.S. water quality criteria and with the EPA trigger concentrations (Maximum Concentration of Contaminants for "Characteristic of EP Toxicity" (6)). The latter are defined as 100 times the quality criterion for water.

At this time only a limited amount of information is available. For our first efforts we have chosen only a few low-rank coals (and one AFBC bed material) from several utilization processes or installations. Direct comparison of pc-fired fly ash, AFBC fly ash, and gasification ash for each of several representative coals would be useful.

9.3.4 Discussion

Each of these coals was formed in different depositional environments (North Dakota non-marine swamps, Texas marine, etc.). With the limited data at hand, it is premature to develop many generalizations. There is some evidence that the three alkaline earths (Ca, Ba, Sr) are interdependent. Under natural conditions, these elements commonly form solid solutions of sulfates ($CaSO_4$-$BaSO_4$-$SrSO_4$) and carbonates ($CaCO_3$-$BaCO_3$-$SrCO_3$), and such may also be occurring in these ashes.

As we develop a larger body of data, we will be able to test this hypothesis and others. In addition, Fe, Cd, and Hg may accompany Zn because

TABLE 9-1
ASH DESCRIPTION AND FILTRATE CHEMISTRY AS DETERMINED BY ICAP

Sample No.:	GF81-2126	GF81-4846	GF83-1668	GF82-1766	GF83-1693 (BUI-342)	GF83-1763A (1st)	GF83-1763B (Duplicate)	GF83-1666
Coal:	Decker Std. (DS)	Dolomite bed mtl., high Na Beulah burn (BA)	High-Na Beulah (BU)	San Miguel (TL)	Indian Head (I3)	Indian Head (I3)	Indian Head (I3)	Pike Co., Ala., lignite (PK)
Process:	AFBC	AFBC	AFBC (oxygen deficient)	pc-fired[1] utility station	pc-fired[2] utility station	Wellman-[3] Gelusha gasifier ash	Wellman-[3] Gelusha gasifier ash	PTC
Run No.:	DS1-0681	BA5-2581	BU4-0383	--	--	--	--	PK-241
Ash Description:	Light gray with white specks[4]	Light brown[4]	Gray[4]	Homogeneous gray	Homogeneous gray[5]	Homogeneous dark gray[4]	Homogeneous dark gray[4]	Light gray[5]
Filtrate Description:	Colorless	Dark yellow	Dark yellow brown	Colorless	Pale yellow	Colorless	Colorless	Light green
Concentration in mg/ℓ (ppm):								
Filtrate pH	12.3	12.7	10.9	9.7	12.5	11.7	11.8	11.0
Al	3.70±0.02	138±9*	51.51±C*	8.33±0.60	1.66±0.04	87.19	90.33	4.47±3
Ca	209±2	12.C4±3**	499±133	293±45	532±72	136.2	121.7	637±38
Fe	0.16±0.01	0.24±0.08	0.25±C.08	0.21±0.06	0.42±0.02	0.26	0.17	0.65±0.4
Na	730±9	21500±100*	31300±700*	243±53	6140±10	3338	3329	32.89±1**
Si	5.76±0.04	71.46±2*	1.42±C.12	0.53±0.05**	5.72±0.3	3.29	4.59	12.30±.6*
As	ND	3.74±0.30*	0.55±C.07	0.25±0.07	ND	0.35	0.36	ND
Ba	4.04±0.01*	0.12±0.03	0.15±C.02	0.20±0.02	0.12±0.02	0.29	0.27	0.15±0.05
Cd	ND	Det.	Det.	ND	ND	ND	ND	ND
Cr	<0.01	1.99±0.2	0.06±C.01	0.05±0.01	0.97±0.20	0.02	0.01	4.73±1*
Pb	ND	ND	ND	ND	ND	ND	ND	ND
Se	0.12±0.02	4.53±0.30*	7.39±0.30*	0.51±0.08	0.39±0.10	0.09	0.09	0.32±0.05
Sr	71.70±2*	2.56±0.02	24.88±0.22*	3.50±0.05	31.66±5*	2.24	2.04	11.80±0.5*
Cu	ND	0.02±0.01	0.03±0.01	<0.01	ND	<0.01	<0.01	ND
Ti	<0.01	ND	ND	ND	ND	<0.01	<0.01	ND
Ni	ND	ND	ND	<0.02	ND	<0.01	<0.01	ND
Mn	ND	<0.01	ND	0.01	<0.01	<0.01	<0.01	ND
Mo	0.90±0.01	2.06±0.20	55.11±7*	0.92±0.10	0.94±0.12	0.81	0.86	1.86±0.4
Zn	<0.1	0.31±0.10	<0.1	<0.1	0.17±0.01	<0.1	<0.1	<0.1

[1]San Miguel Station, San Miguel Electric Cooperative, Christine, TX.

[2]Antelope Valley Station, Basin Electric Power Cooperative, Beulah, ND.

[3]U.S. Bureau of Mines, Minneapolis, MN.

[4]Apparently semi-pozzolanic; formed low strength mass on exposure to water.

[5]Apparently pozzolanic; formed hard mass on exposure to water.

*Unusually high concentration.

**Ususually low concentration.

TABLE 9-2

COMPARISON OF U.S. WATER QUALITY CRITERIA, EP TOXICITY CONCENTRATIONS, MAXIMUM CONCENTRATIONS OBSERVED, AND SAMPLES WHICH EXCEED THE EP LIMIT, BY ELEMENT

Element	U.S. Quality Criteria (QC) for Water, ppm	EP† Toxicity Limit, ppm	Maximum Conc. Observed, ppm	Samples Approximating or Exceeding EP Limit GF No.
As	0.05	5	3.7 ± 0.3	None
Ba	1.00	100	4.0	None
Cd	0.01	1	Det[δ]	None
Cr	0.05	5	4.7 ± 1.0	83-1666
Pb	0.05	5	ND[∂]	None
Hg	0.002	0.2	(Not Measured)	
Se	0.01	1	7.4 ± 0.3	81-4846 83-1668
Ag	0.05	5	ND	None
Mo*	--	(50*)	55 ± 7	(83-1668)

*U.S. has no QC for molybdenum. For reference, Soviet value of 0.5 ppm has been converted to its equivalent EP limit as U.S. QC would have been.

†EP toxicity limit (Trigger concentration) is defined as 100 · (QC) (6).

[δ]DET = Detected at or near detection limit (0.005 ppm)

∂ND = not detected

these elements often occur as trace contaminants in ZnS, sometimes observed in coal and fly ash (7). We may expect to find associations of Fe and Cr in the ash.

Future work will include etching experiments (e.g., with H_2F_2) and magnetic separation. These techniques, combined with petrographic microscopy will help us identify and explain some of these assocations.

EPA standards for pH (8) in groundwater are exceeded (pH>9 in all cases) but dilution by groundwater and low buffering capacity of leachate will reduce this concern.

Very little correlation seems to exist between pH and elemental concentration. However, there are numerous other, univestigated, ash characteristics which may also be important. These may include not only the apparent pozzolanic behavior noted earlier, but also specific surface area, particle size, thermal history of the ash, etc.

9.3.5 Future Work

In Table 9-3, we display some of expected trace and major element associations with coal and ash minerals. By no means will all such associations occur in all, or perhaps even many, coals. Leaching, etching, magnetic separation, SEM/microprobe and Auger spectrometry, and polarizing microscopy are tools which will help to clarify the associations in actual ashes.

The simpler ash mineral origins can be explained by reactions such as:

$$\underset{\text{(pyrite, marcasite)}}{4\ FeS_2} + 8\ CaO + 15\ O_2 \rightarrow \underset{\text{(anhydrite)}}{8\ CaSO_4} + \underset{\text{(hematite)}}{2\ Fe_2O_3}$$

$$3\ FeS_2 + 6\ \underset{\text{(calcite)}}{CaCO_3} + 11\ O_2 \rightarrow 6\ CaSO_4 + \underset{\text{(magnetite)}}{Fe_3O_4} + 6\ CO_2 \uparrow$$

$$\underset{\text{(kaolinite)}}{3\ Al_2Si_2O_5(OH)_4} \rightarrow \underset{\text{(quartz, cristobalite tridymite)}}{3\ SiO_2} + \underset{\text{(mullite)}}{Al_6Si_3O_{15}} + 6\ H_2O \uparrow$$

$$\underset{(SiO_2)}{\text{Quartz}} \xrightarrow{870^\circ C} \underset{(SiO_2)}{\text{tridymite}} \xrightarrow{1470^\circ C} \underset{(SiO_2)}{\text{cristobalite}}$$

Unfortunately, most of the ash "minerals" are chemically too complex to derive their origins with any confidence. If the origins of the ash minerals and chemical reactions were known, the behavior of toxic trace elements during combustion could be determined. Unscrambling these uncertainties would be most helpful in developing methods to immobilize specific trace elements.

For these minerals, potential trace clement contaminents may occur as interstitials, substitutional replacements, surface-sorbed species, perhaps epitaxial surface growths, etc. In addition, elemental associations may occur

TABLE 9-3

ELEMENTAL ASSOCIATIONS WITH MAJOR, MINOR, AND TRACE MINERAL COMPOUNDS OF COAL AND ASH

	Coal		Ash	
Element	Minor Trace Components	Major Components	Minor and Trace Components	Major Components
Al	Hematite, magnetite	Clays, feldspar	Hematite, magnetite	feldspar, spinels, gehlenite, oxides
Sb	Pyrite	--	Magnetite	--
As	Pyrite Arsenopyrite	--	Glass	--
Ba	Barite, anhydrite, phosphates	--	Barite, anhydrite, witherite, phosphates	--
Cd	Pyrite, sphalerite, calcite, quartz, organics	--	Glass	--
Ca	Apatite	Calcite, lime dolomite, anhydrite	--	Anhydrite, calcite, lime, pyroxenes
Cr	Magnetite	--	Magnetite	--
Cu	Pyrite, clays, chalcopyrite, organics	--	Magnetite	--
Fe	Siderite	Pyrite, hematite, magnetite	--	Hematite, magnetite spinels, pyroxene
Pb	Galena, organics	--	Glass	--
Mg	Calcite	Dolomite	Magnetite, hematite	Periclase, pyroxene, brucite
Mn	Pyrite, calcite, "pyrolusite" quartz, magnetite	--	Magnetite	--

TABLE 9-3 (Continued)

Element	Coal		Ash	
	Minor Trace Components	Major Components	Minor and Trace Components	Major Components
Hg	Sphalerite, clays, pyrite	--	Gases, sphalerite	--
Mo	Pyrite, calcite molybdenite, organics	--	Spinel (Mo^{+4}) Na_2MoO_4 (Mo^{+6})	--
Ni	Millerite, pyrite organics	--	Magnetite hematite	--
P	Anhydrite, apatite phosphates	--	Anhydrite, apatite phosphates	--
K	Anhydrite	Clays, feldspars	Anhydrite	Feldspars, feldspathoids $KAlSiO_4$
Se	Pyrite, calcite quartz, organics	--	Calcite, quartz hematite, magnetite	--
Si	--	Quartz, clays, feldspars	--	SiO_2, Wollastonite, glass, feldspars, feldspathoids
Sr	Anhydrite, calcite, phosphates	--	Anhydrite, calcite, phosphates	--
Ag	?	--	?	--
Na	Anhydrite	Clays, feldspar, organics	Anhydrite	$(Na,K)_2SO_4$, feldspars, sodalite, noselite
Ti	Ilmenite, magnetite, rutile, clays	--	Magnetite, pyroxene hematite, ilmenite	--
Zn	Sphalerite, quartz, organics	--	Magnetite, hematite	--

in ill-defined, non-stoichiometric glasses. Magnetic separation will permit separation of spinels (magnetite, spinel, etc.) from non-magnetic ash components (9) and H_2F_2 etching will distinguish many glasses from mullite, for example (10).

We can split the ash minerals into three groups.

1. Spinels and other magnetic materials.
2. Non-magnetic crystalline phases.
3. Many of the glasses.

The three groups may be analyzed for target trace elements, or be subjected to further treatment. The latter can include etchants other than H_2F_2 and pyrolysis. There remains also the possibility of identifying and isolating specific crystalline phases using the polarizing microscope, followed by electron microprobe analysis in the SEM, or Auger/ESCA analysis.

Appropriate combinations of these approaches will be applied with special emphasis on those wastes displaying high leachate concentrations of specific deleterious elements. The much longer range goal of developing immobilization, ash treatment, or resource extraction schemes as alternatives to conventional disposal will depend rather sensitively upon defining the associations of the deleterious elements with specific ash phases.

9.4 REFERENCES

1. ASTM: 1979 Annual Book of ASTM Standards, Pt 31, "Proposed Methods for Leaching of Waste Materials," p. 1258.

2. U.S. EPA "Hazardous Waste Management System-Identification and Listing of Hazardous Waste," Federal Register, 45 FR (#98) 33127, May 19, 1980.

3. Ness, H.M. Private communication, June 1982.

4. Anderson, S.B. "Molybdenum," Mineral and Water Resources of North Dakota, Bull. 63, North Dakota Geological Survey, 1973, p. 159.

5. Hart, Fred C. and B.T. DeLaney. The Impact of RCRA (PL94-580) on Utility Solid Wastes: Electric Power Research Institute, FP-878, Technical Planning Study 78-779, 1978, p. 90.

6. U.S. EPA, "Hazardous Waste Management System-Identification and Listing of Hazardous Waste," Federal Register, 45FR (#98) 33122, May 19, 1980.

7. Valkovic, V. Trace Elements in Coal, Vol. I, CRC Press Inc. Boca Raton, Florida, 1983, p. 61.

8. U.S. EPA, Quality Criteria for Water: U.S. Dept. of Commerce Nat. Tech. Infor. Service, PB-263 943, (1976) p. 337.

9. Groenewold, G.H. "Characterization, Extraction, and Reuse of Coal Gasification Solid Wastes": North Dakota Mining and Mineral Resources Institute. Quarterly report to the Gas Research Institute, Apr-June 1983, Ed. 1983, 41 pp.

10. Hulett, L.D. A.J. Weinberger, N.M. Ferguson, K.J. Northcutt, and W.S. Lyon. Trace Element and Phase Relations in Fly Ash: Electric Power Research Institute, EA-1822, Research Project 1061, 1981.

10. - COMBUSTION RESEARCH AND ASH FOULING

Project No.: 7205 B&R No.: AA1505000

Submitted by: M.L. Jones, Division Manager, Coal Utilization

Prepared by: M.L. Jones, Division Manager, Coal Utilization
D.P. McCollor
B.G. Miller

Assigned UNDERC Personnel: M.L. Jones
D.M. McCollor
B.J. Weber
B.G. Miller
R.J. Kadrmas

Assigned AWU Personnel: V.K. Nangia
R.E. Conn

10.1 GOALS AND OBJECTIVES

The Combustion Research and Ash Fouling project has two primary goals. The first is the development of fundamental data and correlations on the combustion reactions of low-rank coals. Special attention will be given to effects related to the unique properties of low-rank coals such as high moisture content, lower heating value, highly variable and alkaline ash, and high porosity.

The second objective of the project is to maintain and expand the technical data base at UNDERC on ash fouling and slagging behavior in pulverized fuel and cyclone-fired furnaces burning low-rank coals.

The specific objectives of the project in the current budget year are:

1. Completion of the construction and checkout of the bench-scale combustor and its diagnostic and sampling systems.

2. Initial testing and calibration of the bench-scale combustor with model compounds, and with low-rank coal particles.

3. Pilot-scale testing to evaluate the effects of ultra-fine coal grinding on ash fouling.

4. Evaluation of systems for in situ examination of deposits.

5. Completion of the ash fouling topical report.

6. Examination of alkali species in combustion systems, focusing on analysis of gas and solid phases to be sampled and collected by Midwest Research Institute.

7. Testing of selected low-rank coals to expand the existing data base on fouling and slagging maintained at UNDERC.

The planned activities for the current quarter included the following:

1. Shakedown and initial testing of bench scale combustion device.

2. Combustion testing of micronized coals.

3. Evaluation of systems for determination of gas temperatures in combustion systems.

10.2 ACCOMPLISHMENTS

10.2.1 Bench-Scale Combustor

To obtain information on single low-rank coal particles as they experience devolatilization, ignition, and char burn out, a bench-scale combustor has been constructed at the UNDERC. The combustor is designed to provide non-obtrusive probing of an entrained flow of coal particles in a simulated combustion gas using photography and three-color optical pyrometry. The combustion environment experienced by the coal particles can be controlled with respect to both gas temperatures and gas composition.

An overview of the conceptual design of the bench-scale combustor is shown in Figure 10-1. A gas mixing system blends N_2, O_2, CO_2, and SO_2 to simulate a combustion environment. The gas mixture is heated to the desired temperature in two preheaters and a resistance-heated furnace. Water is metered into the gas stream after the first preheater where it flashes to steam. The hot gas stream exits the furnace through a ceramic distribution plate into a vertical quartz observation chimney. Uniformly-sized coal particles are entrained at a constant rate in a small fluidized bed and injected into the hot gas stream through a water-cooled tube terminating at the top of the distribution plate. The square quartz chimney allows photography and optical pyrometry along the other axis, along the axes perpendicular to the particle's trajectry. Data from the pyrometer, thermocouples and other instruments are acquired, stored, and manipulated using an IBM 5150 microcomputer.

Activity in this quarter has been directed toward bringing the bench-scale combustion system near the point of readiness for actual experimental use.

Tests of the bench-scale combustor have been conducted to determine operating characteristics and to test segments of the instrumentation. Overall performance of the system has been satisfactory, although problems were encountered with the coal feed system and portions of the instrumentation. These were subsequently overcome.

The first shakedown tests of the system with coal injection were performed during August, enabling the pyrometer and photographic systems to be tried under actual operating conditions.

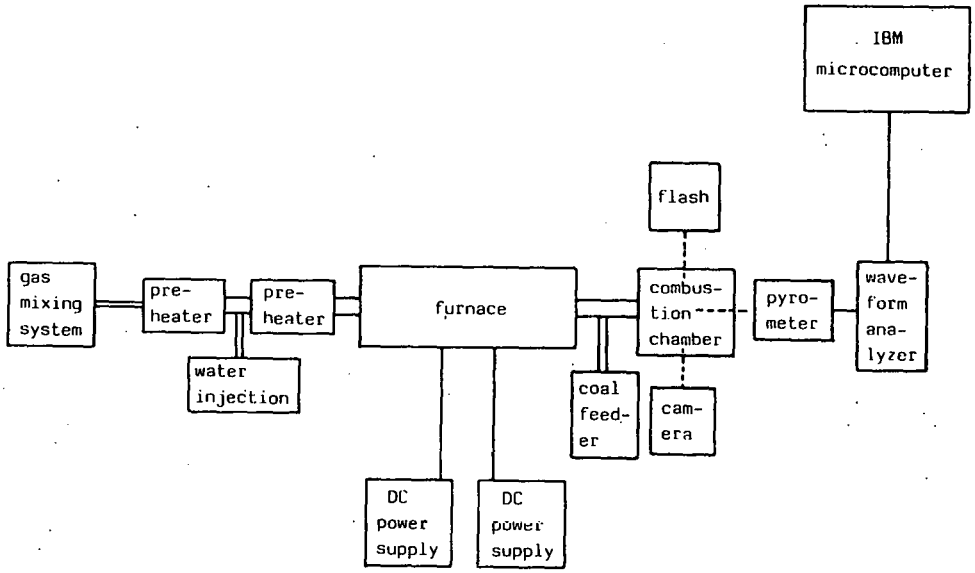

FIGURE 10-1. Overview of the conceptual design of the bench-scale combustor.

The following sections outline the performance of major components of the bench-scale combustor, and solutions of the problems encountered.

Gas Heating System

The performance of the gas heating system has been quite satisfactory. The system has proven rugged and simple to operate, with no problems of design or control. Heat-up and operation of the furnace system is now routine.

A timeline of the normal operational procedure for the gas mixing, water injection, and heating system is shown in Figure 10-2. Since most runs were performed to test instrumentation, the furnace was "idled" at a gas flow of 200 scfm and an exit gas temperature of 1000°-1200°C. However, one high-temperature run made to exercise the furnace reached a peak exit gas temperature of 1500°C. It is anticipated that the design goal of 1650°C will be obtained with all furnace elements installed. Exit gas temperature was found to be controllable to within $\pm$ 10°C at 1200°C. Because of the low thermal inertia of the Zicar insulation, gas temperature quickly responds to charges in power applied to the heating elements and is quite stable at a given power setting.

Coal Feed System

Difficulties and delays in fabrication of the fluidized-bed coal feeder necessitated the design and construction of a modified version, made of plexiglass rather than glass for ease of construction. A drawing of the modified feeder is shown in Figure 10-3. Two tests of the feeder have been satisfactory.

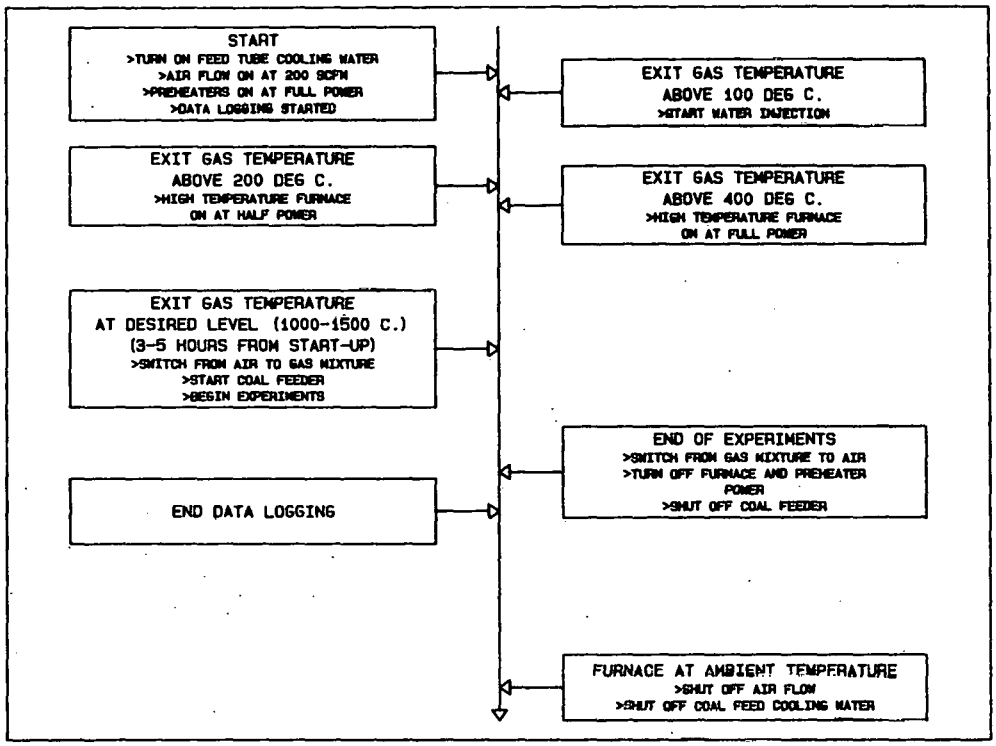

FIGURE 10-2. Timeline of normal operational procedure for the gas mixing, water injection, and heating system.

The coal feed tube used to inject coal particles into the hot gas stream in the observation chimney proved particularly troublesome. As designed, the feed tube consisted of a 1/16 inch transport tube sheathed in a 1/4 inch water jacket extending up through the base of the furnace to the top of the distributer plate. At furnace operating temperatures, the cooling water flow in the jacket proved grossly inadequate. During one of the first tests with the feed tube in place, this led to a weld failure at the distributor plate and injection of steam and water into the observation chimney at a furnace temperature of 1200°C. This incident, although spectacular, proved less catastrophic than had been feared, and no damage resulted to the furnace or observation chimney.

A new feed tube was designed and constructed with the goal of providing the maximum possible cooling water flow while keeping the tube cross-section as small as possible. The result, shown in Figure 10-4, uses thin-wall tubing and a stepped-down configuration to achieve a cooling water flow of 2.2 lpm. In addition, a thermocouple was installed to monitor exit cooling water temperature. No overheating problems have occurred with the new feed tube.

A second problem arises from the substantial cooling of the gas stream in the vicinity of the water-cooled coal feed tube. This results in a "cold spot" in the center of the distributor plate surrounding the coal injection point and persisting higher in the chimney. This is shown in the temperature profile of Figure 10-5, obtained 5 cm above the distributor plate.

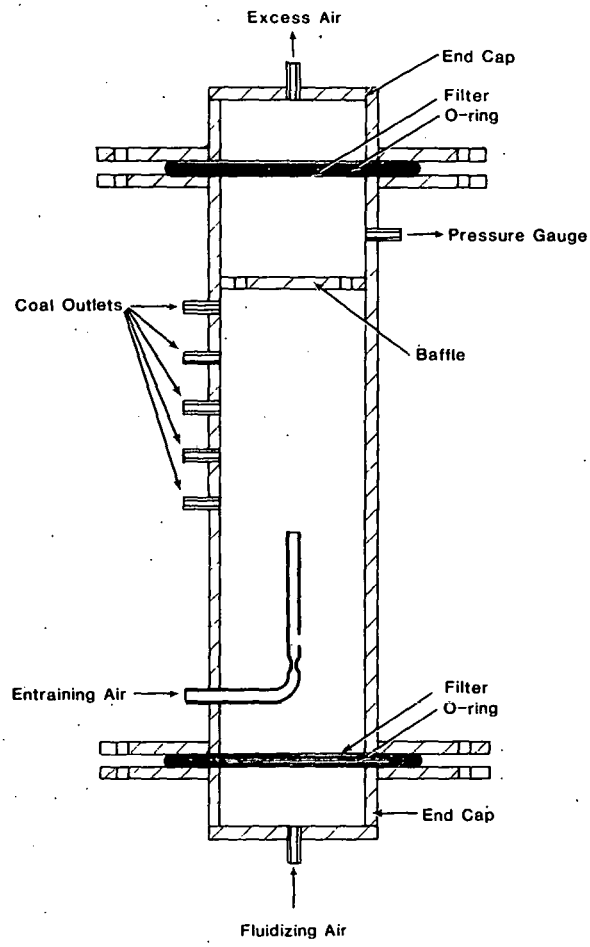

FIGURE 10-3. Drawing of the modified coal feeder.

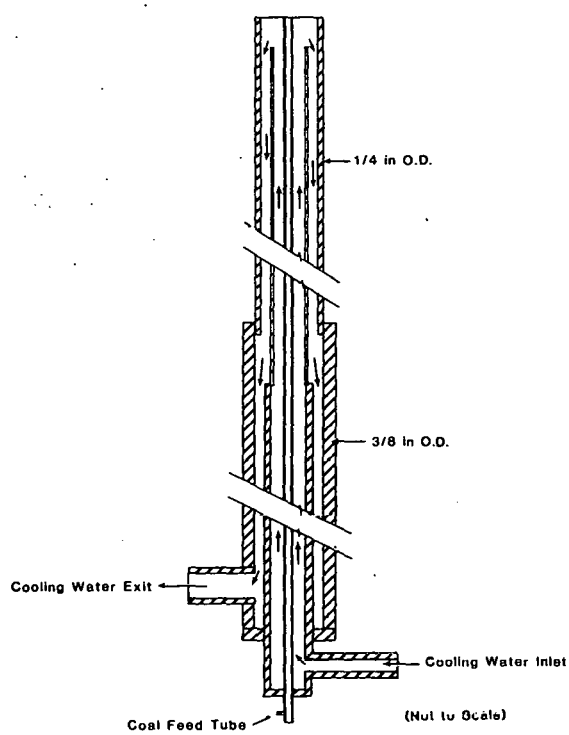

FIGURE 10-4. New feed tube design.

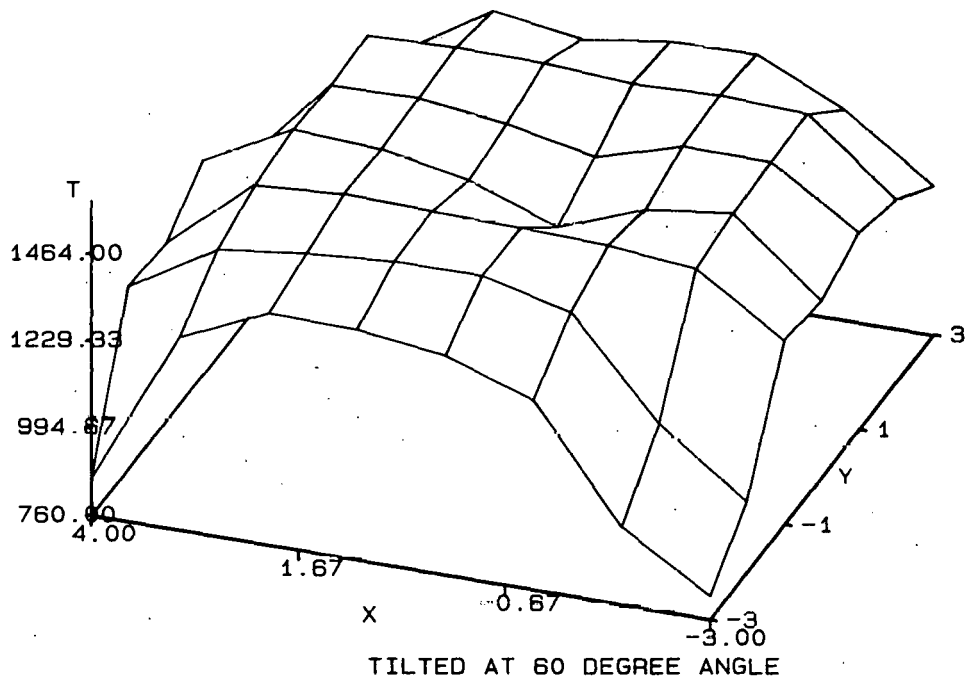

FIGURE 10-5. Temperature profile obtained 5 cm above the distributor plate.

A round 1/2 inch OD sheath of Zircar was machined to cover the feed tube. The sheath gradually tapers inward to minimize flow disturbance around the coal injection point. A small 1/4 inch thick Zircar cap with a hole to match the coal transport tube was also fabricated and fitted to the tip of the coal feed tube to minimize heat loss there. In subsequent tests, the presence of the insulating sheath does not appear to disturb the gas flow significantly, and greatly reduces the "cold spot" at the chimney center.

Computer System and Instrumentation

Expansion and improvement of the data acquisition programs has continued, along with modification necessitated by instrumentation changes. New programs have been written to control the Data 6000, collect and perform statistical analyses of the data as part of the pyrometer callibration.

After an inexplicable failure and subsequent factory repair of the Tecmar Analog-to-Digital converter (ADC) board, no additional problems have been noted. To improve accuracy for thermocouple inputs, the ADC inputs were changed from bipolar to unipolar mode.

The only major problem with data acquisition instrumentation has been with the panel meters which monitor voltage and amperage output of the furnace power supplies. The basic cause of the problem is a strong AC ripple on the DC output, which at operating power is passed through the meters' analog outputs to the ADC, causing spurious readings on most input channels. Factory modification of the meters moderated but did not eliminate the problem.

As filtering of the meter inputs and analog outputs had marginal effect, it was decided to completely isolate the meter output from the ADC. This will be accomplished by storing the analog output voltage in a capacitor which is alternately shunted across the meter outputs and across the ADC inputs. Tests with a manually switched system were successful, and a device to accomplish this under computer control (Figure 10-6) is nearly completed.

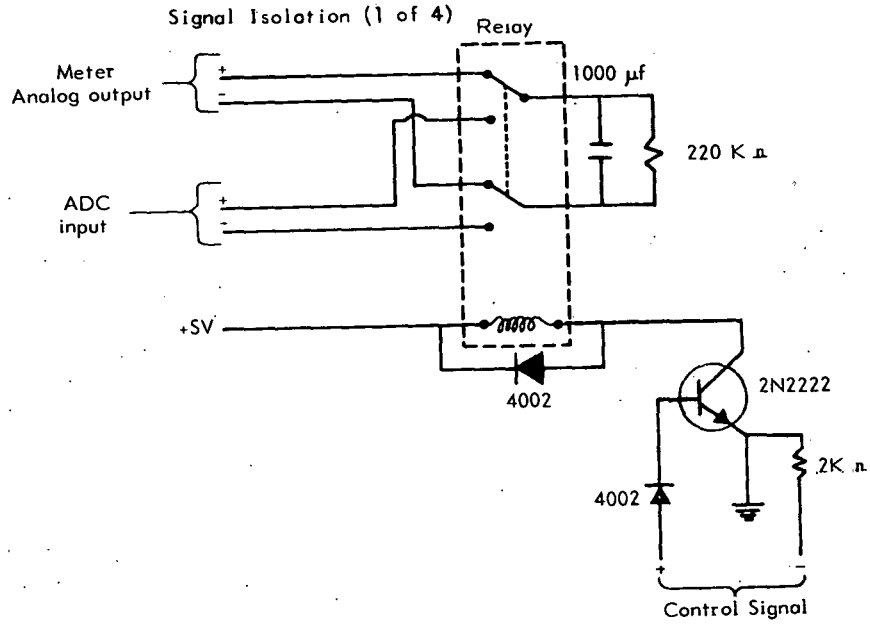

FIGURE 10-6. Schematic of signal shunting device.

Photographic and Pyrometer System

The completion of the coal feed system allowed testing of the photographic system and optical pyrometer under actual operating conditions. Qualitative visual observations at a temperature of 1200°C and an air flow of 200 scfh show particles igniting 1-2 cm above the feed tube exit, with burnout occurring below the top of the observation chimney. Definitive measurements will be made at a later date, but the smooth path of the particles up the chimney centerline indicates the flow is laminar.

Photographs of coal particles obtained under operating conditions at different microscope magnifications were obtained. Work is continuing to determine the best combination of film and strobe intensity for each magnification. Focusing on the coal particle stream proved unexpectedly easy, either by using the tip of a small thermocouple as a target or by focusing on the incandescent streaks of the burning particles. It was also found to be possible to visually observe momentary images of the coal particles through the microscope using the strobe 60 Hz viewing mode.

Calibration of the optical pyrometer is continuing to provide temperatures and to optimize signal/noise. Although particle temperatures were not obtained during the furnace tests with coal feed, it was shown that the pyro-

meter had sufficient sensitivity to readily detect light emissions from the burning particles. Several samples of these signals were stored on disc for subsequent use in developing sampling and analysis procedures. It was also found that operation of the strobelight had no grossly adverse effect on the optical pyrometer.

10.2.2 Combustion Testing of Ultra-Fine Ground Coal

Pilot-scale testing to evaluate the effects of ultra-fine coal grinding on ash fouling is one of the objectives of the research program at the Energy Research Center. Currently, testing is ~50 pct complete. The test schedule developed consists of three test burns using Beulah high sodium lignite with coal particle sizes as follows;

1. ~80 pct <75μm (Standard grind ~80 pct <200 mesh),
2. ~80 pct <44μm (~80 pct <325 mesh), and
3. <15μm (micronized).

Combustion testing was performed using a standard grind and the micronized samples. The coal properties of the two tests are shown in Table 10-1. Coal ash analyses are shown in Table 10-2. The moisture content of the two samples differed by approximately 10 pct; and in the attempt to keep as many parameters constant as possible, the standard grind will be repeated with the moisture content approximately 17 pct. The test burn using coal particle sizes of ~80 pct <44μ will be conducted with an identical moisture content of 17 pct.

TABLE 10-1

COAL PROPERTIES OF TESTS PERFORMED USING BEULAH HIGH SODIUM LIGNITE

Coal size:	80%<74μm		<15μm	
	As Burned	Dry Basis	As Burned	Dry Basis
Proximate Analysis (pct):				
Moisture	26.7	N/A	16.7	N/A
Ash	6.7	9.1	8.5	10.2
Volatile Matter	28.2	38.5	31.8	38.2
Fixed Carbon	38.4	52.4	43.0	51.6
Heating Value, Btu/lb	7,856	10,718	8,856	10,631
Ultimate Analysis (pct):				
Carbon	47.7	65.1	53.3	64.0
Hydrogen	6.2	4.4	5.2	3.3
Nitrogen	0.6	0.8	0.7	0.8
Sulfur	0.9	1.2	1.1	1.3
Ash	6.7	9.1	8.5	10.2
Oxygen (diff.)	37.9	19.4	31.2	37.5

TABLE 10-2

COAL ASH ANALYSIS (PCT)[1]

	80% <74μm	100% <15μm
SiO_2	19.7	20.7
Al_2O_3	12.1	12.2
Fe_2O_3	8.1	7.8
TiO_2	0.8	0.2
P_2O_5	1.0	1.0
CaO	18.2	18.2
MgO	5.9	5.5
Na_2O	9.4	8.6
K_2O	0.3	0.2
SO_3	24.5	24.9

[1]All values are normalized to 100 pct.

The test using micronized coal did not result in an appreciable decrease in the amount of ash deposited on the probes as compared to results from the standard grind. However, the deposit formed on the probes during the test burn using the micronized coal differed from the deposit obtained during the standard grind test in several ways. First, the shapes of the deposits were dissimilar. The micronized coal deposit had a very depressed center that appeared to extend down to the inner white ash layer next to the tube as can be seen in Figures 10-7, 10-8a, and 10-8b. Figure 10-7 is a photograph of the standard grind test deposit and Figures 10-8a and 10-8b are photographs of the deposit formed during the micronized test burn.

Second, the structures of the deposits for the two tests were different. The deposit from the standard grind was of the typical outer sinter layer appearance and resembled "feathering" whereas the deposit formed during the micronized test resembled "brush bristles" or "pine needles."

The relative amount of ash deposited as the inner white layer or the outer sinter layer also differed between the tests. More inner white layer ash (3.5 times) was deposited during the micronized test than during the standard grind test. The chemical analyses of the probe ash layers are presented in Table 10-3.

FIGURE 10-7. Photograph of the standard grind test deposit.

FIGURE 10-8a. Photograph of the deposit formed during micronized test burn.

FIGURE 10-8b. Photograph of partially removed deposit formed during micronized test burn.

The strength of the ash deposited during the micronized test was weaker than the deposit formed by combusting the standard grind coal. The micronized deposits were removed easily and crumbled into smaller fractions; however, the smaller fractions were extremely hard.

10.2.3 Evaluation of System for Determination of Gas Temperatures in Coal Combustion Systems

A project has been undertaken to evaluate the available methods for the point measurement of flame temperatures, i.e. temperature mapping of the flame zone, in a coal fired combustor.

A thorough literature search was made to identify the various types of measurement techniques available. In general, thermocouple systems appear to be the best system available for point temperature measurements, despite the errors involved in their application. A thorough analysis of the errors and the methods used to reduce them has been completed.

For the application of point temperature measurements in UNDERC's pilot scale coal fired combustors, a high velocity thermocouple appears to be the best choice. A design tailored to this application is being considered and will most likely be implemented in the near future.

TABLE 10-3

PROBE ASH CHEMICAL ANALYSIS[1] (PCT)

Ash Layer:	Inner White Layer		Outer Sinter Layer	
Coal Size:	80%<74μm	<15μm	80%<74μm	<15μm
Composition (SO_3 free):				
SiO_2	22.7	28.8	25.1	34.7
Al_2O_3	13.7	14.1	14.5	11.1
Fe_2O_3	9.7	12.9	10.5	17.3
TiO_2	1.1	1.1	1.1	0.8
P_2O_5	1.1	1.0	0.8	0.6
CaO	25.9	21.3	30.8	19.3
MgO	6.1	5.7	8.0	4.8
Na_2O	19.2	14.6	9.0	11.2
K_2O	0.5	0.5	0.1	0.2

[1]All values are normalized to 100 pct.

11. - FLUIDIZED-BED COMBUSTION OF LOW-RANK COALS

Project No.: 7206

B&R No.: AA3505450
AA3510100

Submitted by: M.L. Jones, Manager, Coal Utilization Research Division

Prepared by: D.R. Hajicek, Research Supervisor, Fluidized-Bed Combustion

Assigned UNDERC Personnel:
B.J. Zobeck
B.G. Miller
D.R. Hajicek
B.M. Gumeringer
D.S. Willson
R. Patel
A.L. Severson

Assigned AWU Personnel:
M. Bobman
R. Gehringer

Assigned UND Faculty:
N.S. Grewal

11.1 GOALS AND OBJECTIVES

The Fluidized-Bed Combustion (FBC) project at the University of North Dakota Energy Research Center (UNDERC) has two major goals: first, to resolve identified problems such as bed agglomeration, low turndown ratio, and enhanced utilization of SO_x sorbents; and second, to continue the development of a data base on the FBC process and systems utilizing low-rank coals.

Specific objectives of the Fluidized-Bed project for the first year of the Cooperative Agreement which contribute to these major goals are:

1. The preparation of a comprehensive topical report on the performance of low-rank coal in Atmospheric Fluidized-Bed Combustion.

2. The development of a data base on the formation of bed material agglomerate, including pilot plant testing with various levels of ion exchanged lignite, effects of operation under reducing conditions, design and construction of a gas and particulate sampling probe for insertion into the 2.25 sq ft combustor bed, and analytical studies to formulate a mechanism and define the role of sodium in the formation of agglomerates.

3. An engineering evaluation of alternative coal feeding systems, and possible testing of an alternative system for effects on agglomeration.

4. The examination of advanced FBC concepts being developed under METC contracts for applicability to low-rank coals.

5. Evaluation of heat transfer coefficients in AFBC of low-rank coals.

11.2 ACCOMPLISHMENTS

During the second quarter of the Cooperative Agreement, work was completed in the following areas:

11.2.1 Pilot Scale Testing

11.2.1.1 Bed Agglomeration

The two runs in a scheduled test series to determine the effect of a reducing atmosphere (0 pct excess air) on bed agglomeration were completed with the 2.25 ft^2 atmospheric fluidized-bed combustor at UNDERC. It had been suspected that reducing conditions in isolated areas of the bed could be contributing to the agglomeration problem associated with burning a high sodium North Dakota lignite. A third run has not yet been completed. It was determined that Beulah lignite should be burned in a silica sand bed with 20 pct excess air for the purpose of providing baseline data on bed agglomeration for comparison with results from the two 0 pct excess air runs.

Run conditions and results from Runs BU4-0383 and BU5-0483 are presented in Table 11-1. Run BU4-0383 was a 76-hour run (actual hours burning coal) in which Beulah North Dakota lignite was burned in a silica sand bed with approximately 0 pct excess air and no ash reinjection (20 pct excess air was usually specified in previous runs). A 1650°F bed temperature was used for the run.

Run BU5-0483 (100 hours on coal) was designed to be identical to the previous run except that the fly ash collected by the primary cyclone was reinjected into the combustor and the test duration was longer. Lignite from Beulah, North Dakota was used during this run, although the coal was not identical to that burned during Run BU4-0383. The coal and coal ash analyses are presented in Table 11-2. It is important to note the difference in sodium levels for the two coal samples.

Neither of the two reported runs was shortened because of loss of fluidization due to severe bed agglomeration. No significant agglomeration occurred, though some clumps of bed particles were observed on the lower walls of the bed. These formations apparently formed in the static bed as it cooled after shutdown. Also, slight slag build-up on the upper side of the top bed cooling coil was noted.

Bed agglomeration was noted after Run BU5-0483. Large fused bed material formations were noted between and above the upper two bed cooling coils (the upper formation fell from tubes before the photograph was taken). The inner portions of the deposits were quite friable, but the deposits were coated with a hard fused layer on the bed side of the deposits. The walls of the bed also had similar deposits.

Bed composition is plotted as a function of run time in Figure 11-1 (BU4-0383) and Figure 11-2 (BU5-0483). The sodium concentration in the bed increased rapidly during both runs. End-of-run sodium concentrations of the beds exceeded levels at which bed agglomeration has previously occurred when burning an untreated Beulah high sodium lignite in a silica sand bed.

TABLE 11-1

RUN CONDITIONS AND RESULTS FROM
BU4-0383 AND BU5-0483 AFBC RUNS

Run Number	BU4-0383	BU5-0483	
Test Duration, hr	76	100	
Purpose of Test	Bed agglomeration testing with silica sand bed, 0 pct excess air, and no ash reinjection.	Bed agglomeration testing with silica sand bed, 0 pct excess air, and ash reinjection.	
Type of Coal:	Beulah North Dakota lignite (7.4 pct Na_2O in ash)	Beulah North Dakota lignite (10.5 pct Na_2O in ash)	
Bed Material	Grade #10 Silica Sand	Grade #10 Silica Sand	
Ash Reinjection	No	No	Yes
Ash Reinjection Rate, lb/hr	0	0	15.1
Additives	None	None	None
Velocity, ft/sec	5.6	6.0	5.8
Excess Air, %	0.3	1.3	-1.6
Flue Gas, Conc., %:			
O_2	0.3	0.5	0.2
CO_2	18.3	18.6	18.5
CO	0.6	0.5	1.1
Alkali/Sulfur Ratio	1.15	1.20	*
Sulfur Retention, %	61.1	64.6	65.8
Emissions, lb/MM Btu:			
SO_2	1.41	1.29	1.24
NO_x	0.16	0.17	0.13
Combustion Efficiency, %	98.38	99.51	
Overall Heat Transfer Coefficient, Btu/hr ft^2 °F	44.9	45.28	44.92

*Analysis not yet received.

TABLE 11-2

COAL AND COAL ASH PROPERTIES
BEULAH HIGH SODIUM NORTH DAKOTA LIGNITE

Run Number:	BU4-0383		BU5-0483	
	As Burned	Dry Basis	As Burned	Dry Basis
Proximate Analysis:				
Moisture	22.7	N/A	18.4	N/A
Ash	10.0	12.9	9.1	11.2
Volatile Matter	30.1	39.0	29.4	36.0
Fixed Carbon	37.2	48.1	43.1	52.8
	100.0	100.0	100.0	100.0
Ultimate Analysis:				
Moisture	22.7	N/A	18.4	N/A
Ash	10.0	12.9	9.1	11.2
Carbon	46.9	60.6	51.9	63.6
Hydrogen	2.9	3.8	3.3	4.0
Nitrogen	0.7	0.9	0.7	0.9
Sulfur	1.1	1.4	1.2	1.5
Oxygen (diff.)	15.7	20.3	15.4	18.8
	100.0	99.9	100.0	100.0
Heating Value:				
Btu/lb	7,646	9,896	8,479	10,388
Elemental Ash Analyses:				
SiO_2		25.3		18.5
Al_2O_3		11.9		12.4
Fe_2O_3		11.3		8.5
TiO_2		0.8		0.8
P_2O_5		0.7		1.0
CaO		15.8		17.7
MgO		5.4		5.8
Na_2O		7.4		10.5
K_2O		0.2		0.1
SO_3		21.2		24.7
		100.0		100.0

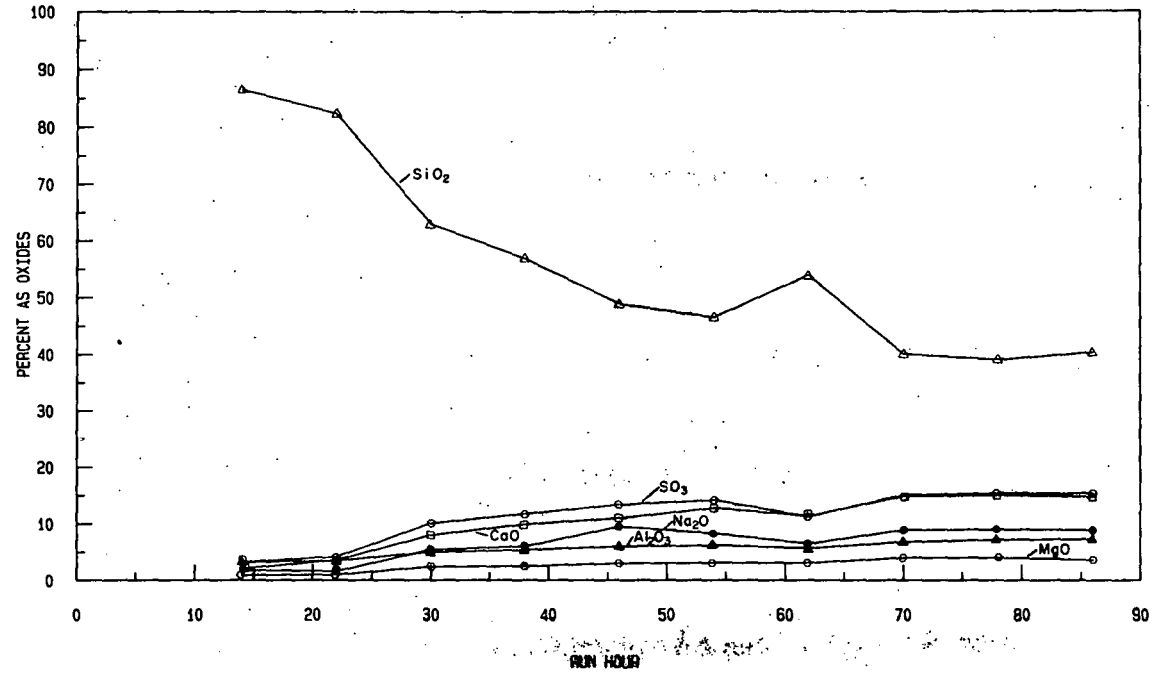

FIGURE 11-1. Change in bed composition with time (FB2-BU4-0383).

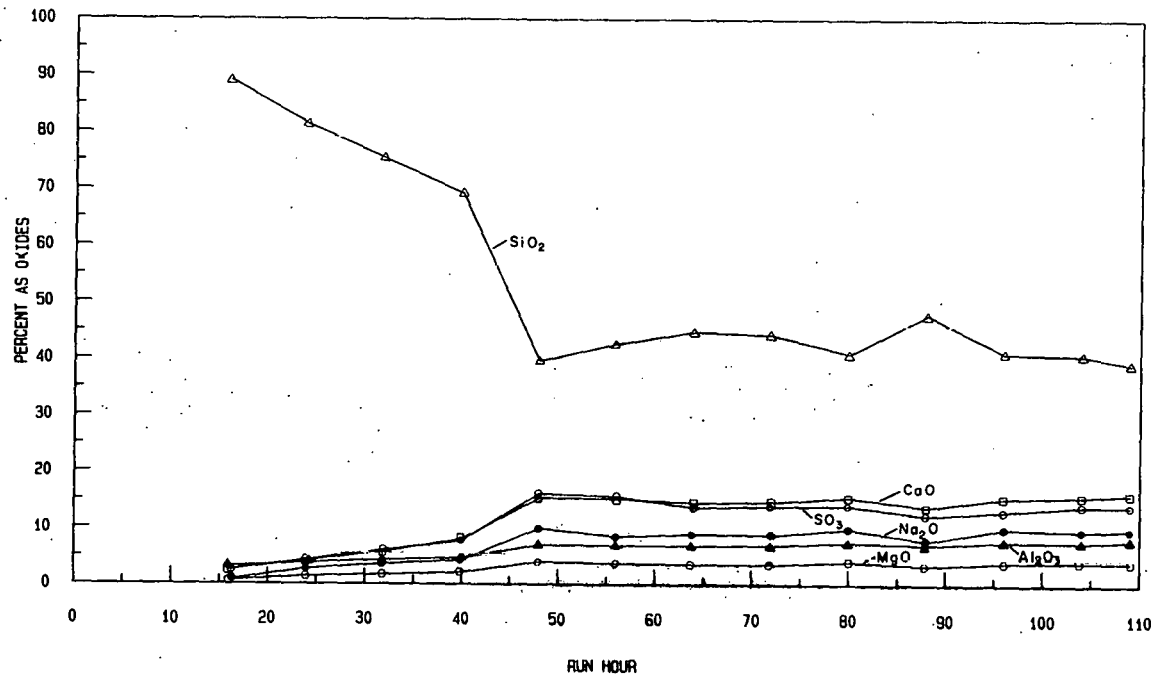

FIGURE 11-2. Change in bed composition with time (FB2-BU5-0483).

It is probable that the bed material agglomeration would have caused loss of fluidization in a short time if the reported runs had been continued. This conclusion is based on 1) a more rapid increase in sodium levels in the bed than is typically noted, 2) a rapid growth of the bed particle size, and 3) the end-of-run agglomerates that were observed. Based upon the analytical results it appears that low excess air (reducing conditions) increases the agglomerating tendencies of the silica sand bed when burning a high sodium Beulah lignite, even though these tests did not result in severe agglomeration during their duration. A more definite conclusion will be possible after completion of the base line test with oxidizing condition.

11.2.1.2 Heat Transfer

Bed particle size and overall heat transfer coefficient are plotted as a function of run time in Figure 11-3 (BU4-0383) and Figure 11-4 (BU5-0483). Extremely rapid growth of the bed particle size was seen in both runs. As a result the overall heat transfer coefficient for the bed cooling coils decreased steadily during the runs.

11.2.1.3 Emissions and Operational Performance

A significant reduction in NO_x emissions was noted with the 0 pct excess air runs. Less than 0.2 lb NO_x/MM Btu input was observed during the two runs. This level is significantly below the NO_x emission level encountered in previous runs when 20 pct excess air has been supplied with the coal. The reduction in NO_x emissions with low excess air would be expected due to the lower bed oxygen concentration (1).

Higher carbon monoxide concentrations in the flue gas were also noted and can be attributed to lower oxygen concentrations during the runs.

A relatively low combustion efficiency, 98.38 pct, was obtained during Run BU4-0383. Generally, combustion efficiencies of 99.5+ are observed when burning Beulah lignite. Ash reinjection was not used during Run BU4-0383 but was used during Run BA5-0483. A significant increase in combustion efficiency, 99.51 pct, was observed during the second run.

11.2.2 Bed Material Analysis

In order to increase the understanding of the mechanisms of the agglomeration process occurring during the fluidized combustion of low-rank coal, microscopic, and x-ray elemental mapping are being used in addition to routine elemental analysis. Samples of bed material from BA1-2181, run hour 40; BI2-0782, run hour 35; BI4-0982, run hour 46; and BU5-0483, run hour 100, were placed in a Jeol Model JXA-35 electron probe x-ray microanalyzer (SEM) and area and point analyses were obtained using energy dispersive x-ray fluorescence. Micrographs were taken to identify the sample regions corresponding to specific x-ray spectra, thus yielding an elemental composition for a known area or point of the sample. Samples were then heated in a Leitz Metallux II Heating Stage Microscope at temperatures ranging from 1292° to 1832°F to determine the effect of heating on chemical composition.

Table 11-3 gives the results of select tests for the elements Na, S, Si, and Ca, where the percentage change is negative for a decrease, and positive for an increase in relative occurrence after heating.

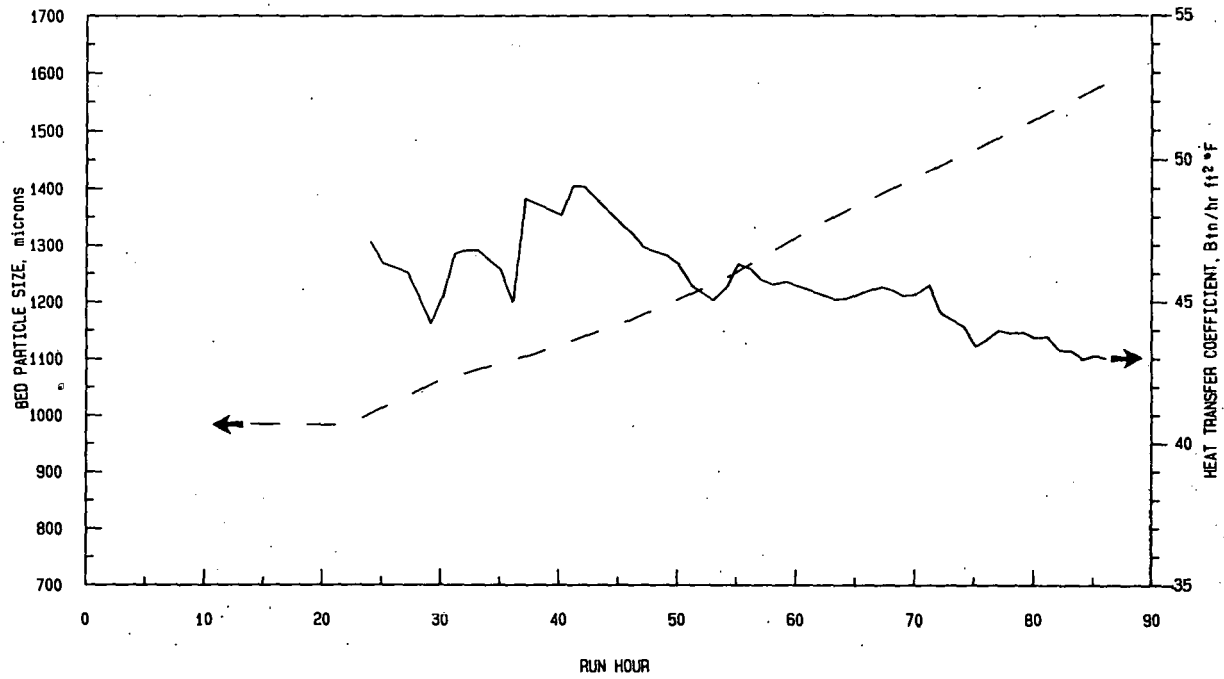

FIGURE 11-3. Heat transfer coefficient and bed material size versus run hour (FB2-BU4-0383).

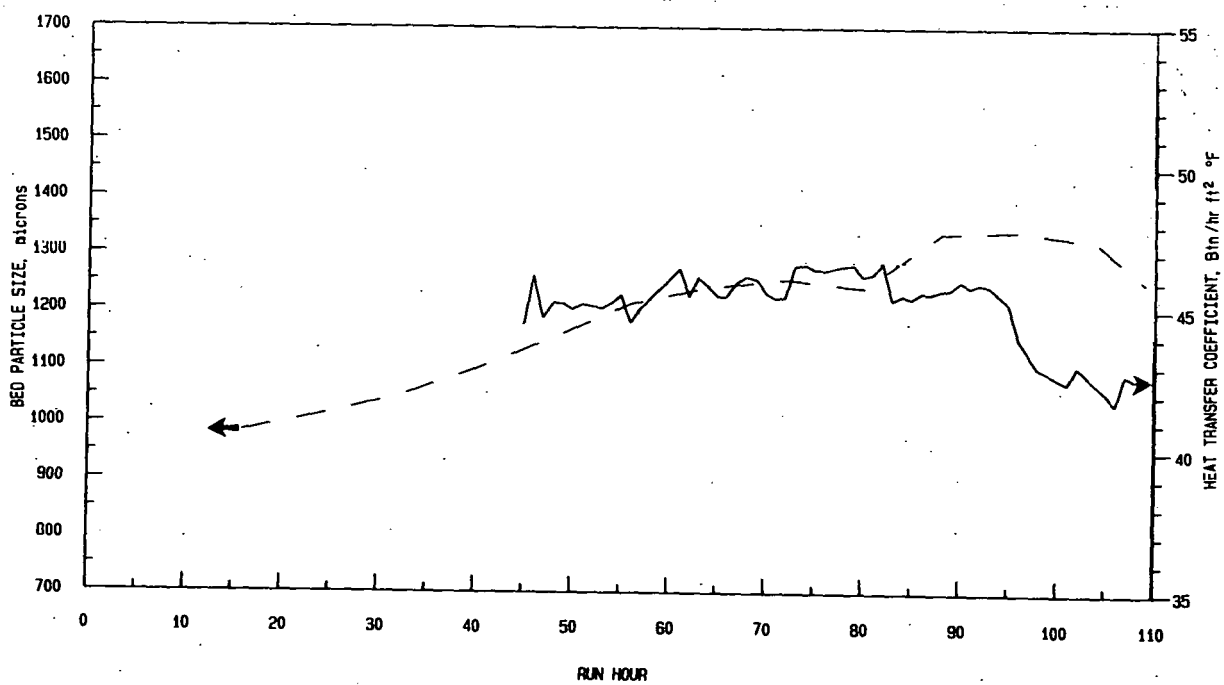

FIGURE 11-4. Heat transfer coefficient and bed material size versus run hour (FB2-BU5-0483).

TABLE 11-3

CHANGE IN CHEMICAL COMPOSITION OF BED MATERIAL SAMPLES UPON HEATING

Sample	Heat Treatment Temperature, °C	°F	Change in Composition, % Na	S	Si	Ca
BA1-2181	800	1472	-61	- 9	0	64
	900	1652	-28	-27	14	42
	900	1652	-36	-38	70	47
BI2-0782	800	1472	-37	- 3	5	10
BI4-0982	750	1382	-36	-14	43	43
	800	1472	-17	- 6	11	11

Though only a few tests have been completed, evidence suggests that Na and S are volatilized at temperatures as low as 1382°F. One of the perplexing phenomena of the agglomeration problem is the formation of stable crystalline phases at temperatures well below their actual melting points, as is seen in the case of the melilite series; the melting point of gehlenite ($Ca_2Al_2SiO_7$) is 2894°F, and that of akerminite ($Ca_2MgSi_2O_7$) is 2649°F. Melilite species have been identified in agglomerates formed in the UNDERC combustor by x-ray diffraction analysis. The loss of Na and S from bed material samples at 1382°F, coupled with similar investigations on ash fouling deposits (3), suggests that low temperature sublimation may contribute to the initial deposition and subsequent crystallization noted on boiler tubes or bed material particles.

Future work will be performed to clarify the relationship between temperature, gaseous environment, chemical composition, and agglomeration. Of particular interest are the associations of Na in coals and how they contribute to particle size growth in the fluidized bed. To isolate specific factors which promote agglomeration, laboratory ash samples will be prepared, consisting of coal ash, mineral mixtures, and carbonaceous material containing ion-exchanged Na.

11.2.3 Test Burn of Lignite at French Island

In discussions with Otter Tail Power Company, UNDERC has agreed to participate in planning and analysis of a full-scale AFBC test. The test will use a high sodium Beulah, North Dakota lignite at the French Island utility boiler owned and operated by Northern States Power Company (NSP). The French Island unit is a retrofit atmospheric fluidized-bed combustor located in LaCrosse, Wisconsin, designed to burn wood and rated at 15 MW(e).

It was agreed that UNDERC's involvement in the test would include:

1. assistance with preparing a test plan,
2. monitoring during the test burn,
3. sample analyses of bed material and fly ash collected during the test, and
4. preparation of a test report.

It is also understood that since UNDERC's involvement is sponsored by funding supplied through the Cooperative Agreement, the test report would be public information. Thus far, a proposed test and sampling procedure have been prepared by UNDERC and reviewed and approved by both Otter Tail and NSP. The test burn was scheduled to occur in October 1983, but due to an over supply of wood, NSP has rescheduled the test for April 1984.

11.2.4 2.25 Ft^2 AFBC Modifications

The access door to the combustor was modified to allow the use of five 1½" diamter bayonet heat transfer probes. Previously only 1" tubes could be inserted through the door. These tubes along with three more tubes in the freeboard will be used for heat transfer tests to simultaneously measure heat transfer coefficients in the bed, the splash zone, and the freeboard. The tubes will be air-cooled to an operational surface probe temperature of approximately 1150°F as measured by thermocouples embedded in the surface of the tubes. Air cooling allows for operation at temperatures that would more accurately simulate actual conditions encountered with steam cooled tubes. The purpose of the test is to measure heat transfer coefficients that occur in the different zones during the fluidized bed combustion of low-rank coal and evaluate the amount of turndown that can be accomplished by varying the bed height.

11.2.5 Heat Transfer Paper

A paper entitled "Heat Transfer to Horizontal Tubes in a Pilot-Scale Fluidized-Bed Combustor Burning Low-Rank Coal", was presented at the jointly sponsored meeting by AIChE and ASME in Seattle, Washington during July 24-27, 1983. The authors were N.S. Grewal and G.M. Goblirsch. The paper's principal conclusion was that the heat transfer coefficient determined experimentally using UNDERC's 2.25 ft^2 AFBC (5) was within ±25 pct of the value obtained using the correlation of either Grewal (6) or Bansal, et al (7). The calculated outside heat transfer coefficient included the radiation contribution determined from the estimates of Baskakov et al (8).

11.2.6 Topical Report

Work on the topical report covering atmospheric fluidized-bed combustion is proceeding with sections being completed at UNDERC, Combustion Power Company, and Radian Corporation.

Progress to date can be summarized in the following manner:

Combustion Power Company submitted the following first drafts for the topical report:

-AFBC Applications
-Cost Comparisons
-Cost Sensitivity Analysis of Low-Rank Coal AFBC Systems (with Appendix)

First drafts of the following sections were completed at UNDERC during this quarter:

-Sulfur Emissions and Sorbent Utilization
-Oxides of Nitrogen
-Particulates

Sections for which no first drafts have been completed include:

-LRC Deposits and Properties
-Problems with Utilization in Conventional Combustion Systems
-Agglomeration and Fouling
-Other Emissions (CO, THC, Trace Elements)
-Solid Waste Characterization

Present plans call for completion of the first draft of the report during the first year of the cooperative agreement. It is anticipated that this schedule will be met.

11.2.7 Advanced Concepts in AFBC of Low-Rank Coals

A trip was made to METC to review information on advanced concepts for FBC to determine their applicability to low-rank coals. A discussion was held on some of the technical aspects of the seven advanced concepts that show the highest potential for exceeding conventional FBC technology. The technical evaluation of the seven proposals was not available at this time, but is expected to be released by next quarter.

11.3 REFERENCES

1. Jonke, A.A. Reduction of Atmospheric Pollution by Application of Fluidized-Bed Combustion, Annual Report, July 1968-June 1969, (ANL/ESCEN-1002).

2. Goblirsch, G.M. S.A. Benson, F.R. Karner, D.K. Rindt, and D.R. Hajicek. AFBC Bed Material Performance with Low-Rank Coals. Twelfth Biennial Lignite Symposium, Grand Forks, ND, May 18-19, 1983.

3. Rindt, D.K., S.J. Selle, and W. Beckering. Investigations of Ash Fouling Mechanisms for Western Coals Using Microscopic and X-ray Diffraction Techniques, ASME 79-WA/CD-5, Winter Annual Meeting, New York, December 2-7, 1979.

5. Grewal, N.S. and D.R. Hajicek. Experimental Studies of Heat Transfer from an Atmospheric-Fluidized-Bed Combustor to an Immersed Array of Horizontal Tubes. 7th International Heat Transfer Conference, Paper No. HX23, Munchen, Federal Republic of German, September 1982.

6. Grewal, N.S. A Gernalized Correlation for Heat Transfer Between a Gas-Solid Fluidized Bed of Small Particles and an Immersed Staggered Array of Horizontal Tubes. Powder Technology, Vol. 30, 1981, pp. 145-154.

7. Bansal, R.K., P.V. Kadaba, and P.V. Desai. Heat Transfer from Horizontal Tubes in Gas Fluidized Bed. Paper No. 80-HT-115, ASME/AIChE National Heat Transfer Conference, Orlando, Florida, July 27-30, 1980.

8. Baskakov, A.P., B.V. Berg, O.K. Vitt, N.F. Filippovsky, V.A. Kirakosyan, J.M. Goldobin, and V.K. Maskaev. Heat Transfer to Objects Immersed in Fluidized Bed. Powder Technology, Vol. 8, 1973, pp. 273-282.

12. - COAL/WATER SLURRY COMBUSTION

(New project; no work planned during this reporting period.)

13. - ASH AND SLAG CHARACTERIZAION

Project No: 7302 B&R No.: AA1515050

Submitted by: H. H. Schobert, Manager, Coal Science Division

Prepared by: H. H. Schobert, Manager, Coal Science Division; S. A. Benson, Research Supervisor; and Sharon Falcone, Postgraduate Fellow

Assigned UNDERC Personnel:
S. A. Benson
W. B. Hauserman
J. P. Hurley
F. R. Karner
W. A. Kinney

Assigned AWU Personnel:
S. Falcone
S. Braun
N. Forsman

13.1 GOALS AND OBJECTIVES

The goal of the Ash and Slag Characterization project is to develop a fundamental understanding of the properties and behavior of the inorganic constituents of low-rank coals at high temperatures. The project is therefore directed at studying the chemical changes occurring when low-rank coals are ashed and at measuring thermophysical properties of the resulting ashes and slags, with observed chemical changes or measured data then correlated with the chemical and mineralogical composition of the inorganic species in the coals.

A second goal of the project is to investigate slag-refractory interactions in the UNDERC slagging fixed-bed gasifier. This aspect of the project seeks to take advantage of opportunities to study actual slags and refractories in an actual operating gasifier--as opposed to laboratory simulations--and hence to add to the coal conversion data base on slag and refractory behavior. The slag-refractory interaction study is "target of opportunity" research in that it is wholly dependent on the operating schedule of the gasifier and on interesting or unusual effects arising during the run.

The objectives of the Ash and Slag Characterization project during this reporting period were to continue work on ashing of low-rank coal samples under controlled laboratory conditions, with attendant chemical and mineralogical analysis of the ashes; second, to continue measurements of the viscosity-temperature relationships of low-rank coal ash slags, with collateral development of mathematical relationships of viscosity to composition; and, third, to study the interaction of slag and refractory in the gasifier.

13.2 ACCOMPLISHMENTS

13.2.1 Coal Collection

Samples of low-rank coals have been collected from various mines in North Dakota, Montana, Colorado, New Mexico, and Texas. These coals are being characterized and will be used by all the Coal Science projects. The samples were carefully collected, homogenized, and stored in an inert atmosphere. The coals are available in several different sizes from -1 inch to -60 mesh and quantities from five gallons to 250 grams.

13.2.1.1 Sample Collection Procedure

Selection of coals to be used for characterization is based on specific properties of interest (i.e., Na content, slag viscosity, etc.) or on production tonnage. When the selection of mine and specific location within the mine has been made, the face of the seam is cleaned to expose a fresh non-weathered coal free from extraneous mineral matter which may have fallen from overburden. The seam is then measured and a megascopic description is made of the various features (lithotypes). Samples of coal are collected to obtain a channel sample. In some cases samples are also collected at various intervals throughout the seam, including overburden, interburden (if two seams are sampled) and underclay. All samples are stored and sealed in plastic and transported to UNDERC for preparation. A list of samples collected to date is in Table 13-1.

TABLE 13-1

COAL SAMPLES OBTAINED FOR CHARACTERIZATION

Mine	Rank	State
Absaloka (Sarpy Creek)	Subbituminous	Montana
Indian Head	Lignite	North Dakota
Beulah (High-Na)	Lignite	North Dakota
Beulah (Low-Na)	Lignite	North Dakota
Gascoyne (Red)	Lignite	North Dakota
Gascoyne (Blue)	Lignite	North Dakota
Velva	Lignite	North Dakota
Spring Creek	Subbituminous	Montana
Falkirk	Lignite	North Dakota
Glenharold	Lignite	North Dakota
Colorado Coal Co.	Subbituminous	Colorado
Navajo	Subbituminous	New Mexico
San Miguel	Lignite	Texas
Martin Lake	Lignite	Texas
Savage	Lignite	Montana
Center	Lignite	North Dakota

13.2.1.2 Preparation and Characterization

The channel samples are crushed, split, and stored under an inert atmosphere. A diagram which illustrates the procedure in detail is shown in Figure 13-1. The final splitting is done by a rotary riffler in an argon-purged glove box. The larger five-gallon sized samples are purged with argon in the vessel used for storage.

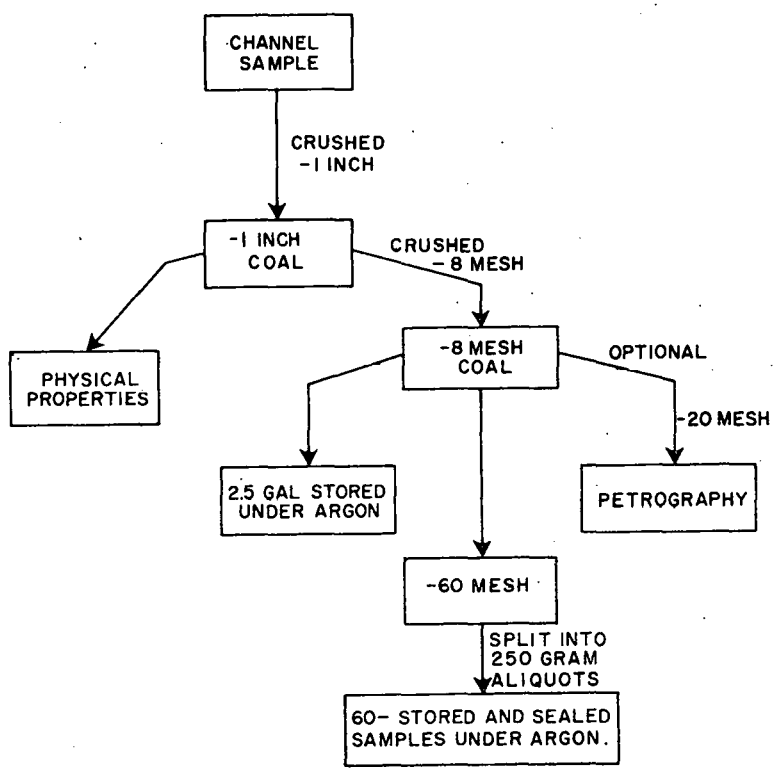

FIGURE 13-1. Schematic of sample preparation procedure for channel sample.

The samples collected at various locations within the seam are prepared for selected characterization techniques, such as petrography and separation of lithotypes.

The 250-gram samples of coal will be characterized by many different techniques, which will include the standard ASTM analyses, chemical fractionation, organic chemistry, pyrolysis, supercritical solvent extraction, distribution of mineral matter, trace element analysis, ash and slag chemistry. The results of the analytical determinations will be stored on computer for easy access and analysis. Indian Head lignite from North Dakota is used here as an example of some of the results obtained to date on the sample. This data is summarized in Table 13-2.

13.2.2 Ashing of Low-Rank Coals With Respect to Mineral Transformations

To date five coals have been low-temperature ashed and the resulting ash analyzed by x-ray diffraction: Beulah (Mercer Co., North Dakota), Velva/

TABLE 13-2

RESULTS OF ANALYSES FOR INDIAN HEAD LIGNITE

Ultimate Analysis	Wt %
C	44.08
H	6.36
N	0.64
S	0.38
Proximate	
Moisture	34.0
Volatile Matter	27.4
Fixed Carbon	33.8
Ash	4.8
Heat Content	7329 Btu/lb

Ash Analysis	Wt %
SiO_2	21.1
Al_2O_3	11.9
Fe_2O_3	8.5
TiO_2	1.0
P_2O_5	0.5
CaO	20.9
MgO	6.5
Na_2O	11.9
K_2O	0.1
SO_3	15.6
TOTAL	98.1

Carboxylic Acid Group Content	2.45 meq/gram maf Basis
Aromaticity of lithotypes determined by pressure differential scanning calorimetry	Whole Coal - 0.71 Fusain - 0.77 Durain - 0.71 Vitrain - 0.71
Mineral matter by Low Temperature Ashing	Quartz (SiO_2) Pyrite (FeS_2) Kaolinite ($Al_2Si_2O_3[OH]_4$)

TABLE 13-2 (Continued)

NEUTRON ACTIVATION ANALYSIS OF INDIAN HEAD LIGNITE FROM NORTH DAKOTA

Element	Concentration, ppm
Titanium	108.43 ± 20%
Iodine	<3.0
Manganese	4.58 ± 5%
Magnesium	411.91 ± 15%
Copper	<25.0
Vanadium	3.00 ± 2%
Chlorine	15.98 ± 20%
Aluminum	3024.14 ± 1%
Samarium	0.36 ± 2%
Uranium	0.29 ± 10%
Lanthanum	4.69 ± 1%
Cadmium	<1.0
Gold	<0.001
Arsenic	5.02 ± 1%
Antimony	0.22 ± 1%
Bromine	1.13 ± 1%
Sodium	6220.63 ± 1%
Potassium	<500.0
Cerium	7.80 ± 10%
Calcium	3759.80 ± 10%
Selenium	0.50 ± 10%
Thorium	1.02 ± 1%
Chromium	2.04 ± 15%
Europium	0.09 ± 10%
Ytterbium	0.35 ± 20%
Barium	518.77 ± 5%
Cesium	0.12 ± 10%
Silver	<0.08
Nickel	<25.0
Scandium	1.26 ± 1%
Rubidium	<5.0
Iron	3566.79 ± 3%
Zinc	6.39 ± 20%
Cobalt	1.60 ± 1%
Silicon	<35,000.0
Molybdenum	<10.0

Coteau (McHenry Co., Noth Dakota), Gascoyne Red and Blue Pits (Bowman Co., North Dakota) and Absaloka (Horn Co., Montana). All coals ashed are lignites except for the Absaloka subbituminous. Preliminary examination of x-ray diffractograms reveals the following trends in mineral transformations from ash samples generated at low temperature (~110°C) and those samples generated at 750° or 1000°C.

1. Oxidation of iron in the form of pyrite (FeS_2) to hematite (Fe_2O_3) and magnetite (Fe_3O_4).

2. Sulfur fixation of organically-bound calcium forming anhydrite ($CaSO_4$) at high temperatures.

3. Dehydration of bassanite ($CaSO_4 \cdot \frac{1}{2}H_2O$) to anhydrite ($CaSO_4$).

4. Formation of anhydrite in higher temperature ash due to reaction between calcite ($CaCO_3$) and/or bassanite ($CaSO_4 \cdot \frac{1}{2}H_2O$) and kaolinite ($Al_2Si_2O_5\ [OH]_4$).

5. Formation of aluminosilicate solution series, notably the melilite group $(Ca, Na, K)_2\ [Mg, Fe^{+2}, Fe^{+2}, Al, Si)_3\ O_7]$. Other minerals include lazurite $(Na, Ca)_8\ (AlSiO_4)_6\ (SO_4, S, Cl)_2$ and augite (Ca [Mg, Fe] Si_2O_5).

6. Dehydration of clays (i.e. kaolinite).

Figures 13-2 (A, B, C) and 13-3 (A, B, C) respectively, represent a series of diffractograms of Gascoyne Red and Gascoyne Blue ashes obtained at different temperatures (i.e. 110°C, 750°C and 1000°C). The oxidation of iron is apparent in both samples in the ash produced at 750°C (Figures 13-2B and 13-3B). According to Mitchell and Gluskoter (1976), hematite forms at 500°C and is often accompanied by anhydrite forming from reactions between pyritic sulfur and calcite. In both samples hematite (Fe_2O_3) and magnetite (Fe_3O_4) are found in high temperature ashes.

Although bassanite ($CaSO_4 \cdot \frac{1}{2}H_2O$) is not present in either of the low-temperature ashes of Gascoyne coals, anhydrite is present in ashes produced at high temperatures. Anhydrite, in high temperature ashes, may form from the dehydration of gypsum ($CaSO_4 \cdot 2H_2O$) or form due to the reaction of sulfur released from sulfides upon ashing with calcite or organically-bound calcium. The formation of bassanite in low temperature ashes is avoided due to the removal (by ion exchange with ammonium acetate) of organically-bound calcium available for sulfur fixation. Samples were pretreated twice with 100 ml of 1N ammonium acetate for 24 hours at 70°C. Samples were subsequently washed with 50 ml 1N ammonium acetate followed by 50 ml distilled water. Coals ashed at 750° and 1000°C were not pretreated with ammonium acetate and therefore conceivably contain significant amounts of organically-bound calcium which may experience sulfur fixation, thereby forming anhydrite.

Aluminosilicate solid solution series appear in ashes at 750°C and increase in intensity up to 1000°C, corresponding to a decrease in relative quartz (SiO_2) peak intensities and the disappearance of kaolinite. The Gas-

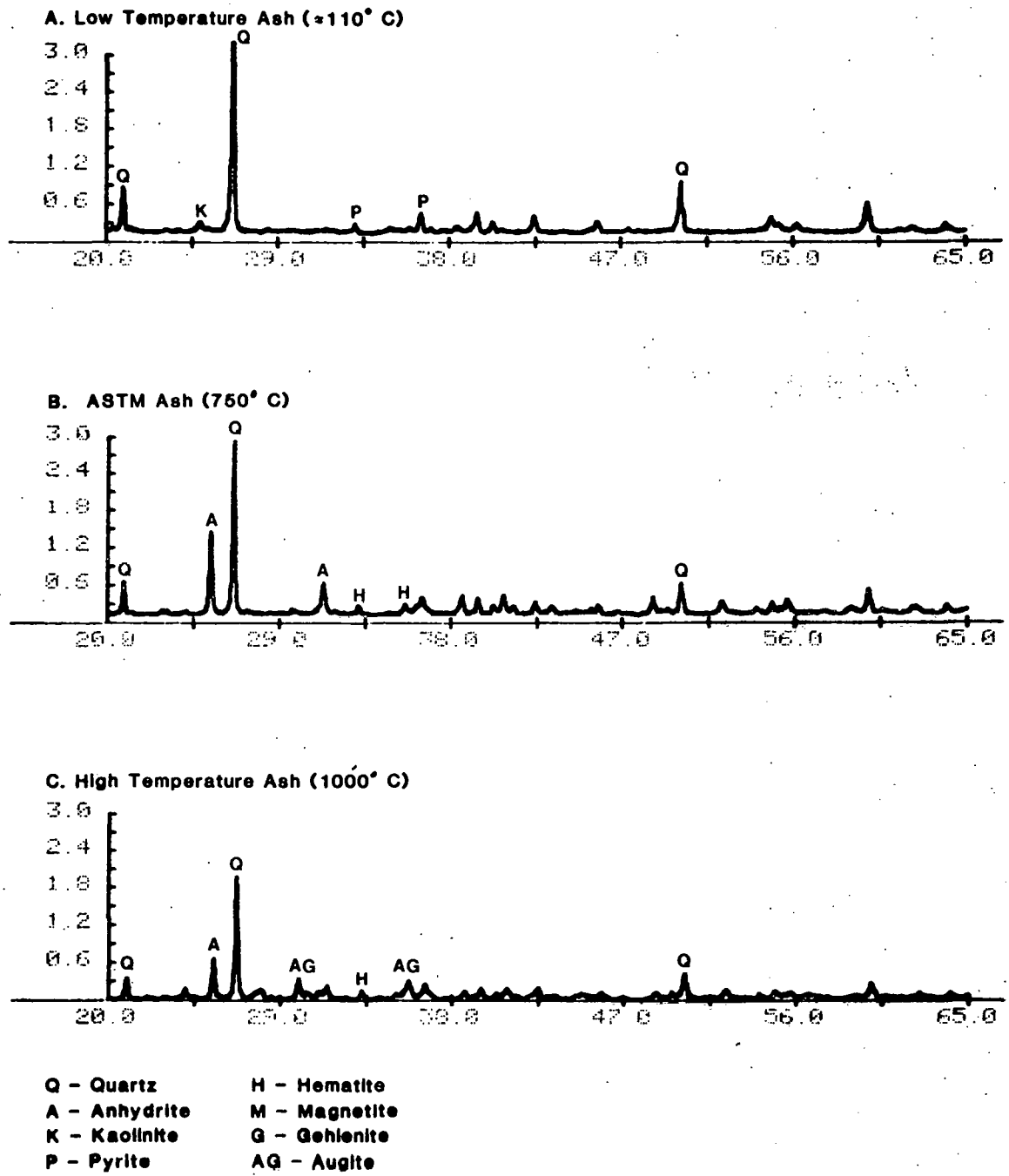

FIGURE 13-2. Gascoyne Red Pit

coyne Blue high-temperature ash (Figures 13-3B and 13-3C) contains predominately aluminosilicates (feldspathoids) exhibiting sodium and calcium substitution within the silica tetrahedra. The melilite solid solution series,

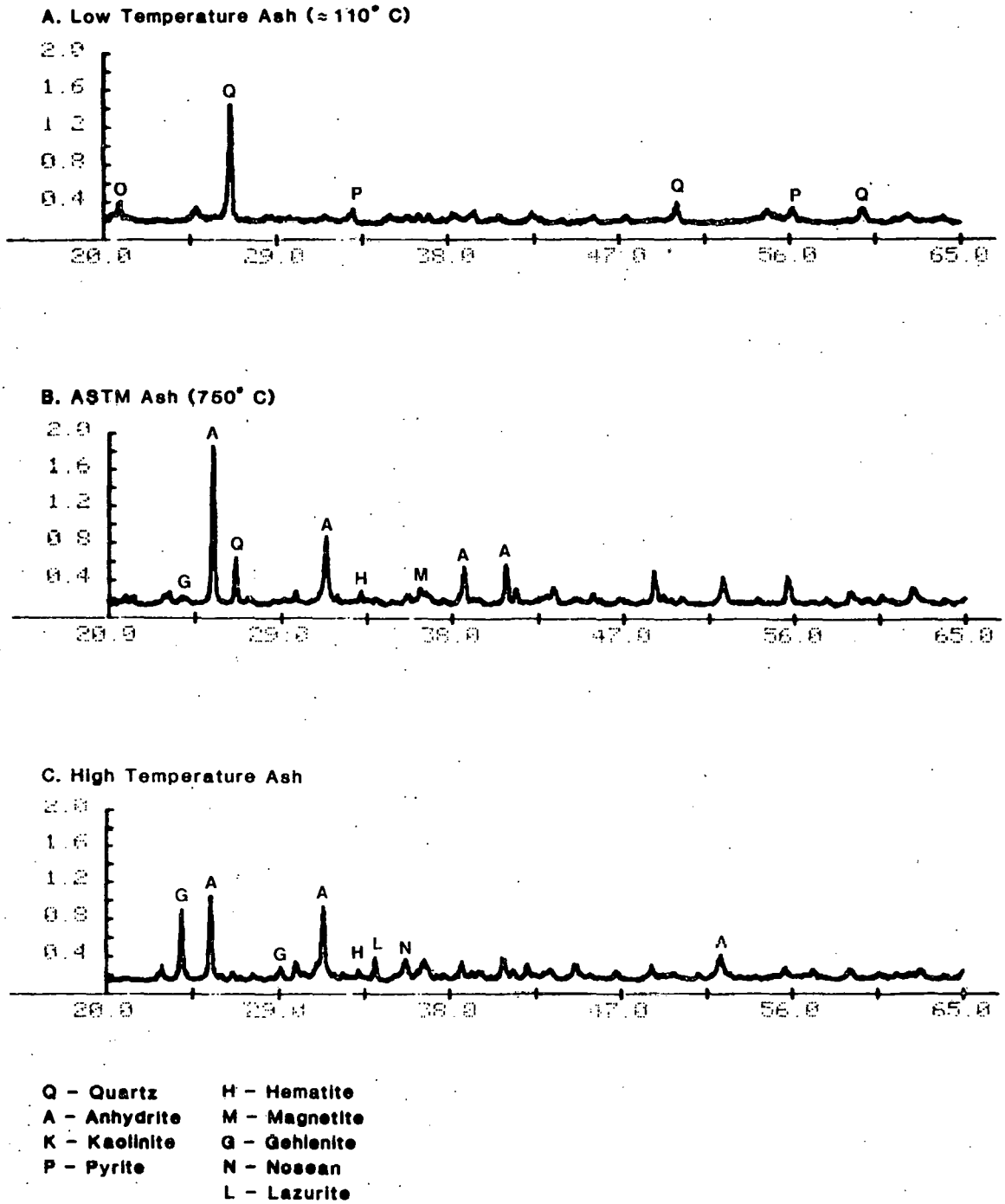

FIGURE 13-3. Gascoyne Blue Pit.

in the form of gehlenite ($Ca_2[Al_2SiO_7]$), appears in both Figures 13-3B and 13-3C, as does nepheline ($NaAlSiO_4$). The melilite structure solid solution phases are common in slags poor in Al_2O_3 and rich in CaO, and may arise from reactions of bassanite and kaolinite. Aluminosilicates appear only in the

high-temperature ash sample of the Gascoyne Red coal (Figure 13-2C) in the form of augite ($Ca[Mg,Fe]Si_2O_5$) and gehlenite.

The difference in the types of aluminosilicates that form at high temperatures from the two coals may relate to the types of cations available for substitution within the silica tetrahedra structure, and may have a relationship to boiler fouling behavior. The Gascoyne Blue is known to be a high fouling lignite, suggesting an abundance of organically-bound sodium in the coal, and possibly explaining the tendency for sodium and calcium substitution along with aluminum within the silica structure. The Red Pit, on the other hand, is not a high fouling coal, and exhibits mostly calcium and aluminum substitution in the silica tetrahedra.

X-ray diffraction data along with x-ray fluorscence data, petrographic identification of minerals, and SEM work will be completed on at least ten coal samples to determine the applicability of low-temperature ashing in preserving the original integrity of minerals within coal and to trace their transformation through high-temperature ashing to the slag stage. A study by Mitchell and Gluskoter (1976) with bituminous and subbituminous coals identified similar mineral transformations seen in lignites presented here. Their study indicates that most coal minerals are stable up to 380°C. At this time the correlation of the minerals seen in high-temperature ash to the minerals present in the original coal sample can only be speculative, but the correlation will be elucidated as more data is gathered.

13.2.3 Slag Viscosity

13.2.3.1 Rockdale

Tests with Rockdale (Texas lignite) in reducing (20/80 H_2/N_2), inert (N_2), and oxidizing (air) atmospheres were conducted. A graph showing plots of log viscosity vs. temperature is given as Figure 13-4. Also shown for comparison is the curve from the original 1981 alumina-crucible test in reducing atmosphere (dashed line). The results of the reducing- and inert-atmosphere tests were quite similar; in both tests, the temperature of critical viscosity (T_{cv}) was about 2450°F, and the increase in viscosity below this temperature was quite rapid. (This same behavior was observed in an earlier test, in a carbon crucible, where T_{cv} was slightly higher at 2475°F.) Also, typically viscosities in an inert atmosphere were slightly higher than those in a a reducing atmosphere.

In each of these tests, as the temperature was decreased below 2450°F the slag tended to congeal into a lumpy mass, and the shear stress vs. shear rate curves became very erratic. In the reducing atmosphere, the agglomerated slag tended to cling to the bob. Also, there was a substantial amount of hysteresis as the slag was reheated.

It is not yet clear why the results of the latest reducing atmosphere test were so different from those of the earlier 1981 test. Although a different batch of coal was ashed for the latest tests, it seems unlikely that any inhomogeneities in the coal (ash) sample would have been large enough to account for the observed discrepancy.

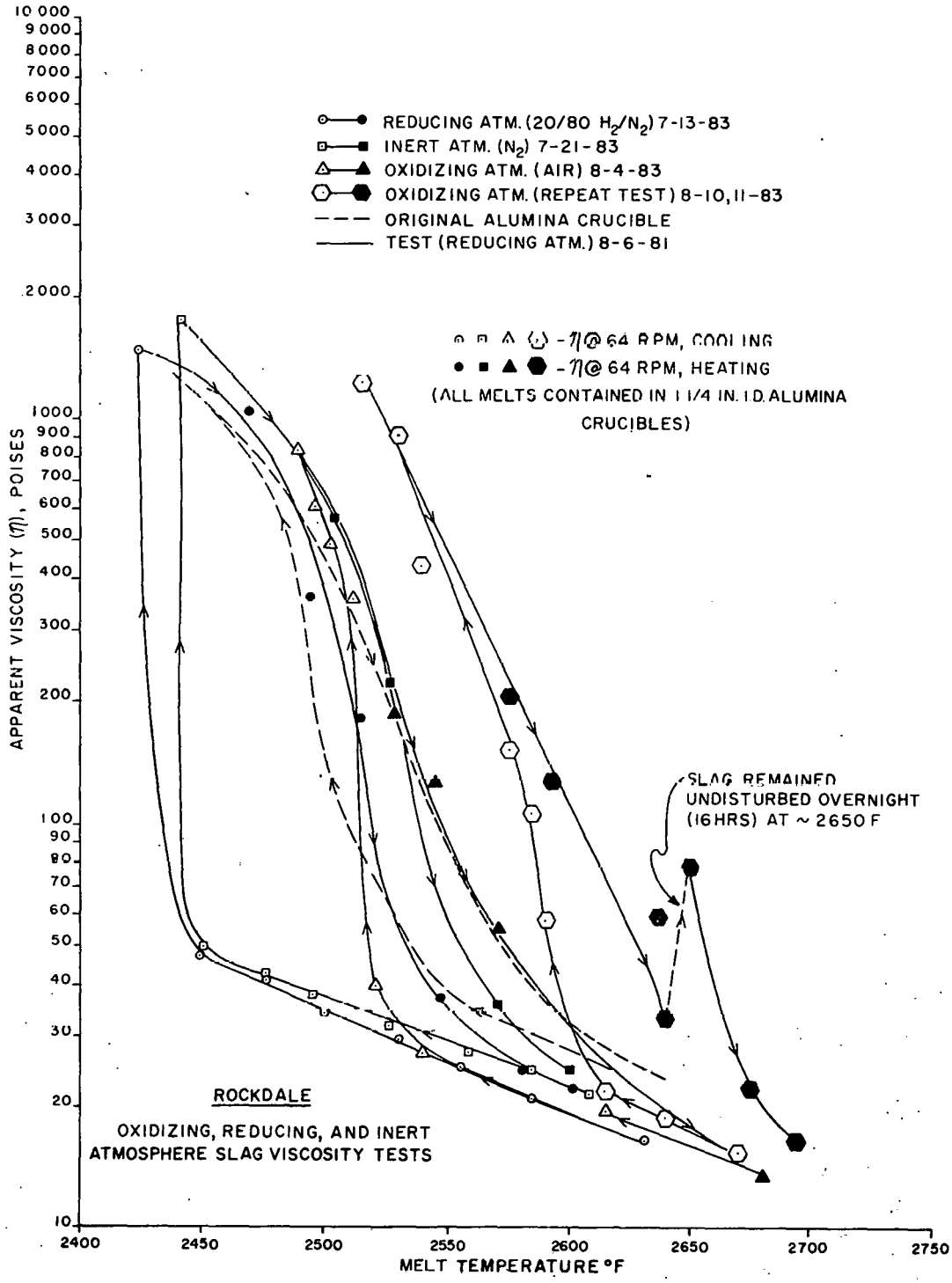

FIGURE 13-4. Viscosity-temperature curves for Rockdale lignite.

Since the Fe_2O_3 content of the Rockdale slag was moderately low (9 pct compared to a range of 7 to 19 pct for slags from previous alumina-crucible tests), it might be anticipated that the behavior of the slag in an oxidizing atmosphere would not be much different from its inert-atmosphere behavior. Such was not the case, as shown by the test results. In the first oxidizing atmosphere test (data points shown by triangles on the graph), initial viscosities at ~2250°F were virtually identical to those obtained in the reducing-atmosphere test. However, after only two data points on the cooling curve, the shear stress vs. shear rate curves become erratic, indicating the onset of slag solidification, and the viscosity began to increase very rapidly. The resulting T_{cv} of ~2525°F was approximately 75 degrees higher than that observed for the reducing- and inert-atmosphere tests. Furthermore, there was significantly less hysteresis during the reheating cycle. Because of some problems at the beginning of this test (discussed below), it was decided to reheat the slag to ~2680°F and repeat a portion of the cooling cycle. Interestingly, the data indicate that the slag reverted to Newtonian behavior and apparently retraced the original cooling-cycle line.

Because of an apparent problem with the temperature control microprocessor, as well as the rather divergent nature of the overall test results, it was decided to repeat the test, planning to repeat the cooling cycle in the normal fashion, partially reheat the slag, and allow it to "soak" at some intermediate temperature overnight to observe any changes in viscosity with time.

The results of the second oxidizing-atmosphere test (hexagons on the graph) were even more dissimilar compared with those of all previous tests on this sample. The Newtonian portion of the viscosity curve was essentially in the same area as before, but the T_{cv} was shifted upscale to about 2615°F. Once again, the slag began to assume a "lumpy" appearance below 2575°F, and as the viscosity increased one large lump of semisolid slag was observed clinging to the bob and rubbing on the side of the sample crucible (which behavior, of course, tended to show up as irregularities in the shear stress vs. shear rate curves).

Only minimal hysteresis was observed on the reheating curve. After the slag had reached 2640°F, the heating process was interrupted and, after stopping but without removing the bob, the slag was allowed to remain overnight (16 hrs) at this temperature. The following morning, after the slag was first stirred for 15 minutes at 16 rpm, the viscosity was measured and had actually increased from 33 to 78 poises. There were also some humps on the shear stress vs. shear rate curve, suggesting that solid or semisolid phases were still present in the slag. A similar, although smaller, increase in viscosity during a 3-hour equilibration period at the end of an earlier heat-soak test with Decker was observed in 1982. Continued heating of the slag to 2694°F resulted in a further decrease in viscosity, as shown by the graph, although it did not return to the original baseline value. In fact, after the final reading at 2694°F, that temperature was maintained for 3 hours and there was no further change in the slag viscosity.

These observations, as well as those from the Decker heat-soak test, seem to suggest that thermal equilibration periods are at least on the order of hours, if not days, when the slag is in the plastic state. There is also the matter of possible Al_2O_3 contamination from the sample crucible, which may be

the main reason why viscosities do not return to their original values when the slags are reheated above their liquidus temperatures.

The results of material balance calculations on the four Rockdale tests are summarized below:

Test Atmosphere	Wt. of Ash Melted, g	Wt. of Slag Produced, g	Weight Loss, % of Ash Wt.
Reducing	70.2430	62.9538	10.4
Inert	70.4187	64.3237	8.7
Oxidizing*	68.5681	61.9574	9.6
Oxidizing (repeat)	69.7603	61.9384	11.2

*Slag overflowed sample crucible.

The weight losses are all of the same order of magnitude.

13.2.3.2 Choctaw

Choctaw (Alabama lignite) turned out to be a unique sample in several respects. First of all, unlike any previous samples the ash had a tendency to sinter during ashing at 1850°F. Most of the sintered particles were of a regular, inverted "V" shape in the ashing dish. Secondly, the ash had a distinct reddish color, indicating the presence of high iron, probably a higher Fe_2O_3 content than any of the earlier low-rank coal ashes that have been tested.

Not surprisingly, therefore, the results of the viscosity tests in the three atmospheres showed some rather dramatic differences (Figure 13-5 - note the temperature scale has been compressed by a factor of 2 compared with the Rockdale graph). For the reducing-atmosphere test, it appears that there is a short region of Newtonian behavior with a T_{cv} of about 2200°F. In the inert atmosphere test, Newtonian behavior is indicated down to about 2275°F. However, at and below a temperature of 2300°F, the shear stress versus shear rate curves showed increasing irregularities, indicating the presence of crystallized phases in the melt. There was no well defined T_{cv}, and (within the limits of experimental error), essentially no hysteresis on reheating (note that the latter situation also pertained in the reducing-atmosphere test). Finally, with the oxidizing atmosphere, erratic behavior was seen after the second reading (at 2530°F), and a lump of material was observed clinging to the bob. As cooling continued, the bob tended to bind on the wall of the crucible, and the irregular movement of the bob evidently "confused" the microprocessor to the extent that it could no longer step the bob speed through the 0 to 64 rpm range (the bob got stuck at 16 rpm several times). Consequently, all readings below 2500°F were taken from the shear-stress meter with the bob spinning continuously at 64 rpm. At 2450°F, the viscosity suddenly appeared to be decreasing; visual examination of the slag revealed what appeared to be a rigid, semisolid mass, but it had shrunk away from the bob, and the bob was turning in a hole. This observation accounts for the dashed line on the viscosity/temperature curve.

The results of material balance calculations on the three Choctaw tests are summarized below:

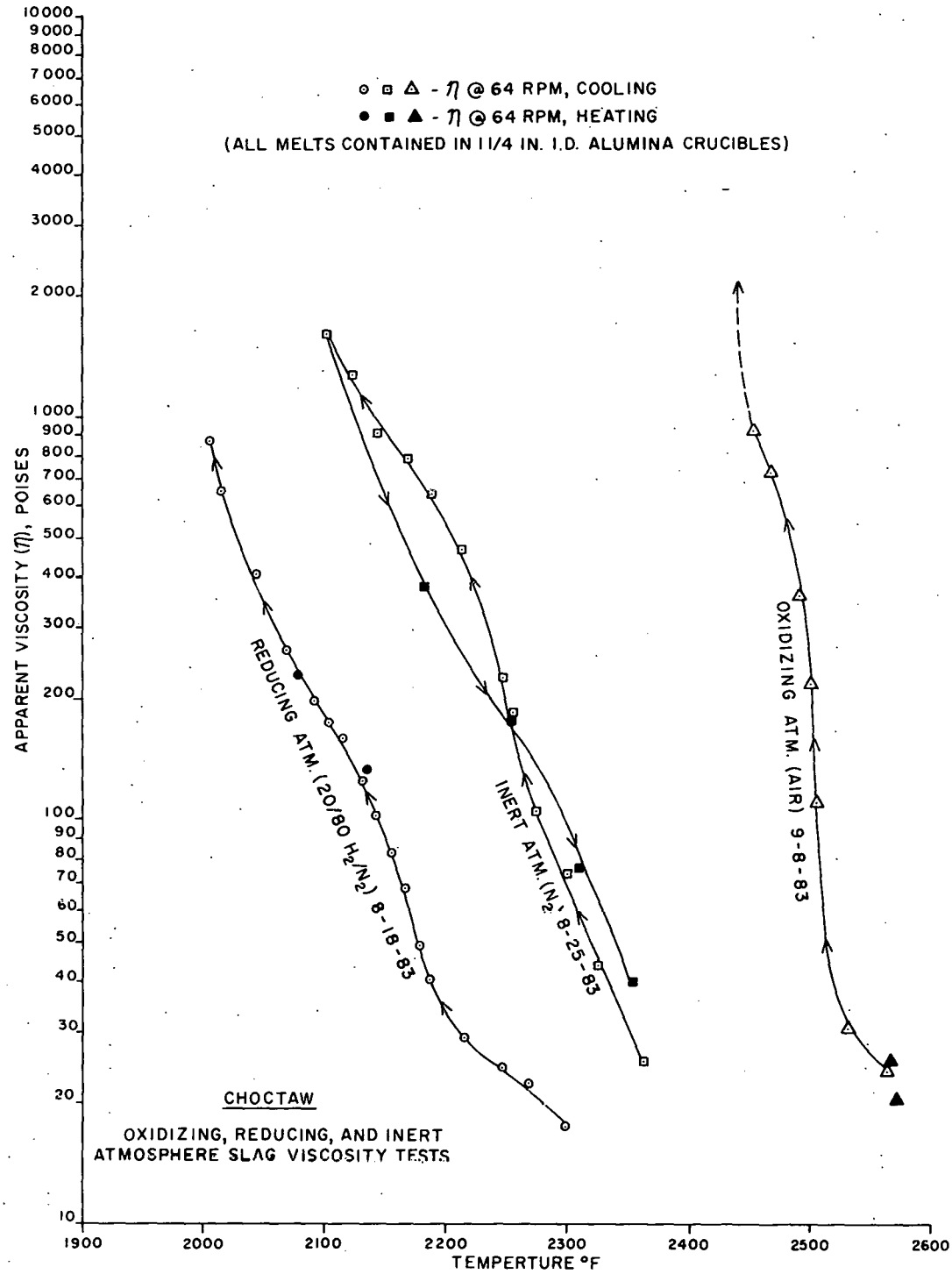

FIGURE 13-5. Viscosity-temperature curves for Choctaw lignite.

Test Atmosphere	Wt. of Ash Melted, g	Wt. of Slag Produced, g	Weight Loss, % of Ash Wt.
Reducing	68.0381	61.7791	9.2
Inert	74.8101	69.6467	6.9
Oxidizing	73.5212	68.3140	7.1

The larger weight loss for the reducing-atmoshpere test is presumably due to reduction of Fe_2O_3.

13.2.3.3 Indian Head

The viscosity test on the Indian Head (North Dakota lignite) sample was conducted on September 21, 1983, using a reducing atmosphere. As shown in Figure 13-6, this slag appeared to be one of those "glassy" types like Naughton and Black Butte in that (1) no point of critical viscosity was observed, and (2) on reheating, the viscosity values essentially retraced the cooling curve line.

The ash fusibility values for this sample in a reducing atmosphere were: I.D. = 2200°F, S. T. = 2260°F, F. T. = 2300°F. These values, plus the appearance of the shear stress vs. shear rate curves and visual observations of the slag during the test, suggest that the slag was probably in the region of non-Newtonian (plastic) behavior over the entire temperature of measurement; i.e., if there is a temperature of critical viscosity, it is above 2400°F and below a viscosity of 20 poises.

It is very interesting that the initial deformation temperature of 2200°F was almost reached before there was any evidence of total solidification of the slag. As in the Choctaw oxidizing-atmosphere test, the apparent viscosity began to decrease as the solidus temperature was approached; the bob was turning in a hole, and the bulk of the slag was a rigid, immobile mass attached to the walls of the crucible. This sample of Indian Head behaved quite differently from the earlier one tested back in 1980. Incidentally, the earlier Indian Head slag was one of the few that significantly attacked the alumina crucible; no such behavior was observed in this latest test.

In this test 72.8118 g of ash produced 64.0820 g of slag, corresponding to a weight loss of 12.0 pct (there was some overflow of slag into the guard crucible, however, so slag recovery weighings involved both the sample and guard crucibles).

13.2.4 Slag-Refractory Interactions in Gasification

X-ray microprobe analyses were performed on samples of solidified slag collected from the taphole and hearth area of the slagging gasifier after runs that had suffered an early shutdown. A hypothesis for the early shutdowns is that some component(s) of the slag may react with the refractories to produce a high-melting phase which may be fluid enough to flow out of the very high temperature region of the tuyere blast but which then solidifies in the relatively cooler regions of the hearth or taphole.

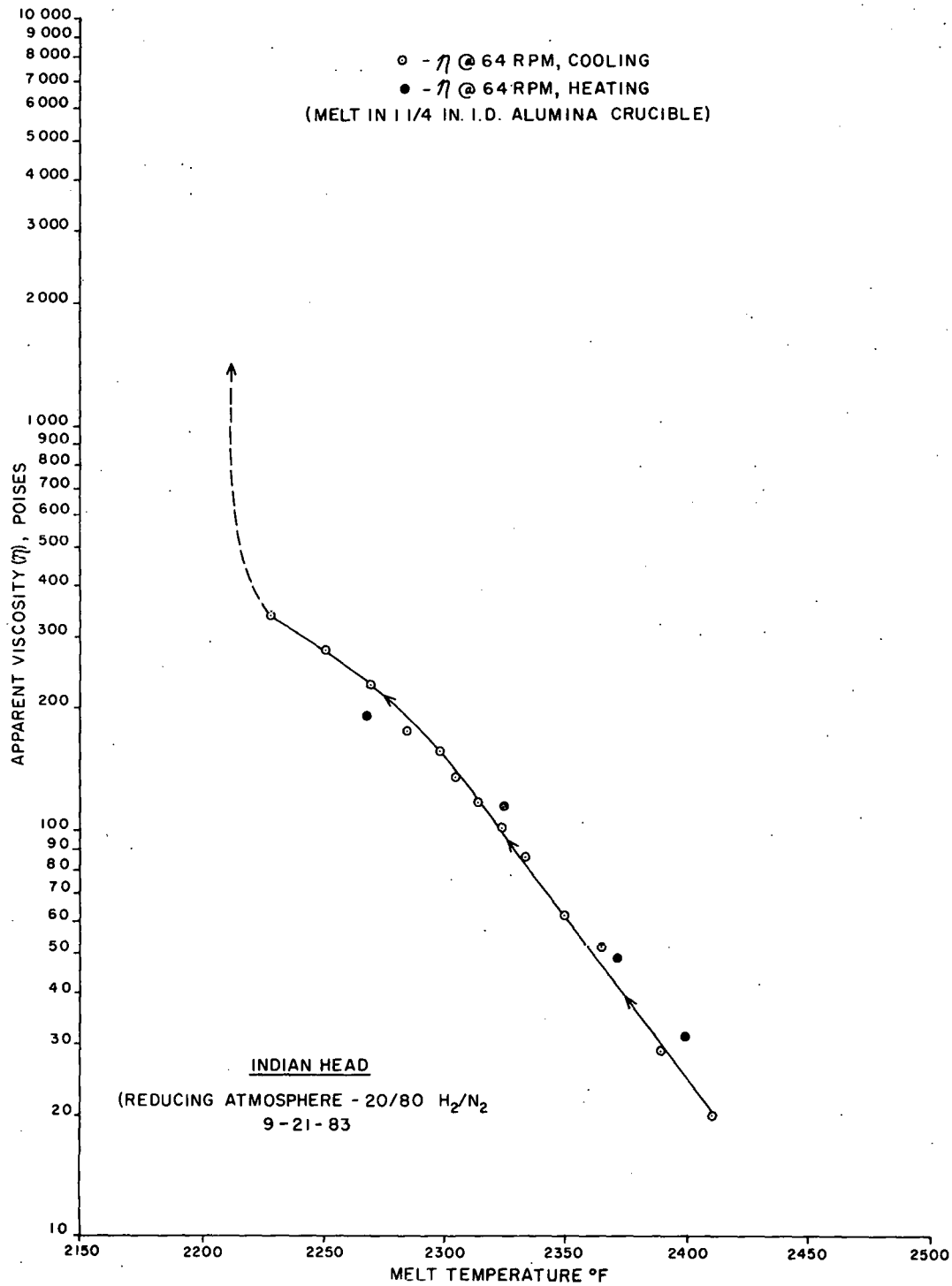

FIGURE 13-6. Viscosity-temperature curve for Indian Head lignite.

The first specimens studied were pink cenospheres found in and under the taphole. An average composition from microprobe analyses is shown in Table 13-3 along with the composition of the hearth refractory (A. P. Green "Jade-Pack") for comparison.

TABLE 13-3

AVERAGE COMPOSITIONS OF PINK CENOSPHERES AND REFRACTORY, WEIGHT PERCENT

Component	Cenospheres	Refractory	Component	Cenospheres	Refractory
Al_2O_3	88	87	MgO	1.7	0.1
Cr_2O_3	2	9.5	Fe_2O_3	0.25	0.2
SiO_2	4	2.5	$(Na_2O + K_2O)$	1.2	0.1
CaO	2.5	0.1	SO_3	2.4	-

The presence of Cr_2O_3 in the cenospheres is an immediate indicator that they must be a product of reaction with the refractory, since the chromium content of North Dakota lignites is typically only a few parts per million.

Since the Al_2O_3, SiO_2, and Fe_2O_3 contents of the cenospheres and refractory are reasonably comparable, it appears that on a macroscopic scale the alkali and alkaline earth components of the slag have attacked the refractory, replacing the chromium. (It is not meant to imply that the reaction mechanism on an atomic scale is necessarily a direct replacement of Cr^{+3} by Na^{+}, K^{+}, Ca^{+2}, or Mg^{+2}). The effect of such a replacement would almost certainly be a reduction in melting point. For example, the melting point of 90 Al_2O_3 - 10 Cr_2O_3 system would be about 2100°C. If all of the alkalies and alkaline earths were counted as MgO (for convenience in reading readily available ternary phase diagrams), an 88 Al_2O_3 - 2 Cr_2O_3 - 10 MgO system would have a melting point of about 1950°C. MgO is a very refractory material in its own right; it seems reasonable to speculate that the alkalies Na_2O and K_2O would be even more effective in reducing melting point.

It is generally regarded that the temperature in the "fireball" of the tuyere blast is approximately 1700°C, while slag discharge temperatures, measured on the outlet side of the taphole, are about 1300°-1350°C. Extrapolating the known effect of MgO on the melting in the Al_2O_3 - Cr_2O_3 system, it may be likely that the combined effects of MgO, CaO, Na_2O, and K_2O could produce a reaction product fluid at about 1700°C and hence able to flow within the highest temperature region of the hearth. On the other hand, it is not likely that a phase containing nearly 90 pct alumina would still be liquid at 1300°C, regardless of the other components.

It is not yet known why cenospheres were formed. It is possible that they are the solid product of a reaction:

Liquid → Solid + Gas

and thus are in effect bubbles blown by the gas as it is liberated. Our studies are not far enough along to explain this reaction further. It is interesting to note that the reference compilation Phase Diagrams for Ceramists shows a pseudobinary in the quinquenary system $CaO-MgO-Al_2O_3-Cr_2O_3-SiO_2$, which is said to have a "vapor" phase, unfortuantely otherwise unidentified.

The second material to be studied was a crystalline deposit found in the taphole and on the hearth. In Table 13-4 the average microprobe analyses are again compared with those of the refractory. It seems evident by inspection that the principal difference is the very high amount of calcium incorporated in the crystalline product, suggesting an attack by CaO on the refractory. The composition of the product of the hypothetical reaction of 25 grams CaO with 100 grams refractory was calculated and is also shown in Table 13-4 in the column "calculated product."

TABLE 13-4

AVERAGE COMPOSITIONS OF CRYSTALLINE DEPOSIT AND REFRACTORY, WEIGHT PERCENT

Component	Deposit	Refractory	Calc'd Product	Component	Deposit	Refractory	Calc'd Product
Al_2O_3	71	87	70	MgO	1.0	0.1	-
Cr_2O_3	1.7	9.5	7.6	Fe_2O_3	3	0.2	-
SiO_2	6	2.5	2	(Na_2O+K_2O)	-	0.1	-
CaO	21.5	0.1	20	SO_3	2.6	-	-

The relatively good agreement between the actual and calculated compositions suggests the hypothesis of attack by CaO is reasonable. Again as with the cenospheres there has also been a macroscopic replacement of Cr_2O_3 by, in this case, SiO_2, MgO, and Fe_2O_3.

Even though CaO by itself is a very high-melting material (handbook value of the melting point is 2580°C), it has a potent effect on reducing the melting point of alumina-containing systems. For example, the $CaO-Al_2O_3$ binary system has a melting point of about 1625°C for the 30 CaO-70 Al_2O_3 and about 1725°C for the 20 CaO - 80 Al_2O_3 compositions. Here again it seems that the product of slag attack on the refractory could be a liquid at "fireball" temperatures but would solidify around or in the taphole.

While this work is by no means complete, it appears that the attack of slag components on the refractory can produce phases which would be fluid at

1700°C in the immediate vicinity of the hottest region of the gasification/combustion reaction zone, but which solidify at the relatively cooler 1300°C temperatures of the taphole and hearth plate. The solidification of material in the taphole has the consequence of forcing termination of the gasification test shortly thereafter.

13.3 REFERENCES

1. Mitchell, Richard S., and Gluskoter, Harold J., 1976, Mineralogy of Ash of Some American Coals: Variations With Temperature and Source, Fuel, v. 55, p. 90-96.

14. - ORGANIC STRUCTURE

Project No.: 7303 B&R No.: AA1515100

Submitted by: H.H. Schobert, Manager, Coal Science Division

Prepared by: E.S. Olson
J.W. Diehl
S.A. Benson

Assigned AWU Personnel: M. Froehlich
K. Groon

14.1 GOALS AND OBJECTIVES

Our approach to the study of the organic structure of coal has been to use a model based on substructures, the same as were present in the original wood (cellulose, hemicellulose, lignin) and those derived from these original substructures. The extraction of these substructures from the coal required much investigation, since the methods applicable to wood did not necessarily work with coal. In the first quarter, new methods incorporating gas chromatography were developed for the analysis of the components derived from depolymerization of the macromolecular substructures.

Our work on the quantitation of cellulose and lignin substructures in North Dakota lignites continued in this quarter. We wished to examine some modifications of the cadoxen method for extraction of cellulose (1) to improve the yield. A study of the completeness of the cadoxen extraction was another important objective. Finally a comparative study of the three lithotypes of Beulah lignite was desired.

Since the methoxy determination reported last quarter (1) using oxidation with CF_3CO_3H followed by hydrolysis and quantitative analysis of the liberated methanol was giving consistent and reasonable values, the comparison of various lignite samples was undertaken. The amount of methoxy groups is believed to be proportional to the amount of lignin in the coal sample. Several delignification methods were planned with lignite samples. These were all methods previously used for the delignification of wood samples. If some of these would work with lignite, not only could lignin be determined directly, but the residue might be more easily extracted to remove the carbohydrate. We previously reported the failure of the Klason method (72 pct H_2SO_4) in the separation of lignin from cellulose (1) and coal matrix.

The objective of pressure differential scanning calorimetry (PDSC) studies of low-rank coals is to develop a method of inferring aromaticity and extent of ring condensation from the characteristic patterns of the thermogram. PDSC characterization of model compounds and model polymers is used to provide supporting information. The PDSC can be applied to investigate comparative structural features among lithotypes and to study structural changes within a coal seam.

14.2 ACCOMPLISHMENTS

14.2.1 Effectiveness of Cadoxen Extraction

One important goal was to try to determine whether the cadoxen was extracting all of the cellulose and hemicellulose from the lignite. Thus a sample of the dull Beulah lithotype which had been previously extracted by stirring with cadoxen was reextracted with cadoxen for another day and the yield of cellulose was determined by hydrolysis in 1N H_2SO_4, reduction of monosacchlarides to the alditols, esterification to the alditol acetates which were quantitatively measured by gc on a SP2330 capillary column with inositol acetate as an internal standard. The results of this and other experiments with cadoxn are summarized in Section 14.2.1.1.

Several experiments were carried out with the goal of increasing the effectiveness of cadoxen extraction of North Dakota lignites. A sample of Beulah 3 lignite was sonicated with cadoxen for 24 hours and the yield of cellulose extracted was determined by conversion to glucitol acetate. Extractions with cadoxen at higher temperatures were also carried out. One sample of Beulah lignite was refluxed with cadoxen and one was heated in a stirred autoclave with cadoxen at 250°C. Cellulose was determined as above.

Pretreatment of the coal with base and mild oxidizing agents was also studied as a technique for improving the yield of cellulose obtained by cadoxen extraction. A sample of Beulah lignite was stirred with sodium hydroxide solution to remove humic acids and possibly hemicellulose before the cadoxen extraction. A second sample was oxidized by refluxing with iodine in pyridine followed by silver oxide in base (2). The residue from this procedure was then extracted with cadoxen.

14.2.1.1 Results of Cadoxen Extractions of Beulah 3 Lignite

Experiment	% Cellulose (As Received)
1. Extraction of dull lithotype	0.015
2. Reextraction of above sample	0.010
3. Extraction of composite Beulah lignite by stirring	0.003
4. Extraction of composite Beulah lignite by sonication	0.000
5. Extraction of composite Beulah lignite by refluxing	0.010
6. Extraction of composite Beulah lignite at 250°C	0.004
7. Extraction of NaOH treated Beulah lignite	0.003
8. Extraction of mildly oxidized Beulah lignite	0.007
9. Reextraction of mildly oxidized Beulah lignite	0.005
10. Extraction of hypochlorite oxidized Beulah lignite	0.009

14.2.1.2 Conclusions of Cellulose Determinations

Although cadoxen is able to extract cellulose from lignite where the Klason method failed completely, the extraction is not complete. A reextraction of the lignite residue gave more cellulose (2/3 of the originally extracted amount). The amount extracted probably depends somewhat on the depolymerization or degradation of the coal matrix to expose the cellulose.

Sonication of the lignite with cadoxen was not effective. Refluxing with cadoxen gave the best improvement in yield. Heating in an autoclave at 250°C did not significantly affect the yield. Perhaps degradation of the cellulose or other coal reactions at 250°C might have been a factor in this experiment.

Treatment with NaOH to remove humic acids did not affect the yield. The oxidation with iodine in pyridine followed by silver oxide depolymerized the coal somewhat; however, the cellulose value obtained was not significantly different. Reextraction of the residue with cadoxen gave additional cellulose, indicating that pretreatment to oxidatively depolymerize the coal did not expose all the cellulose, although slightly more was obtained than with no pretreatment. A vigorous reaction with sodium hypochlorite removed 60 pct of the coal, however the cellulose content in the residue was not greatly changed.

14.2.2 Comparison of Cellulose Content in Various Lithotypes of Beulah Lignite

The cellulose contents of vitreous, dull, and fragmental lithotypes of Beulah lignite and a specimen resembling a tree stump from the Beulah mine were investigated. Although the extraction of cellulose was considered to be incomplete using the cadoxen method, a comparison of the cellulose extracted might be of some use in characterizing the lithotype samples and in understanding their properties and possible origin.

14.2.2.1 Results of Cellulose in Lithotypes

Lithotype Sample (Beulah lignite)	% Cellulose (As Received)
Composite	0.003
Vitreous	0.003
Dull	0.015
Fragmental	0.014
Tree Stump	0.010

14.2.2.2 Conclusions of Cellulose Comparisons in Lithotype

The values for the cellulose content are very small for all the lithotypes, thus whatever chemical differences there are between the lithotypes which give rise to their different reflectance or other physical properties must involve other structural components. The somewhat higher values for the dull and fragmental lithotypes may have resulted from some interruption of the biochemical depolymerization process such as might have occurred in charring. The low cellulose content of the tree stump specimen indicates that the physical appearance of a sample is not necessarily related to its chemical resemblance to the original plant structures.

14.2.3 Methoxy Determinations of Lignite Samples

The methoxy ether content of three lithotypes of Beulah 3 lignite were investigated by oxidation with CF_3CO_3H, hydrolysis and gc determination of methanol. A sample from the tree stump specimen (Beulah mine) was also investigated. Since Indian Head lignite is currently being used extensively in gasification tests and supercritical extraction runs at UNDERC, the methoxy

ether content of this coal is an important parameter for comparison with the yield of methanol in the aqueous products from processing this coal.

14.2.3.1 Results of Methoxy Determinations

Lignite Sample	% MeOH (As Received)
Beulah composite	0.8
Vitreous lithotype	0.8
Dull lithotype	0.4
Fragmental lithotype	1.1
Beulah tree stump	0.2
Indian Head composite	0.7

14.2.3.2 Conclusions of Methoxy Determinations

The fragmental lithotype has the highest methoxy ether content and also has one of the highest cellulose contents; by inference then, it has the highest amount of lignin present in the sample. The same charring process which interrupted the degradation of cellulose may also be responsible for preventing decomposition of the lignin.

The methoxy content of Indian Head is consistent with the methanol yields observed in supercritical water extraction and steam drying (0.6 and 0.5 pct).

The low value observed for the tree stump specimen may result from easier access of fungal enzymes to the isolated specimen than was the case of packed or compressed material. Anyway this illustrates again that physical resemblance may not be associated with a chemical resemblance to the original plant.

14.2.4 Delignification Studies

A number of methods have been used previously for the delignification of wood samples. We have tried to use some of these for the delignification of coal (Beulah lignite). As we pointed out earlier, 72 pct H_2SO_4 does not yield a lignin sulfate or sulfonate type of product as it does with wood.

Two hydrolytic methods for degradative removal of lignin were attempted. Lignite was heated with ethanol and HCl and with dioxane and HCl in an effort to depolymerize the lignin present by acid-catalyzed ether cleavages.

A thermal decomposition in a dioxane-water solvent was carried out at 180°C on a Beulah lignite sample.

Finally an oxidative lignin degradation was attempted using sodium hypochlorite. The residue was analyzed for methoxy groups to determine the extent of delignification.

14.2.4.1 Results of Delignifications

The delignifications under acidic conditions were a total failure in that no soluble products were obtained.

A dioxane-water extraction at high temperatures gave a 10 pct yield of soluble products. These products are currently being studied.

The sodium hypochlorite oxidation resulted in a loss of 60 pct of the sample into solution. The methoxy content of the residue gave a value of 0.3 pct.

14.2.4.2 Conclusions of Delignifications

The coal matrix renders useless many of the deligification reactions which were used with wood. Although the hypochlorite oxidizes a considerable portion of the lignite, the residue which should have been delignified was actually only about half delignified.

14.2.5 Periodate Oxidation of Lignites

The oxidation of aromatics with sodium periodate is specific for ortho-methoxyphenols which are converted to methanol and ortho-benzoquinone. Thus a measurement of the methanol released in this oxidation gives a measure of the number of free guaiacol groups present in the sample. Beulah 3 lignite was oxidized by sodium periodate and the methanol was determined by quantitative gc.

14.2.5.1 Results of Periodate Oxidation of Lignite

Experiment	% MeOH
Periodate oxidation of Beulah lignite	0.25
Periodate oxidation of Beulah lignite (larger sample)	0.24
Repeated oxidation on same sample	0.08
Periodate oxidation (refluxing)	0.44

14.2.5.2 Conclusions of Periodate Oxidation of Lignite

This experiment establishes that at least one-third of the methoxy groups (0.25 out of 0.8 total) are present as guaiacol groups (ortho to a free hydroxy group). The remaining methoxy groups are then either inaccessible to the reagent or are present in an ortho-methoxyphenyl ether. Since the coal does not dissolve at all during the reaction, the coal matrix may be preventing the periodate from reacting with all the ortho-methoxyphenol groups. On the other hand the ratio of one-third is found in some wood samples.

The increase in methanol liberated at refluxing temperatures may be attributed either to depolymerization which makes more of the methoxyphenol groups accessible or to hydrolysis of the phenyl ether linkage which liberates o-methoxyphenols.

14.2.6 Pressure Differential Scanning Calorimetry

Pressure differential scanning calorimetry (PDSC) has provided insight into the structural characteristics of coals. The PDSC thermograms have features which can be used to interpret coal "structure" in terms of the aliphatic and aromatic portions. This interpretation was developed on the

basis of similarities related to solid state nuclear magnetic resonance and infrared spectroscopy of coals, and to the thermograms of pure organic compounds and polymers.

The thermograms of coals consist of two to three exothermic peaks depending upon the coal. The number of these peaks, intensity of the peaks, and the temperature at which they occur vary with coal rank. This variation in the thermograms as a function of rank fits the model of increasing aromatic and loss of aliphatic character with increasing rank.

The experimental procedure involves heating 1-1.5 mg of -100 mesh sample at a linear heating rate of 20°C/min from 150° to 600°C, in a 3.5 MPa atmosphere of oxygen. The coals analyzed originated from core samples, high vitrinite samples from the Exxon Coal Characterization Library, carefully selected coal lithotypes and bulk process samples used at UNDERC. The organic compounds and polymers are commercially available.

14.2.6.1 Results

The interpretation of changes in the shapes of the thermograms produced in the PDSC experiment, show a shift in peaks from peat to anthracite. The peat sample produced a major exothermic peak at approximately 260°C and a small shoulder at 360°C, whereas anthracite has a major peak at 470°C and a small shoulder at 350°C.

The thermogram produced in a PDSC experiment can be regarded to consist of a low-temperature peak which arises from the aliphatic or alicyclic moieties in the coal and of a high temperature peak which arises from the aromatic portion of the coal. A typical thermogram of a subbituminous coal is shown in Figure 14-1. It is possible to determine an apparent aromaticity by taking the ratio of the height of the high temperature peak to the sum of the heights of both peaks. To correct the apparent aromaticity calculated from the PDSC thermograms to the actual aromaticity an equation was derived based on the relationship of the aromaticity, f_a, to the maf carbon content. Figure 14-2 shows the relationship of f_a to the apparent aromaticity for run-of-the-mine coals and for the high vitrinite samples from the Exxon Coal Characterization Library. It is particularly interesting that the two sets of samples give the best least square fits if treated separately. The run-of-mine samples plot along a line given by

$$y = 0.263 + 0.868x$$

with $r^2 = 0.852$; the high vitrinite samples plot on the line

$$y = 0.397 + 0.753x$$

with $r^2 = 0.884$. If the two groups of samples are treated as one population the linear correlation coefficient for an attempted least squares fit drops to 0.741.

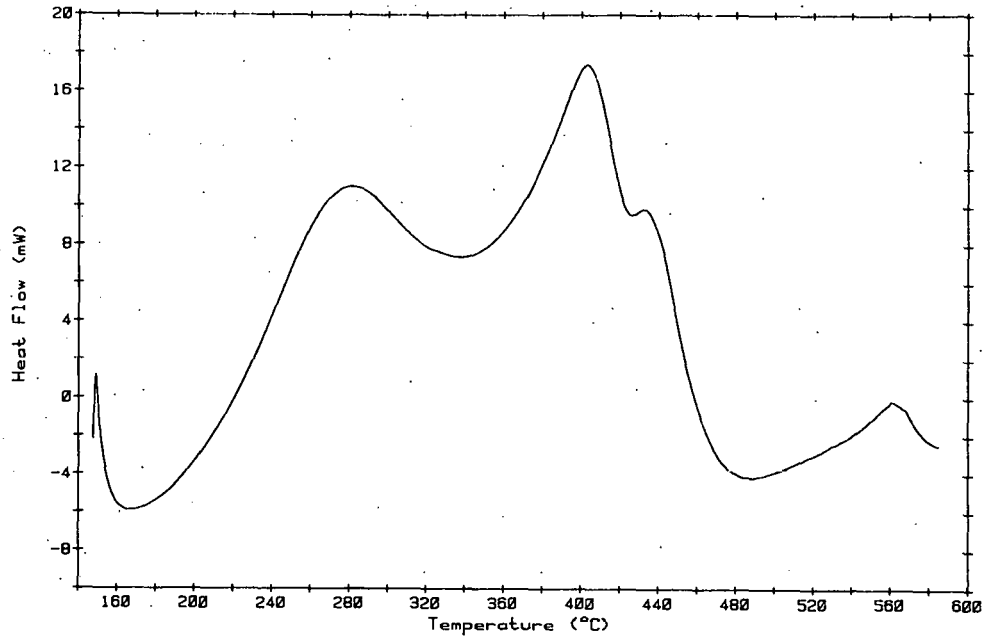

FIGURE 14-1. PDSC thermogram of Bighorn subbituminous.

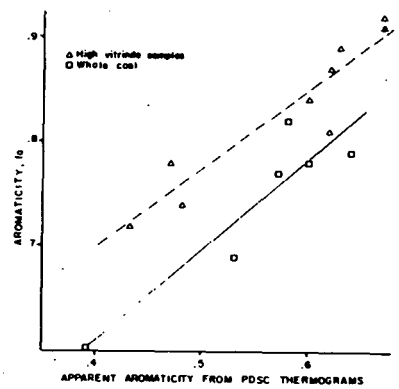

FIGURE 14-2. Aromaticity from Teichmuller plot, reference as a function of peak ratio from PDSC thermograms. Dashed line-high vitrinite samples, reference solid line - whole coals from UNDERC.

The PDSC was used to examine various lithotypes from Beulah, North Dakota lignite. The thermograms reveal distinct differences. The fragmental portion shown in Figure 14-3 represents a portion of the coal that is charcoally in nature and was located between non-vitreous and woody zones. This sample has very little aliphatic and alicyclic character and consists largely of aromatic structures. The aromaticity is 0.94. The vitreous lithotype, which can be described as having a black luster and being very hard, has an aromaticity of 0.64. The third lithotype was a dull woody portion which is almost brown in color. This is the most abundant lithotype in the coal seam and has an aromaticity of .63. The fragmental and vitreous lithotypes include higher temperature peaks above 400°C which could be due to small portions of condensed aromatics.

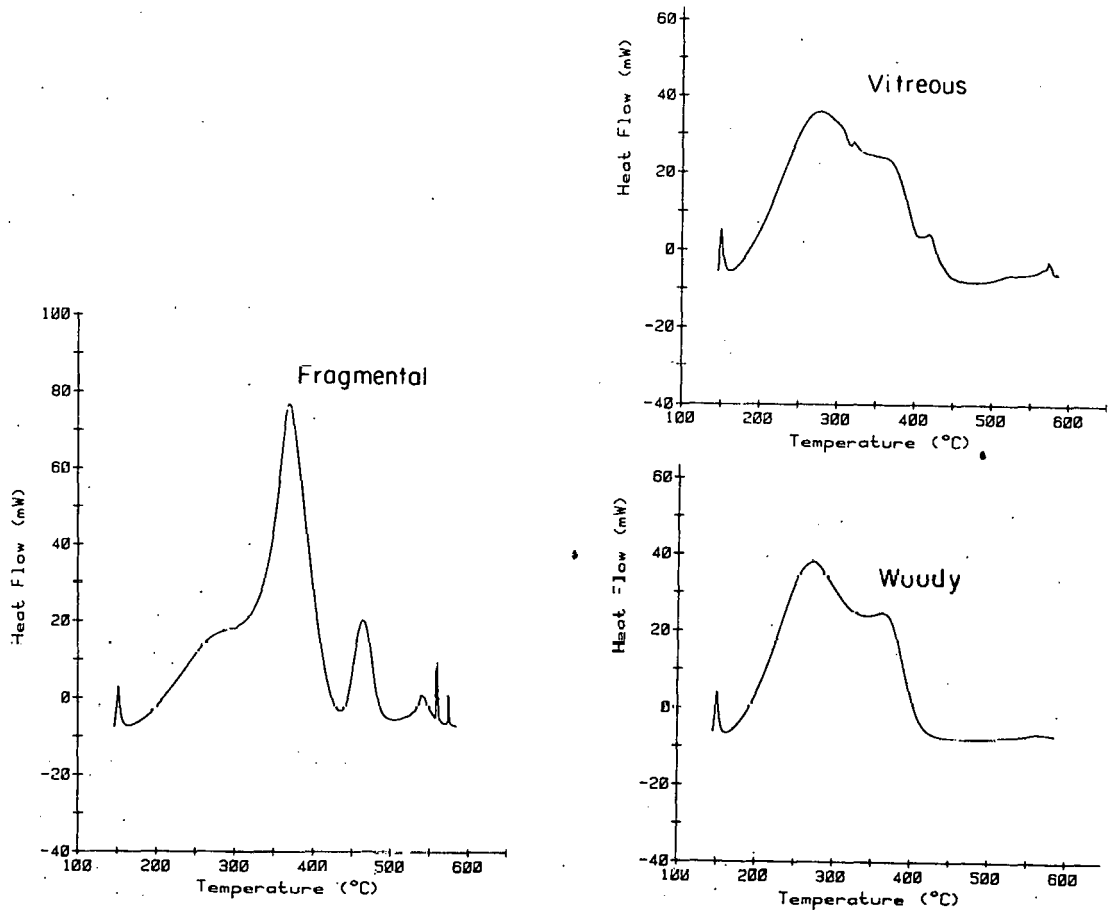

FIGURE 14-3. PDSC thermograms of various lithotypes separated from Beulah lignite.

The variations in aromaticity for a set of core samples for Ledbetter (Texas) lignite reveals trends with depth in the seam. In Table 14-1 the results show decreasing aromaticity with increasing depth. This trend may be due to the depositional environment of the Texas lignite, but is not yet well understood.

Approximately 50 polymers of known structure were tested using PDSC, and the resulting thermograms were compared to those of coals in an attempt to learn more about the structure of coals. Polyethylene, which is a totally aliphatic substance, produced a thermogram with a single low-temperature peak having a maximum temperature of 230°C. This is shown in Figure 14-4 along with the polyethylene structure. On the other hand, the completely aromatic substance poly(p-phenylene) produced a thermogram with a single high-temperature peak. As evidenced in Figure 14-4, the maximum temperature of the peak was 450°C.

TABLE 14-1

VARIATIONS IN AROMATICITY IN LEDBETTER (TEXAS) LIGNITE

Seam	Depth	Corrected Aromaticity
Brown seam	21-23 26-28	.65
Red seam	36.6-39.6 41.1-44.1	.64
Upper blue seam	43-46 47-51.5	.62
Lower blue seam	51.5-56.4 55-56.4	.60
Green seam	55.5-58.2	.56

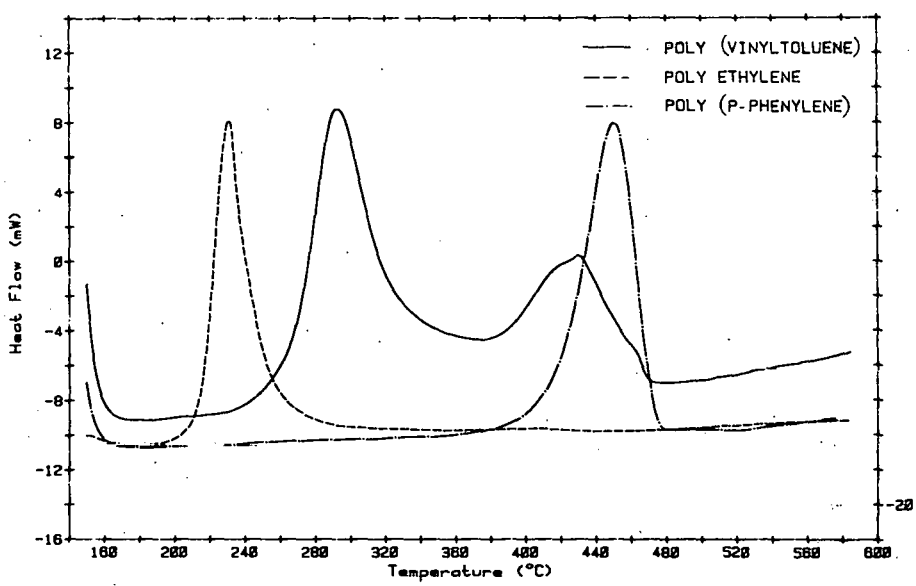

FIGURE 14-4.. PDSC thermogram of Polyethylene, Poly(p-phenylene), and Poly(vinyltoluene).

Poly(vinyltoluene) exhibited a thermogram (Figure 14-4) which looked very similar to those of the Ledbetter Texas lignites. The maximum temperature of the aliphatic peak was 293°C and that of the aromatic peak was 424°C. Both values fall within the temperature ranges of the Texas lignite peaks. The aromaticity of poly(vinyltoluene) is approximately 0.51, which is only slightly below the aromaticities calculated for the Texas lignites.

14.2.6.2 Conclusions of Pressure Differential Scanning Calorimetry

The PDSC work has shown insight into understanding coal structural properties for various ranks of coal, coal lithotypes, and changes in aromaticity with seam. The study of pure organic compounds and polymers provide a means of understanding aliphatic and aromatic character of the PDSC thermograms. Along with other analytical techniques such as solid state NMR work, electron spectroscopy for chemical analysis, and infrared spectroscopy, PDSC can discern differences in the structural relationships among coals and may serve as a bridge to understanding coal-specific process responses.

15. - DISTRIBUTION OF INORGANICS

Project No: 7304 B&R No: AA1520150

Submitted by: H.H. Schobert, Manager, Coal Science Division

Prepared by: S.A. Benson, Project Manager, Distribution of Inorganics

Assigned UNDERC Personnel: S.A. Benson
J.P. Hurley
F.R. Karner

Assigned AWU Personnel: P.L. Holm
D.R. Kleesattel
E.N. Steadman
C. Zygarlicke

15.1 GOALS AND OBJECTIVES

The goals of this work are to better understand the distribution of inorganics in low-rank coals and examine the geochemical factors which affect their distribution. Methods are being developed to selectively remove inorganics in ways dependent upon their association in the coal. Knowledge of how these inorganics are associated can be used to predict the fate or impact of the elements during utilization.

The objectives for this reporting period were to:

1. Continue extending the chemical fractionation procedure used to selectively extract inorganics to include more steps which would possibly determine more inorganic associations.

2. Examine methods used to determine carboxylic acid groups in low-rank coals and quantitatively determine carboxylic acid content.

3. Begin examining the organic and inorganic features recognizable by microscopic techniques; also, begin examining coal minerals and lithotypes by a variety of analytical techniques.

15.2 ACCOMPLISHMENTS

15.2.1 Chemical Fractionation

The work to extend the chemical fractionation procedure involved using a greater number of NH_4OAc extractions to remove all the ion exchangeable cations, and developing a procedure to determine the optimum pH of ion exchange of the carboxylic acid groups. The procedure is being tested to determine the pH at which cations will exchange with the organic acid groups in demineralized coal. For example, to determine the optimum pH where Na^+ will exchange, the following procedure is used: Na^+ is exchanged by adding 50 ml

each of 0.1 N NaOH and 0.9 N NaCl to two grams of coal and stirring in an inert atmosphere for two days. The pH is then adjusted to 11 with 1 N NaOH. The sample is allowed to cool and the pH is adjusted to 5 with HCl to aid in flocculation of humic and fulvic acids. (Very little ion exchange should occur with addition of HCl because the Na^+ level is 10,000 times greater than the H^+ at the pH of 5.) The sample is then treated with 30 ml of 0.1 N triethanolamine to achieve a high pH without exchanging Na^+ and to act as an ion strength adjuster so that the exchange of Na^+ with H^+ can be detected with a sodium specific electrode. The pH is then lowered by 0.1 pH units and the Na^+ level measured.

Chemical fractionation with an extended technique, which uses three NH_4OAc extractions, was performed on two samples from the Gascoyne mine (North Dakota). The Gascoyne Blue sample is from a region in the mine which causes ash fouling. The Gascoyne Red is from a pit which causes little or no problems with ash fouling. The results of these tests are summarized in Tables 15-1 and 15-2. (The data reported in these tables are preliminary results and may be subject to revision.) These samples have been submitted for neutron activation analysis at North Carolina State University but results have not been received.

TABLE 15-1

CHEMICAL FRACTIONATION OF GASCOYNE BLUE PIT LIGNITE

Element	Initial Conc., ppm	% Extracted by NH_4 OAc	% Extracted by HCl	% Remaining in Coal
Al	7300	22.6	38.8	38.6
Ca	22790	85.1	14.3	0.6
Fe	2540	0	42.5	57.5
K	1430	89.0	0	11
Mg	17890	98.0	2	0
Si	10920	11.6	16.7	71.7
Sr	313	94.6	5.4	0
Cu	11	0	0	100
Ti	546	0	57.0	43
Ni	5	0	--	--
Mn	25	28	72	0

15.2.2 Carboxylic Acid Group Determinations

Work was continued to find the best method for determining carboxylic acid functional groups in low-rank coals. The method found to give the best results involved refluxing ~1 gram of demineralized coal under an inert atmosphere with 100 ml 1N barium acetate. The acetic acid liberated was titrated with 0.05N $Ba(OH)_2$. Titrations were performed after 2 hours, then after ~20 hours and after 40 hours of refluxing to determine if an endpoint could be reached. The endpoint was found at approximately 20 hours of refluxing. Several low-rank coals were analyzed by this technique to determine carboxylic acid functional group content. The results are summarized in Table 15-3.

TABLE 15-2

CHEMICAL FRACTIONATION OF GASCOYNE RED PIT LIGNITE

Element	Initial Conc., ppm	% Extracted by NH_4 OAc	% Extracted by HCl	% Remaining in Coal
Al	8740	22.2	27.6	50.2
Ca	17370	78.1	19.8	2.1
Fe	3890	0	55.8	44.2
K	1260	62.8	3.7	33.5
Mg	20540	95.4	4.6	0
Si	28640	17.2	8.1	74.7
Sr	276	77.5	22.5	0
Cu	10	0	0	100
Ti	1180	0	13.6	86.4
Mn	18	22	88	0

TABLE 15-3

CARBOXYLIC ACID GROUP DETERMINATIONS FOR SOME LOW-RANK COALS

Coal	Carboxylic Acid, meq/gram, maf
Center lignite, ND (4088)	2.74
Center lignite, ND	3.58
Beulah lignite, ND (high Na)	2.32
Beulah lignite, ND (low Na)	1.46
Beulah lignite, ND (CPC)	2.97
Indian Head lignite, ND	2.45
Velva lignite, ND	2.55
Big Brown #2 lignite, Texas	2.26
Bryan lignite, Texas	2.25
Ledbetter lignite, Texas	1.82
Pike County lignite, Alabama	2.04
Choctaw lignite, Alabama	2.83
Absaloka (Sarpy Creek) subbituminous, Montana	1.55
Rosebud subbituminous, Montana	1.88
Arapahoe subbituminous, Colorado	0.93

15.2.3 Mineral Analysis by Scanning Electron Microscopy

This work involved the systematic identification and analysis of inorganic constituents distributed throughout a vertical section of a North Dakota lignite seam using a scanning electron microscope/microprobe (SEM). The characteristics and properties of the inorganics analyzed were not altered by crushing, grinding, or ashing the coal. Thus, the inorganics are described and analyzed in their original form.

15.2.3.1 Experimental

Sample Collection

Lignite samples were collected from the Beulah Mine, Mercer County, North Dakota, which is part of the Fort Union Coal Region of the Northern Great Plains Coal Province. The lignite bed which was sampled, called the Hagel bed, varies from 3-5 meters in thickness and is part of the Sentinel Butte Formation. Nine samples were collected at 0.5 meter intervals from a 3.5 meter thick coal seam located in the Orange Pit between markers 15-18. A vertical section of the seam was freshly exposed and swept to minimize the possibility of contamination. The nine samples were collected in plastic-lined one-gallon cans.

Sample Preparation

Coal chips of approximately 1-2 cm^2 were placed in molds with premeasured quantities of epoxy to form stubs suitable for analysis in the SEM. Three lignite samples from each of nine locations in the seam were mounted in the epoxy stubs. The epoxy stubs were sliced using a diamond-bladed low deformation rock saw to expose a fresh surface of coal. The fresh surface was ground using a succession of 240, 300, and 600 grit grinding papers and then finely polished using a sequence of 9 μm, 3 μm, 1 μm, and ¼ μm diamond pastes. Finally, the polished stubs were cleaned in an ultrasonic bath of trichlorofluorethane solvent and coated under high vacuum with carbon to provide a conductive surface for SEM analysis.

SEM-EDX Analysis

A JEOL JXA-35 electron probe x-ray microanalyzer was used to examine the lignite samples for inorganics. This instrument is an SEM with energy dispersive x-ray analysis (SEM-EDX) capabilities. The secondary electron imaging mode of the SEM allowed for easy observation of most minerals and other inorganics found in the coal maceral. The EDX system was used to identify the various inorganic particles (primarily minerals) by analyzing their elemental compositions.

A systematic use of the SEM was devised, which employed some of the methods proposed by Finkelman (1983) and Cecil et al (1979), whereby minerals *in situ* could be identified, sized, and photographed. This systematic examination was executed consistently for the samples at each location in the seam for the purpose of acquiring statistically reliable data. One of the three samples for each location was analyzed systematically and the other two samples were scanned randomly. In this manner, an area of approximately 1.5 cm^2 was scrutinized for each of the nine locations in the Beulah seam. This area was

observed thoroughly for minerals by employing a back and forth grid-type scanning procedure. The electron beam in the SEM was focused on the particle in question, and the resulting x-rays coming off the particle were analyzed by the EDX analyzer for 200 seconds, with the characteristic elemental spectra being stored in the computer memory of a Tracor Northern NS-880 unit programmed to record the normalized oxide concentrations of Na_2O, MgO, Al_2O_3, SiO_2, P_2O_5, SO_3, K_2O, CaO, TiO_2, Fe_2O_3, SrO, and BaO. The average diameter of each particle in microns was recorded. Polaroid photographs, approximately 10-15 per sample location, were taken of representative minerals present at each location in the seam.

Computer Application

The data compiled using the SEM-EDX system were entered into computer storage via Virtual Storage Personal Computing (VSPC). The data for each particle consisted of: the particle identification number; size; height in seam; the 12 normalized oxide concentrations; and the closure or sum of the oxide concentrations. Various statistical and graphic operations were then performed on the data using Statistical Analysis Systems (SAS).

15.2.3.2 Results and Discussion

The majority of the inorganic constituents discovered and analyzed in the Beulah lignite were minerals. The majority of these minerals were easy to see with the SEM when observing the coal samples at magnifications of 200x to 700x. The minerals observed in this study, and their frequency of occurrence, coincide relatively well with the findings of others who studied the lignites of this particular region (Paulson et al., 1972; Karner et al., 1983).

Mineral Descriptions

The most frequently encountered minerals were quartz, clays (kaolinite, montmorillonite, and illite), and pyrite. Other minerals that were less commonly found, yet still significant, were carbonates, rutile, and hematite. Some rare mineral occurrences were zircon, feldspars, barite, and gypsum.

The significant minerals which were detected and analyzed using the SEM-EDX system are listed and briefly described below in order of abundance.

Quartz - Quartz was the most frequently encountered mineral throughout the seam. The grains averaged 20-30 microns in diameter and were subrounded to angular in form (Figure 15-1). One peculiar quartz grain had the form of a hexagonal crystal.

Clays - Clay minerals occurred as relatively massive mineralized areas, 30-400 microns in diameter, dull in appearance and flat or platy in form (Figure 15-2). There were no sure ways to distinguish between the different compositions of the clays except by EDX analysis, although illite seemed to be slightly brighter than kaolinite.

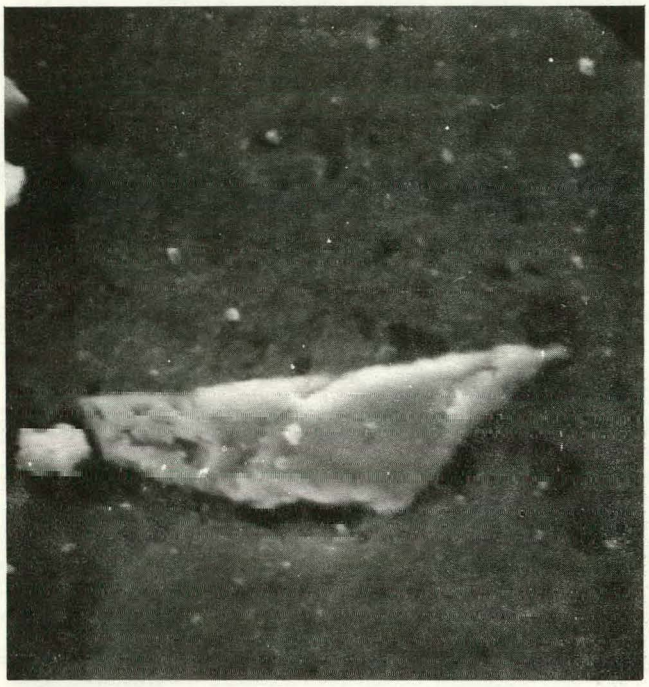

FIGURE 15-1. Angular quartz grain (2000x).

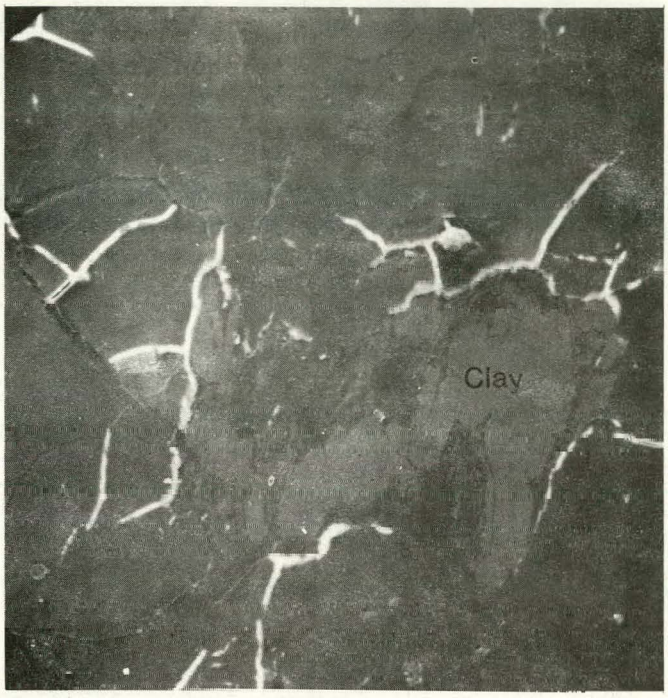

FIGURE 15-2. Massive kaolinite mineral; note dull appearance (160x).

Pyrite - Pyrite was found mainly as small rounded features or framboids with diameters averaging 20-30 microns (Figures 15-3 and 15-4). Basal sections of the seam revealed massive bands of pyrite which followed the woody structure of the coal. An unusual pyrite framboid which is intergrown with quartz is seen in Figure 15-5.

Carbonates - Carbonate minerals were detected in small amounts as calcite ($CaCO_3$), magnesite ($MgCO_3$), and dolomite ($CaMgCO_3$). Calcite plates were 25-40 microns in diameter and were found in coal crevices and cracks or in massive surface patches. Magnesite and dolomite occur mainly as crevice or cleat growths.

Hematite, Rutile, Zircon - Thin plates of hematite approximately 15 μm in diameter, were found in very minor amounts. Small quantities of rutile and rutilated quartz were identified which ranged in size from 5-25 microns. The grains are definitely embedded in the coal and were very weathered and rugged in appearance. One fairly large zircon particle (17 micron) which still retained some of its crystal form was identified.

Origin of Minerals

The source and origin of the minerals can be postulated using data accumulated through the SEM-EDX system. Many studies have been done concerning the epigenetic, syngenetic, authigenic, and detrital origins of minerals in low-rank coals (Cecil et al., 1982; Finkelman, 1982; Finkelman, 1983). The numerous photographs which were taken of the minerals distributed throughout

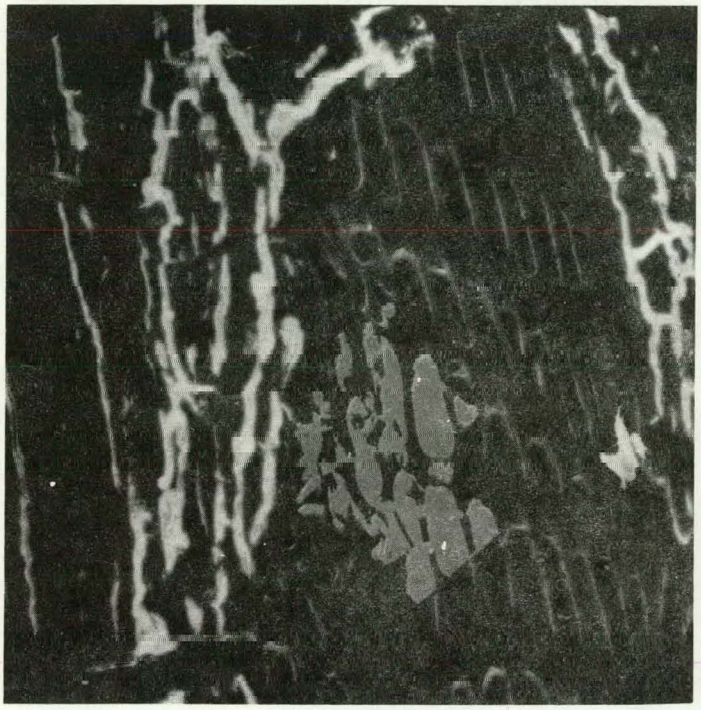

FIGURE 15-3. Pyrite intergrown in coal structure (300x).

FIGURE 15-4. Pyrite framboids (150x).

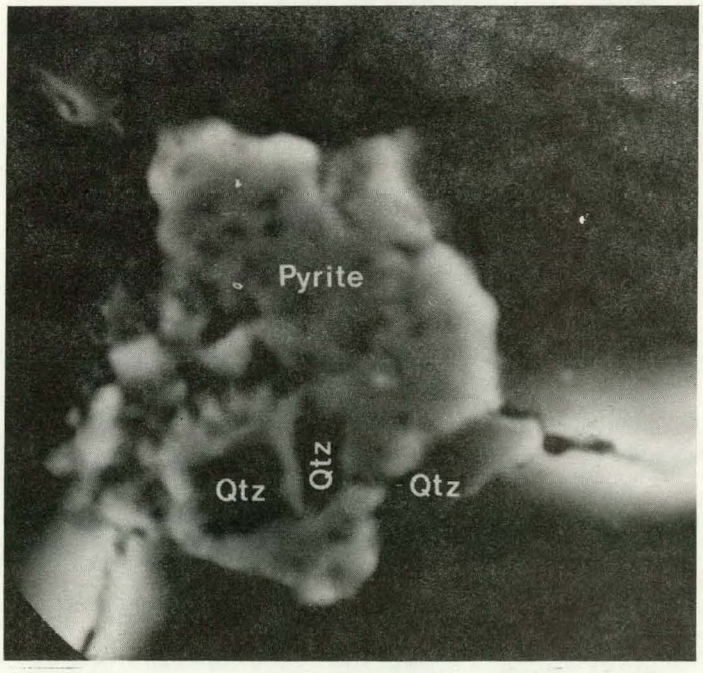

FIGURE 15-5. Pyrite framboid with quartz inclusion (6000x).

this particular Beulah seam provide textural evidence for the origin of the minerals. More specifically, textural evidence in support of the authigenic origin of minerals, consists of: mineralization in pores and pods of the coal mass; isolated crystals or crystal growths in cavities and cleats; and minerals intimately intergrown within the coal organic matter (Finkelman, 1982). Evidence in support of a detrital origin of minerals includes: subangular to subrounded grains; banding; aligned minerals; and v-shaped impact indentations in mineral grains.

Modern studies (Altschuler et al., 1983; Cecil et al., 1982) have shown that pyrite begins forming syngenetically as small framboids (Figure 15-6) during the peat stage of coal formation. Nearly all of the pyrite in the Beulah lignite is syngenetic. The textural relationship between the pyrite framboids and the coal maceral as pictured in Figure 15-4 reveal the syngenetic nature of the Beulah pyrite. The framboids occur as isolated blebs and do not follow cracks or fissures in the coal maceral.

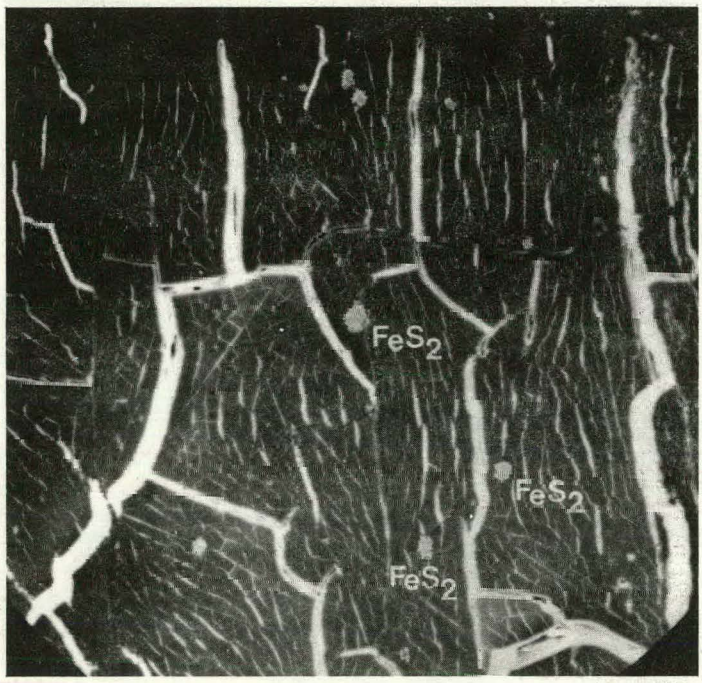

FIGURE 15-6. Very small pyrite framboids.

Epigenetic pyrite mineralization occurs after the coal has already been formed. This mineralization is brought about by the action of iron-bearing solutions within the coal body. The lignite studied in this project revealed some pyrite mineralization that may be epigenetic. Pyrite was noted in fracture zones of the woody coal structure. Epigenetic pyrite will only be deposited in cracks, crevices, or woody tissue zones of weakness.

Textural relationships also aid in determining the origin of the quartz grains noted in this study. The subrounded-subangular nature of the quartz grains and surface impact dents suggest a detrital origin (Figure 15-1). The

size distribution signifies that the quartz fraction within the Beulah seam is fairly well sorted with a slight skew to the larger grains (i.e., 30 microns). The distribution is similar to that expected of detrital quartz transported by wind or water and deposited. Other detrital minerals found were clays and rutilated quartz.

The carbonate minerals that were observed might be authigenic because they are seen lining cracks in the coal or in cavities, pores, and pods in the maceral structure. Siliceous matter was discovered on occasion, lining cracks in the coal. The shape, smooth surface, and relationship with the coal of this siliceous matter may indicate an authigenic origin.

Mineral Distributions

Karner et al., 1983, completed work on a similar lignite and noted trends in elemental distribution of four general types: 1) concentration of elements (in this report, minerals) in the margins of the seam: 2) concentration in the lower part of the seam; 3) even distribution; and 4) without a clear pattern.

In this study, the trends of mineral distribution are not always clearly visible. The clay minerals are concentrated more at the margins of the seam. The quartz distribution shows higher concentrations at the middle and upper portions of the seam. Pyrite is usually concentrated at the margins of lignite seams (Karner et al., 1983), but in this study it remains fairly even throughout the seam. An unusually high frequency of pyrite occurs at the 1.0 meter level from the base of the seam.

Most of the TiO_2 discovered in this coal was in the form of rutile or rutilated quartz. The TiO_2 distribution is uneventful except for a sudden high concentration at the 2.0 meter level, which corresponds with a high concentration of quartz at the same level. Rutile usually occurs as an accessory mineral in detrital mineral matter.

15.2.3.3 Conclusions

The inorganic constituents observed in the Beulah lignite seam can have a pronounced effect on coal utilization processes. Therefore, it is important to understand the physical and chemical relationships and characteristics of the inorganic matter. The SEM-EDX system provides an excellent means of studying lignite inorganics in situ.

By examining minerals in situ, the textural and distributional relationships can be discerned, which lead to interpreting mineral origins. SEM photography shows a distinction between syngenetic pyrite and epigenetic pyrite. Syngenetic pyrite is seen as small rounded blebs or isolated framboids throughout the coal seam. It is the product of early peat stage processes. In contrast, epigenetic pyrite is primarily concentrated in the basal sections of the lignite seam. It follows cracks, fissures, and other zones of weakness in the lignite and is usually massive in form. Epigenetic pyrite is the result of postdepositional processes related to the flow of meteoric or hydrothermal aqueous solutions through the lignite.

Textural relationships also aid in determining the origin of quartz in this lignite. The subrounded-angular nature of the quartz grains and their well sorted size distribution, point to a detrital origin.

Authigenic mineral types, such as carbonate minerals, were found in this study lining pores, pods, fissures, and cavities in the coal.

15.2.4 Distribution of Inorganics within Coal Seams

The distribution of major, minor, and trace elements within a seam of coal is very complex and is dependent upon many factors. These factors include the characteristics of the environment of deposition, types of plant material, ground water flow pattern, etc. The distribution of these elements relate to how they are associated or bound in the coal, which may in turn be related to the chemistries of the underlying and overlying strata.

The distributions noted in a section of the Beulah mine which includes two coal seams reveal several trends. These trends are as follows: elements concentrated at the margins of the coal seams include Co, Se, Eu, Sm, Sb, and Br; elements concentrated at the base of the lower seam include V, Cr, and Sb; elements concentrating at the top of the upper seam are Ba, Yb, U, V, and Cr; elements which have shown even distributions include Mg, Ti, Ru, Cu, Zn, Ni, K, Al, and Si; elements concentrated at or near the center of the coal seam include Na, Ca, and Se. Examples of these plots are shown in Figures 15-7 through 15-10.

15.2.5 Low-Rank Coal Lithotypes and Petrographic Techniques

The separation of low-rank coal lithotypes into durain, fusain, and vitrain has been accomplished successfully for both lignite and subbituminous coals. These lithotypes have been characterized by several analytical techniques, such as pressure differential scanning calorimetry, which has been used to examine the differences in aromaticity; and scanning electron microscopy, which has been used to examine and analyze organic and mineral fractions within the lithotypes.

The application of petrographic techniques to low-rank coals has involved solving problems associated with high-moisture contents of the coals. The approach used to get around the problem is to always keep the exposed part of the polished section of coal covered with the oil used for oil-immersion optical microscopy work. The identification of the microscopic constituents of coal (macerals) is then possible. The identification of certain macerals has been made. Samples of selected lithotypes fusain, durain, and vitrain were prepared and examined. Examples of photographs are shown in Figures 15-11, 15-12, 15-13, and 15-14. Figure 15-11 is a reflected light image of a portion of the vitrain lithotype, which shows huminite and liptinite macerals. Figure 15-12 is an image of liptinite macerals (the dark lines are characteristic of the liptinite group which are hydrogen rich). Figure 15-13 is a photograph of a section of fusain showing the highly reflective fusinite maceral which is carbon rich. Figure 15-14 is a photograph of a suberinite maceral, which is part of the liptinite maceral group. This maceral is derived from a cork-like material.

15.3 REFERENCES

1. Altschuler, Z.S., M.M. Schnepfe, C.C. Silber, and F.O. Simon. Sulfur Diagenesis in Everglades Peat and Origin of Pyrite in Coal. Science, Vol. 221, No. 4607, (1983), pp. 221-227.

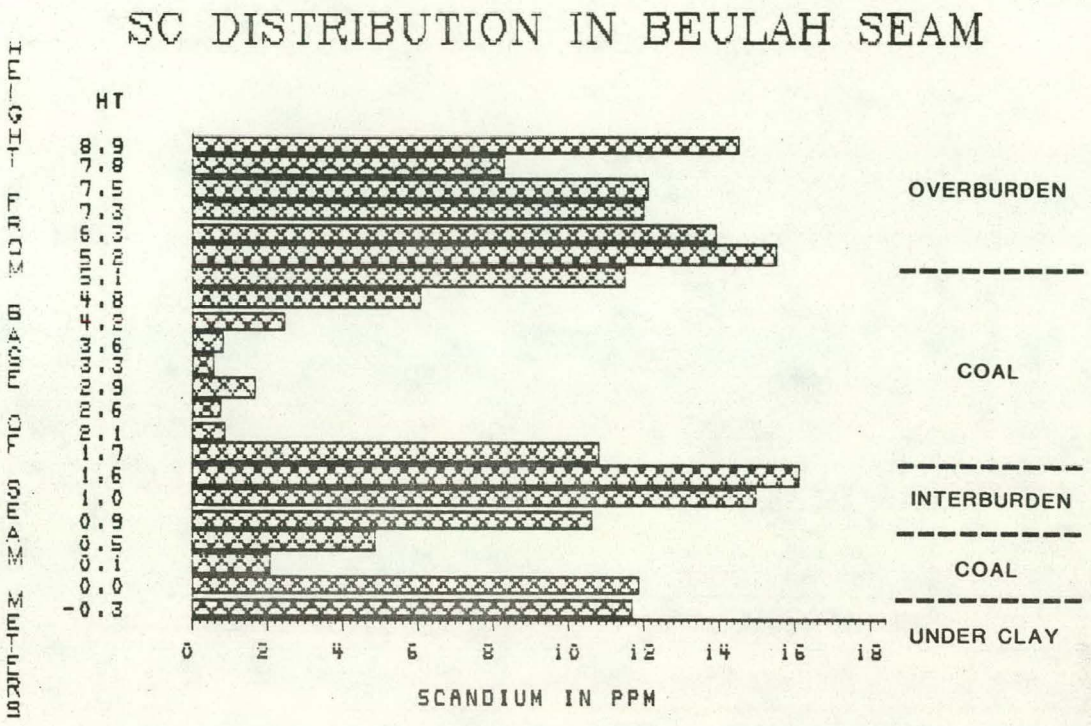

FIGURE 15-7. Concentration at the margins of the coal seam.

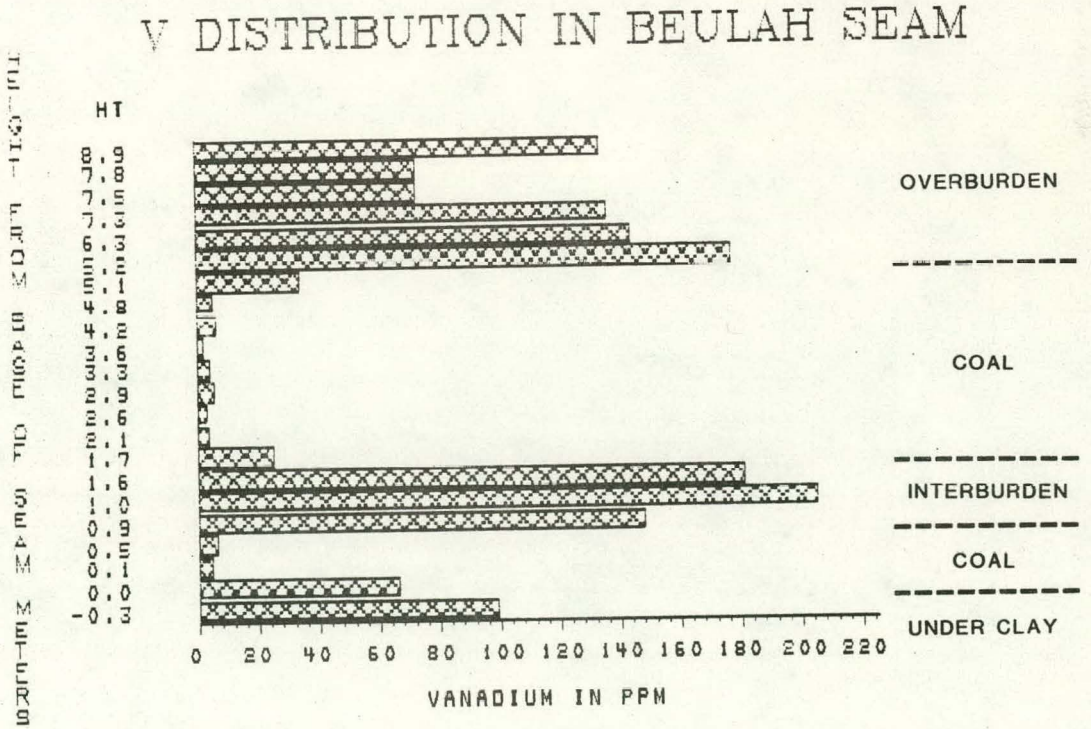

FIGURE 15-8. Concentrations at the top of upper seam and base of bottom seam.

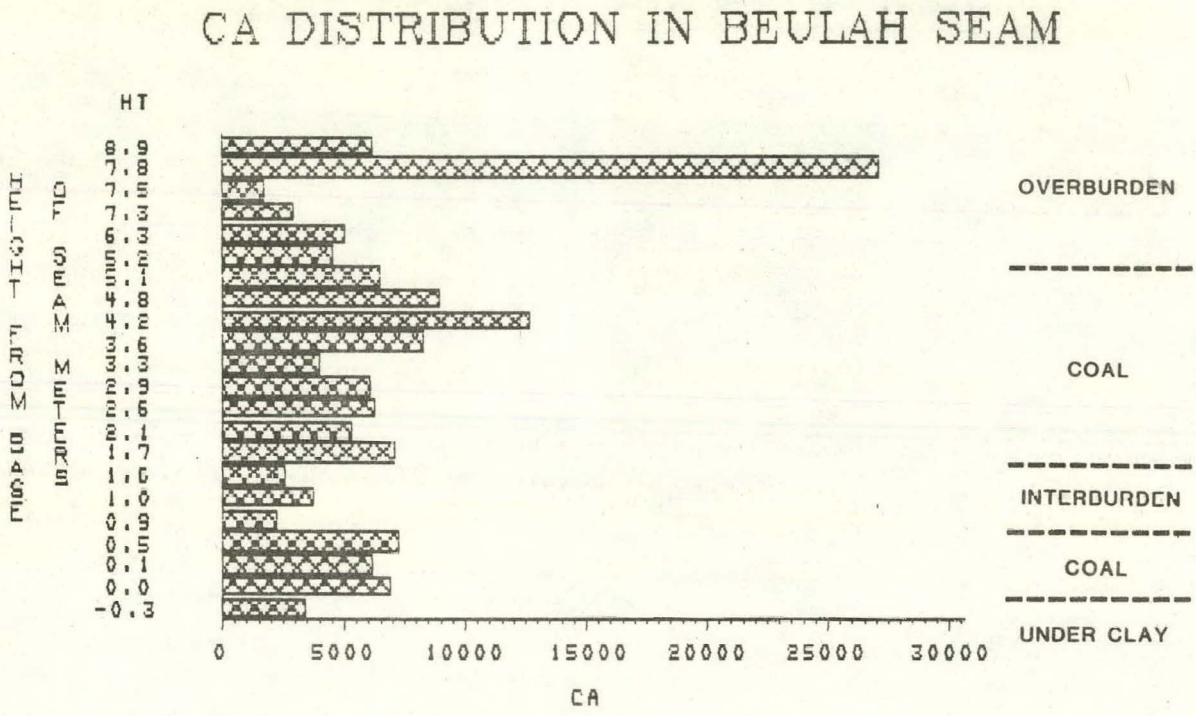

FIGURE 15-9. Concentration at or near the center of coal seams.

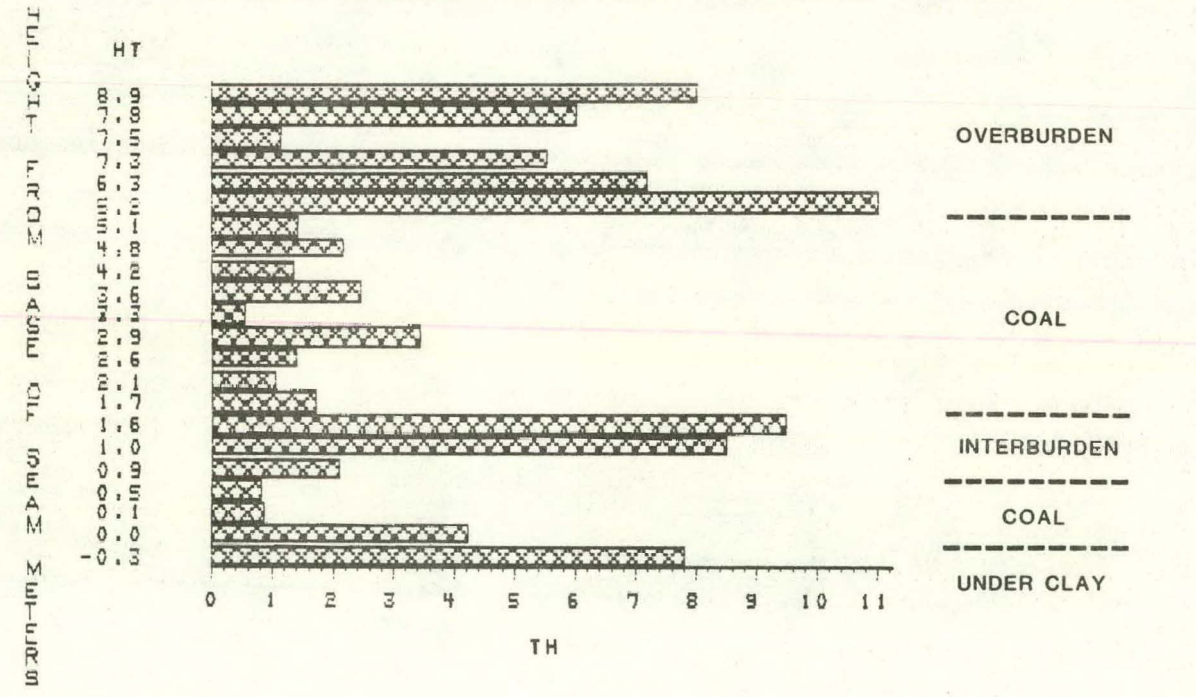

FIGURE 15-10. Random distribution.

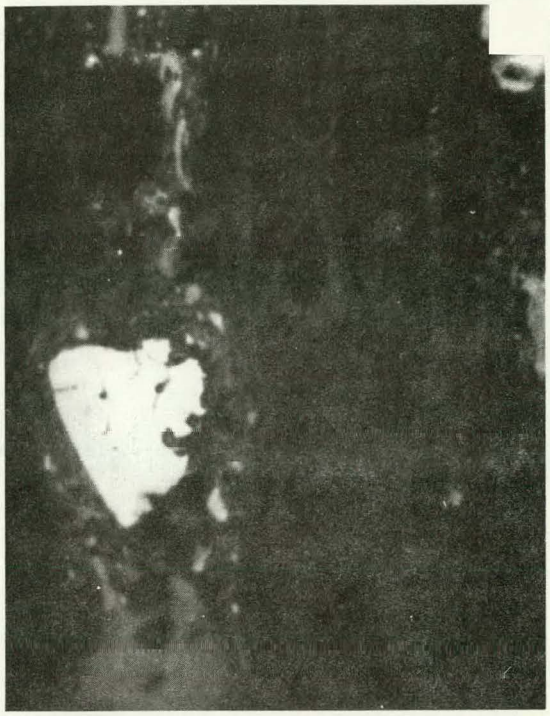

FIGURE 15-11. Reflected light image of a vitrain lithotype from Beulah lignite.

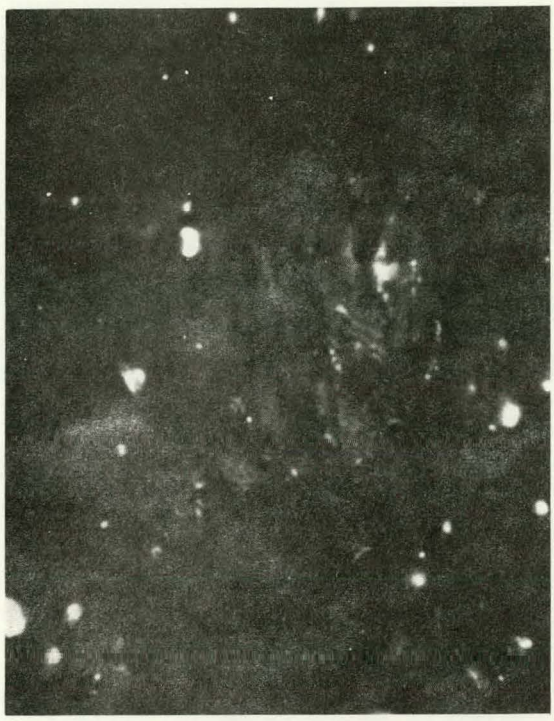

FIGURE 15-12. Reflected light image of some liptinite and macerals.

FIGURE 15-13. Reflected light image of fusain lithotype of Beulah lignite.

FIGURE 15-14. Suberinite maceral characteristic of cork material.

2. Blank, L.T. Statistical Procedures For Engineering Management, and Science. McGraw-Hill, (1980), 649 p.

3. Cecil, C.B., R.W. Stanton, S.D. Allshouse, R.B. Finkelman, and L.P. Greenland. Geologic Controls on Element Concentrations in the Upper Freeport Coal Bed. American Chemical Society, Division of Fuel Chemistry, preprints of paper presented at Honolulu, Hawaii, April, 1979, 24.

4. Cecil, C.B., R.W. Stanton, F.T. Dulong, and J.J. Renton. Geologic Factors that Control Mineral Matter in Coal. In Atomic and Muclear Methods in Fossil Energy Research, edited by R.H. Filby, Plenum Press, New York, (1982), pp. 323-335.

5. Finkelman, R.B. Modes of Occurrence of Trace Elements and Minerals in Coal: An Analytical Approach. In Atomic and Nuclear Methods in Fossil Energy Research, edited by R.H. Filby, Plenum Press, New York, (1982), pp 141-149.

6. Finkelman, R.B. The Inorganic Geochemistry of Coal: An SEM View. Unpublished paper written for: Exxon Production Research Company, Houston, Texas, (1983), 27 p.

7. Karner, F.R. S.A. Benson, H.H. Schobert, and R.G. Roaldson, Geochemical Variation of Inorganic Constituents in a North Dakota Lignite. U.S. DOE Report FC-1019 (submitted to the 186th American Chemical Society National Meeting Division of Fuel Chemistry, Washington, D.C., August 1983).

8. Kiss, L.T. and T.N. King. Reporting of Low-Rank Coal Analysis--the Distinction Between Minerals and Inorganics. Fuel, Vol. 58, (1979), pp. 547-549.

9. Morgan, M.E., R.G. Jenkins, and P.L. Walker, Jr. Inorganic Constituents in American Lignites. Fuel, Vol. 60, March, 1981, pp. 189-193.

10. O'Gorman, J.V. and P.L. Walker, Jr. Mineral Matter Characteristics of Some American Coals. Fuel, Vol. 50, (1971), pp. 135-151.

11. Paulson, L.E., W. Beckering, and W.W. Fowkes. Separation and Identification of Minerals from Northern Great Plains Province Lignite. Fuel, Vol 51, July, 1972, pp. 224-227.

16. - PHYSICAL PROPERTIES AND MOISTURE*

Project No.: 7305 B&R No.: AA1520150

Submitted by: H.H. Schobert, Manager, Coal Science Division

Prepared by: W.B. Hauserman, Project Manager, Physical Properties & Moisture
H.D. Bale, Faculty Research Associate (Physics)

Assigned UNDERC Personnel: W.B. Hauserman
W.A. Kinney
H.D. Bale
R.M. Neumann

Assigned AWU Personnel: C.M. Randleman
S. Kotalik

*A major portion of this section is being published for the ASME 7th Annual Energy-Sources Technology Conference in New Orleans, Louisiana on February 12-16, 1984.

16.1 GOALS AND OBJECTIVES

There are three major goals of this project. The first is to develop methodologies and data on mechanical properties of crushed and finely-ground low-rank coals and their mineral residues, relevant to their behavior and handling problems. The second is to relate observed mechanical or physical properties to the three-dimensional structural arrangement of the coal macromolecules via the theories and models of polymer science. The third is to determine the distribution and modes of incorporation of water in low-rank coals, and to develop approaches for the measurement of "moisture" which can be interpreted in ways meaningful for low-rank coal utilization.

Major objectives for the current budget year are as follows:

1. Establish credible testing procedures to define the following properties of coarsely-crushed coals, which define their behavior in a settling bed gasifier.

   a. Free sliding, bulk shear strength, as a function of particle size;
   b. Permeability to gas flow, as a function of particle size;
   c. Mechanical friability as a function of dryness; and
   d. Thermal friability.

2. Determine the pore size distribution in coals by small angle x-ray scattering, and any change therein that results during heating, drying, and pyrolysis, which is relevant to the release and reabsorption of moisture during processing. (This study is being done under a subcontract with Dr. Harold Bale of the UND Physics Department.)

3. Establish a methodology and simple apparatus to measure the relative hardness of finely-ground solids, such as coal and its ash in slurry streams, and candidate materials of construction. The hardness will be expressed on Mohs scale, which has hitherto been applied only to large surfaces by means of a scratch test. Process and equipment materials will thus be characterized with respect to the rates of erosion to be expected in slurry handling systems.

4. Apply physical characterization methods of polymer science, such as measurements of internal friction, elasticity, or solvent swelling, to elucidation of three-dimensional structural order of low-rank coals.

The objectives for the current reporting period have focused on measurements of shear strength, permeability, mechanical and thermal friability, and pore size distribution.

16.2 ACCOMPLISHMENTS

16.2.1 Shear Strength, Permeability, and Friability

Summarizing and essentially concluding the work done in pursuit of Objective 1, above, the following paper has been prepared for presentation at the ASME 7th Annual Energy-Sources Technology Conference, New Orleans, Louisiana, on February 12-16, 1984.

INTRODUCTION

This is a report on methods for simple, empirical measurement of mechanical properties of coarse, granular solids that determine their rate of settling against gases flowing upward through a packed bed. Data reported are primarily for a North Dakota lignite used as feed stock in a pilot scale, settling bed gasifier. The design is usually called "fixed-bed" in applicable literature and occasionally "traveling bed." One conclusion of a long program of pilot operation (1,2) was that the gasifier's capacity, and hence the rate of return on capital invested in it, is limited to the rate at which coarsely crushed fuel can settle against the upward flow of product gases. It is desirable to predict the settling behavior of potential gasifier feeds, in terms of fundamental, easily measurable parameters. These parameters, for nonagglomerating coals, are permeability and shear strength, which are functions of their particle size, which in turn is a function of their mechanical and thermal friability.

Consider any mass of crushed, solid material, settling down a vertical vessel, resisted by an upward flow of gas through it. The rate and stability of its motion are limited by its ability to form stable bridges or domes that can support part or all of the weight of material above it. Design assumptions and mathematical models of settling beds traditionally assume slug flow behavior, in which the material's bulk density, porosity, rate of descent, degree of compaction, particle size, and distribution of internal forces are assumed uniform and constant. In no way does this describe an actual gasifier vessel, nor anything but the most uniform, free-flowing solids sliding down a

tube against a relatively small gas flow. Figure 16-1 is submitted as a more realistic description, showing the condition where a minor part of the settling mass is compacted to a degree that it can, hopefully only temporarily, sustain shear forces, either against itself or the vessel wall. The weight supported by the bridge, dome, or impacted zone is equal to the weight of material above it minus the supporting force of the upward pressure drop through it. The bubble under the dome can be a cavity or a zone of very uncompacted or fluidized material. As this unfilled zone moves downward, the dome will normally collapse, either all together or by the dropping of single particles. The impacted zone can grow upward as settling particles come to rest and are sufficiently compacted to provide the radial, compressive stress (See free body diagram of Figure 16-1) which determines the vertical shear strength. The larger the pressure drop due to upward gas flow, the less shear strength is needed to support the effective weight of material above. As this effective weight approaches zero, with increasing gas flow and reduced permeability, the material may become locally fluidized.

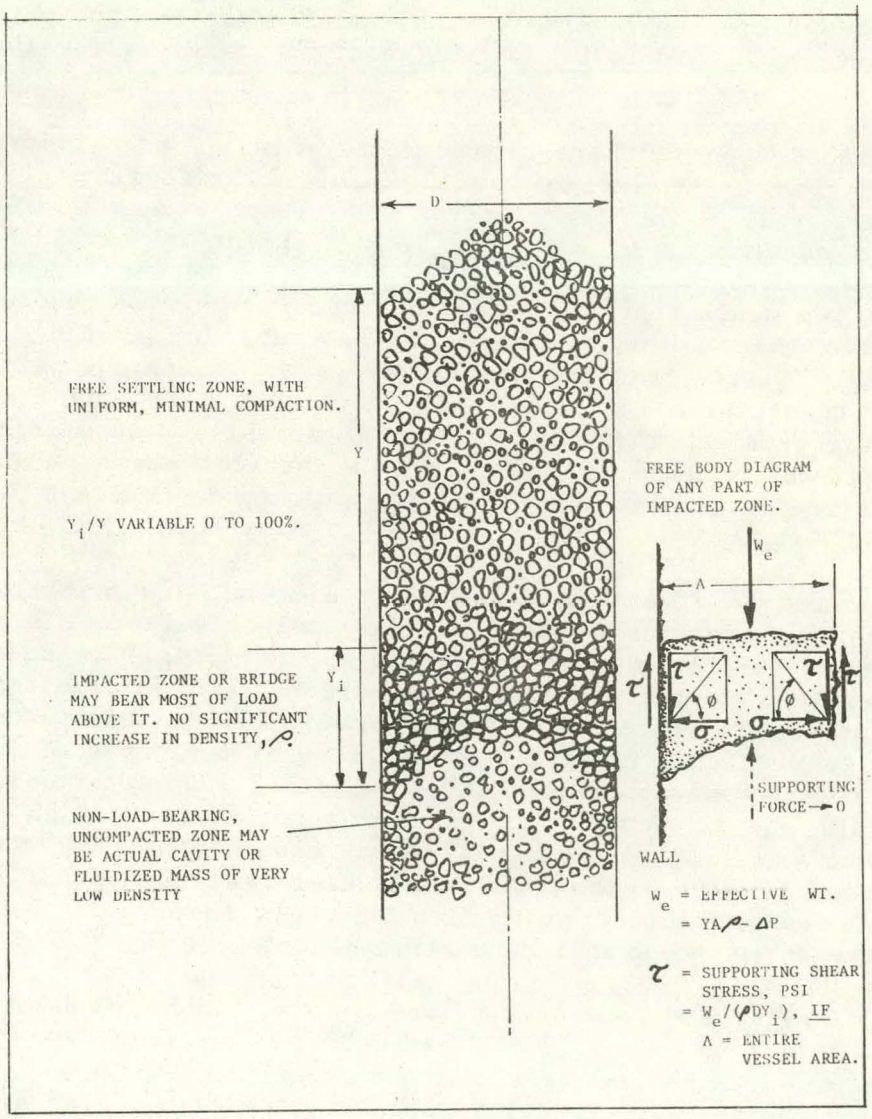

FIGURE 16-1. Irregular compaction of settling solids in a fixed-bed gasifier or other vertical vessel.

Even with completely "free-flowing" solids, such as uniform, dry sand flowing down a glass tube several inches in diameter, the phenomenon discussed above can be observed if the sand is flowing into a closed vessel, displacing an equal volume of air up the tube. Thin, lenticular bubbles are seen to travel harmlessly up the tube, at roughly the speed of the settling sand. In studies of solid flows through large bins and chutes (3), strain gages in the sides of vessels have measured the radial, compressive stress shown in the free body diagram of Figure 16-1. These stresses are seen at levels of even slight irregularities on the vessel surface. In a gasifier vessel, the actual volumetric flow of gases upward is over a hundred times that of the coal settling downward. Thus even apparently minor decreases in permeability can result in a pressure drop approaching the weight of the fuel bed, so that even an apparently insignificant shear strength can support the reduced, effective load on a bridge or dome. With highly friable lignites, mechanical and thermal attrition within the fuel bed often produce enough dust to reduce permeability to this critical level. With even slightly caking or agglomerating coals, the shear strength of impacted masses can be greatly increased. Fortunately, caking tendency and extreme friability are not encountered in the same coal. Also fortunately, under any set of fuel bed conditions, the minimum shear strength to support the bed decreases inversely with vessel diameter, so that variations in bulk shear strength tend to be insignificant in commercial scale gasifiers.

The experimental methods reported here are extremely simple, even primitive, and easy to replicate. The thermal and mechanical friability are characteristic of a given coal. The permeability and shear strength are determined mainly by the particle size and to a lesser extent by particle shape. Thus there is not likely to be detectable difference between these latter variables for any two coals that break down to roughly the same shaped particles. It is possible that a more isotropic anthracite, for instance, that fractures into "pebbly," less flat fragments, may have a different permeability and structural characteristics than a lignite of the same particle size range. Of the measurements reported here, it is the friability or degree of comminution under a given sequence of thermal and mechanical abuse, that determines the particle size distribution, which is the primary determinant of shear strength and permeability.

The experiments reported here were done with very limited, low-priority man-hours and funding for the intrinsic scope of the subject matter. They serve to define a family of related mechanical variables and minimal methods of measuring them, rather than complete data arrays to establish fundamental correlations. Results persistently revealed the importance of unanticipated variables in attempting to predict completely the behavior of a given coal in a settling bed gasifier. It became apparent that a complete array of tests to characterize various coals and to predict pressure drop reliably through a gasifier for a given fuel bed size distribution would consume many time the man-hours expended on this project. The data are therefore presented as a sampler of the range of the mechanical properties of coals that can affect their performance, to give an overview of the relative impact of each.

The work on shear strength and permeability was done with a North Dakota lignite from the Indian Head mine, which UNDERC has used for the past 3 years as feed to a pilot scale, settling bed gasifier, providing operating experience for correlation with the physical property data reported here. Typical-

ly, this coal analyses 25-32 pct moisture, 6 pct ash, and 28 pct volatiles. Ultimate analyses run 67 pct carbon, 4 pct hydrogen, 1 pct nitrogen, and 8 pct sulfur on an ash and moisture free basis.

FREE SLIDING SHEAR STRENGTH

In the fuel bed model of Figure 16-1, the shear force that can be sustained at any point in the material is in some proportion to the normal or perpendicular stress applied to the shear plane, which in turn is a result of the degree of consolidation of the compacted region. For any given compressive stress, the resulting shear strength is a bulk property of the material. Comparing different materials, it is a measure of their relative probability of forming a stable bridge or dome. Knowing that excessive dust in a gasifier's fuel bed results in severe settling problems, the purpose of the following tests was to relate the shear strength of a typically friable lignite to the particle size range.

Figure 16-2 shows two variants of the simple direct shear tester used for these tests. Established procedures for predicting flowability of fine solids

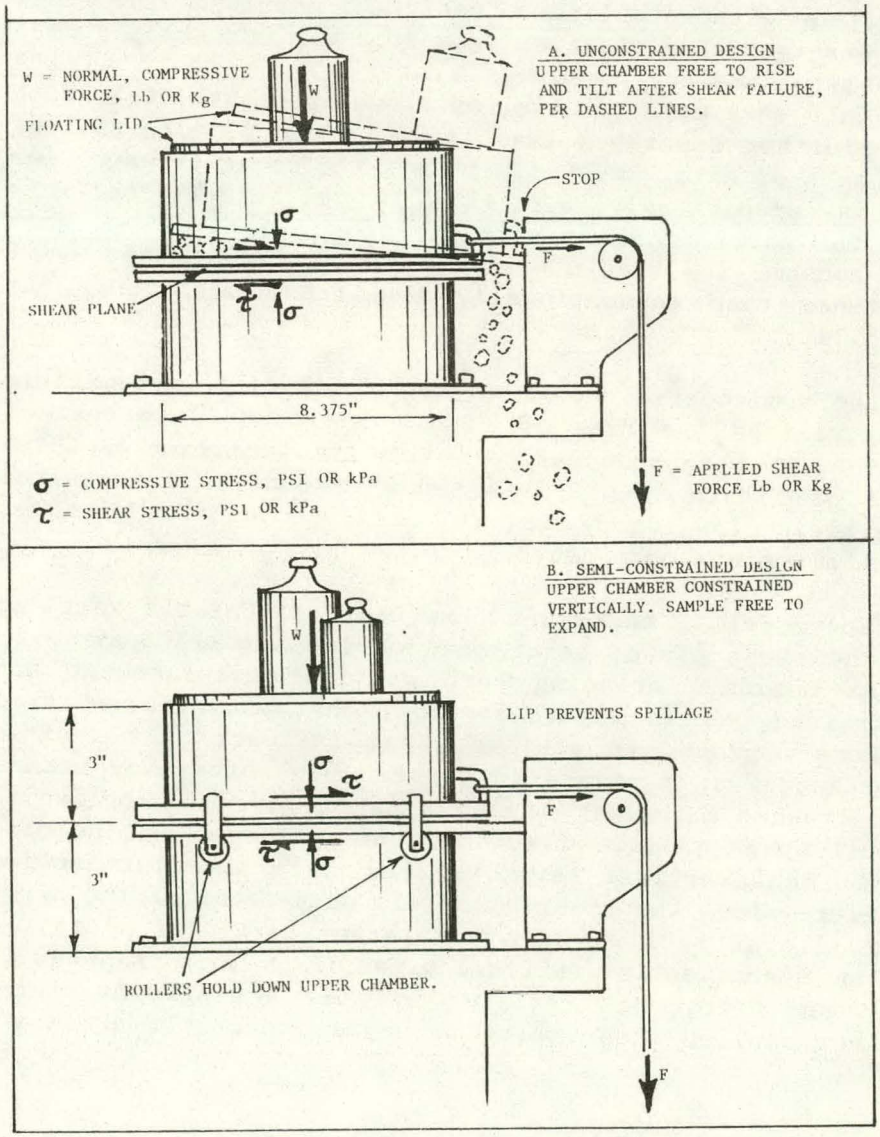

FIGURE 16-2. Shear test cells for coarse, crushed coal.

(4) to date have used a standard shear test cell of about three inches in diameter, yielding consistent results for materials below 20 mesh (.79 mm or .031 inch) which behave as uniform substances, the test cell diameter being roughly a hundred times the largest particles tested. In the case of feed to the UNDERC gasifier, the specified feed range is -3/4"+1/2" (-19+13 mm) for a minimum vessel ID of only 16", or only 21 times the maximum particle size. It is obvious that examination of this material requires a bigger test cell than the standard three inch (76 mm) unit. Even the 8.375" (203 mm) cell of Figure 16-2 is only 11.2 times the maximum particle size tested, raising the question of whether the data describes a "substance" or a random assortment of objects.

Initial tests were done with the completely unconstrained device of Figure 16-2A. The tendency to scatter the sample and weights randomly about the immediate area of the laboratory upon shear failure motivated the design of the semiconstrained design in Figure 16-2B. The adding of constraining rollers imposed further, nonyielding vertical forces on the sample, resulting in more erratic data but yielding insight into the mechanism of shear failure.

Initial data, using the unconstrained shear test cell, for two adjacent size ranges of crushed lignite are shown in Figure 16-3. The lines represent a visual best fit, consistent with established theory (4) developed for finer solids, which predicts a straight line starting from some minimum shear stress intercept. While the semiconstrained cell was neater with respect to its operation, the resulting data were more erratic, as shown in Figure 16-4, with two particle size ranges further separated than in Figure 16-3. The salient feature of both of these sets of data, however, is that the shear strength for the smaller sizes tested is conspicuously lower than for the larger size. This would indicate that, on the basis of shear strength alone, a fixed bed gasifier should be able to consume its feed somewhat faster or more smoothly if the feed were ground finer than conventionally specified, neglecting the effect of reduced permeability.

A further test on the semiconstrained shear cell, using a 50 pct mixture of the two size ranges, yielded the data of Figure 16-5, added to that of Figure 16-4. Note that the new points appear to follow the same line as those of the finer size range of Figure 16-4. This tends to confirm the general presumption from fine particle flow theory that the shear behavior of mixtures is dominated by that of their finer components.

During all of the above tests, there was observed considerable vertical deformation, normal to the shear plane, before and during actual shear failure. When this complex motion, including both vertical displacement and rotation, was semiconstrained, as in Figure 16-2B, higher shear forces were required, at each compressive load, to achieve shear failure. A plausible model of the failure mechanism is sketched in Figure 16-6. Starting with a randomly packed mass of crushed material (16-6A) a shear force is applied to deform the sample, resulting in some reorientation of particles in the direction of shear, with a small vertical reduction (16-6B). With further increased shear force, failure along the shear plane can only occur if the upper part of the sample can literally climb over the larger particles along the shear plane, resulting in a substantial vertical expansion. This is shown in 16-6C, where complete shear failure is resisted by only a single particle, which will require further applied shear force to either rotate or break it.

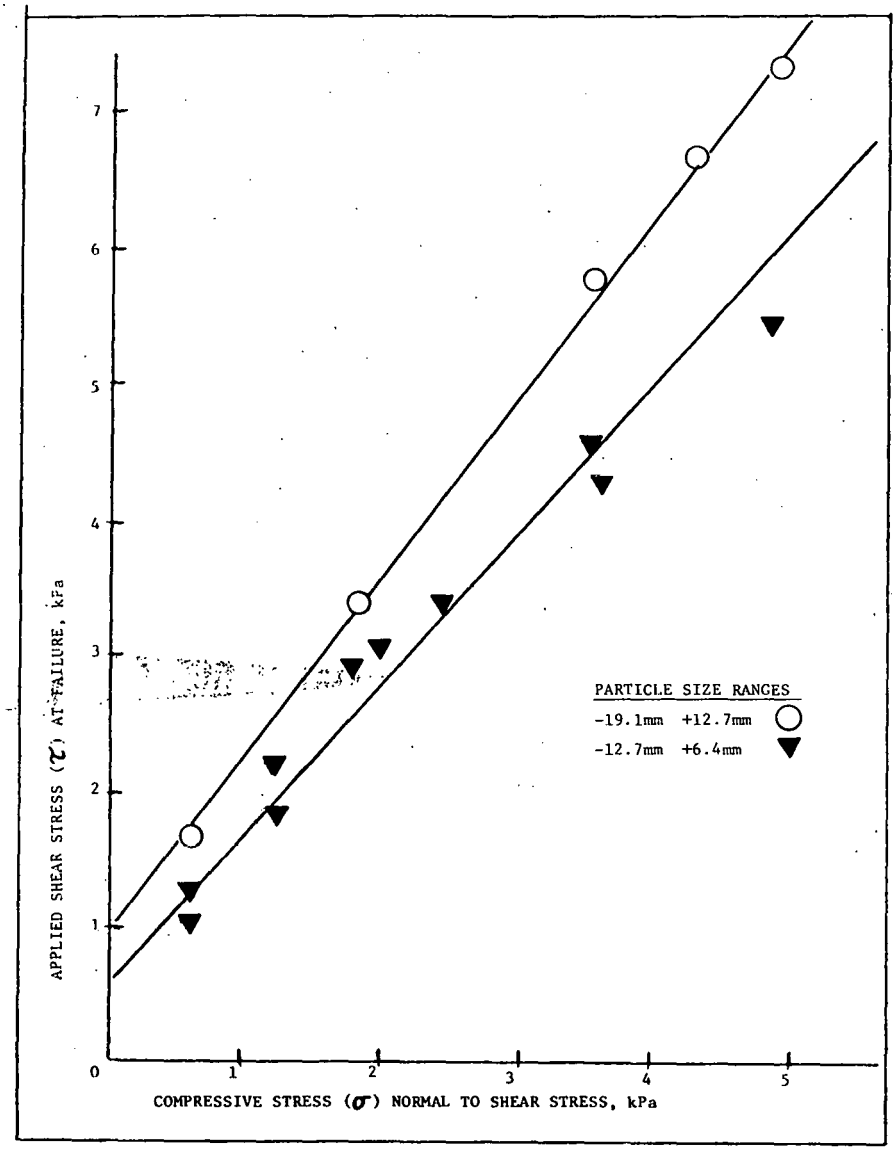

FIGURE 16-3. Shear strength verus normal compressive stress for crushed lignite in unconstrained shear test cell.

The above shear mechanism is evident in the deformation measurements of Figure 16-7. Note that the plastic deformation curves do not preceed smoothly to shear failure, indicated by their slope approaching infinity, but get there by jerks and stops, as individual particles are rearranged along the shear plane. The pattern was essentially identical for all three size ranges shown in Figure 16-3 and 16-4. The vertical displacement of the floating lid and weights (See Figure 2) was extremely erratic, nonrepeatable and varied greatly from one position on the lid to the next. It was consistent, however, as sketched in the crude approximation at the bottom of Figure 16-7, in that every measurement showed first a slight consolidation and then a much larger vertical expansion at or just before shear failure.

It is apparent then, form Figures 16-6 and 16-7, that shear failure cannot occur unless the associated normal stresses can be relieved by some displacement perpendicular to the shear plane. To demonstrate this further, a final experiment is reported in Figure 16-8, using a completely constrained shear cell. Here the floating lid was held down so that no vertical stress relief was possible. Increasing shear stress was applied, with the load cell initially zeroed. The result was an increasing, induced compressive stress,

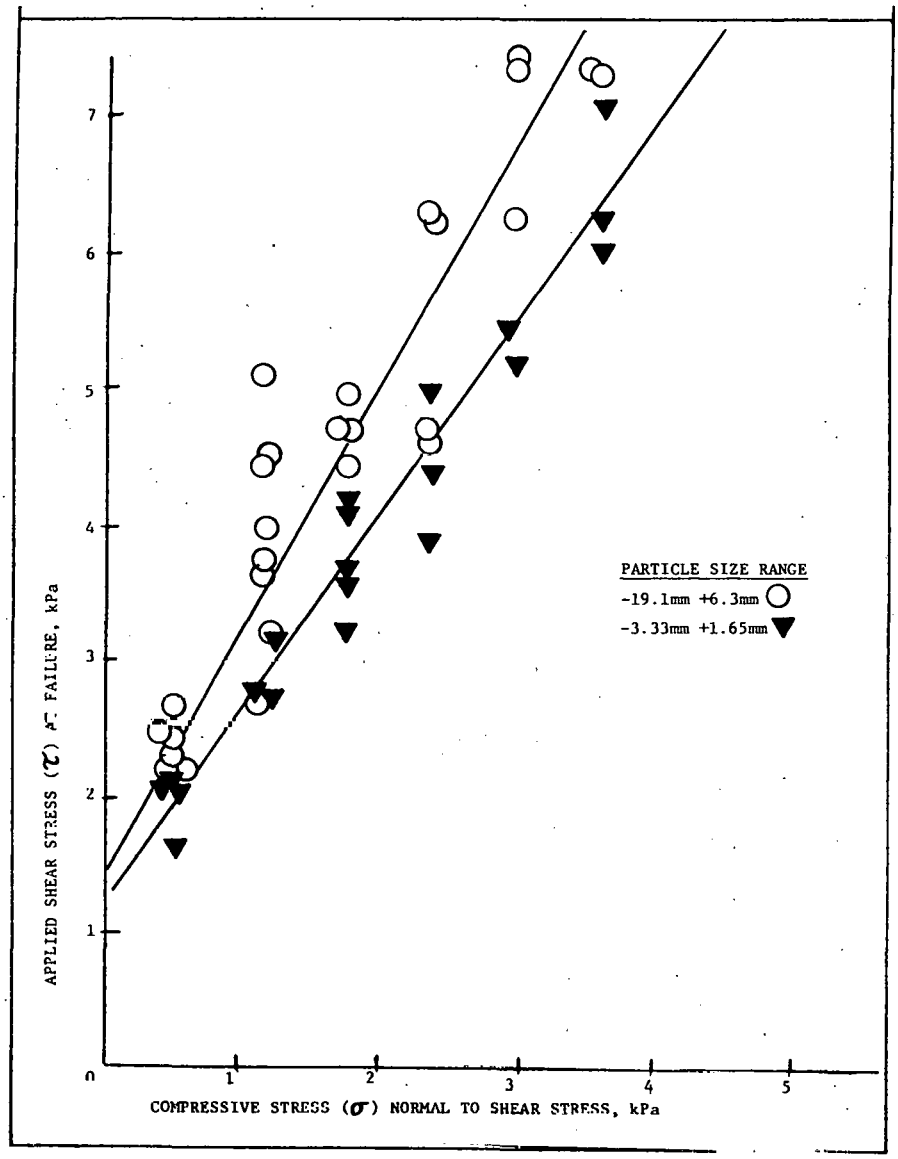

FIGURE 16-4. Shear strength versus normal compressive stress for crushed lignite in constrained shear test coal.

without ever achieving shear failure. In Figure 16-8, these data are compared with unconstrained shear strength data for the same sample. The line indicates the border between the shear strength as a function of compressive stress and the induced compressive stress as a function of shear stress. The experimental scatter in the induced compressive stress measurements indicates significant rearrangement and consolidation during variation of the applied shear stress, which was done several times over the range of the apparatus. At no point, however, did this result in enough internal stress relief to permit any gross motion along the shear plane. Intuitively, from inspection of Figure 16-6, the necessary normal stress relief should be at least equal to the minimum dimension of the largest particles, which is consistent with the approximate range shown for the semiquantitative data at the bottom of Figure 16-7.

In an actual packed column, however, where the shear planes are vertical and the normal compressive forces are radial, the material is most nearly approximated by the completely constrained condition simulated in Figure 16-8. This is especially true in a small column, with a small ratio of diameter, D, to particle size, d. With increasing D/d ratios, as in commercial scale gasifiers, the required radial compression for stress relief, expressed as

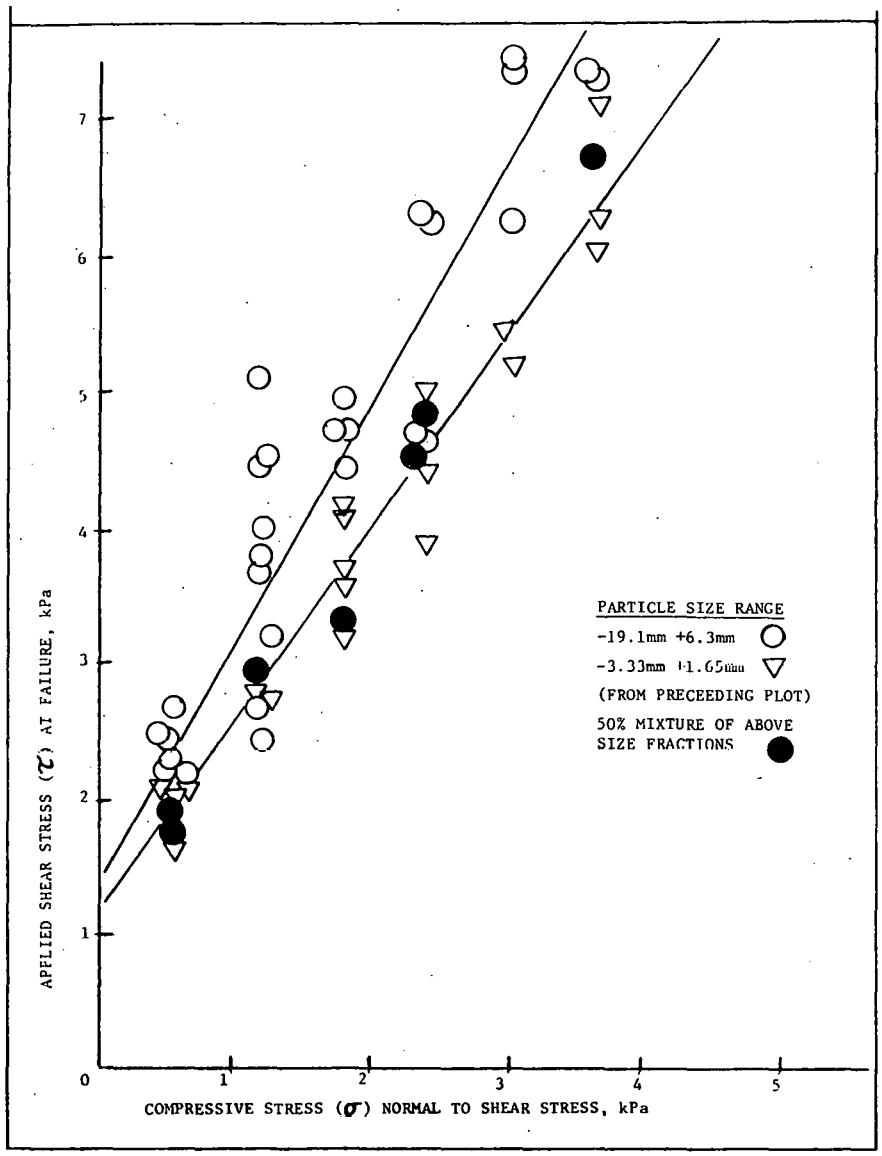

FIGURE 16-5. Shear strength verus normal compressive stress for crushed lignite in constrained shear test cell, showing effect of mixed sizes.

$\Delta y/D$ becomes smaller and more easily achieved. For the conventional, uniform, slug flow model to be valid, the material must be in a uniformly incomplete state of consolidation, such that the essential stress relief can be accommodated by rearrangement of particles across the vessel. The problems arise with the formation of impacted zones, as in Figure 16-1, where stress relief is possible only at the bottom of the zone, as the ceiling of the dome drops off, single particles at a time. Where the "bubble" is not in fact a cavity, but merely a filled volume of low density, it can impede disintegration of the ceiling, further maintaining the impacted zone. In the case of gasification of noncaking (low-rank) coals in which the solids are consumed, shrinkage of the fuel bed occurs due to drying and devolatilization in the upper part of the vessel and due to the gasification and combustion reactions in the lower part. The specific location of these reactions, however, will vary with the durability of the temporary domes. In short, either the dome must collapse to supply the reactants below it with fuel or the reactants must shift upward to burn out the dome, with adverse affects on process dynamics and stability (2).

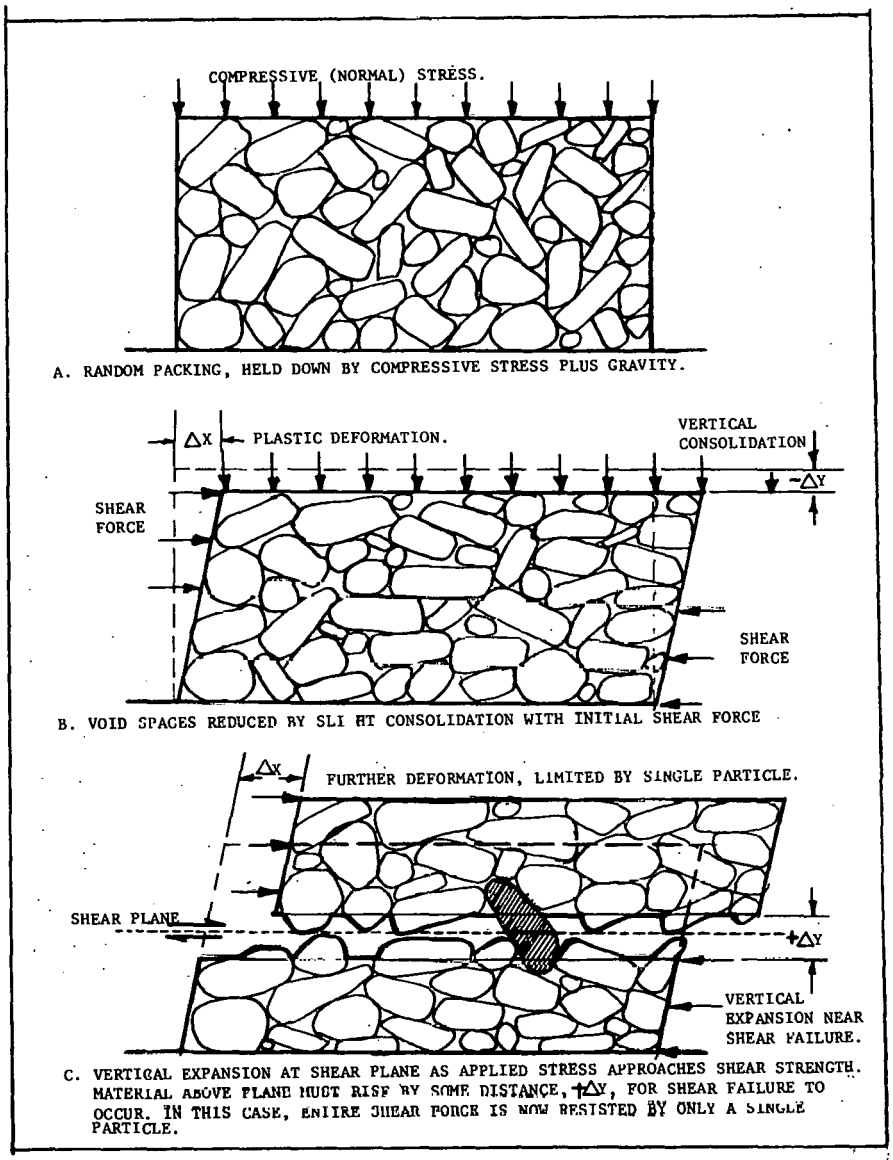

FIGURE 16-6. Realignment of crushed lignite particles with increasing shear stress.

Fixed-bed gasifiers have been effectively equipped with stirrers to break up bridges formed by caking bituminous coals. In such cases, the agglomerating tendency of the coal causes even a very temporary bridge to become rapidly more rigid. It is analogous to a fitted stone arch that would stand without mortar but becomes rapidly more durable as the mortar sets. When operating the same gasifiers on lignite, at less than their limiting capacity, stirrers are not necessary and generate excessive dust, due to mechanical attrition of the delicate feed, as discussed later. It would be desirable to provide stress relief in impacted zones with minimal stirring of the fuel bed. This defines a need and opportunity for a novel approach to the design of stirrers. As a design variable, the bulk shear strength need not be included in normal engineering calculations for well-designed gasifiers. At the upper end of a settling bed gasifier's operating range, where the pressure drop (discussed next) approaches the bed weight, the shear strength of a moderately compacted mass may become significant, as indicated in Figure 16-1. Under any set of bed geometry, state of compaction and pressure drop, the shear strength required to support the fuel bed is inversely proportional to diameter.

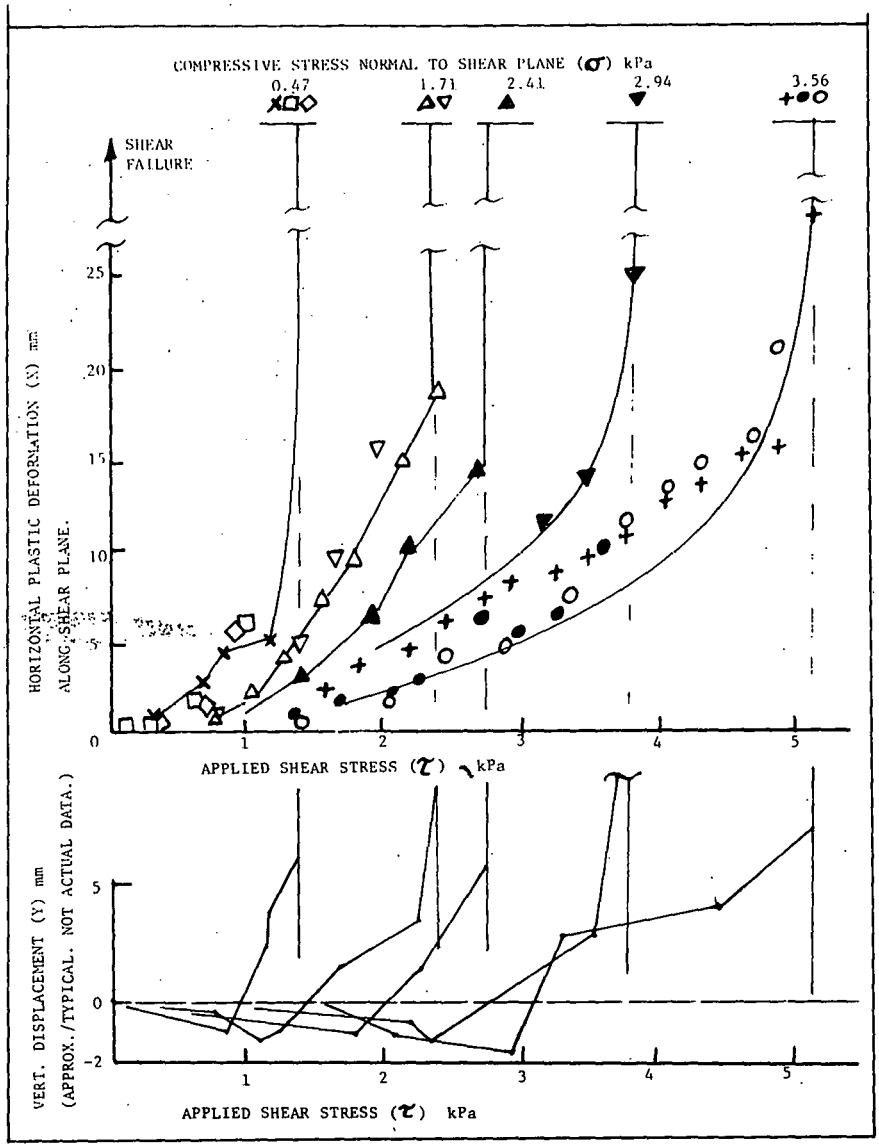

FIGURE 16-7. Plastic deformation proceding shear failure of crushed lignite particle size range: -6.3mm+3.3mm.

PERMEABILITY

In order for a settling bed gasification process to operate uniformly and near its maximum volumetric conversion efficiency, or even to operate predictably, the gas flow must be reasonably uniformly distributed over the entire reactor cross section. If the fuel bed's permeability, even over limited areas, should result in pressure drops approaching the bed weight minus the local shear strength, impeded settling will occur. A self-supporting bridge or bubble can permit a large void space below it, reducing the gas-solid contact volume, radically disrupting the vertical temperature profile and temporarily stopping the flow of solids. Where the bridge or bubble is not self-supporting, then the excessive upward pressure may relieve itself through some random channel of least resistance, resulting in a major part of the gas stream bypassing much of the fuel bed, with greatly reduced contact time and incomplete reaction. In an operating gasifier, this is indicated by dangerously high product gas temperatures. Qualitatively, operating experience suggests that channeling is caused mainly by excessively fine fuel bed material, while stable bridges are associated mainly with excessive gas flows.

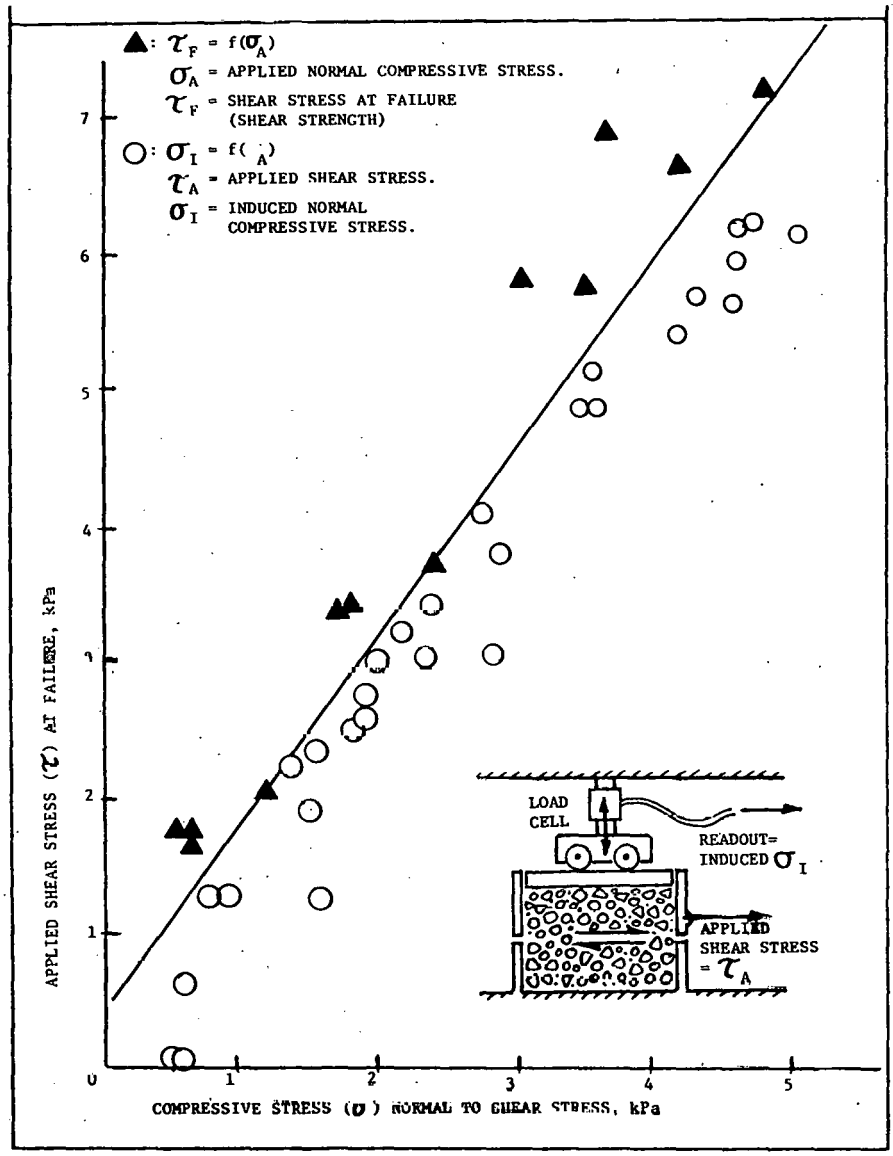

FIGURE 16-8. Comparison of unconstrained and completely constrained shear stress relations for crushed lignite, -19.1mm+12.7mm.

Here we shall explore empirically the relative sensitivity of pressure drop through a bed of crushed coal to its particle size distribution.

Apparatus was extremely simple. A plastic cylinder of 6.5" diameter (165 mm) by 24" (600 mm) tall was filled with crushed coal of selected, nonoverlapping size ranges. Air flow through it was measured by an orifice assembly for the upper flow ranges and by a rotary, positive displacement gas meter for the lower ranges. Pressure drops through the coal column and across the orifice were measured by water manometers. Air flows were determined by an orifice flow slide rule (from Robinson Orifice Fitting Co.) for the higher ranges and by a stopwatch for the lower. Air was at essentially ambient conditions, simplifying assumptions as to density and viscosity. All data were logged into a processing system for computation and plotting.

An example of the point-by-point data is shown in Figure 16-9. The considerable nonrepeatability is due to irregularity of packing, incipient fluidization at higher flows, some channeling for the smaller size ranges and visible segregation (fines migrating to upper surface) for the wider particle size ranges. The onset of all these effects defines roughly the upper limit

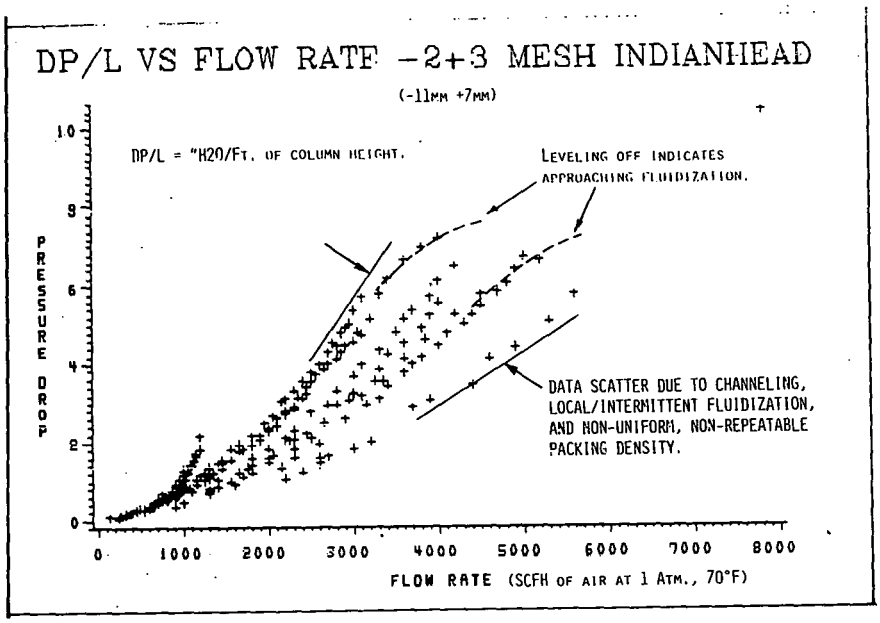

FIGURE 16-9. Example of permeability data.

of the experimental range of interest, beyond which orderly or predictable "fixed-bed" behavior is no longer possible. The actual column height varied considerably, being shorter for the finer size ranges with higher pressure drops. Pressure drop was recorded per unit of column height, for uniformity of comparison. For smaller particle sizes, there was some bed expansion. Also for smaller sizes, the initial bed depth varied, depending on whether the column was merely filled gently or rapped several times to settle the coal. Composites of pressure drop data for five, nonoverlapping particle size ranges are sketched in Figures 16-10 and 16-11.

The packing density or weight of fuel bed in actual gasifier is highly variable, due to the continual rearrangement of the settling solids, not to mention decreasing particle densities due to drying and devolatilization, all complicated by shrinkage and fracturing of single particles. On Figures 16-10 and 16-11, the weight of the coal, expressed as pressure drop per column height is indicated for different assumptions as to the coal's effective bulk density. In all cases, except for the largest size range, the upper limit of data was determined by some visual rearrangement of the coal surface, that is, spouting dust, expansion or size segregation. For the largest size range (-.75"+.5" or -19+12.7 mm), capacity of the compressed air supply system was limiting. In all cases, it is of interest that decreasing slopes of single data runs (per example of Figure 16-9) and of upper limits of composites in Figures 16-10 and 16-11, which indicate approaching fluidization, begin as the pressure drop passes that corresponding to an average column density of 30 lb/cu. ft. (40-50 gm/cc). This establishes upper limits to applicability of mathematical models using any fundamental relationships derived specifically for packed column or "fixed-bed" systems.

It is readily apparent why the ideal or specified feed size range for settling bed gasifiers is above 0.5" (12.7 mm) and that highly friable lignites present severe capacity limitations, in spite of their being free of the agglomerating tendencies that are the major problem source in gasification of higher rank coals. To observe qualitatively the effect of wide ranges of particle sizes, the highest range studied here (-19+12.7 mm) was blended with 25 pct and 50 pct of lowest size range (-3.4+2 mm), with the results shown in

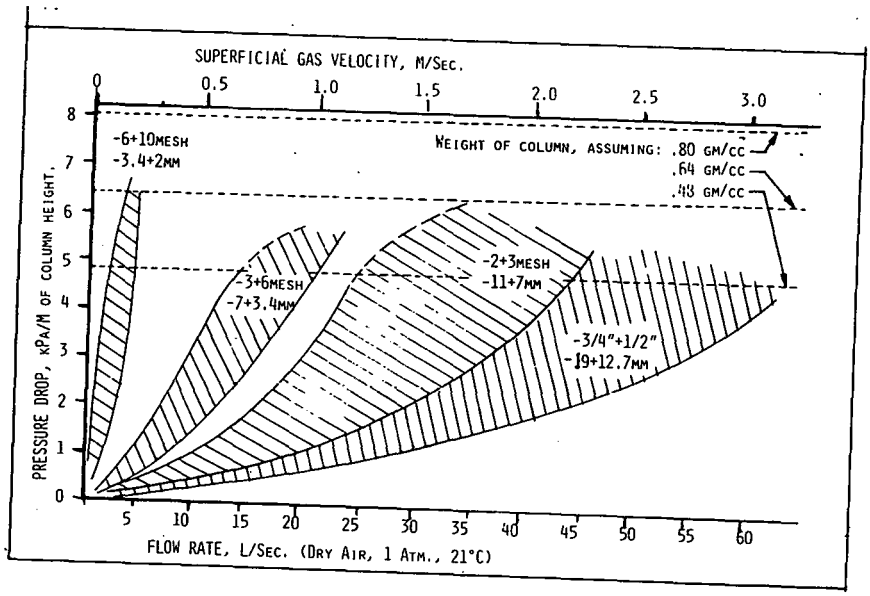

FIGURE 16-10. Pressure drop versus air flow rate through crushed coal, high range composite.

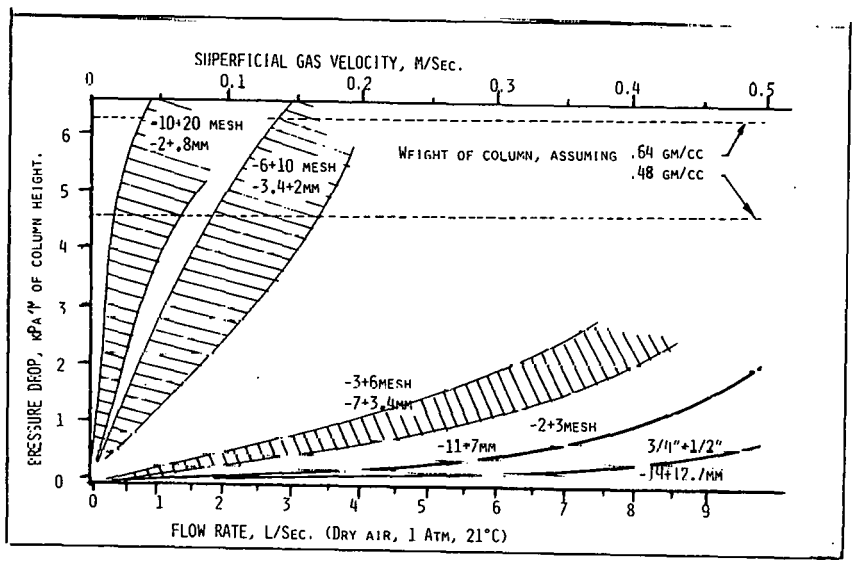

FIGURE 16-11. Pressure drop versus air flow rate through crushed coal, low range composite.

Figure 16-12. Clearly, permeability is dominated by the finest components present in any significant quantity. At an air flow of 1000 scfh (7.9 L/sec) through the specified fuel bed material, an addition of 25 pct of the -10+20 mesh (-3.4+2 mm) portion increases the pressure drop by 3 to 8 times, while a 50 pct addition would result in a pressure drop exceeding the weight of the column.

To relate these idealized data more closely to gasifier performance, Figure 16-13 shows size distribution for both normal and unacceptable gasifier feeds and their associated fuel bed condition. Curve A is typical of the Indian Head lignite fed to the UNDERC pilot gasifier (1,2). In spite of inadequacies of the screening and feed handling system, it is at least 60 pct greater than the desired .5" minimum and no more than 2 pct below 10 mesh (2 mm). Following a normal shutdown (not due to the upper fuel bed's misbehavior), the residual fuel in the vessel's upper two thirds typically has a size distribution indicated by Curve B. As an experiment during the final hours of one operating run (Run 4) the feed was switched to an as-ground, unscreened bunker of lignite, having the size distribution indicated by Curve

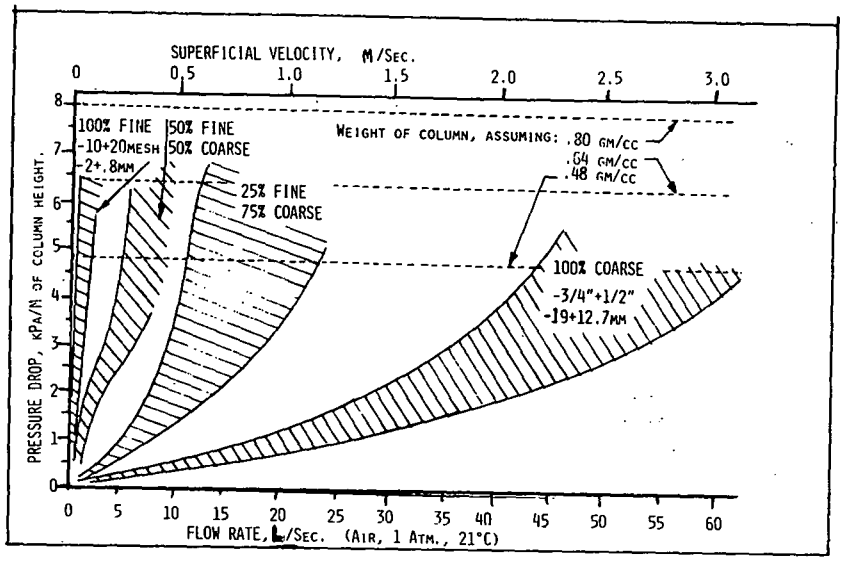

FIGURE 16-12. Permeability of mixtures of coarase and fine crushed coal.

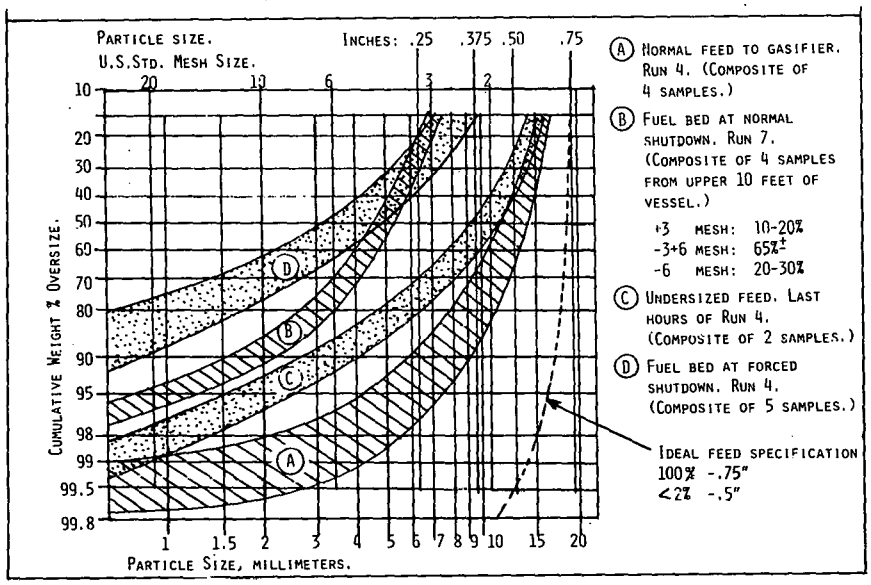

FIGURE 16-13. Size distribution of gasifier feed and fuel bed.

C. The gasifier was operating well within its proper capacity and even this un-screened feed caused no immediate symptoms of major bridging or impeded settling. After the vessel was completely filled with the new feed, however, the product gas temperature increased abruptly, exceeding the equipment's safety rating and forcing a hurried shutdown. This indicates chanelling, where very hot gases from the reaction zone, which exceed 2000°F (1100°C), bypass most of the upper fuel bed. Following shutdown, a composite of 5 samples from the upper 10 feet of the fuel bed showed the size distribution of Curve D. Note the correspondence of shapes between A and B and between C and D. Within the area covered by Figure 16-13, the limiting specification for operating the gasifier could be the upper edge of composite Curve B, to the extent that the fuel bed size could be controlled by any means other than screening the feed. A composite sample of the inoperable fuel bed material of Curve D was tested for permeability, with the results shown in Figure 16-14. Superimposed on the data of Figure 16-14 is the range of equivalent data on -3+6 mesh material, from Figure 16-11. It is of interest that this describes the middle 24-31 pct of the fuel bed material, implying that the permeability of a broad range of particle sizes is roughly approximated by mass median size.

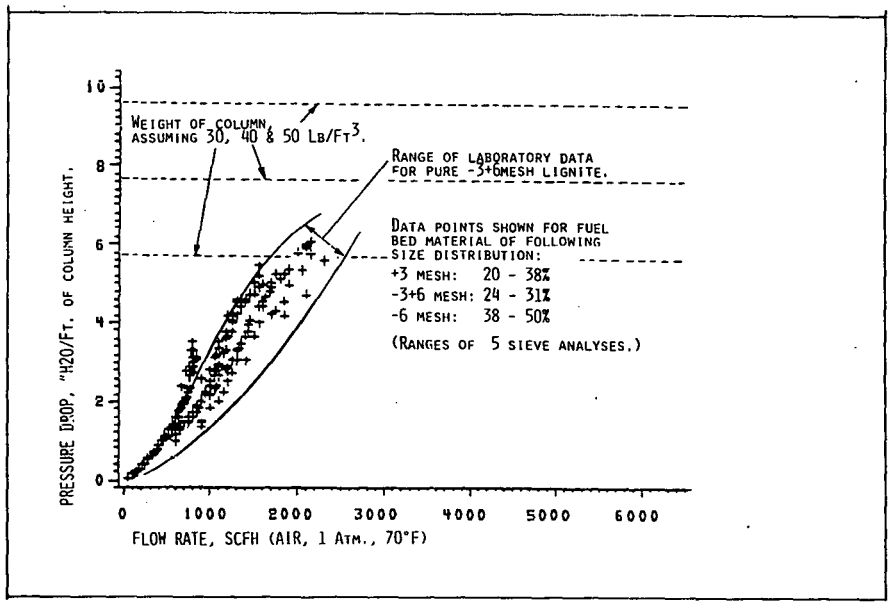

FIGURE 16-14. Permeability of undersized gasifier fuel bed material at shut-down.

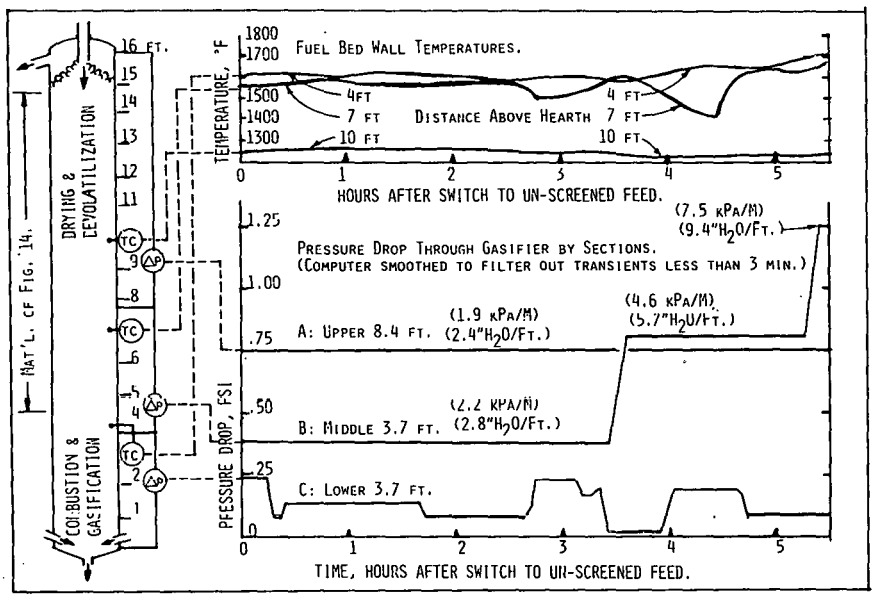

FIGURE 16-15. Temperature and pressure drop through gasifier fuel bed with undersized feed.

The time sequence of events leading to the forced shutdown is shown in Figure 16-15. The entering feed (Curve C, Figure 16-13) is thermally fractured to the distribution of Curve B within the upper 4 or 5 feet, by mechanisms discussed later as the temperature reaches 1000°F (540°C) during drying and devolatilization. There is presumably a size gradient in the upper few feet of the fuel bed, although the available sampling method made considerable vertical mixing unavoidable. Before the switch to unscreened feed, fuel bed temperatures and pressure drops had been steady at the levels shown at time zero in Figure 16-15. As the unscreened feed and its resulting char filled the fuel bed, the temperature at the 7-foot level began a slow cycling, which is believed to indicate formation and collapse of "bridges" or zones of reduced permeability (1). This coincided roughly with an increasing pressure drop through the same general section of fuel bed, though the pressure drop in the upper half of the vessel appeared unaffected. The lower end of the vessel normally shows a more erratic pressure drop, due to the continual rearrangement of the char as it is consumed in a violent, fluidized zone in the lower foot or so. In Figure 16-15, the observed pressure drops are expressed in parentheses as ΔP/depth over vertical range spanned by the pressure drop

measurements. Comparing these with the column weight limits in Figure 16-14, note that the pressure drop in the middle 3.7 feet was enough to render this section of fuel bed weightless for the last 2 hours of operation, even ignoring any additional support from the materials' shear strength which contributed at least another .05 psi/ft, at the vessel diameter of 22", and possibly several times as much, depending upon the degree of compaction. In the final 10 minutes of operation, the mid-section pressure drop rose to 9.4 "H_2O/ft, which is enough to support itself, even at an assumed maximum density of 50 lb/cu ft. The apparent result was that a major portion of the upper bed became temporarily weightless and rearranged itself to permit a path of least resistance to the surface, releasing product gases to the discharge line at a dangerous 1300°F+ (700°C). Why then, during this scenario, was the upper 8.4 feet of the fuel bed so serenely unaffected by the violence immediately below and even passing through it, as suggested by its remarkably unvarying pressure drop and temperature? The effect on coal's structural properties of drying and devolatilization, which are completed in this zone, are described in the following section.

FRIABILITY - THERMAL AND MECHANICAL

Having reviewed the effects of particle size on settling behavior of coal, we now consider some key properties of specific coals that determine their relative suitability as gasifier feed stocks. Specifically, the shift in size distribution of a specific coal during heating and mechanical abrasion will determine its particle size distribution as a fuel bed material.

As brittle solids are subjected to mechanical tumbling, size reduction proceeds by several mechanisms. According to fundamental brittle fracture theory, when particles of a given size distribution are subjected to impact or crushing action, all particles will break into a roughly equal number of smaller particles of an identical relative size distribution. The result is parallel shifting upward of a standard size distribution curve. As an example, Figure 16-16 shows the result of an equal, mild tumbling action on two different size distributions of the Indian Head (North Dakota) lignite commonly used as feed to the UNDERC gasifier. In both cases, the line was shifted by a roughly equal vertical displacement, which defines the mechanical friability of a given material. Replication of tests on one sample indicates high repeatability.

As any brittle solid is heated, thermal fracturing occurs by differential expansion of the outer and inner portions of each particle or of internal components of different composition. Where any devolatilization takes place, as in the case of lignites that typically contain over 30 pct moisture, the expanding vapors push apart the particles along their planes of weakness around the pores wherein the water is contained. Furthermore, removal of chemically bound water from the molecular structure creates further points of weakness. At higher temperatures, removal of volatile organics produces further, similar effects. While all the micro-mechanisms of thermal fracture form an extremely complex package of interrelated phenomena, beyond the scope of this work, their combined result follows very closely the same size distribution behavior that describes mechanical brittle fracture. An example is shown in Figure 16-17, in which two samples of the same Indian Head lignite were heated to 1000°F (540°C), driving off all moisture and essentially all

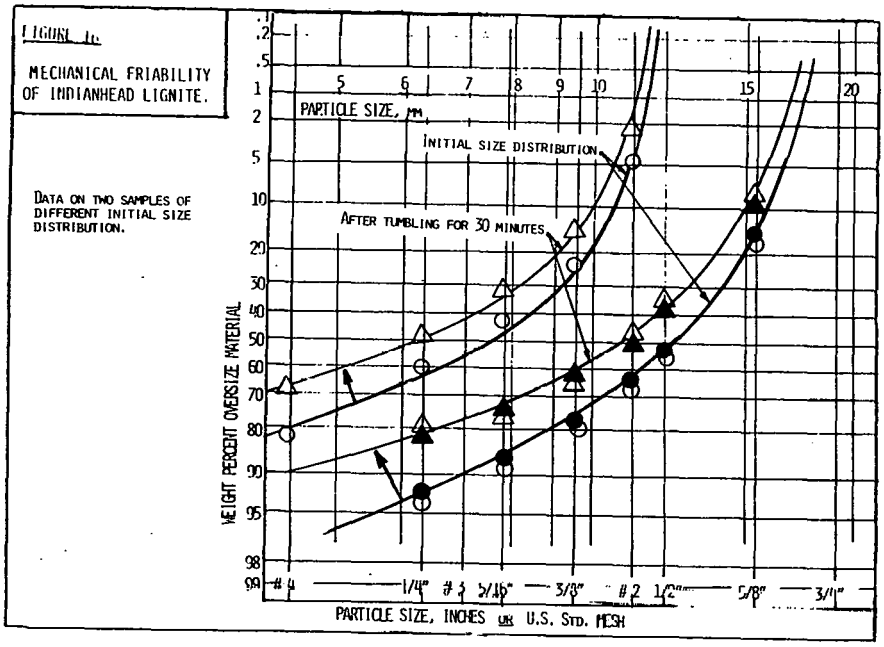

FIGURE 16-16. Mechanical friability of Indian Head lignite.

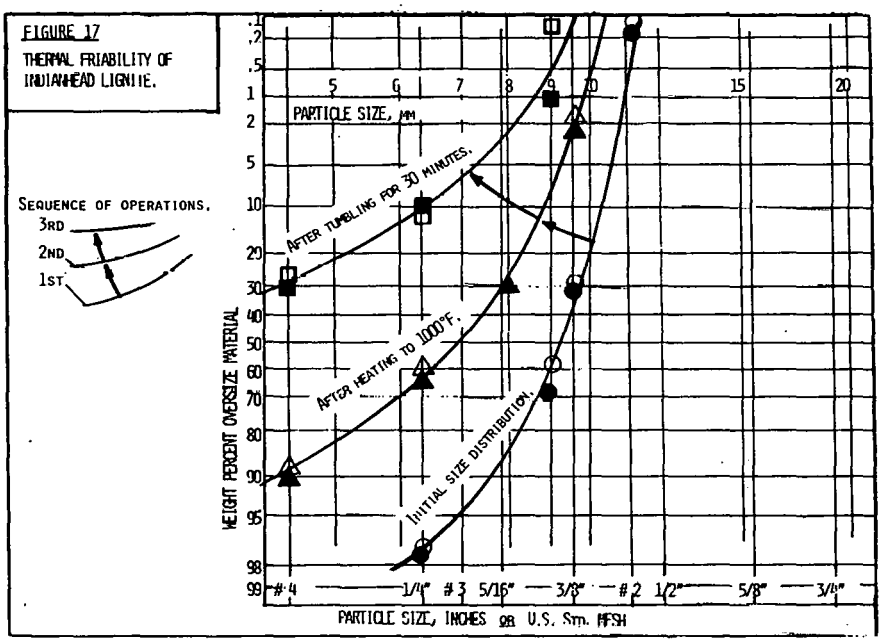

FIGURE 16-17. Thermal friability of Indian Head lignite.

volatile organics. Note that the resulting degree of comminution is substantially greater than for mechanical tumbling alone, per Figure 16-16. When the devolatilized char is subjected to the same mild tumbling action, however, the degree of destruction is far greater, as indicated by the upper line of Figure 16-17. This combined friability predicts what can be expected of a given coal in a gasifier fuel bed.

To compare the relative cold mechanical, thermal and combined friability of a different coal, Figure 16-18 shows on one plot the equivalent test data for a single sample of Elgin-Butler (Texas) lignite. Note that the cold tumbling shifted the line far less than in the case of the Indian Head lignite (Figure 16-16). Thus the Elgin-Butler is said to have a lower mechanical friability. Note, however, that the Elgin-Butler shows a change in shape of the curve, rather than a vertical shift alone, specifically indicating a

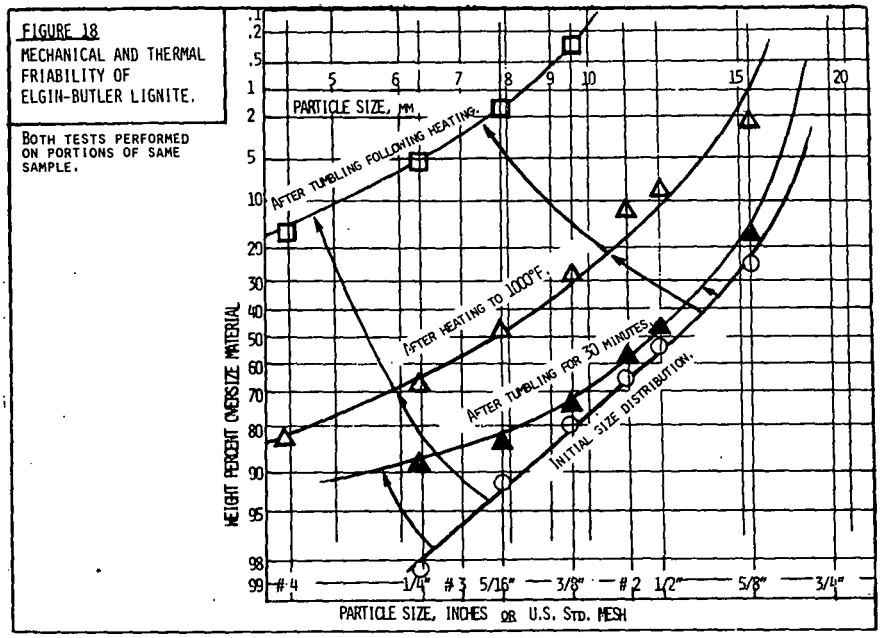

FIGURE 16-18. Mechanical and thermal friability of Elgin-Butler lignite.

preferential generation of relatively fine particles, rather than equally probable fracturing of the largest particles. This provides a measure of deviation from ideal brittle fracture theory, indicating that Elgin-Butler lignite is less homogeneous or less isotropic than the Indian Head lignite, in some way that leaves it more subject to abrasion than to impact or compressive destruction. When heated, however, comparison of thermal and combined friability curves in Figures 16-17 and 16-18 indicates the Elgin-Butler lignite to be significantly more subject to thermal damage than is the Indian Head. Figure 16-19 shows the thermal and combined friabilities of delicate Spring Creek subbituminous coal, which are indistinguishable from those of a lignite. Absaloka subbituminous, on the other hand, in Figure 16-20, shows a barely detectable shift in its size distribution curve with heating alone and a pattern of combined friability (tumbling after heating) that indicates a susceptibility to abrasion more than to impact or compressive failure. In short, the rank of a coal does not necessarily coincide with its mechanical or thermal friability, although higher rank coals tend to be more durable.

The difference in shape of the initial curve in Figure 16-20 merely indicates that the sample was first screened to -20+7 mm, eliminating the fines that define the left end of the previous curves. The shift without distortion during heating, indicated here by narrow ranges rather than single lines, confirms that thermal comminution of Absaloka coal follows ideal, brittle fracture theory. Upon tumbling after heating, however, there is a deviation from ideal behavior, favoring dust-forming abrasion over massive fracturing. A similar thermal friability study (5) of a dozen nonagglomerating, Wyoming bituminous and subbituminous coals also showed an upward shifting of size distribution plots by varying amounts. That study (6) was done entirely with -8 mesh (0.093 inch, 2.3 mm) material. Sieve analyses down to -200 mesh indicated essentially ideal brittle fracture behavior over the entire size spectrum.

Thermal comminution of higher rank coals may be retarded by their agglomerating tendency. This property, or set of related properties, can be

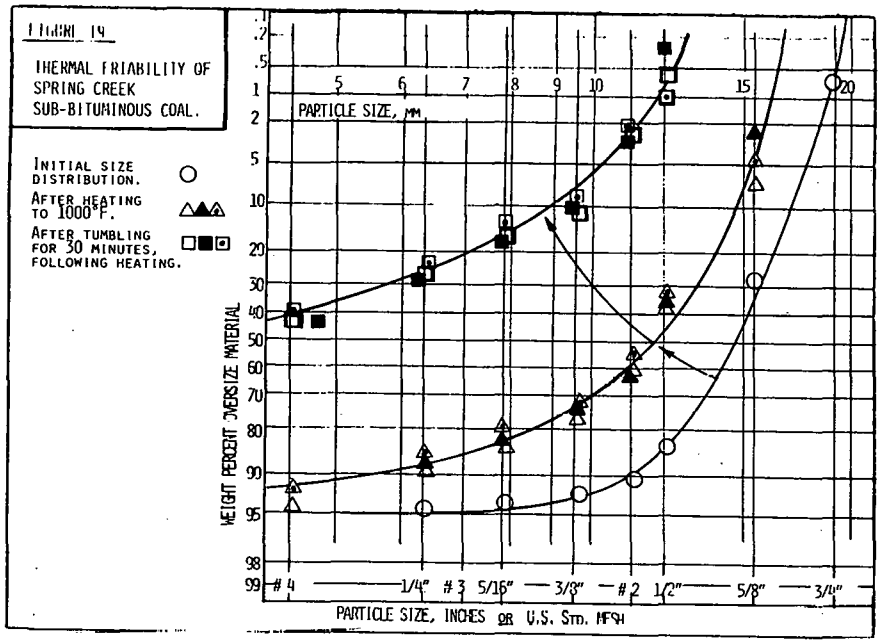

FIGURE 16-19. Thermal friability of Spring Creek subbituminous coal.

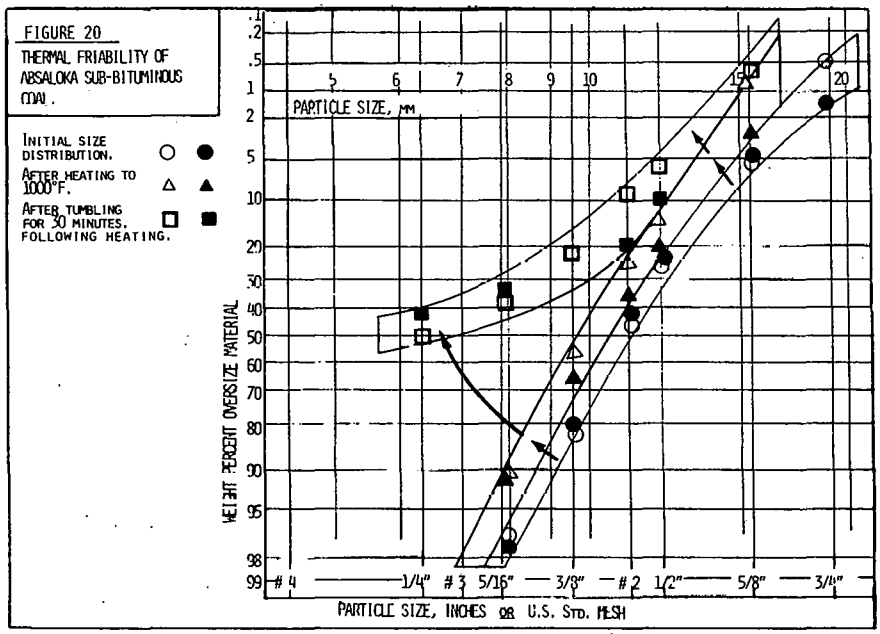

FIGURE 16-20. Thermal friability of Absaloka subbituminous coal.

described in part by their coke shear strength (1) and the Free Swelling Index (ASTM Std. D 720-57). In actual gasifier performance, a Utah (Emery) subbituminous coal with an FSI of only 1.5 to 2.0, on a scale of 0 to 9, tended to agglomerate into large, continuous, stable masses, under operating conditions of the UNDERC gasifier (1), completely offsetting the desirable effects of its relatively low mechanical and thermal friabilities. Friabilitiy tests of this coal are revealing. Figure 16-21 shows simply that the raw, preheating mechanical friability is lower than for the Indian Head, Elgin-Butler and Spring Creek coals. (No such test was done for the Absaloka.) The Emery coal's mildly caking nature shows up in the thermal friability data of Figure 16-22. Here the downward shift of the curve indicates the extent to which agglomeration more than offset comminution, forming larger particles rather than

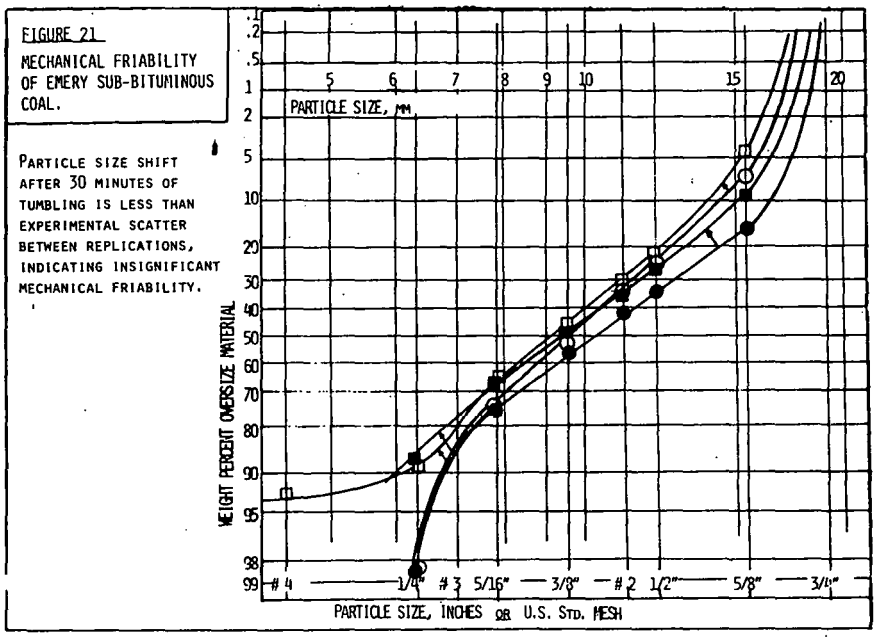

FIGURE 16-21. Mechanical friability of Emery sub-bituminous coal.

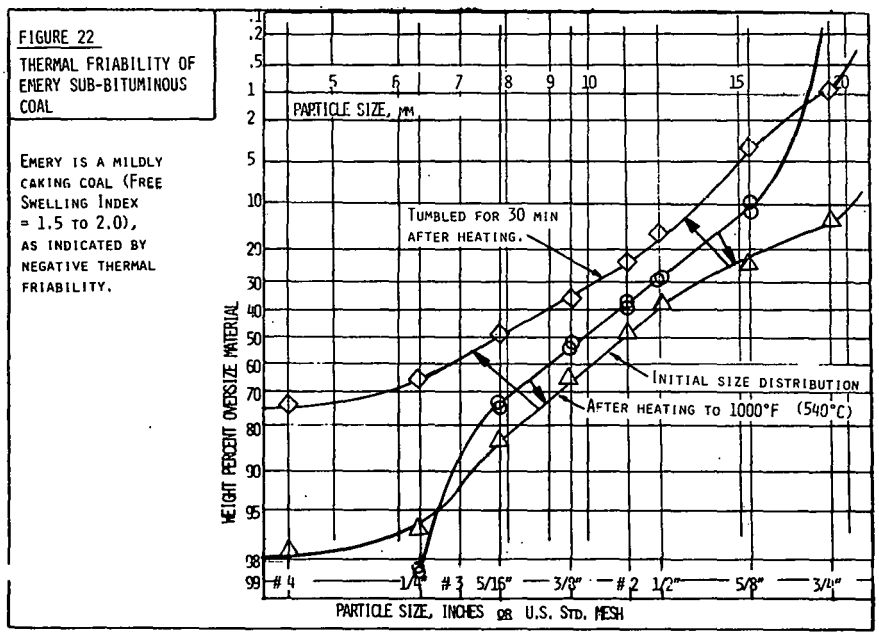

FIGURE 16-22. Thermal friability of Emery sub-bituminous coal.

smaller, though some fine dust was liberated. The larger particles were visible conglomerates, formed of initial particles, slightly smoothed, loosely stuck together. Such a coal, with a free swelling index greater than one, defines the upper limit of nonagglomerating coals, whose thermo-mechanical behavior can be defined by their free-sliding bulk properties. Figure 16-22 suggests, however, that this limit is not abrupt but indicated by a smooth transition, in which the thermal friability, defined here by a shift in the size distribution curve, simply becomes negative. It may be that extending this test to other mildly caking coals may indicate some correlation between the negative mechanical friability and the standard FSI. This defines an unexpected dimension to the project's scope.

Also unexpected was the curve shift during tumbling after devolatilization of the Emery subbituminous coal, also shown on Figure 16-22. It indicates a far more friable material than the raw coal, per Figure 16-21, which is consistant with the embrittled coke of other coals, per Figures 16-18 through 16-20. The fact that the shape of the line is preserved indicates ideal, brittle-fracture behavior, which is intuitively surprising when recalling that the newly formed composite lumps are now held together by internal structures quite dissimilar from the original coal.

It would have been desirable if all the above tests could have been conducted on initial samples of uniform size distributions. However, a conspiracy of seemingly trivial problems in logistics and equipment availability precluded obtaining adequate samples of all coals in repeatable size ranges approaching the 40 pct to 70 pct, -0.75"+0.50" (-19+12.7 mm) normally used for gasifier feed. While the curve shifts of Figures 16 through 22 tell a lot about the mechanical and thermal fracture mechanisms of coal, it was initially intended to compare all coals tested with single numerical data points, by performing all tests on standard -0.75" +0.50" samples, reporting mechanical, thermal and combined friabilities as the fraction reduced to -0.50" (-12.7 mm), for condensed tabulation and comparison. A similar tumbling test of mechanical friability is ASTM Std. D 441-45, which calls for -1.5"+1" sample. The smaller range selected here, -0.75"+0.5", was selected because it is also the feed specification for the UNDERC pilot gasifier. Tumbling was done in a jar mill with baffles identical to that specified by D 441-45. An earlier work (1), comparing Indian Head lignite and Emery subbituminous gasifier feeds by this single point test reports the following:

	Indian Head Lignite	Emery Subbituminous
Mechanical Friability, %	38.7, 37.9	17.2, 19.0
Thermal Friability, %	84.9, 87.0	9.6
Combined (Tumbling after thermal test), %	97.3	62.9

An example of single point characterization of coals with respect to their mechanical friability is given in Figure 16-23, to illustrate its dependence upon yet another structural parameter, the initial dryness. This is not to be confused with the effect of destructive drying at high temperatures, reflected in the combined friability curves of preceding figures. Here the mine-fresh samples of -0.75"+0.50" coal were gently dried at 140°F (60°C) for increasing multiples of roughly 30 minutes, following which the moisture content was determined and correlated with the single point definition of mechanical friability in Figure 16-23. This amounts to another dimension to the plots of mechanical friability in Figures 16-16, 16-18, 16-19, and 16-21. It also tells us that any meaningful comparison of mechanical friability curves for two coals will require that both be mine fresh or at least no drier

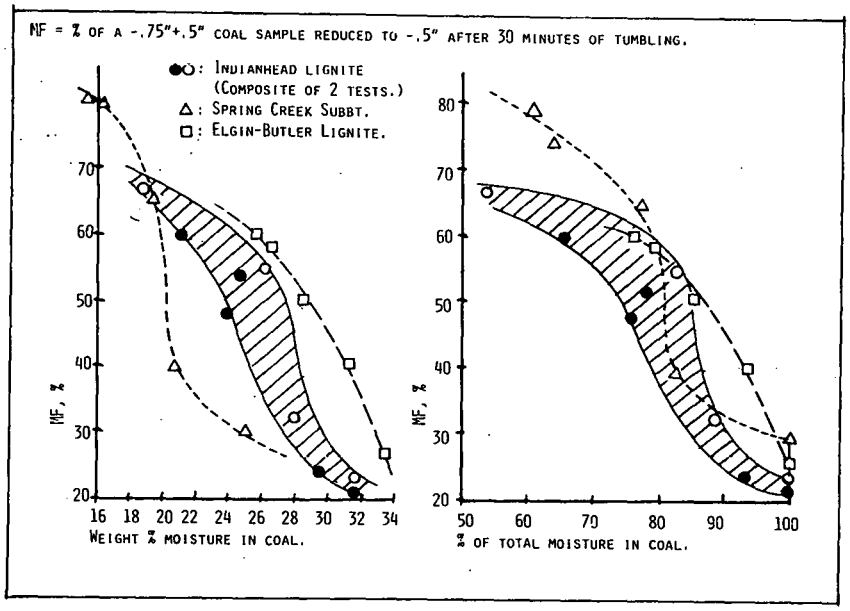

FIGURE 16-23. Effect of dryness on mechanical friability of coals.

than they would be if/when fed into a gasifier. (In nearly all the work reported here, samples were mine fresh and kept in sealed containers until used.) The curves of Figure 16-23 convey more information about the structure of coal and mechanisms of bonding or entrainment of moisture than current theory can explain. The changes in slope, for example, indicate that the first and last water driven off from the Spring Creek and Indian Head samples had less disruptive effect on the particles' mechanical integrity than did the water removed at around 80 pct of the total present.

The Elgin-Butler sample, on the other hand, showed no such behavior. That is not to say, however, that the Elgin-Butler sample could not have had a still higher initial moisture content than the 34 pct determined here, some of which was lost during mining and packaging. Therefore, future measurements like those of Figure 16-23 must include some knowledge of the samples' origin. The Indian Head sample was taken from a railroad car received for gasifier feed, with a minimum of storage between mine and loading, while the Spring Creek subbituminous was collected directly from the mine face by a geological sampling team, expressly for this and other research conducted by the Coal Science Division at UNDERC.

Another important factor in the settling behavior of coal during heating is its volume change. For higher rank coals, a key property is the Free Swelling Index, a rough measure of the amount by which they swell during softening, pyrolysis and/or devolatilization, occurring between about 500° and 1300°F (260° to 700°C) in a neutral atmosphere. It is a good indication of a coal's coking or agglomerating tendency. Lignites and other nonswelling, nonagglomerating coals are arbitrarily assigned an FSI of one. In reality, lignites actually shrink substantially under these conditions, thus defining fractional FSI values. For this study, a quick, simple test was to fill a graduated cylinder with crushed lignite, -2+10 mesh (-10+2mm), settled to maximum compaction by tapping, and note its volume reduction after heating (drying), again settled by tapping. Indian Head lignite consistently showed a shrinkage of 12 pct after a gentle, nondestructive drying at 60°C for seven hours. After an additional, complete drying at 105°C for 16 hours, causing noticeable thermal comminution, the cumulative shrinkage was 20 pct, indicating the loss of further moisture, more tightly bound than that driven off

at 60°C. After heating to 540°C (1000°F), by which temperature most pyrolysis is complete, the total shrinkage was 35 pct. This defines an approximate FSI, perhaps better called the Free Shrinking Index, of 0.65.

The implication of volumetric shrinkage for the data of Figures 16-17 through 16-23 is that observed phenomena are not purely thermal and mechanical comminution, since some part of the size reduction is due to shrinkage of individual particles, in addition to breakage alone. The distinction is more important from an academic than a practical point of view, since the shear strength and permeability are determined by the changes in size distribution, regardless of how they are achieved. Particle shrinkage becomes the property of critical importance, however, in preventing bridging in perhaps the entire upper half of a lignite fuel bed, where drying and pyrolysis are not yet complete. From Figure 16-8, we observed that unless there is some freedom of motion normal to a shear plane, for relief of compressive stresses, the effective shear strength of a compacted solid can reach relatively enormous values, precluding shear failure. This appears to be what occurs in a filled cylinder, where there is no room for expansion in the radial dimension, normal to the vertical shear planes. Returning now to the gasifier failure scenario of Figure 16-15, the high pressure drop through the middle 3.7 feet, and the temperature range at which drying and pyrolysis or devolatilization are complete but gasification ($H_2O + C \rightarrow H_2 + CO$) has not yet started, all suggest a compacted mass of stable char, with no means of internal stress relief short of the reaction zone shifting upward to consume it. Since the pressure drop through this section was greater than its weight, it remained stable only because it had settled into place with a channel of relatively enhanced permeability through it. This condition presumably described the 3.7 feet spanned by the differential pressure taps plus perhaps another foot or two, to some level at which the bed temperature was roughly 1000°F (540°C). Above that level, drying and pyrolysis would still have been in progress, resulting in a constantly shrinking, and thus uncompactable mass, which would explain the low, steady pressure drop. That is, the mass of shrinking coal, not yet char, was continually rearranging itself, allowing the collapse of any local impervious or structurally stable concentrations. Although the high, terminal product gas temperature indicates a channel through this section, the low, stable pressure drop suggests that the channel remained quite generous for the gas flow, due to the freely shifting coal, and probably limited to a location directly above a more constricted channel in more rigidly compacted coke layer beneath it.

Earlier operating data (1), with gas production and steam-oxygen injection rates per vessel cross section of nearly twice those of Figure 16-15 showed a far more violent but similar relation between the two upper zones. The middle or stable coke zone showed violent vertical temperature excursions and pressure drop peaks, corresponding to periods of roughly an hour during which stable bridges, partly supported by the excessive pressure drop, would eventually collapse only when the oxidation-combustion zone climbed the column to burn them out from below, indicated by temperatures of 2000°F (1100°C) at the seven foot level. The upper zone, meanwhile, consistently showed high temperature peaks that were far less excessive and started much later, though the combined pattern resulted ultimately in the same shutdown scenario. The UNDERC gasifier is a thirty-year old relic of preliminary phases in the development of slagging, fixed bed gasification. It is now apparent that the ratio of height to diameter is far greater than necessary, and that if it were

four or five feet shorter, the superfluous middle section of stable, compactable char would not exist. A fuel bed of optimal or minimal depth, on the other hand, is more prone to burn-throughs with less severe upsets in the height of the combustion-gasification zone.

CONCLUSIONS AND RECOMMENDATIONS

The scope of this work to date has not permitted orderly experimental planning to include the full range of mechanical properties of crushed coal. It does reveal, however, the relative importance of the various, measurable properties, some of which were "discovered" during the work reported. Most importantly, this work has established which of several properties of nonagglomerating coals are the major contributors to limitations of design capacity of gasifiers and other packed column, thermal processes. By demonstrating methods for cheap, simple determination of these properties, this work provides clear guidance for continued, orderly research in the area.

CONCLUSIONS

* Mechanical behavior of packed columns of coal during thermal processing is so strongly dependent on major changes in its structural properties that mathematical models of such processes based on the ideal, slug flow assumption of constant and isotropic bulk properties are essentially useless.

* Accepted feed size specifications for gasifier operation are conservative with respect to tolerable levels of undersize material. Gasifiers can be operated with finer feeds than normally specified, especially for nonfriable coals, if their thermal and mechanical friabilities and volumetric shrinkage are predictable.

* The pressure drop through a bed of material with a broad range of particle sizes is dominated by the finer particles present, to a degree well beyond their weight fraction of the mixture.

* The relationship between free sliding shear strength and normal or perpendicular compressive stresses for coarsely crushed coal is similar in form to established theory for finer materials. The shear strength of mixtures is dominated by the finer components present.

* The primary effect of particle size on the settling rate of packed solids in gas-solid contact operations is on permeability rather than on shear strength, the latter becoming a crucial factor only when pressure drop through a packed bed approaches the weight of the solids, which situation exceeds normal, stable or recommended design practice. Furthermore, the contribution of shear strength to the stability of an impacted zone is inversely proportional to the vessel's diameter.

* The relative suitability of nonagglomerating coals as gasifier feeds is dominated by their thermal and mechanical friabilities. Simple tests can predict and compare the shift in particle size for different coals subjected to the same degree of thermal and mechanical abuse. The shape of the resulting size distribution curves indicates which coals are most subject to

thermal or mechanical comminution, and whether they are mechanically more subject to fracture by impact and compression or by abrasion. Correlations with the rank of coal, between lignite and subbituminous, are not consistent.

* Mechanical friability of low-rank coal increases sharply with the amount of drying prior to tumbling. The rate of change of mechanical friability with dryness shows striking changes in slope, believed to indicate that the removal of water bound to the coal structure in different ways has significantly different effects on its structural integrity.

* Lignite particles shrink during drying, having an effect on size distribution in addition to that caused by fracturing alone. The combined bulk volume shrinkage of lignites, through drying and pyrolysis, can reach 35 pct. This shrinkage is an important factor in providing compressive stress relief normal to planes of shear failure through compacted zones.

RECOMMENDATIONS

While the work reported above is continuing with a minimal level of effort, an expanded and more orderly program could provide a valuable compendium of data, completely characterizing low-rank coals with respect to their thermo-structural behavior. Such a program will include the following:

* Coarse samples (say +2' or 50 mm) should be crushed and sieved to a standard size distribution curve for quantitative comparison of thermal and mechanical friability data.

* Mechanical friability, weight loss and volume shrinkage should be correlated for each coal through temperature ranges to 1000°F (550°C), to cover ranges of drying and devolatization.

* Particle shrinkage should be measured by liquid displacement, to separate this result from the bulk volume shrinkage associated with tighter compaction following comminution.

* Further permeability tests should be run, covering different blends of crushed coal of the same, narrow size ranges, to develop reliable predictive equations by which pressure drop can be predicted from sieve analyses alone.

* Recognizing that laboratory permeability measurements are based on compacted or "fixed" beds, work recommended above, and that reported here should be replicated in a laboratory device where the solids are continuously withdrawn from the bottom of a column, more nearly simulating the actual behavior of a gasifier fuel bed.

16.2.2 Pore Size Distribution

In pursuit of Objective 2, above, work to date in observing micro-pore size distribution by small angle x-ray scattering is summarized by the following contribution by Dr. Harold Bale of the UND Physics Department.

INTRODUCTION

Our recent experimental work was carried out with a Bonse Hart small angle diffractometer. This unit which we have borrowed from Amoco Research Center at Naperville, Illinois, makes it possible to measure the scattering into one-tenth of the smallest angle that we had previously examined with our Beeman collimation system. Scattering measurements made with the Bonse Hart have been performed on most of the lignite samples that we previously studied with our Beeman system. We have combined the two sets of data for each sample to obtain composite scattering curves extending from 0.1 to 100 milliradians. The corresponding range in h is from 0.0004 Å^{-1} to 0.400 Å^{-1}, $h = (4\pi \sin \theta/2)/\lambda$. The most striking feature of these composite curves is that on a log-log graph of intensity versus angle, the curves (corrected for atomic scattering) have nearly a constant slope over the entire angular region. The significance of this behavior will be discussed in the next section.

We have also analyzed our composite curves using the pore model that we previously applied to our Beeman measurements.

SAMPLE MATERIALS

Sample 1. Beulah lignite obtained by standard sampling techniques was ground sufficiently so that the entire sample passed through a 200 mesh screen. This sample was prepared by the UND Energy Research Center and has their designation, "Beulah CPC."

Sample 2. This sample is a size fraction of sample 1 retained on a 325 mesh screen.

Sample 3. U.S. Bureau of Standards subbituminous powder sample #1635.

THE ANALYSIS

Earlier we adopted a pore model for data analysis purposes similar to the one used by Schmidt (ACS Symposium Series 169, 1981, 1-22) which assumes that the coal contains three distinct classes of pores; macropores, transition pores and micropores. We have found that this model can still be used to analyze the composite scattering curves if two modifications are made. 1) Since the scattering curves now include the very small angle region where the scattering curve may be affected by the size of the macropores, the macropore term in the model equation was changed to a Lorentzian form similar to the transition and micropore terms. The fit of the model is improved if the inverse 4th power term is retained. We labeled the term, S^1/h^4, where S^1 is the surface area of very large components such as, ash inclusions, powder particles and very large pores. The model then has the form,

$$I(h) = I_o \left(\frac{S^1}{h^4} + \frac{S_{ma}}{(h^2+g^2)^2} + \frac{S_{tr}}{(h^2+g_2)^2} + \frac{S_{mi}}{(h^2+g^2)^2} + C \right)$$

S_{ma}, S_{tr}, and S_{mi} are respectively the specific surfaces for the micropores. Also the micropores of the parameters, g_1, g_2, and g_3, are characteristic lengths for the three classes of pores and C is a constant term which accounts for the atomic scattering. The fit of this model to an experimental curve then becomes an eight parameter least-square fit. Figures 16-24, 16-25, and 16-26 show that the model (solid line) fits the slit corrected experimental points quite well over the entire curve. In the discussion that follows this model will be referred to as, "model A."

It was pointed out above that if a constant term is subtracted to account for the atomic scattering, the corrected scattering curve is nearby a straight line in a log-log graph. Consequently we have fit the curves to a three parameter equation $I(h) = A\ h^{-\alpha} + C$. Figures 16-27, 16-28, 16-29 show this model (solid lines) fit to the experimental points for the three samples. The fit is best for Figure 16-28, the sample 2 scattering curve, and poorest for Figure 16-29, the sample 3 scattering curve. In the discussion that follows this 3 parameter model will be referred to as, "model B."

PORE DIAMETER DISTRIBUTION

We have calculated a diameter distribution for both of our models. The results of these calculations are shown in Figure 16-30 for samples 1 and 2. For both samples, the two distributions are in close agreement. The distributions are unusual in the sense that they have neither an upper or lower bound for particle size and have no extremum. However, the characteristics of the observed scattering curves require that the distribution be unbounded or that the bounds be undetermined. Despite the fact that the basic premise of model A is the existence of three classes of pores, we see that the pore size distribution for this model shows no indication of any maxima. The uniqueness of the three types of pores is therefore questionable. However, this problem does not invalidate the model as a means of determining the specific surface for coal samples. Likewise values for the characteristic lengths can be determined although their exact measuring suffers from the same uncertainty as the distinctness of the three classes of pores.

THERMAL TREATMENT EXPERIMENTS

Figure 16-31 shows our composite scattering curves for the unheated lignite and for the sample heated at 550°C for 4 hours. The graph clearly shows that the primary effect of the heat treatment is to enhance the scattering at the largest angles. Qualitatively, this increased scattering at the larger angles can be attributed to the creation of very small pores following the escape of volatile matter upon heating. The fact that there is little thermal change in the scattering over the smaller angles suggests that the coal matrix has remained more or less intact.

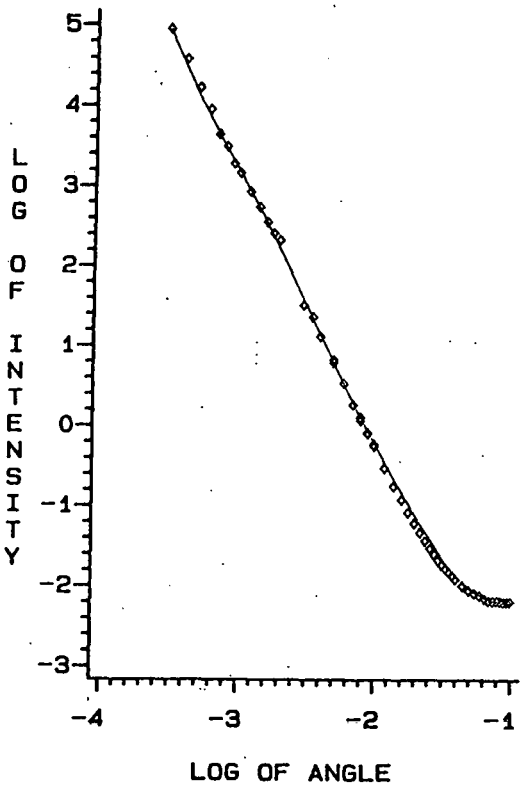

FIGURE 16-24. Sample 1 composite data points fit to model A (solid line).

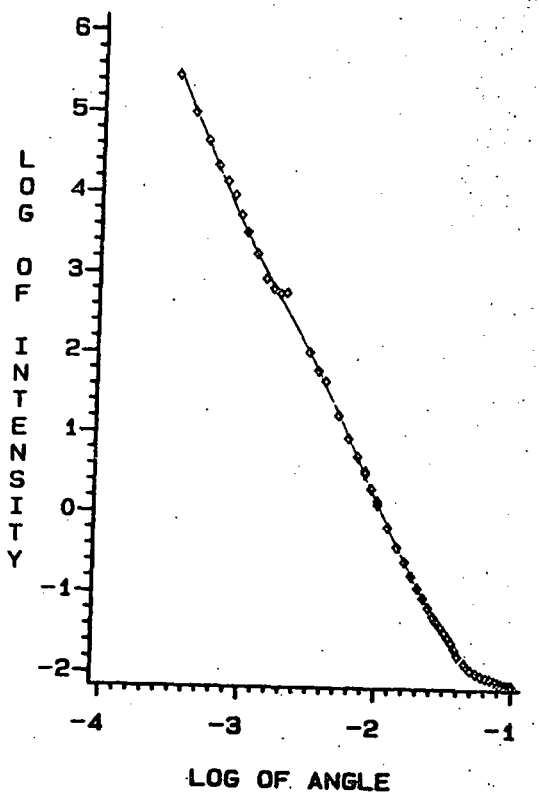

FIGURE 16-25. Sample 2 composite data points fit to model A (solid line).

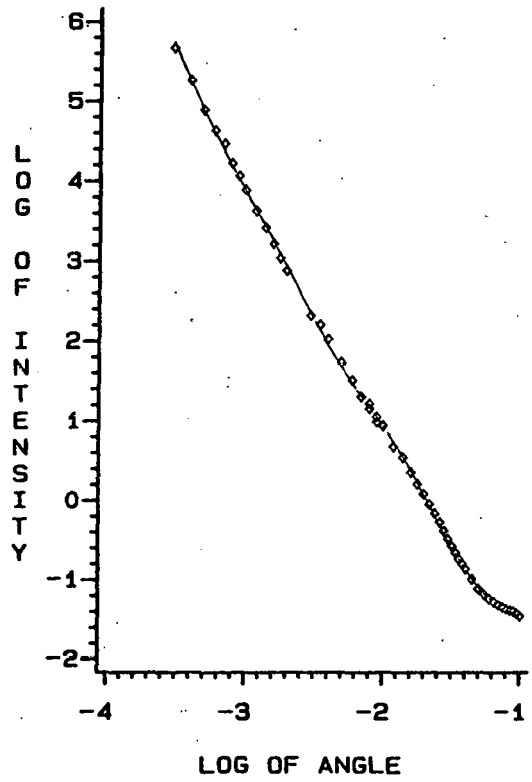

FIGURE 16-26. Sample 3 composite data points fit to model A (solid line).

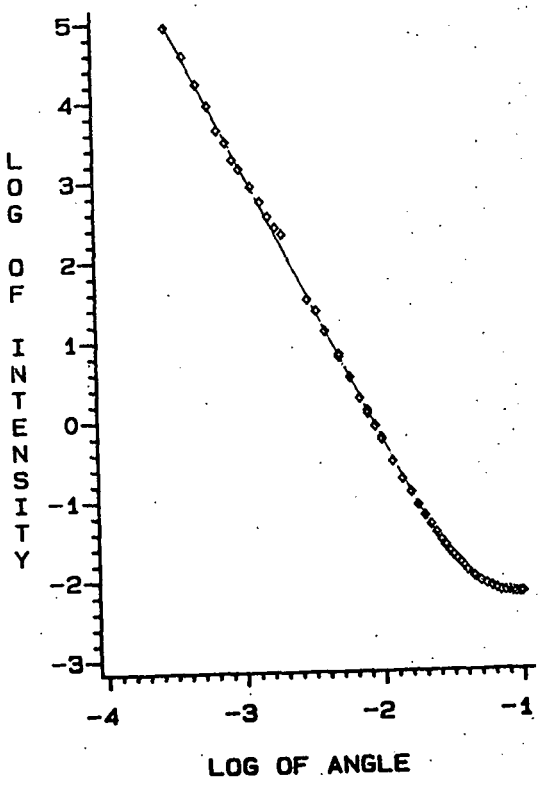

FIGURE 27. Sample 1 composite data points fit to model B (solid line).

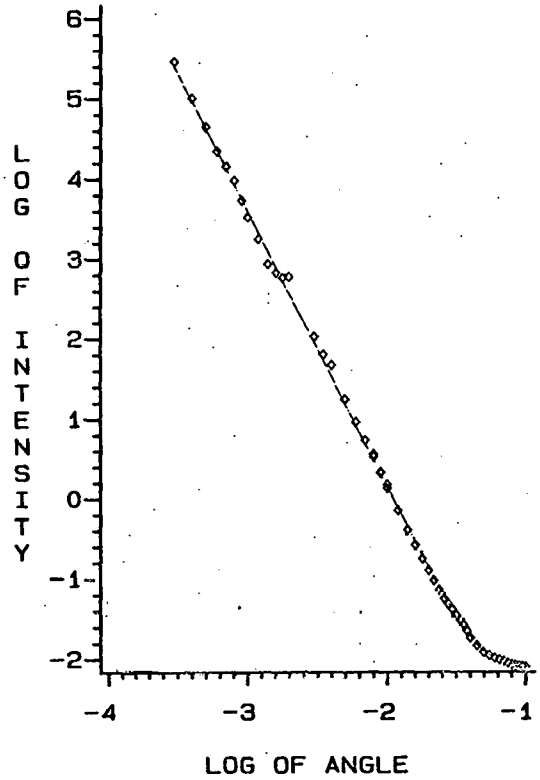

FIGURE 16-28. Sample 2 composite data points fit to model B (solid line).

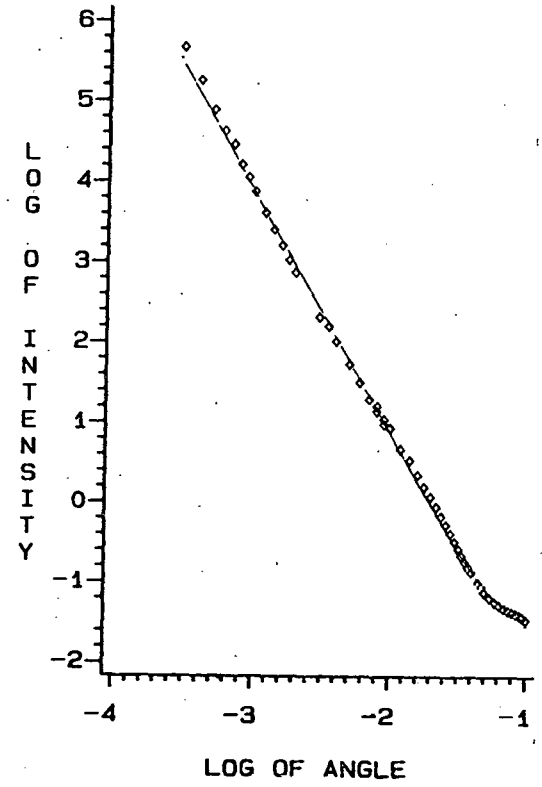

FIGURE 16-29. Sample 3 composite data points fit to model B (solid line).

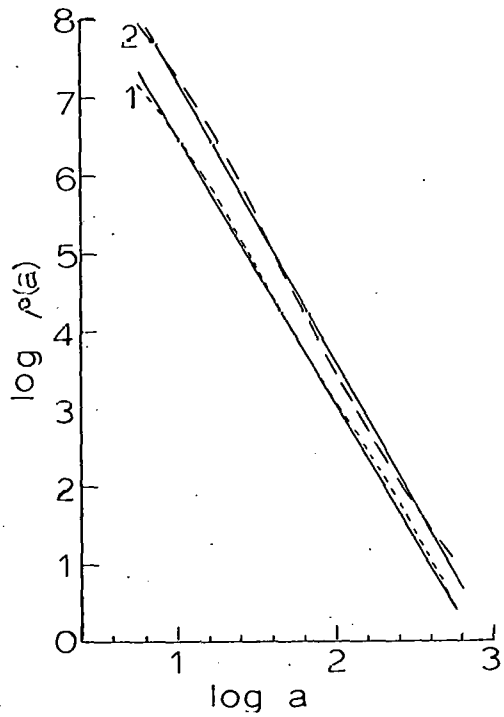

FIGURE 16-30. Pore diameter distribution function, p(2) versus particle diameter in Å. Curve 1 is for sample 1 and curve 2 is for sample 2. The dashed lines are based on model A and the solid lines are based on model B. The two curves have been displaced for clarity.

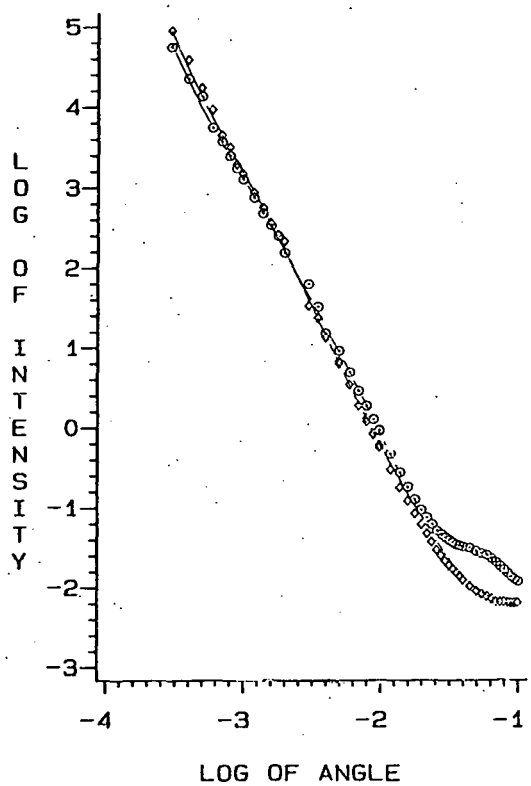

FIGURE 16-31. Sample 2 composite data points ◇ unheated sample, o sample heated 4 hours at 550°C in argon atmosphere. The data points are fit to model A (solid line).

16.3 REFERENCES

1. Hauserman, W. B. and Willson, W. G. "Mechanical Problems in the Design of a Fixed-Bed Slagging Gasifier." ASME, Energy-Sources Technology & Exhibit, Houston Texas January 30-February 2, 1983.

2. Hauserman, W. B. and Willson, W. G. "Conclusions on Slagging, Fixed-Bed Gasification of Lignite." UND 1983 Lignite Symposium, Grand Forks, North Dakota, May 18-19, 1983.

3. Jenike, A. J., Johanson, J. R. and Carson, J. W., "Bin Loads--Part 2: Concepts," ASME Transactions, 1972 (Paper No. 72-MH-1).

4. Jenike, A. J. and Johanson, J. R., "Storage and Flow of Solids," Bulletin No. 123 of the University of Utah Engineering Experiment Station.

5. Landers, W. S., et al, U.S. Bureau of Mines, "Carbonizing Properties of Wyoming Coals." RI5731, 1961.

17. - SUPERCRITICAL SOLVENT EXTRACTION

Project No: 7306 B&R No: AA2530100

Submitted by: H.H. Schobert, Manager, Coal Science Division

Prepared by: J. Dollimore, Research Supervisor, Coal Reactivity and
M.L. Swanson, Research Engineer, Supercritical Solvent Extraction Project

Assigned UNDERC Personnel: J. Dollimore
M.L. Swanson
J.W. Diehl
E.S. Olson

17.1 GOALS AND OBJECTIVES

The two main goals of the Supercritical Solvent Extraction project (SCSE) at the University of North Dakota Energy Research Center (UNDERC) are to:

1. Use SCSE as a means for determining the composition of various molecular fractions present in low-rank coals.

2. Evaluate the use of the SCSE process as a method of obtaining liquid fuels and chemical feedstocks from coal.

These two major areas of research have the following objectives for fiscal year 1983:

1. Determine the product yields and compositions of the SCSE process as functions of the solvent properties (i.e. T_c, P_c, ρc, and solubility parameters), operating conditions, solvent flow rate, and the residence time of the coal.

2. Characterize the extraction products by the following analytical methods: ^1H NMR, IR, and GC-MS on the extract, C/H ratio on the extract and residue, thermogravimetric analyses on the residue, and GC on the product gas.

3. Determine the effects of adding reducing gases to the supercritical solvent or using a solvent with H-donor capabilities.

4. Conduct basic studies on the thermodynamic properties and fluid behavior in the supercritical regime particularly with respect to selected solvent mixtures and recycled solvents.

5. Perform a limited number of autoclave or tubing bomb tests using the optimum extraction conditions and solvents determined previously.

Objectives for the quarterly period (July through September 1983) were as follows:

1. To continue to perform several series of experiments using various solvents at certain selected conditions to determine the effects of different operating conditions on product yields and composition.

2. Characterize the SCSE products using ^1H, NMR, IR, GC-MS, C/H ratios on the extract, C/H ratio and thermogravimetric analyses on the residue and the GC analyses on the product gas.

17.2 ACCOMPLISHMENTS

Experiments on supercritical solvent extraction by benzene, toluene, and water on Indian Head lignite were reported in the previous quarter (April-June 1983). Water extraction was a massive 50 pct conversion compared to 3.8 to 20 pct for the other solvents. It was therefore decided to concentrate on the water extraction. This quarterly report is therefore concerned with supercritical water solvent extraction in relation to objective 1. This work also leads to interesting structural considerations about lignite decomposition, which will continue to be developed in future reports.

Address to objective 2 has been less satisfactory. All extracts presented for analysis produce problems by being rather heavy materials that are only partially soluble. Powdered coal persists in the extracts, although this may be because of the form of the decomposition of the starting coal. These and related problems may result in a different approach to the product characterization being developed in the future.

Twenty-three runs using supercritical water as the solvent were performed during the quarter. Operating conditions, solvent density and percentage conversions are summarized in Table 17-1. Twelve runs were made to determine the effects of varying the coal residence time and the solvent flow rate on the product yields. Figure 17-1 is a plot of the coal residence time for water extraction versus the percentage conversion for two different flow rates. From this figure, it can be seen that approximately 39 pct of the Indian Head lignite is extracted in 15 minutes. After 15 minutes, the percentage conversions showed a steady increase of approximately 1.8 pct per hour of coal residence time. Coal residence time had no effect on the percentage yield of product gas.

It appears that increasing the solvent flow rate decreases the percentage conversions especially at low residence time as shown in Figure 17-1. This suggests that the organic constituents are not reaching their equilibrium concentration in the solvent. Solvent flow rate also had no effect on the percentage yield of product gas.

The effects of varying the operating temperature and pressure were investigated by performing seven runs at 380° or 440°C (1.01 or 1.10 T_R) and 3265, 4011, or 4815 psia (1.02, 1.25, or 1.5 P_R) with a 4-hour residence time. Results of these runs are also summarized in Table 17-1. Figure 17-2 is a plot of the reduced pressure P_R versus the percentage conversion at both reduced temperatures.

This figure shows a slight increase in the percentage conversions with an increase in the operating temperature. The percentage conversion showed a sig-

TABLE 17-1

RUN CONDITIONS, SOLVENT DENSITY, AND PERCENTAGE CONVERSION
FOR SUPERCRITICAL WATER EXTRACTIONS

Run No.	Operating Temp., (°C)	Operating Press., (psia)	Residence Time, hrs	Solvent Flow Rate @ RT (cc/hr)	Solvent Density (∂/cc)	Conversion pct, (maf)	Yield gas pct, (maf)
17	380	3265	5.75	120	0.18	47.0	ND**
18	380	3265	5.5	120	.18	33.9++	11.9
19	380	3265*	5.5	120	.18	43.5	ND
20	380	3265	4.0	120	.18	49.4	10.4
21	380	3265	4.75	120	.18	45.4	11.9
22	380	3265	5.0	120	.18	48.1	6.6**
23	380	3265	4.0	120	.18	43.3	10.9
24	380	3265	2.0	120	.18	41.3	11.6
25	380	3265	1.0	120	.18	42.1	13.1
26	380	3265	0.5	120	.18	37.6	13.1
27	380	3265	1.0	240	.18	34.9	11.1
28	380	4011	4.0	120	.51	50.6	12.6
29	380	4815	4.0	120	.56	46.9+	10.4
30	440	4011	4.0	120	.14	53.5	22.2
31	380	3265	6.0	120	.18	49.8	11.9
32	380	4815	4.0	120	.56	50.3	12.1
33	440	3265	4.0	120	.096	43.3	19.3
34	440	4011	4.0	120	.14	52.9	17.0
35	440	4815	4.0	120	.20	54.4	16.3
36	380	3265	3.5	200	.18	49.0	12.5
37	380	3265	3.0	120	.18	48.2	5.8**
38	380	3265	1.0	120	.18	43.4	ND**
39	380	3265	0.25	120	.18	38.4	

*Pressure fluctuated substantially during run.
**Lost some product gas.
+Used 10 micron sintered metal disc in extraction vessel instead of 65 micron discs used in other runs.
++Appeared to some contamination in residue causing low pct conversion.

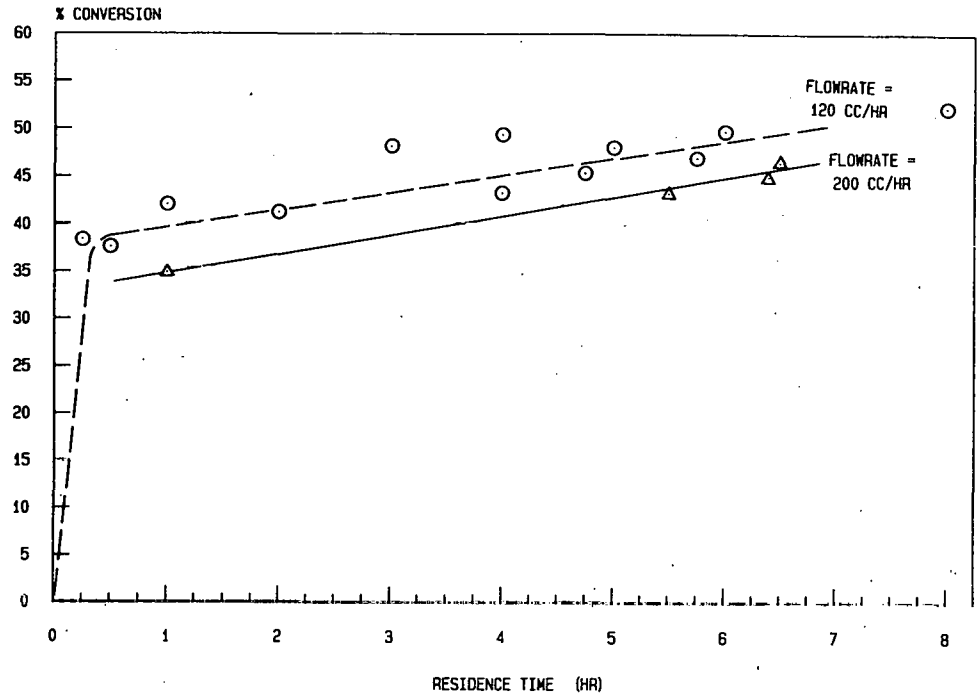

FIGURE 17-1. Supercritical H_2O extraction of Indian Head lignite at 380°C and 3265 psia.

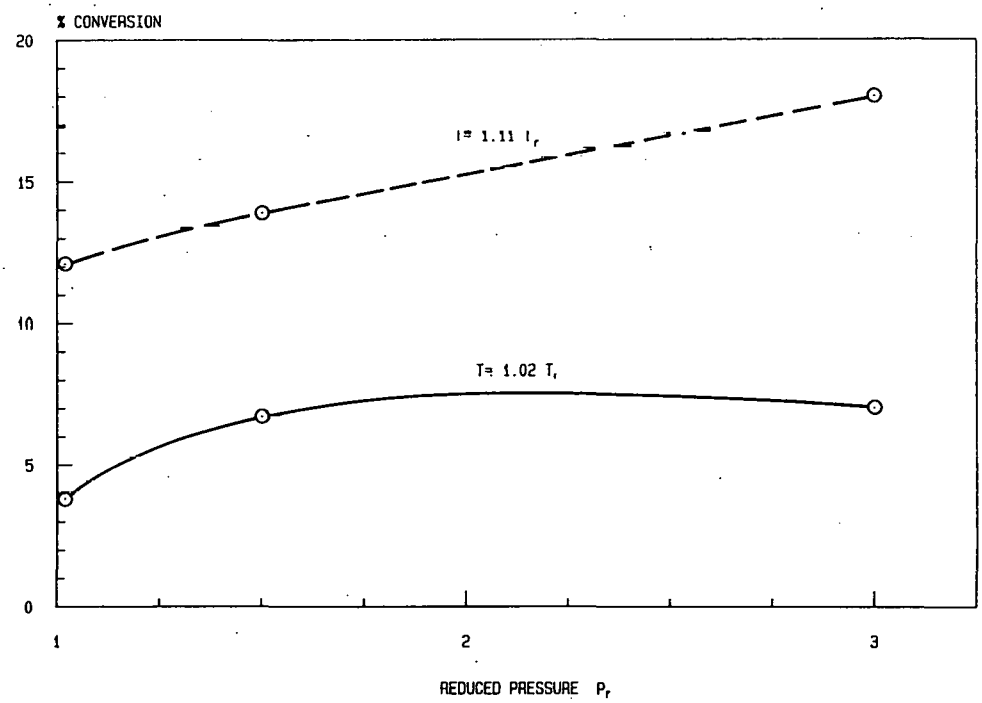

FIGURE 17-2. Supercritical H_2O extraction of Indian Head lignite at 4 hours residence time and 120 cc/hr of room temperature solvent.

nificant increase with an increase in the operating pressure up to 4000 psia. Above 4000 psia, there appeared to be no significant effect on the percentage conversions. Figure 17-3 is a plot of the reduced density of water versus reduced pressure at various reduced temperatures. This figure shows the effect operating temperature and pressure have on the solvent density. It can be seen from this figure that the significant increase in the percentage conversion with an increase in pressure was due to increases in the solvent density. The increase in the percentage conversion with the increase in the operating temperature was due to the increased thermal decomposition of the lignite at higher temperatures. The increase in product gas yields with the increase in operating temperature also indicated that significantly more thermal decomposition was occurring. There appeared to be no relationship between the percentage yield of product gas and the operating pressure.

Figure 17-4 is a plot of the solvent density at operating condition versus the percentage conversion. This figure shows that for increasing temperatures the percentage conversion reaches a maximum at lower solvent densities. This agrees with results obtained by Jezko et al. (1) using toluene to extract South African coals.

Analysis of the solvent recovered after supercritical extraction shows that methanol, acetone, phenol, o-cresol and m,p-cresols are present. Table 17-2 summarizes the percentage yields of all the identified organic constituents. It appears that residence time and operating temperature had no effect on the percentage yields. It appears that increasing the pressure caused an increase in the percentage yield of the organic constituents.

TABLE 17-2

RUN CONDITIONS AND PERCENTAGE YIELDS OF IDENTIFIED ORGANIC CONSTITUENTS IN RECOVERED WATER SOLVENT

Run No.:	20	21	24	28	29	30	37
Operating Temp., °C	380	380	380	380	380	440	380
Operating Press., psia	3265	3265	3265	4011	4815	4011	3265
Residence time, hrs	4.0	4.75	2.0	4.0	4.0	4.0	3.0
Yield, %:							
MeOH	.93	.77	ND	ND	.84	.51	.80
Acetone	.92	.84	ND	ND	.80	.68	.91
2-Butanane	.20	.20	ND	ND	NF	.14	NF
Phenol	ND	ND	.40	.49	.68	.42	.63
o-Cresol	ND	ND	.07	.16	.25	.17	.17
m,p-Cresol	ND	ND	.18	.25	.34	.25	.17
$m/^2$ K	ND	ND					.23

ND = Not Determined
NF = Not Found

Table 17-3 shows the CHN analysis for the original Indian Head lignite and supercritically extracted residue and the resultant extract. From the CHN analysis, it can be seen that the hydrogen-rich portion of the lignite is extracted while the hydrogen-lean portion of the lignite remains in the residue. It can also be seen that the extract is lower in ash than the original coal.

TABLE 17-3

CHN RATIOS FOR ORIGINAL LIGNITE AND SUPERCRITICAL H_2O EXTRACTS AND RESIDUES (DRY BASIS)

	C	H	N	Ash
Individual lignite	67.31	3.93	1.18	6.74
SCSE 20 residue	75.15	3.51	1.20	10.0
SCSE 20 extract	64.54	6.88	0.80	2.5
SCSE 21 residue	73.25	3.39	1.10	10.1
SCSE 21 extract	69.32	6.16	1.0	2.4

A single point nitrogen surface adsorption system was used to determine the effect of supercritical extraction on the initial lignite structure. The surface areas for the residues ranged from 13 to 17 m^2/g while an unstable result was obtained for the original sample. This unstable result was possibly due to activated diffusion into the "ink bottle" pores present in the unreacted coal. This result leaves a question. Does the water extraction of tars leave behind a psuedomorph crystalline structure related to the original Indian Head lignite? The alternative would be a broken down particulate residue, with perhaps some sub-micron coal particles escaping into the extracted resins.

17.3 REFERENCES

1. Jezko, J., P. Gray, and J.R. Kershaw. The Effect of Solvent Properties on the Supercritical Gas Extraction of Coal. Fuel Processing Technology, May 1982, pp. 229-239.

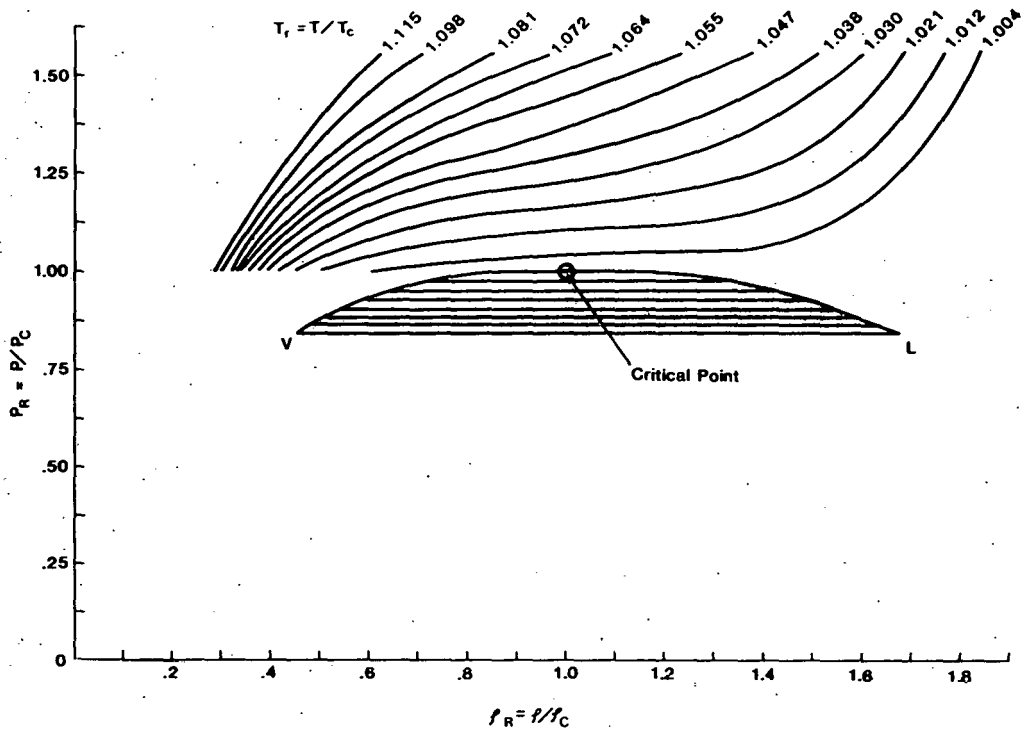

FIGURE 17-3. Plot of reduced density of H_2O versus reduced pressure at various reduced temperatures.

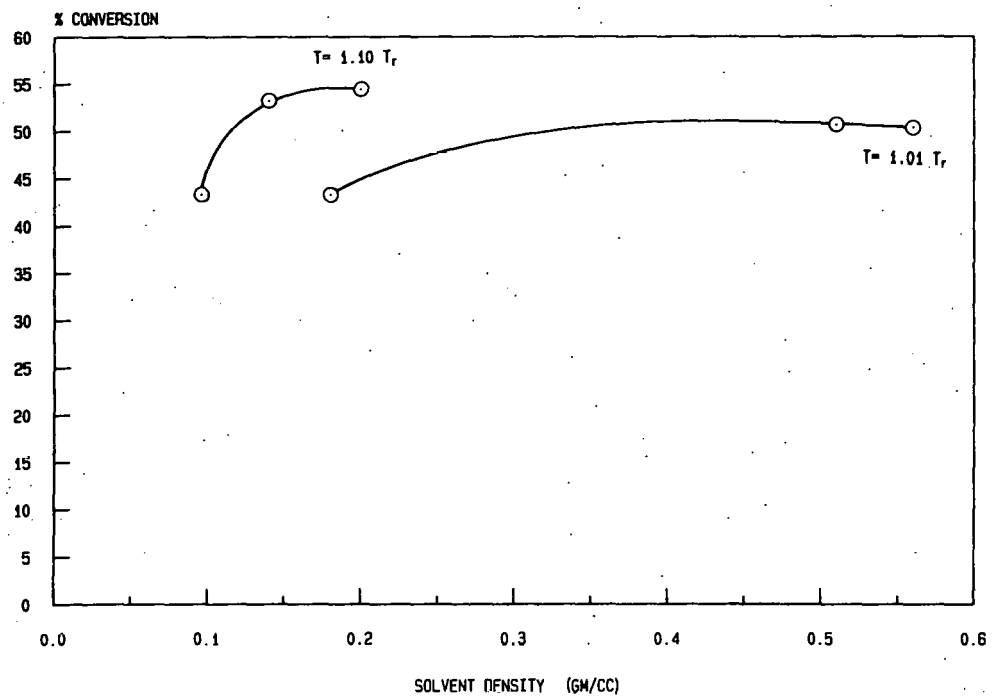

FIGURE 17-4. Plot of solvent density versus pct conversion at T^2 1.01 and 1.10 T_R.

18. - PYROLYSIS AND DEVOLATILIZATION

Project No.: 7307 B&R No.: AA8545050

Submitted by: H.H. Schobert, Manager, Coal Science Division

Prepared by: J. Dollimore, Research Supervisor, Coal Reactivity

Assigned UNDERC Personnel: G.M. Schelkoph
J.P. Hurley

Assigned AWU Personnel: R. Hefta

18.1 GOALS AND OBJECTIVES

The primary goal of the Pyrolysis and Devolatilization project is to determine the product compositions, mechanisms, kinetics and thermodynamics of the pyrolysis or devolatilization of low-rank coals under heating rates, particle sizes and atmospheres typical of low-rank coal processing. A second goal of this project is to use the pyrolysis experiments as the basis of an understanding of reactivity and effluent production from fixed-bed gasification.

The objectives of the project during this reporting period were to:

1. Continue preliminary experiments in thermal analysis equipment and the small pyrolysis reactors.

2. Continue construction, design and installation of a large scale (1-lb sample) thermogravimetric analyzer.

18.2 ACCOMPLISHMENTS

18.2.1 Small Scale Pyrolysis Experiments

Small scale (30-60 gm) pyrolysis experiments were performed on Indian Head lignite. At present not all the supporting analytical work is complete. The effects of particle size, moisture content, heating rate and nitrogen flow rate were considered. The reactor was a steel tube which contained a porous plug of lignite. Various traps were used to condense and collect reaction products for analysis. The optimum hot zone of the tube was located by an internal thermocouple. In more recent experiments a second thermocouple was located on the outside of the tube.

The conditions of the experiment are not entirely obvious, as shown by Figure 18-1 which is the temperature rise of the empty tube. Figure 18-2 shows the pyrolysis profile of Indian Head for 1/2 inch size, 8 mesh, and 8 mesh freeze-dried. Figure 18-3 shows a comparison of Run 3. The coincidence of T_i (Internal) for tests with 1/2 inch size lignite and a blank run with no

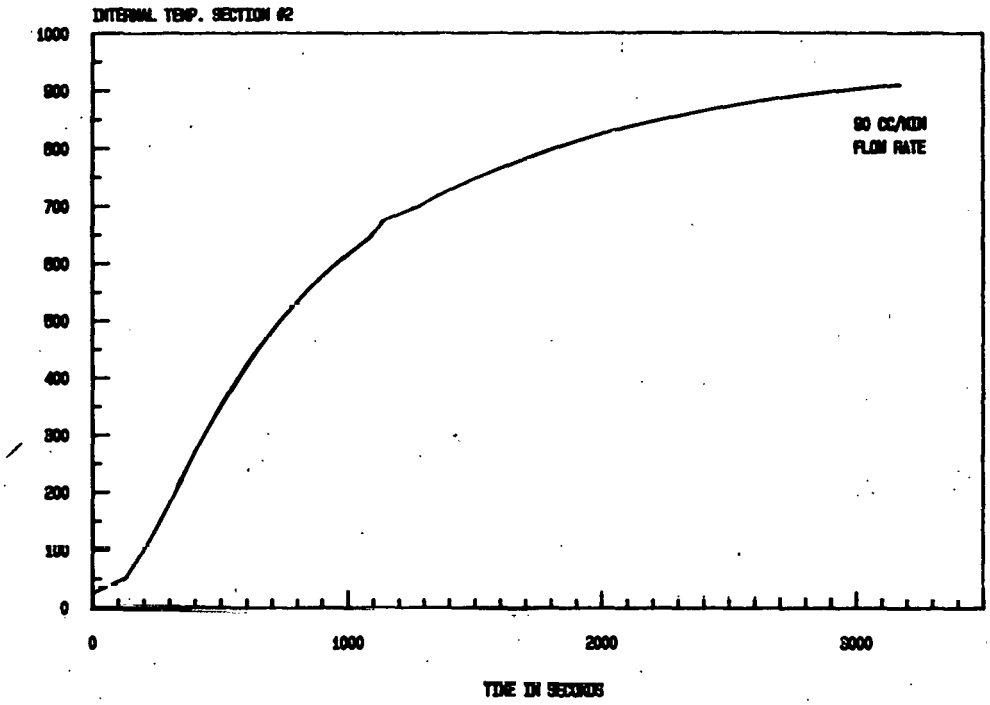

FIGURE 18-1. Heat rates of Spr (furnace start-up).

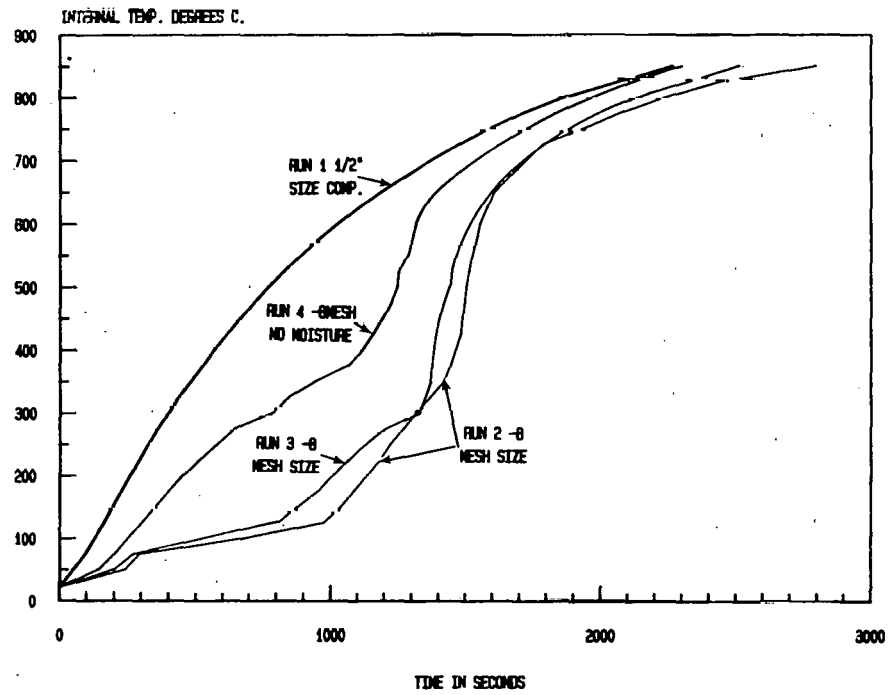

FIGURE 18-2. Pyrolysis profile Indian Head.

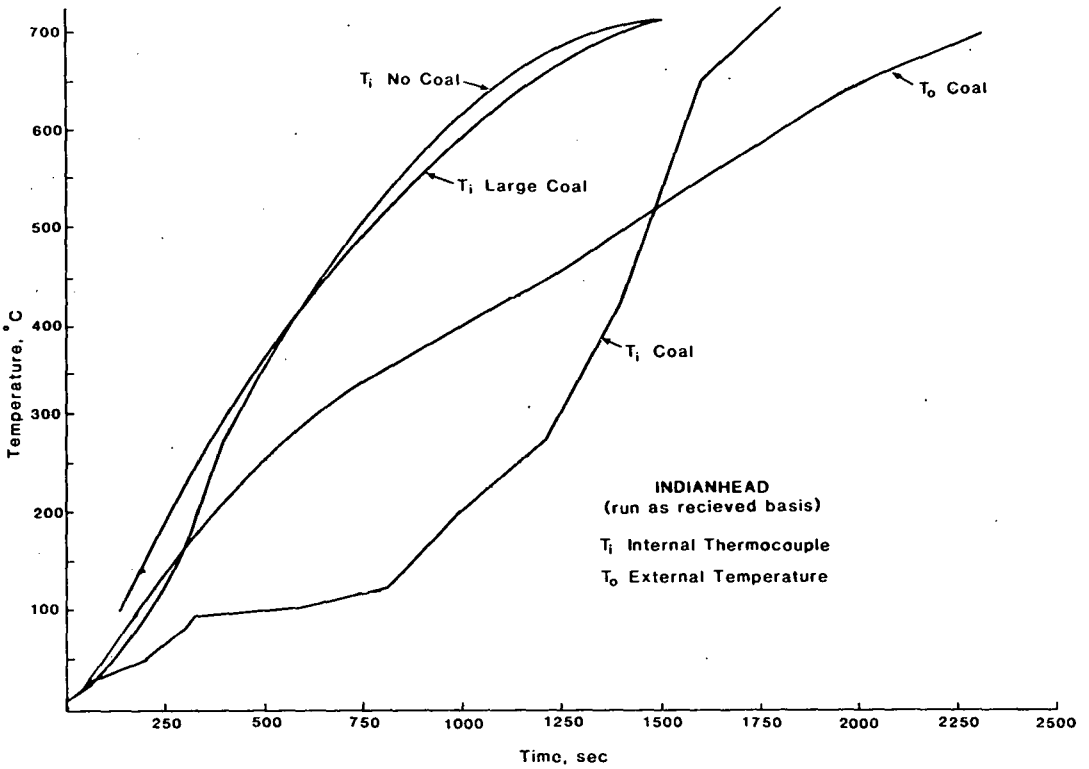

FIGURE 18-3. Internal Ti and external temperature To for Indian Head pyrolysis.

coal suggests that no real conducting path existed to the thermocouple, which behaves as if in a radiation enclosure. The temperature of the lignite is therefore unknown and heat conduction from lignite to thermocouple may not occur. Heat transfer between lignite and thermocouple appears to occur for the 8 mesh samples. The moisture content of the lignite can hold down the lignite temperature to around 130°C for as long as 15 minutes (depending on the mass of sample), by which time the furnace should have reached a temperature above 600°C. The resultant temperature exposure of the lignite may then become rather complex. Figure 18-3 shows the external temperature. Figure 18-2 shows that extensive freeze-drying can remove a large amount of the water from Indian Head. Figure 18-4 shows some results for Beulah high-sodium lignite, where the effect of the water content was quite different. The steel pyrolysis tube appears to act like a DTA system where the endothermic and exothermic reactions are large enough to modify the temperature rise program. The above effects are a guide to possible problems with the 1-lb Large Sample Thermogravimetric Unit. A quartz tube reactor using 5 gm of lignite is now being tested to see if smaller samples and different tube material affect the results.

18.2.2 Thermogravimetric Analysis

The 130°C water loss of Indian Head lignite was of interest in relation to 250°C drying of coal reported previously. Figures 18-5 and 18-6 show a slow temperature rise program on the DuPont TGA Analyzer. The early weight loss around 100°C is probably water. The rate of dehydration may be too slow for the 5°C/min temperature program. The Indian Head lignite was essentially stable at 200°C. Figure 18-7 are approximations to isothermal weight loss curves in that the rise to a steady temperature was performed as quickly as

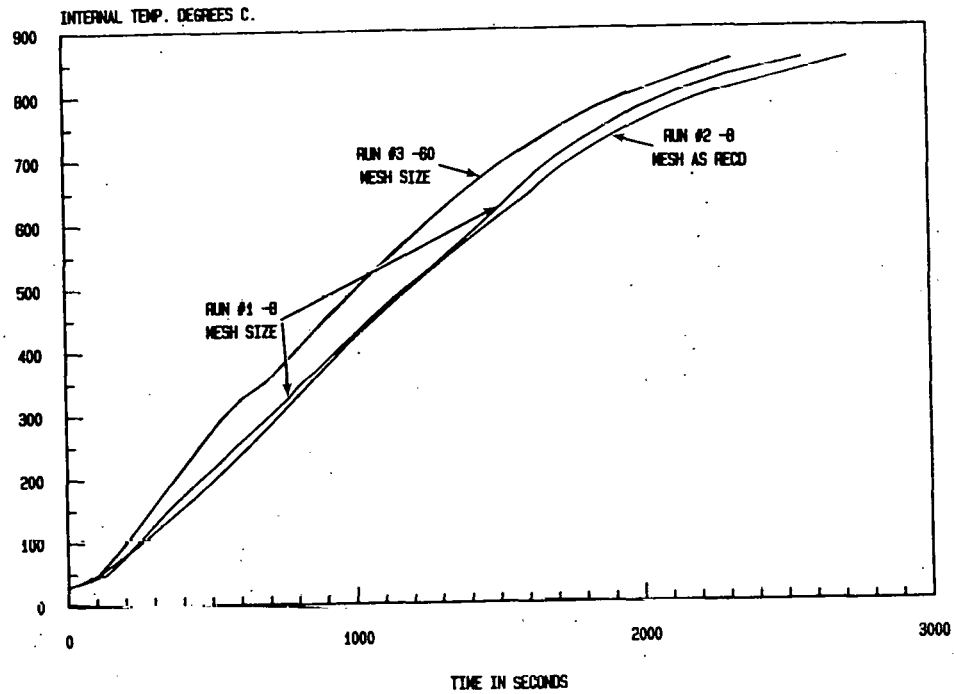

FIGURE 18-4. Pyrolysis profile Beulah high sodium.

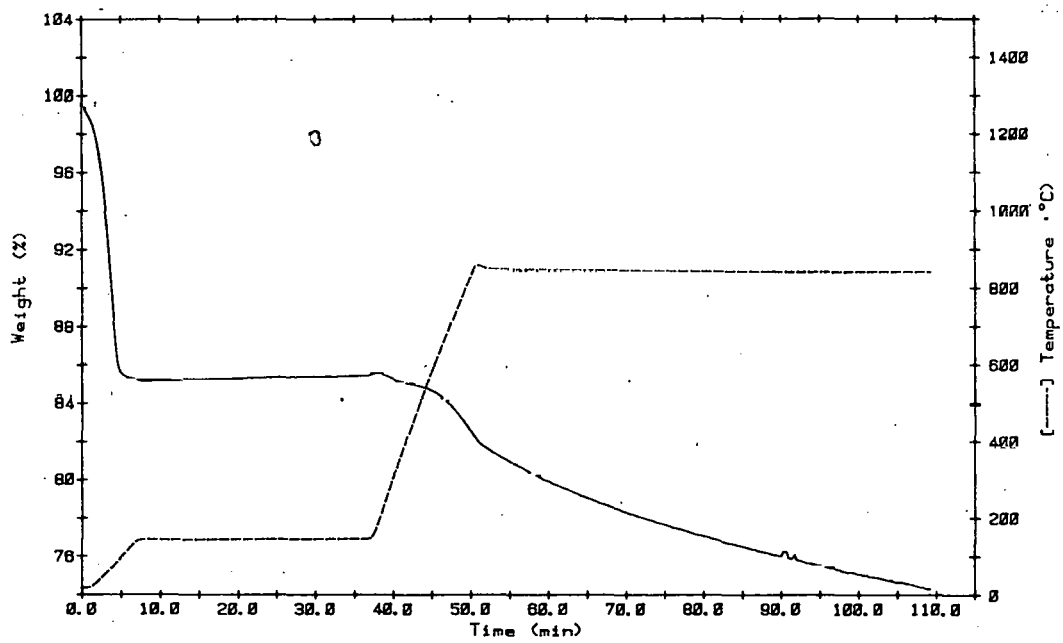

FIGURE 18-5. Thermogravimetric for Indian Head carbonization.

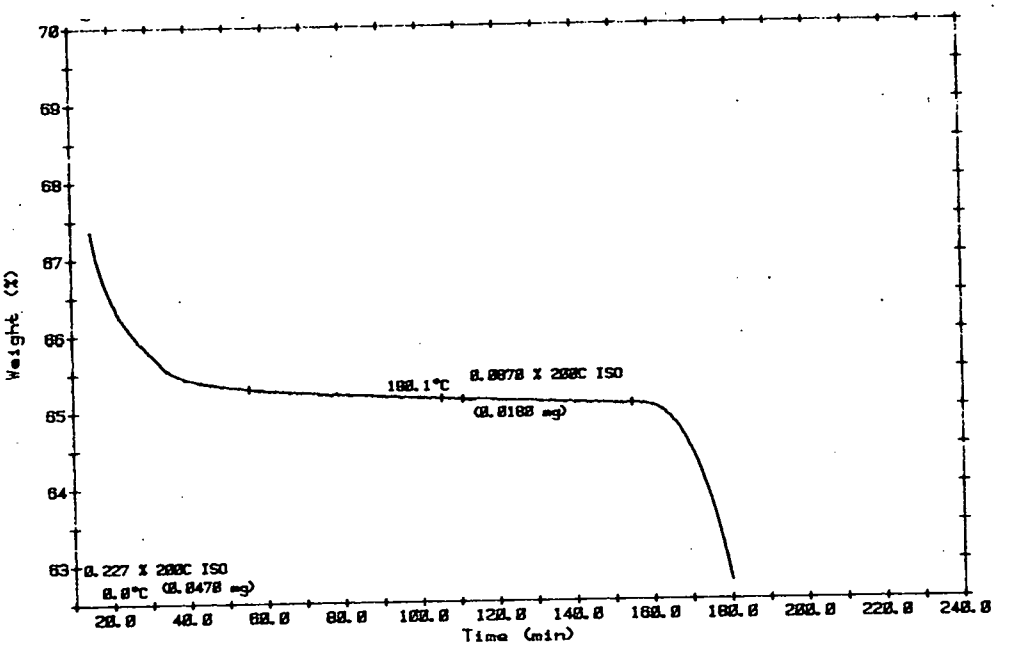

FIGURE 18-6. Expanded version of Figure 18-5.

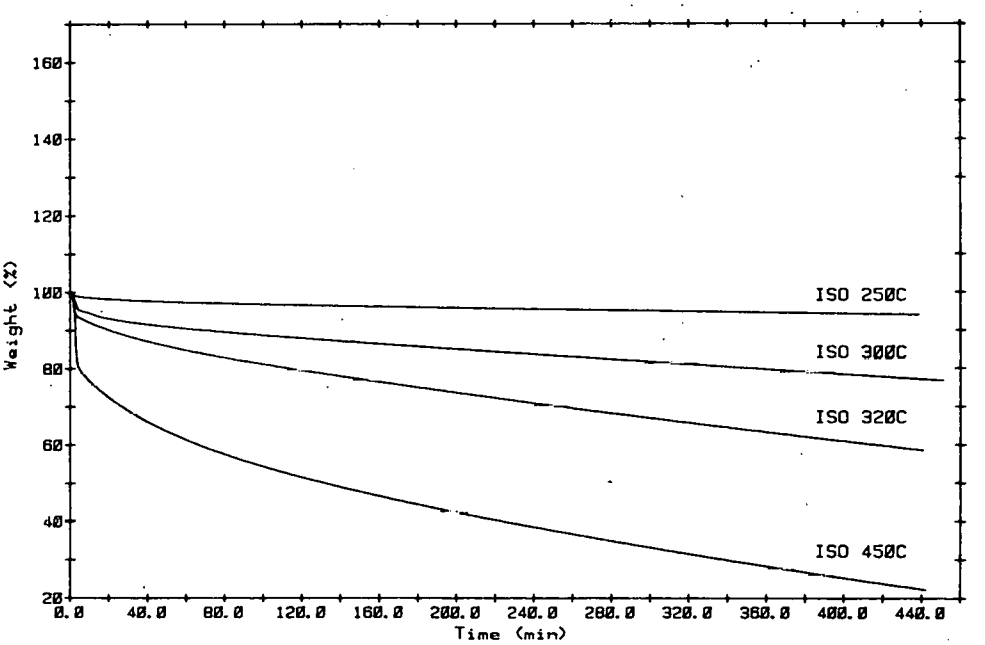

FIGURE 18-7. Isothermal weightless experiments for Indian Head lignite.

possible. These curves indicate that other volatiles are given off soon after 200°C. Interpretation of the thermogravimetric curves becomes uncertain at these extended times and elevated temperatures. The reason is that side reactions with residual water vapor and oxygen in the TGA will become significant in relation to pyrolysis reactions of a 20 mg sample of carbonaceous material. For example, the higher surface area material (curve 15 $mg^2\ g^{-1}$) obtained from the residue of supercritical water solvent extracted Indian Head was reduced to ash by reaction with water vapor or oxygen occurring as impurities in the atmosphere of the TGA apparatus. Similar problems occurred with a test sample of a highly reactive coal-based activated carbon.

18.2.3 Large Sample Thermogravimetric Unit

An apparatus has been designed to allow pyrolysis of samples of up to 1 lb of coal at temperatures to 1000°F and pressures to 1000 psi. It will be possible to run experiments over a matrix of variables including pressure, heating rate, particle size, final temperature, and atmosphere composition. The sample container will be suspended from a load cell to obtain weight loss data as a function of time (or temperature). The outlet of the main vessel will be able to accommodate a variety of condensers or traps to collect samples of tars, water, or oils. Provisions will also be available for on-line gas analysis. The internal features of the unit can be changed easy, in order to accommmodate sample containers or reaction chambers of various configurations. When complete, this apparatus will be a very versatile unit capable of obtaining thermogravimetric data over a range of sample weights and pressures not normally accessible in laboratory-scale equipment.

The main pressure vessel has been fabricated. Virtually all of the internal parts that are commercially available have been ordered. Some non-commercial items have been designed and fabricated. The vessel is being tested for compliance with design specifications and assembly and check-out of the outer unit is in progress. An inner reaction vessel is being fabricated and various spring support systems evaluated.

☆ U.S. GOVERNMENT PRINTING OFFICE: 1984—746-081/2532